Iron-zinc Reaction Kinetics Of Hot-dip Galvanized Interstitial Free Steels.

Iron-Zinc Reaction Kinetics of Hot-Dip Galvanized Interstitial Free Steels

by

Catherine E. Jordan

Presented to the Graduate and Research Committee

of Lehigh University

in Candidacy for the Degree of

Doctor of Philosophy

in

Materials Science and Engineering

Lehigh University

May 1996

Certificate of Approval

Approved and recommended for acceptance as a dissertation in partial fulfillment of the requirements for the degree of Doctor of Philosophy.

5/8/96
Date

Dissertation Advisor

5/x/96
Accepted Date

Special committee directing the doctoral research of Ms. Catherine E. Jordan

Chairperson
Dr. Arnold Marder

Dr. Katayun Barmak

Dr. Michael Notis

Dr. David Thomas

Dr. F.J.J. van Loo

Acknowledgments

I would like to thank Professor Arnold Marder, my thesis advisor, for his technical support and guidance throughout my years at Lehigh University. I am also grateful for the helpful technical discussions and suggestions provided by the members of my committee, Professors Katayun Barmak, Michael Notis and David Thomas, as well as Professor Frans van Loo at Eindhoven University, The Netherlands.

The industrial sponsorshorhip of the work led by Michel Dubois (Cockerill-Sambre, Belgium), Dr. Peter Mercer (BHP Steel, Australia), and Dr. Jean Wegria (Union Miniere, France) is greatly appreciated. Their collective experience in the processing of zinc coatings provided useful insight into my understanding of applied zinc coatings research.

I am truly indebted to Arlan Benscoter for his expertise and advice on the metallography of zinc coatings. The assistance of Kathy Repa with the electron microprobe is also gratefully appreciated. In addition, I thank Larry Clements for his work on the construction of the automated hot-dip galvanizing simulator. The information on sample preparation for hot-dip galvanizing provided by Dr. Yum Gerenrot was also instrumental in the successful production of laboratory specimens. The assistance of Dr. Ray Zuhr of

Oak Ridge National Laboratory with the production and depth profile analysis of ion implanted samples is also greatly appreciated.

I would like to thank Steve Attanasio, my husband, both for his editing portions of this document, and for his patience and support throughout my graduate studies while he himself was also a graduate student.

Lastly, I wish to thank my mom and dad for their encouragement. Their faith and love helped me through the most difficult periods of my graduate work, and to them I extend my heartfelt appreciation.

Table of Contents

List of Tables

List of Figures

Abstract

The objective of the present study was to investigate the effects of interstitial free (IF) steel substrate characteristics (such as grain size and chemistry) on Fe-Zn reaction kinetics and intermetallic phase formation during galvanizing at 450°C in zinc baths containing 0.00 wt% and 0.20 wt% Al. In the 0.00 wt% Al bath, uniform alloying of the substrate steel led to the development of a three phase Fe-Zn alloy layer containing gamma, delta and zeta phases. In the 0.20 wt% Al bath, however, alloying instead took the form of discontinuous Fe-Zn phase growth (outburst formation) at discrete sites along the steel/coating interface due to the initial formation of an Fe-Al inhibition layer.

Grain boundary reactivity was evaluated by testing ultra low carbon steels with identical chemistries but widely varying grain sizes (15 μm and 85 μm). In the 0.20 wt% Al bath, the initial formation of Fe-Zn phases occurred at a far more rapid rate on the 15 μm substrates than on the 85 μm substrates. Only after extended reaction times was localized Fe-Zn growth found to occur on the 85 μm grain size steel, and the location of this growth typically corresponded to substrate grain boundary sites.

The effect of phosphorus as a surface segregation layer was studied by ion implanting phosphorus into the surface of selected steel samples, all of which possessed an extremely large grain size (10-20 mm). Phosphorus surface segregation had no apparent effect on the kinetics of Fe-Zn phase growth on low carbon steel substrates in either 0.00 wt% Al

or 0.20 wt% Al baths. In the 0.20 wt% Al bath, Fe-Zn phase growth occurred on both the P-ion implanted and non P-ion implanted surfaces only after extended reaction times. Fe-Zn phase growth was found to correspond to the location of substrate grain boundary sites, suggesting that the long reaction times needed to produce Fe-Zn phase growth were due to the very large grain size of the steel. Substrate steel grain size (and not P surface segregation) thus appears to be the dominant substrate surface condition which controls the initial formation of Fe-Zn phases in a 0.20 wt% Al-Zn bath.

I. Introduction

Demand for zinc-coated steel sheet has risen dynamically in recent years due to increases in the application of zinc coatings in the automotive industry [1-3]. Zinc coatings provide a relatively low cost method of conferring steel with cosmetic and perforation corrosion protection against aggressive environmental conditions such as road deicing salt and acid rain [4]. The increased use of zinc-coated steel has stimulated a great deal of research aimed at improving coating quality. Alloyed Fe-Zn coatings have received much attention because of their superior weldability, paintability and cosmetic corrosion resistance over that of pure zinc coatings. Alloyed iron-zinc coatings can be manufactured by annealing after hot-dip galvanizing, by electrogalvanizing, or by zinc vapor deposition. For coatings produced by hot-dipping, the annealing step performed subsequent to galvanizing yields the zinc-coated product commonly known as galvanneal. Despite the many advantages conferred by the galvannealing process, the brittle nature of the intermetallic phases that form during the alloying of the coating often lead to surface damage when the metal is press formed. Hot-dip galvannealed coatings can powder and adhere to the press forming dies, resulting in damage to subsequently pressed parts and to the dies themselves (1). As a result, many recent studies have focused on investigating the factors that affect intermetallic phase formation, with an emphasis upon optimizing coating formability.

Interstitial free (IF) steels are finding increased use in the automotive industry due to their superior formability properties over those of plain carbon steels. IF steels are ultra-low

carbon steels (0.001-0.005 wt%) that contain Ti or Ti and Nb as stabilizers. The role of Ti and Nb is to combine with carbon and nitrogen to form Ti and Nb carbides and nitrides.

Previous characterization of zinc coatings has largely been dedicated to coatings deposited on iron and low carbon steels. IF steels possess at least two significant metallurgical differences from iron and low carbon steels: the presence of carbon-free grain boundaries, and the presence of phosphorus as a substitutional alloying agent. IF steel grain boundaries are essentially carbon-free due to the precipitation of Ti and Nb carbides within the grains. It has been postulated [1] that the chemical nature of the grain boundaries increases the thermodynamic activity at grain boundary sites on the steel surface during hot-dip galvanizing, resulting in the preferential nucleation and growth of Fe-Zn phases at these sites. Phosphorus is added to IF steels as a solid solution strengthening agent, in order to prevent denting of automotive steels. Previous work on galvannealed coatings has indicated that substrate chemistry can affect coating formation kinetics, but specific information on the effect of phosphorus is not readily available.

The effects of IF steel substrate characteristics (such as grain size and chemistry) on Fe-Zn reaction kinetics during processing are of great interest to the steel coating industry, as a detailed understanding of their specific effects is a necessary prerequisite to the development of optimally alloyed coatings. The goal of the present study is to investigate the effects of IF steel substrate characteristics on Fe-Zn reaction kinetics and intermetallic

phase formation during galvanizing. Specific emphasis will be placed on the evaluation of grain size effects and on the role of substrate phosphorus concentration.

II. Literature Review

A continuous hot-dip galvanizing/galvannealing process is shown schematically in Figure 1. The substrate sheet is first preheated in a gaseous reducing environment (H_2/N_2) to clean the steel surface and to recrystallize the cold worked grain structure. The sheet is then dipped in a molten bath of zinc (or zinc containing aluminum), and excess liquid zinc is removed from the moving sheet as it exits the pot by pressurized nitrogen gas knives located just above the zinc bath. The hot-dipped coating is subsequently annealed in a reducing atmosphere in a gas-fired or induction furnace. The resulting product is referred to as hot-dip galvanneal.

In an attempt to understand the work that has already been conducted on hot-dip galvanized coatings, the published literature on the topic is reviewed in the present section. The review emphasizes coating structure formation, with a short discussion on interstitial free steels. Studies relating to the initial iron-aluminum intermetallic layer that forms during galvanizing are discussed, as are studies relating to the subsequent iron-zinc phase growth that develops during annealing. The nucleation and growth of these structures are examined in detail, with specific consideration given to the material and processing variables that influence coating phase formation.

Many past studies have concentrated on the variables that affect the formation of galvanized coatings. During these studies, samples were often held for extremely long

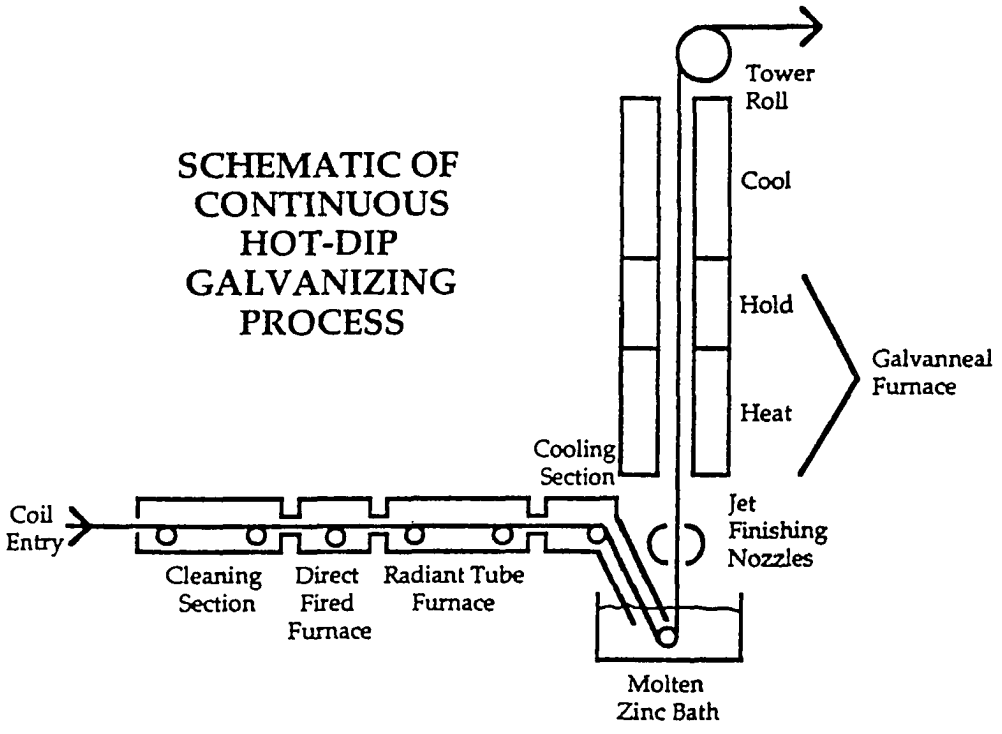

Figure 1. Schematic diagram of the continuous hot-dip galvanizing process (courtesy of Scott Bluni).

immersion times in the zinc bath, allowing a thick iron-zinc alloy layer to form while the sheet was submerged in the bath. Because this growth is morphologically similar to the growth that occurs during galvannealing, many galvanizing studies draw conclusions about the alloy layer growth that develops during galvannealing. Since this situation may occasionally result in confusion, an effort has been made in the following section to distinguish between galvanizing and galvannealing studies.

A. Iron-Aluminum Intermetallic Layer Formation

In the following section, literature data are divided into two categories according to bath Al content: Zn baths containing greater than 5 wt% Al, and Zn baths containing less than 5 wt% Al. The higher Al baths (> 5 wt%) will be discussed first, in order to provide background on the effects of bath Al on galvanizing reaction kinetics. The discussion will then focus on the lower Al baths (< 5 wt%), which are more relevant to the present study.

1. Zn Baths Containing > 5 wt% Al

In 5 wt% Al-Zn coatings formed during hot-dip galvanizing at 450°C, the first solid phase to form at the coating-metal interface is an Fe_2Al_5 phase. Iron has a higher chemical affinity for aluminum than for zinc, resulting in the formation of an iron-aluminum layer upon immersion of the substrate into the bath. The Fe_2Al_5 phase will contain varying amounts of zinc in solid solution (depending upon the bath conditions under study), and it

can thus be referred to alternatively as $Fe_2Al_5Zn_x$; in the present study, however, the more common designation of Fe_2Al_5 will be utilized. The Fe_2Al_5 phase forms as localized growths or outbursts, and with longer reaction times (i.e. immersion times), the outbursts of Fe_2Al_5 increase in number and eventually cover the entire steel surface [5]. The Fe_2Al_5 phase has been found to grow not only into the coating, but also into the steel substrate, with a preferential <001> orientation.

Continued immersion in the bath results in the formation of a second phase, $FeAl_3$ (which may contain zinc in solid solution and can thus alternatively be termed $FeAl_3Zn_x$). At this point, the alloy layer exhibits a two-phase morphology, consisting of an adherent layer of Fe_2Al_5 as well as the $FeAl_3$ phase, which is not in physical contact with the adherent layer of Fe_2Al_5 [5]. The $FeAl_3$ phase is referred to as a "breakaway" phase, since it visually appears to have broken away from the outer edge of the adherent Fe_2Al_5 layer.

A two layer Fe-Al morphology was also found to develop in 45, 55, and 75 wt% Al-Zn coatings [6]. Hot-dip galvanizing in 45-75 wt% Al-Zn baths at 590-635°C resulted in the development of both adherent and non-adherent alloy layers in the coating. The total alloy layer consisted of Fe_2Al_5, $FeAl_3$, and Zn. For the 45-75 wt% Al-Zn coatings, Fe_2Al_5 formed an adherent alloy layer at the steel interface, with $FeAl_3$ forming at the interface between Fe_2Al_5 and the Zn overlay. The $FeAl_3$ was found to have a breakaway structure. The existence of the breakaway morphology is believed to be related to interfacial stresses which develop during the formation and growth of this phase. Both the Fe_2Al_5 and $FeAl_3$

phases contained areas where the liquid zinc had penetrated up to the coating-metal interface; such areas are referred to as zinc channels [6]. The presence of the zinc channels indicates that both of these intermetallic Fe-Al layers have a somewhat porous structure during immersion in the Al-Zn bath.

In summary, for zinc coatings containing 5-75 wt% Al, the first phase to nucleate at the steel/coating interface is Fe_2Al_5 (or a zinc-bearing $Fe_2Al_5Zn_x$). The Fe_2Al_5 layer is stable in coatings containing greater than 5 wt% Al, and is accompanied by the formation and growth of a breakaway $FeAl_3$ layer.

2. Zn Baths Containing < 5 wt% Al

For zinc coatings produced from baths containing less than 0.3 wt% Al, however, the Fe_2Al_5 layer is considered to be *transient* in nature. The Fe_2Al_5 layer is referred to as an inhibition layer [7], because it retards or inhibits the formation of Fe-Zn phases by acting as a physical barrier at the coating/metal interface which protects the underlying iron from rapid zinc attack. Fe_2Al_5 acts to inhibit Fe-Zn phase formation for a certain period of time, but is no longer present at later immersion times, as evidenced by the fact that the alloy layer which develops in these low Al coatings consists only of binary Fe-Zn phases.

An isothermal section of the iron-zinc-aluminum phase diagram at 450°C (shown in Figure 2) [8] suggests that the inhibition layer should be a dual-phase structure [7] consisting of

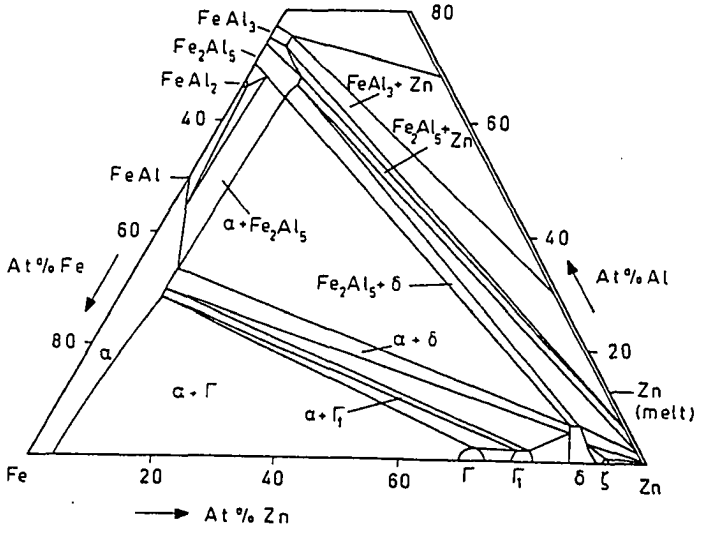

Figure 2a. Isothermal section of the Fe-Zn-Al phase diagram at 450°C [8].

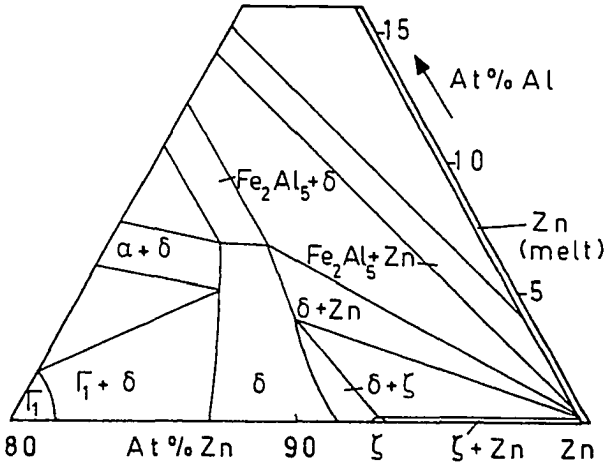

Figure 2b. Zinc rich corner of the diagram in Figure 2a. [8].

zinc-bearing Fe_2Al_5 and $FeAl_3$ (and perhaps $FeAl_2$). It appears, however, that the nucleation barrier for Fe_2Al_5 is relatively low, since this phase forms in preference to other phases predicted to be present by the phase diagram. For short immersion times, Fe_2Al_5 initially forms a stable low-diffusivity layer on the steel substrate. Subsequent to the appearance of Fe_2Al_5, $FeAl_3$ does form on the surface of the Fe_2Al_5 layer. The dual phase inhibition layer then grows in a direction towards the zinc, with a small amount of growth occurring as penetration into the iron alloy substrate.

Ghuman and Goldstein [9] propose a slightly different mechanism for the development of the inhibition layer. For bath temperatures below 600°C, these researchers observed the formation of a thin layer of an iron-zinc-aluminum ternary compound (via electron probe microanalysis and x-ray diffraction), which inhibits the growth of iron-zinc phases. The chemical formula of the Fe-Zn-Al compound is not provided in Reference [9]. According to their study, inhibition is initially caused by a compact layer of primary iron-zinc-aluminum phase, and after a certain period of immersion time, a less compact secondary iron-zinc-aluminum phase inhibits the iron-zinc reaction. Breakdown of the inhibition layer occurs when the secondary phase becomes rich in aluminum and forms the more stable Fe_2Al_5 phase. The diffusing zinc atoms react with iron and begin the formation and growth of iron-zinc phases.

Although the Ghuman and Goldstein interpretation of the inhibition layer seems to be different than that previously described, these alternative explanations may actually be

quite similar. It was mentioned previously that the Fe_2Al_5 phase will contain varying amounts of zinc in solid solution, and that it can be referred to as $Fe_2Al_5Zn_x$. It is possible that the Fe-Al-Zn inhibition phase(s) observed by Ghuman and Goldstein correspond to zinc-containing Fe_2Al_5 layers.

The inhibition layer was found to conform to a parabolic growth rate by Borzillo and Hahn [10], suggesting that its growth is dependent on the diffusion coefficients of iron, aluminum and zinc in the layer. Although little ternary diffusion data exist for the iron-aluminum layer, its small rate of growth as compared to the iron-zinc alloy layer suggests that the diffusion coefficients for the inhibition layer are less than those for the iron-zinc phases at a bath temperature of 450°C [10]. It is estimated that these diffusion coefficients may be approximately two orders of magnitude less than those for the iron-zinc phases. The apparent low diffusivity of Fe, Zn, and Al in the inhibition layer is consistent with its ability to retard Fe-Zn phase formation at the coating/metal interface.

Destabilization of the inhibition layer is relevant to coating microstructure development since destabilization permits iron-zinc phase growth to begin. The growth rate and subsequent destabilization of the inhibition layer was found to be affected by the iron content in the bath. For a constant bath aluminum content, the growth rate of the inhibition layer increased and the time for destabilization to occur decreased as the iron content in the bath was raised to saturation level [7]. Because the inhibition layer grows mostly toward the iron-saturated zinc, iron diffusion through the layer controls the growth

rate of the intermediate phases [7]. If the bath were not iron-saturated, iron would have to diffuse through the alloy layer into the liquid zinc, in addition to contributing to the growth of the iron aluminum inhibition alloy layer formation, thus longer time for the breakdown of the layer would be necessary.

Tang [11] found the inhibition layer to be stabilized for extended time periods in zinc baths containing Al (450°C), which were not saturated in iron. These investigators also found that as the aluminum content of an iron-saturated zinc bath increases, the inhibition layer becomes stabilized. Full inhibition (no Fe-Zn phase growth) was found to occur for Fe saturated zinc baths at 450°C at an aluminum level equal to or greater than 0.15 wt%.

Destabilization of the layer can occur if the aluminum composition of the bath is not maintained at a constant level. A decrease in the aluminum composition can initiate an interfacial instability, such as a column of Fe_2Al_5 growing into the $FeAl_3$ layer. The $FeAl_3$ layer will be consumed by the more stable Fe_2Al_5 phase. Once the $FeAl_3$ layer has been consumed, the Fe_2Al_5 will attempt to withdraw aluminum from the bath. As the aluminum content in the bath decreases at the liquid/solid interface to 0.12 weight percent, a further lowering of the aluminum concentration can only be achieved by the nucleation of the $delta_1$ phase [12]. Aluminum and iron in the bath counteract each other in that an increased aluminum content prolongs the life of the metastable Fe_2Al_5 and $FeAl_3$ phases while an increase in the amount of saturated iron in the bath promotes the destabilization of the inhibition alloy layer.

The determination of bath iron saturation has recently been modified by Tang [11], to include new iron solubility limit data for Zn and Zn(Al) melts in the literature. Iron solubility is shown as a function of bath aluminum content in Figure 3, for a zinc bath temperature of 450°C. The data in Figure 3 indicate that iron solubility reduces to 0.008 wt% in liquid zinc-0.2 wt% Al baths, whereas the Fe-Al-Zn isotherm previously developed by Kirkaldy [12] showed an Fe solubility of 0.03 wt% for a zinc-0.2 wt% Al bath at 450°C. Tang has incorporated new solubility data into an updated 450°C Fe-Al-Zn ternary isotherm, which is shown in Figure 4 [13].

B. Iron-Zinc Alloy Phase Formation: Iron-Zinc phase diagram

The most widely accepted iron-zinc equilibrium phase diagram is that of Kubachewski [14]; the zinc rich portion of this diagram is shown in Figure 5. There are four iron-zinc compounds which exist in the zinc rich region: zeta, delta, $gamma_1$, and gamma. Though not represented in Figure 5, eta phase is a solid solution of Fe in Zn with an Fe solubility of only 0.03 wt%. The primary phases formed during long-time immersion galvanizing (or during post-dipping annealing) are zeta, delta, $gamma_1$, and gamma. Although older iron-zinc equilibrium phase diagrams show the existence both a delta phase and a $delta_1$ phase, the x-ray analysis of Bastin [15] indicates that only one delta phase exists up to 670°C.

Microscopic observations indicate that after a short amount of reaction time, a structure consisting of either fine grained eta or eta plus zeta will form, above a thin delta layer

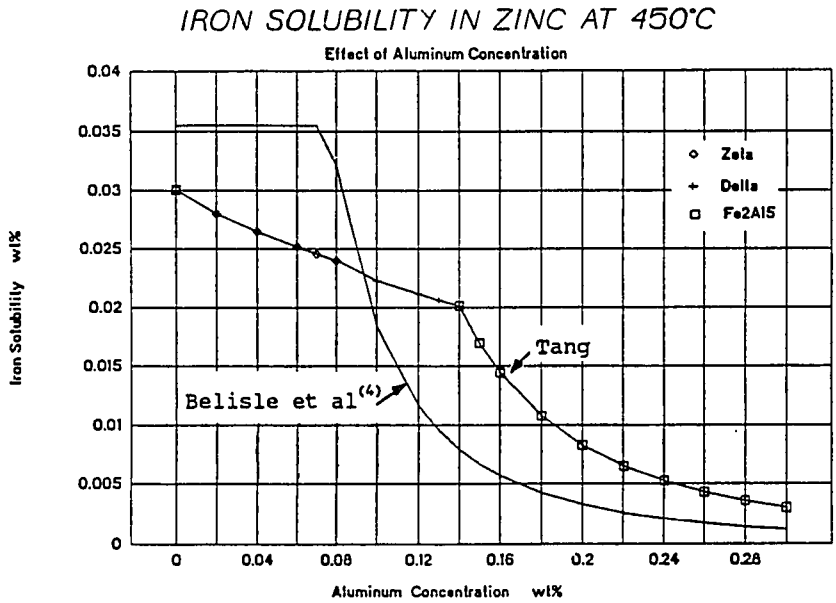

Figure 3. Effect of Al on Fe solubility in molten Zn at 450°C [11].

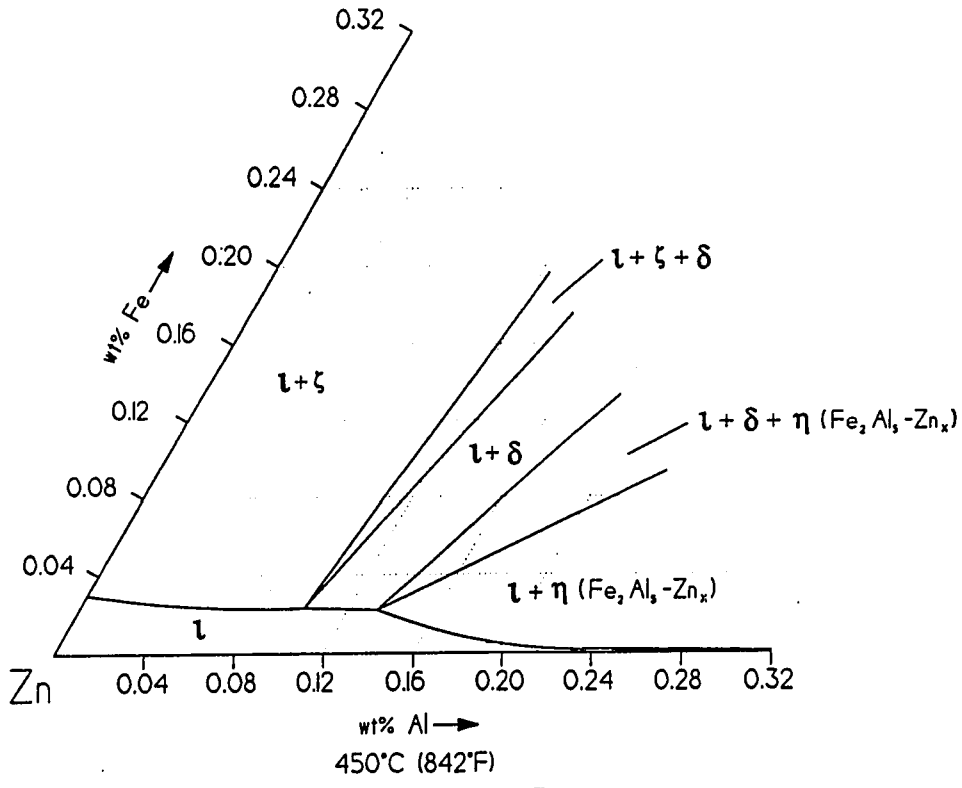

Figure 4. Zinc rich corner of the 450°C isothermal section of the Fe-Zn-Al phase diagram [13].

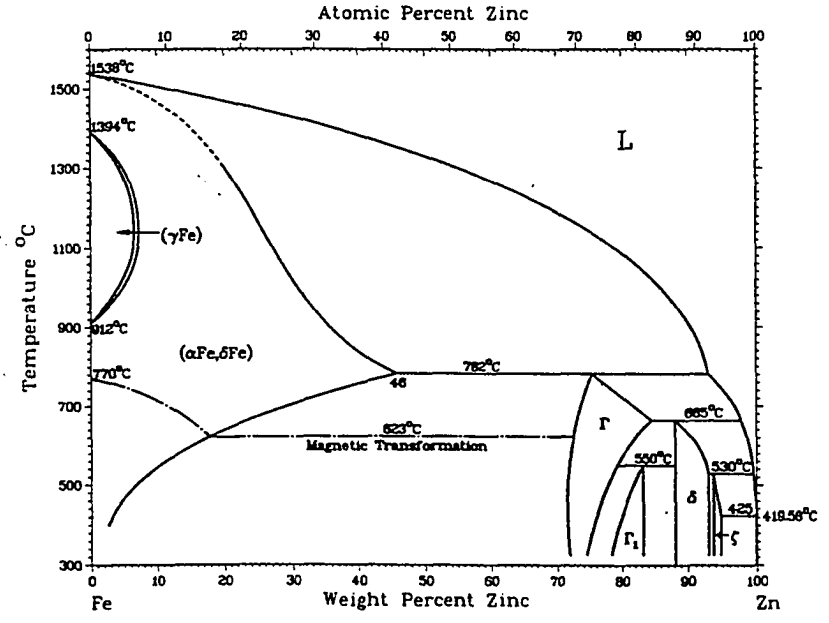

Figure 5a. Complete Fe-Zn binary phase diagram [14].

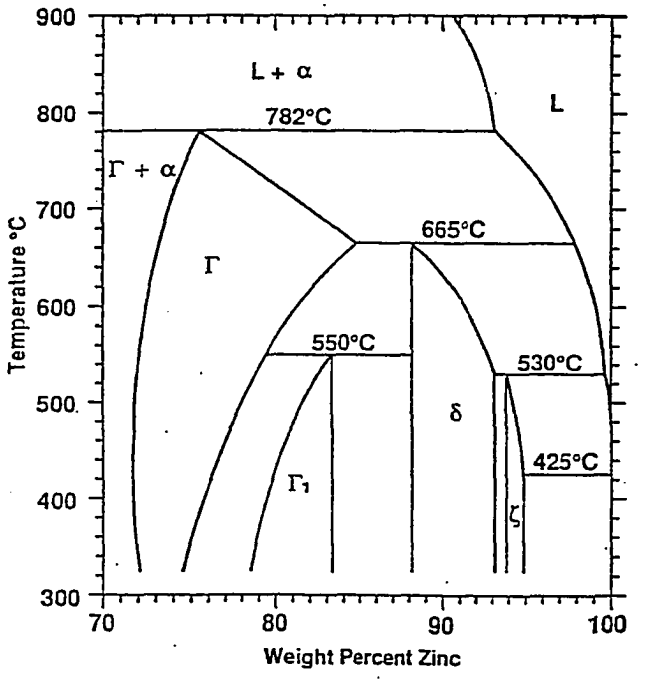

Figure 5b. Zinc rich corner of the Fe-Zn binary phase diagram.

which is adjacent to the substrate steel. As the reaction proceeds, the delta phase grows rapidly and gamma additionally forms between the delta phase and the substrate steel. During galvanizing, eta and zeta phases are believed to form first, followed by delta and then by gamma [16]. The $gamma_1$ phase is believed to form last, after longer times of reaction, as a layer which is located between the gamma and delta phases.

The characteristics of the zinc rich iron-zinc phases are shown in Table I [17].

Table I. Fe-Zn Phase Characteristics [17].

Phases	Formula	Crystal Structure
η	Zn(Fe)	HCP
ζ	$FeZn_{13}$	Monoclinic
δ	$FeZn_{10}$	Hexagonal
Γ_1	Fe_5Zn_{21}	FCC
Γ	Fe_3Zn_{10}	BCC
α	Fe(Zn)	BCC

A brief description of each iron-zinc intermetallic phase typically found in hot-dip galvanized coatings appears below, in order of increasing iron content.

1. zeta phase

The zeta phase, $FeZn_{13}$, has an iron content of approximately 5-6 wt% [18]. It is formed from a peritectic reaction between the delta phase and liquid zinc (at 530 ± 10°C). During controlled diffusion studies in the absence of aluminum, the zeta phase was found to form between the free zinc eta phase and the delta phase, with its growth following a parabolic rate law [19]. The zeta phase is isomorphous with an monoclinic unit cell and an atomic structure similar to that shown in Figure 6 [20], with a transition metal atom (iron) and a zinc atom surrounded by 12 zinc atoms at the vertices of a slightly distorted icosahedron. The icosahedra link together to form chains and the linked chains pack together in a hexagonal array [20].

2. delta phase

The delta phase, $FeZn_{10}$, has an iron composition range of 7.0 to 11.5 weight percent. Delta phase has a hexagonal unit cell and is not isomorphous, but rather has two morphologies. The existence of two morphologies is most likely the result of the zinc and iron concentration gradients that exist across the phase layer. The zinc-rich side of the phase has a columnar morphology and is often referred to as $delta_{1p}$, where p refers to a palisade morphology. The iron-rich side of the phase, which resides closest to the steel/coating interface, has a compact morphology and is designated in the literature as $delta_{1k}$. The palisade and compact morphologies are not separate phases, a fact which has

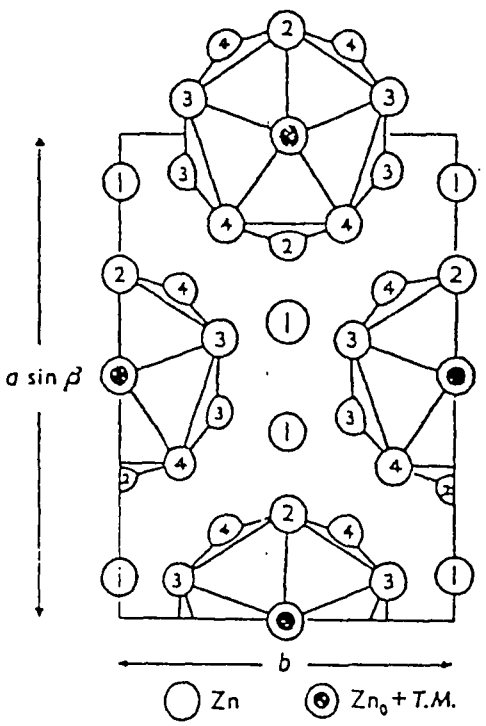

Figure 6. Schematic representation of the zeta phase icosahedron structure as viewed down the [001] plane [20].

been proven by x-ray diffraction analysis [21]. As previously stated, the delta phase was often referred to as the $delta_1$ phase in the past. The two terminologies delta and $delta_1$ actually describe the same iron-zinc phase.

3. $gamma_1$ phase

The $gamma_1$ phase, Fe_5Zn_{21}, has an iron composition range of 17 to 19.5 weight percent (at 450°C). The $gamma_1$ phase has a face centered cubic lattice structure. The $gamma_1$ phase exists up to 550 ± 10°C, and has been proven to be an equilibrium phase because it can be produced upon heating at low temperatures over long time periods [22]. The large composition range listed above decreases with an increase in temperature. The $gamma_1$ phase is an uninterrupted layer that appears between the gamma and delta layers, as shown in Figures 7 and 8 [22]. Figure 7 shows the phase formation after annealing at 380°C for two hours, and Figure 8 shows the growth of the $gamma_1$ phase after annealing at the same temperature for seven hours. After the formation of the $gamma_1$ phase, it is evident that the iron-zinc diffusion couple exhibited cracking at the zeta/zinc interface. Cracking most likely occurred because of gap formation due to the Kirkendall effect. $Gamma_1$, Fe_5Zn_{21}, has the highest microhardness value of intermetallic phases formed during galvannealing, as shown in Table II [22].

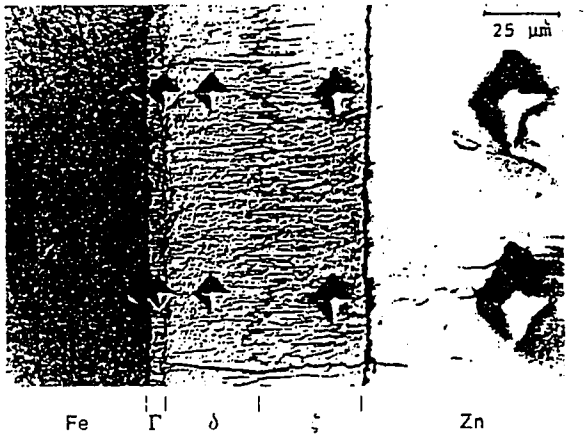

Figure 7. Optical micrograph of an Fe-Zn diffusion couple, annealed for 2 hours at 380°C [22].

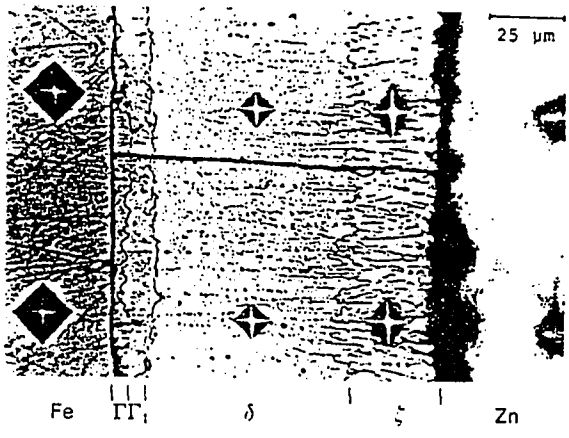

Figure 8. Optical micrograph of an Fe-Zn diffusion couple annealed for 7 hours at 380°C [22].

Table II. Vickers microhardness values (load 25 mg) for various compounds in the Fe-Zn system [22].

Compound	Microhardness value in kg/mm^2
Fe	104
Γ	326
Γ_1	505
δ	358
ζ	208
Zn	52

4. gamma phase

The gamma phase, Fe_3Zn_{10}, has an iron composition range of 23.5 to 28 wt% (at 450°C). Gamma forms in the body centered cubic structure. As the reaction temperature rises, the homogeneity range of gamma increases up until 665°C, which is the peritectic temperature for the reaction gamma + liquid zinc to delta [23].

C. Nucleation and Growth

1. Iron-Aluminum Intermetallic Nucleation and Growth

It has been postulated [10] that the iron-aluminum layer first nucleates as Fe_2Al_5 and then grows at a parabolic rate as a function of bath temperature and the Al:Fe ratio in the bath. The Fe_2Al_5 layer is believed to have a lower nucleation barrier than any of the iron-zinc compounds [8], or any other iron-aluminum intermetallic compounds. Nucleation will occur at a solid/liquid interface because the degree of supersaturation is greatest at the interface, and because the surface area needed for nucleation is available. The zinc-bearing Fe_2Al_5 layer is metastable and breakdown of this layer will eventually occur. The onset of inhibition layer breakdown was identified by the appearance of nodules of a ternary iron-zinc-aluminum phase and the disappearance of the Fe_2Al_5 layer [10]. The nodules were described by Kirkaldy [7] as burst-like. Both the Fe_2Al_5 and ternary Fe-Zn-Al phase transformed to delta upon longer immersion times.

Another explanation for the stated differences in Fe-Al stabilization and growth may be due to metastable equilibrium conditions that arise during short time (less than 30 minute) immersion in Zn(Al) baths. Perrot et al [24] found that for these relatively short times an Fe-Al-Zn ternary isotherm at 450°C generated from EPMA data (Figure 9) showed extended solubility ranges when compared to the accepted equilibrium 450°C isotherm of Kirkaldy [12]. In particular, Fe_2Al_5 was found to have a solubility for Zn up to 22.87

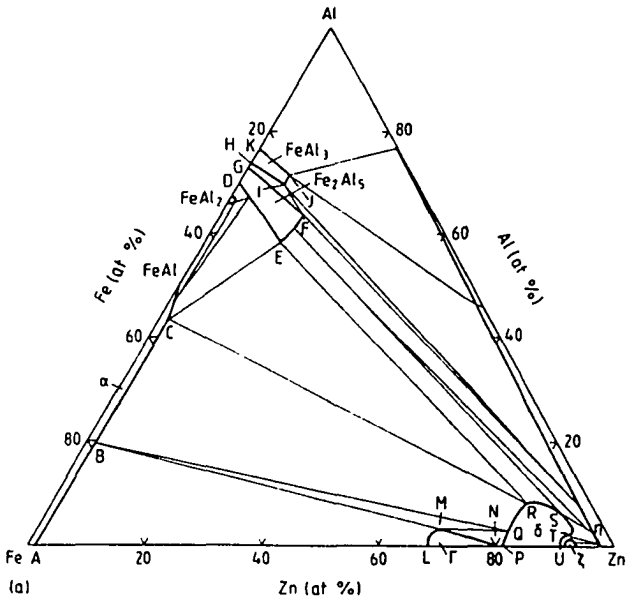

Figure 9a. Isothermal section of the metastable Fe-Zn-Al phase diagram at 450°C constructed from diffusion experiments for short times (< 30 minutes) [24].

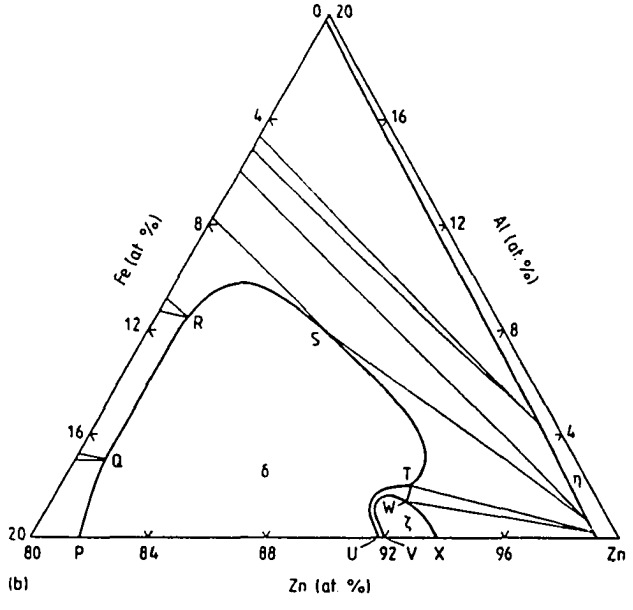

Figure 9b. Zinc rich corner of the diagram in Figure 9a. The compositions labeled A through X are listed in Table IIIA [24].

wt%. Similarly Chen [25] found the extended solubility for Zn in Fe_2Al_5 to be 21 wt%. Chen's short time (less than 30 minutes) immersion data also showed that the maximum solubility of Zn in alpha Fe (at 0 wt% Al in the Zn bath) was 2 wt% and not 12 wt% as reported by Kirkaldy [12].

Perrot [24] found the delta phase to have an extended solubility range for Al (3.71 wt%) at 450°C. Delta phase also had an extended Fe solubility of up to 16 wt% Fe in pure Zn (0 wt% Al) baths. These data indicate that delta becomes supersaturated in Fe (normally 11.5 wt% Fe saturation) in short time immersion samples at 450°C. Similarly, eta phase was also found to be over saturated in Fe for short time immersions. When long time (greater than 1000 hours) immersion samples were analyzed the solubility limits were found to decrease toward equilibrium values. The short and long time immersion experimental solubility data are summarized in Table III.

Table IIIA. Compositions corresponding to phase field boundaries in Figure 9 for short time (< 30 minutes) diffusion experiments at 450°C [24].

Phase	Point	Fe at.%	Zn at.%	Al at.%	Fe wt.%	Zn wt.%	Al wt.%
α	A	99	1	0	98.83	1.17	0
	B	79.15	1.25	19.60	87.86	1.62	10.51
	C	54.65	1.50	43.85	70.43	2.26	27.31
Fe_2Al_5	D	30	0	70	45	0	53
	E	28.38	12.97	58.65	39.47	21.11	39.41
	F	22.47	13.53	64	32.46	22.87	44.67
	G	27.40	0	72.60	43.85	0	56.15
$FeAl_3$	H	26	0	74	42.10	0	57.90
	I	23.89	7.64	68.47	36.24	13.56	50.19
	J	20.66	7.64	71.70	32.16	13.92	53.92
	K	23	0	77	38.20	0	61.80
Γ	L	31.80	68.20	0	28.48	71.51	0
	M	26.92	69.83	3.25	24.42	74.15	1.43
	N	18.93	81.07	0	16.63	83.37	0
δ	P	18.31	81.69	0	16.07	83.93	0
	Q	16	81.04	2.96	14.25	84.48	1.27
	R	10.48	81.11	8.41	9.57	86.72	3.71
	S	6	86	8	5.43	91.07	3.50
	T	6	92	2	5.23	93.92	0.85
	U	8.20	91.80	0	7.09	92.91	0
ζ	V	8	92	0	6.92	93.08	0
	W	6.95	91.40	1.65	6.06	93.24	0.70
	X	6.07	93.93	0	5.23	94.77	0

Table IIIB. Compositions corresponding to phase field boundaries for long time (> 1000 hours) diffusion experiments at 450°C [24].

Phase	Point	Fe at.%	Zn at.%	Al at.%	Fe wt.%	Zn wt.%	Al wt.%
α	A	96.08	3.92	0	95.44	4.56	0
	B	88	4	8	91.15	4.85	4
	C	47.30	2.70	50	63.38	4.23	32.39
Fe_2Al_5	D	25	11	64	36.34	18.71	44.95
δ	E	13.40	86.60	0	11.67	88.32	0
	F	12.39	85.61	2	10.91	88.24	0.85
	G	11.70	85.23	3.07	10.36	88.33	1.31
	H	10	86	4	8.89	89.40	1.71
	I	7.47	88.23	4.30	6.62	91.54	1.84
	J	7.70	89.84	2.46	6.75	92.21	1.04
	K	7.86	82.14	0	6.79	93.21	0
ζ	L	7.50	92.50	0	6.48	93.52	0
	M	6.90	91.25	1.85	6.02	92.20	0.78
	N	6.07	93.93	0	5.23	94.77	0
Γ_2	P	7.45	87.70	4.85	6.62	91.30	2.08
	Q	9.50	83.80	6.70	8.57	88.50	2.93
	R	7	84.40	8.60	6.36	89.86	3.78
$FeAl_3$	S	23.85	4.13	72.02	37.57	7.61	54.82

2. Iron-Zinc Alloy Phase Growth Rates

The nucleation of iron-zinc intermetallic phases is related to a decrease in aluminum concentration of the bath near the solid/liquid interface [8]. The first evidence of iron-zinc alloy layer growth, or outburst structure formation, has been postulated to occur at the grain boundaries of the substrate at the steel/coating interface [1]. A decrease in aluminum concentration is thought to first occur at substrate grain boundaries [1], thus leading to the initial formation of Fe-Zn phases at these substrate grain boundary sites. A proposed sequence of events assumes that as the steel strip is immersed, an iron-aluminum compound initially forms at the steel/coating interface. Because grain boundaries provide fast diffusion paths for Zn, the reaction rate at grain boundaries is rapid, and a decrease in aluminum concentration initially occurs at the location of a substrate surface grain boundary [26]. The iron-zinc delta phase nucleates at grain boundaries and penetrates through the thin iron-aluminum compound as is shown in Figure 10 [1]. Following the equilibrium phase diagram, cooling delta and eta will form zeta, and the zeta phase formed will grow rapidly at sites corresponding to substrate grain boundaries. The iron-aluminum compound at the grain interior is transformed at a later stage, therefore a sidewise growth of the zeta phase is observed similar to that shown in Figure 11 [26].

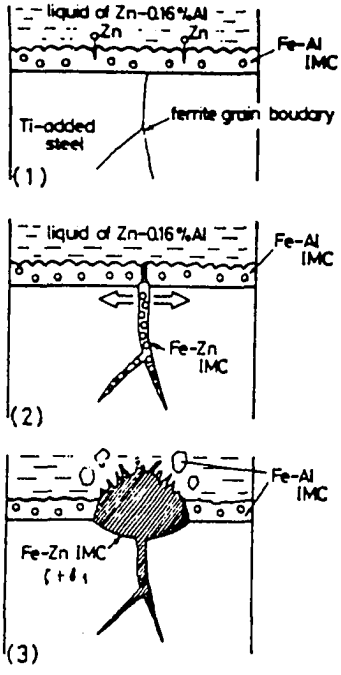

Figure 10. Schematic diagram showing the Fe-Zn outburst growth behavior [1].

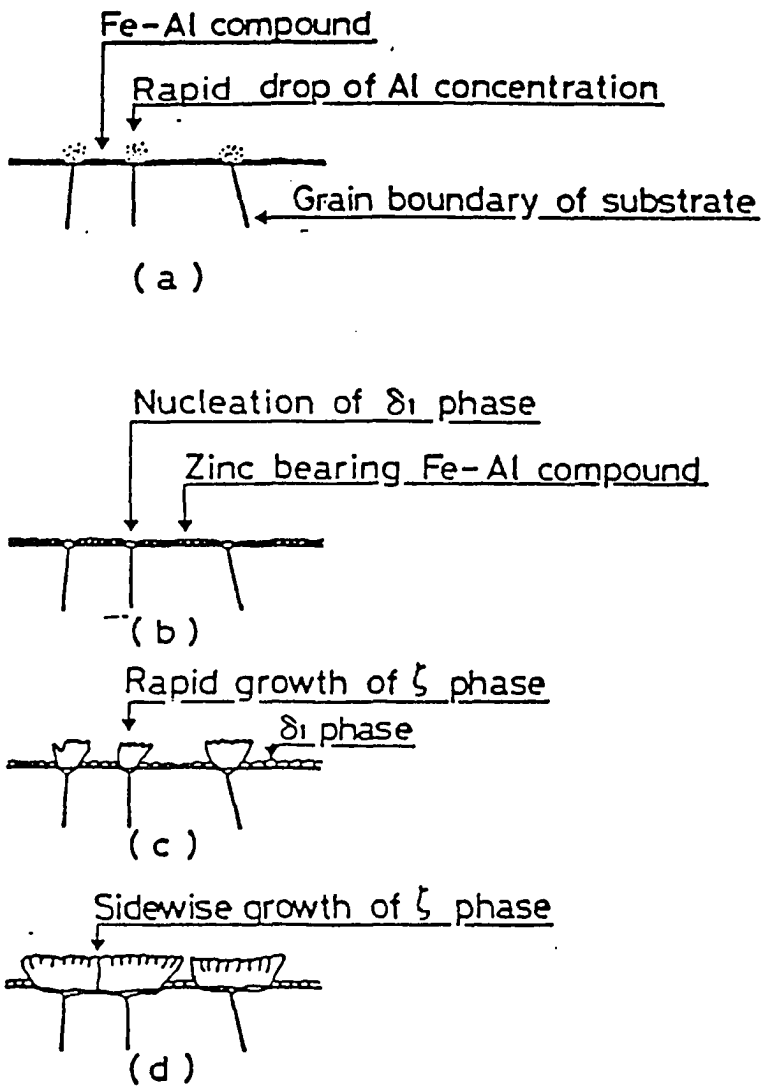

Figure 11. Schematic illustration of the formation of Fe-Zn phase growth at substrate grain boundaries [26].

If the mechanism of iron-zinc phase growth is diffusion controlled, the growth of the phases will be dependent on the square root of immersion time or annealing time. Growth which occurs by diffusion through a concentration gradient results in a layer thickness which increases parabolically with time. Parabolic growth is common for long bath immersion times and high aluminum bath concentrations.

In the iron-zinc system, however, growth can also occur linearly with time. If the delta layer is cracked, it will be penetrated by liquid zinc and subsequent growth will occur at the substrate/zinc interface according to a linear law, with a surface reaction controlling the reaction rate [27]. Linear growth often occurs for short immersion times and for bath aluminum contents between 0.06 and 0.09 weight percent. Yamaguchi [27] also concluded that over a wide range of immersion times, other mechanisms beside parabolic and linear growth rates are likely to occur, as described below.

For short immersion times and a bath content of greater than 0.09 weight percent aluminum, growth may occur according to a reciprocal logarithmic law. An example of this type of growth would be the case of an extremely thin oxide film or an inhibiting alloy layer on the order of approximately 10 angstroms (0.0004 inches) thick. The equation for this type of growth would be:

$$1/e = A - B * \ln(t)$$

where e represents coating thickness.

If the reaction rate increases rapidly with an increased amount of a particular growing phase, the growth is termed autocatalytic and the reacted phase exists as "islands", as shown in Figure 12 [27]. The extent of the reaction over time follows a sigmoidal relationship with the transformation occurring heterogeneously and proceeding in a manner such that the autocatalytic phase consumes the iron-aluminum phase present at the interface. Determination of the rate of heterogeneous nucleation is a complex problem. Johnson and Mehl described isothermal transformations in metals by the equation:

$$y = 1 - \exp(-kt^n)$$

where y is the extent of transformation, and k and n are assumed constant. The above mentioned equation was derived from the experimentally proven transformation equation:

$$dy/dt = kt^n\text{-}1(1 - y).$$

An example of an auto-catalytic reaction would be the outburst structure of the delta phase growing out from the Fe_2Al_5 inhibition layer. The ratio of outburst structure to the total surface area was determined for one aluminum level in the coating by analytical electron microscopy and plotted versus immersion time. The plot gave a sigmoidal curve as is shown in Figure 13 [27]. An isokinetic growth relationship was evident for various aluminum concentrations in the bath. A parallel shift of one curve determined for a given

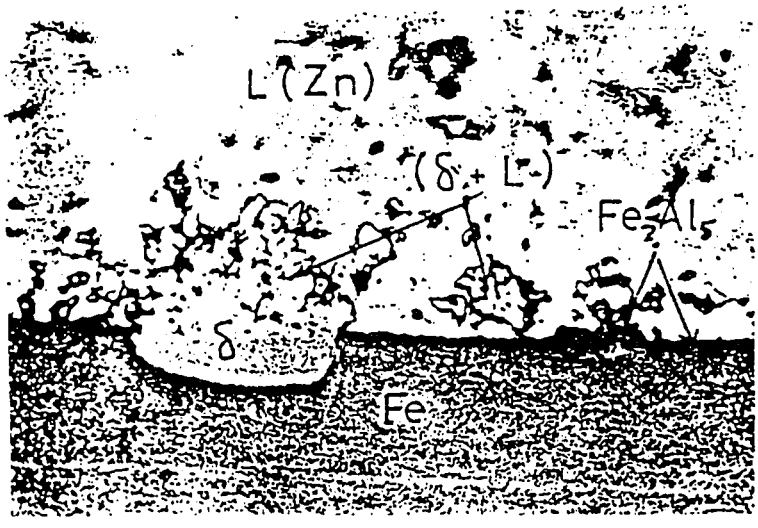

Figure 12. Type-1 surface alloy layer microstructure where transformation from the inhibition layer to the outburst structure is occurring [27].

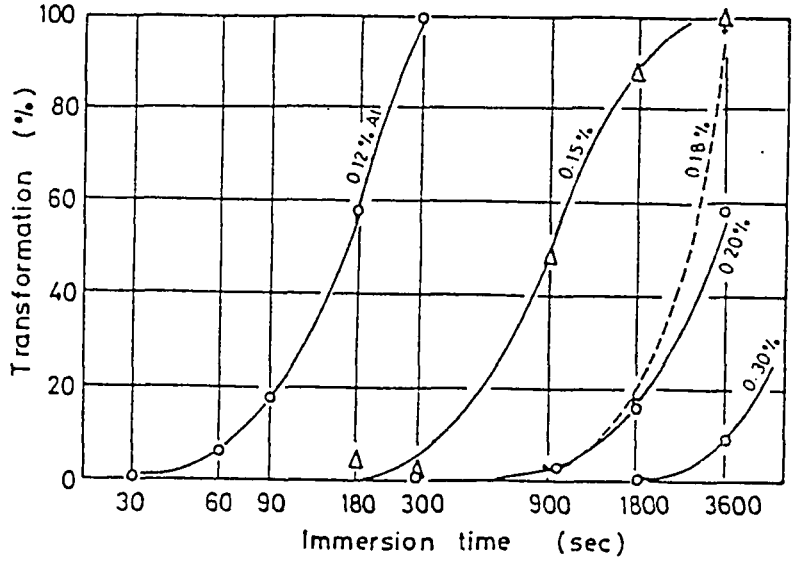

Figure 13. Reaction curves for the transformation from Fe_2Al_5 to delta phase at various Al compositions in the Zn bath [27].

aluminum concentration caused it to coincide with a set of data generated for another aluminum concentration, indicating that the reaction was isokinetic, or followed the same reaction rate behavior, over a range of aluminum concentrations. Yamaguchi [27] investigated whether or not the transformation Fe_2Al_5 to delta and liquid was isokinetic by rearranging the isothermal transformation equation (i.e. $y = 1-\exp(-kt^n)$) to the equation:

$$\log[\log(1/(1-y))] = n * \log t + \log k - \log 2.3.$$

By plotting the following equation:

$$\ln[1/(1 - y)]$$

versus immersion time on a log-log scale, as shown in Figure 14, n for the reaction was determined. The value of n, 0.26, did not vary within the bath aluminum concentration range of 0.12 to 0.30 weight percent aluminum, and supported the belief that the growth of the delta phase outbursts was isokinetic.

For the empirical growth equation:

$$Y = kt^n$$

if n = 0.5 growth follows a parabolic time law. An n < 1 value would indicate a growth rate decreasing with time, while an n > 1 value would indicate a growth rate increasing with time. Therefore n can be used as a basis for comparison among the different alloy phases for the rate at which their growth proceeds. Hortsmann [16] determined n for the total iron-zinc alloy layer, formed from an aluminum free bath, to be 0.5-0.56. He also calculated experimental values of n for the intermediate alloy phases as follows; gamma 0.099-0.5, $delta_1$ 0.5-0.68, and zeta 0.156-0.5. The values indicate that when growth is compared to a parabolic time law, the growth of the entire alloy layer and the $delta_1$ phase will decrease slowly over time, while the growth of the gamma and zeta phase layers will decrease much more rapidly with time. Blickwede [28] found n values for gamma, delta and zeta to be 0.10, 0.60, and 0.16 respectively, for phase layer growth in pure Zn coatings. Figure 15 shows layer thickness measured as a function of the square root of the time of immersion [29]. Straight lines on this plot support the belief that parabolic growth is the rate determining growth mechanism for the long immersion time galvanizing or galvannealing process. The plotted lines in Figure 15 have a break in their slopes after certain time periods, indicating that the growth rates of the phases change during the course of the reaction. The zeta and gamma phases grow rapidly at first, with $delta_1$ phase growth occurring more slowly. Later in the reaction, however, $delta_1$ phase growth becomes rapid. Because the growth rates of the individual phase layers is changing over time, the reported growth rate time constant vales (n values) should be qualified by the reaction time over which they were fitted.

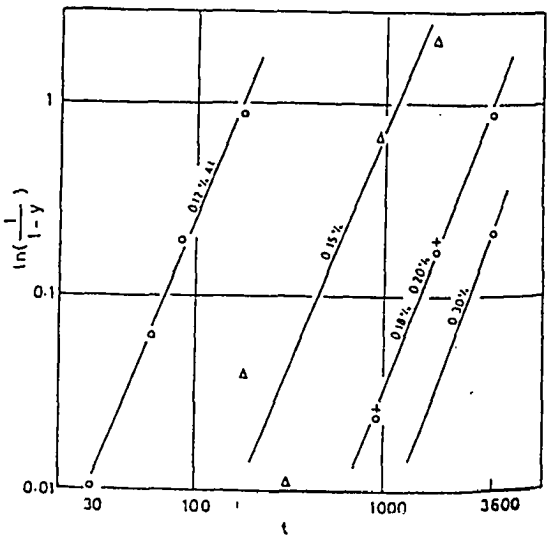

Figure 14. ln (1/(1-y)) curves on log-log scale indicates the consistency of the Johnson-Mehl equation and isokinetic transformation [27].

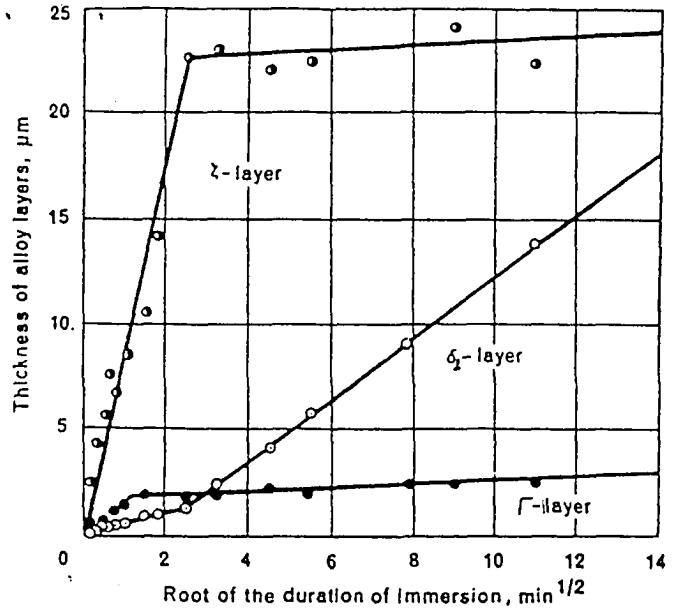

Figure 15. Growth of alloy phase layer at 450°C [29].

D. Diffusion

1. Ternary Fe-Zn-Al Phase Equilibria and Diffusion Paths at 450°C

Ghuman and Goldstein [9] performed hot-dip galvanizing experiments of iron in Al containing baths and found the Fe-Al and Fe-Zn reactions to occur in a sequence of four stages. In stage one, upon immersion of the sample into the zinc bath, a primary Fe-Zn-Al compound was formed which inhibited Fe-Zn reactions. This compound is a primary inhibiting phase represented as point 1 in Fig 16a, a schematic representation of the equilibrium Fe-Zn-Al ternary isotherm at 450°C. At longer immersion times, a secondary inhibiting phase formed from the initial compound, as the primary inhibition phase layer became enriched in iron and aluminum, point 2 in Figure 16b. The observed inhibition period ended with the transformation of the secondary inhibiting phase to the Fe_2Al_5 (Zn) phase. Zinc atoms were able to diffuse through the Fe_2Al_5 (Zn) phase and react with iron to form Fe-Zn phases at the steel/coating interface, Figure 16c. At extended immersion times the Fe_2Al_5 (Zn) phase became enriched with aluminum as shown in Figure 16d, and Fe-Zn phase growth continued, thus both the Fe-Al and Fe-Zn compounds were found to coexist at the steel/coating interface.

To study further the diffusion path through the equilibrium Fe-Zn-Al ternary diagram at 450°C, Osinski prepared liquid Zn -solid Fe-Al diffusion couples by hot-dip galvanizing a number of Fe-Al intermetallic compounds in a zinc bath saturated with iron (0.0 wt% Al)

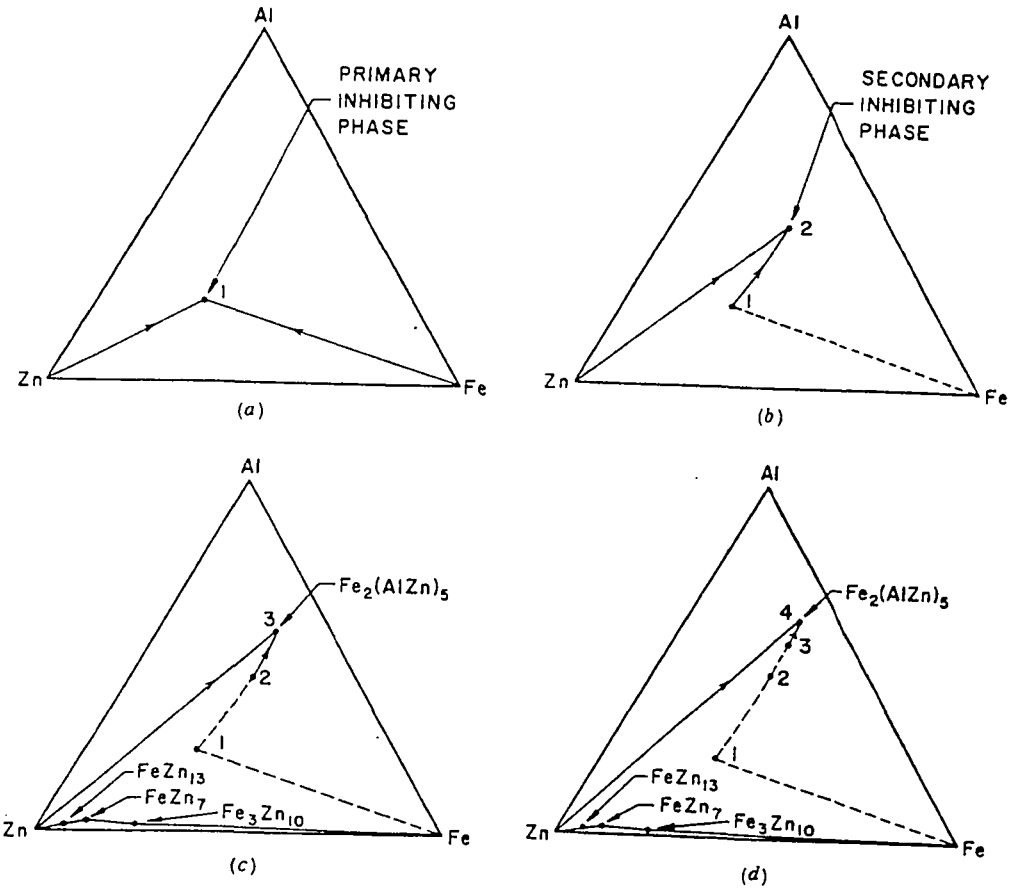

Figure 16. Schematic representations of kinetic changes in composition; reaction paths followed when solid iron is dipped in 0.2 to 3.0 wt% Al-Zn bath. Compositions are in atomic percent. (a) path followed in the initial stage of hot-dipping (b) at slightly longer dipping times phase 1 transforms to phase 2 (c) breakdown of inhibition as phase 2 transforms to $Fe_2Al\ (Zn)_5$, Fe-Zn phases begin to grow (d) for long immersion times $Fe_2Al(Zn)_5$ becomes richer in Al, reaches point 4, Fe-Zn growth continues [9].

for a number of immersion times [8]. The alloys used as the terminal Fe-Al intermetallic compounds were: (1) 10 at% Al - Fe (Fe_9Al), (2) 22.8 at% Al - Fe (Fe_3Al), and (3) 47.6 at% - Fe (FeAl). Osinski characterized the composition of the layers formed in the couples immersed for many hours, and the diffusion paths determined from these experiments are shown in Figures 17, 18, and 19.

On the equilibrium Fe-Zn-Al 450°C isotherm shown in Figure 20, straight lines a, b, c correspond to the Fe_9Al-, Fe_3Al-, and FeAl- and Zn (Fe) diffusion couples, and connect the terminal compositions of the end members of these diffusion couples. The diffusion couples Fe_9Al-, Fe_3Al- and Zn (Fe) formed Fe-Zn phases only, as shown in Figures 17 and 18. However, line c, the mass balance line for the FeAl-Zn(Fe) couple, however, does not cross an Fe-Zn phase region, indicating that during the reaction between FeAl and Zn (Fe) an aluminum rich alloy containing more aluminum than the terminal FeAl compound must develop. In Figure 19 a schematic representation of the diffusion path for the FeAl-Zn (Fe) couple predicts the formation of the Fe_2Al_5 phase, according to mass balance arguments. It also follows from line c that in addition to the formation of an Al-rich compound, Fe-Zn compounds will also eventually develop, and this was observed to occur in the FeAl-Zn (Fe) diffusion couple. In principle the diffusion path cannot be predicted by mass balance arguments alone, therefore in order to predict the layer configuration in the FeAl-Zn (Fe) couple more diffusion and/or thermodynamic data are needed. It must be noted that Osinski analyzed these alloys dipped in a bath containing no aluminum,

therefore aluminum in the above mentioned experiments would have only been supplied from the solid terminal alloy.

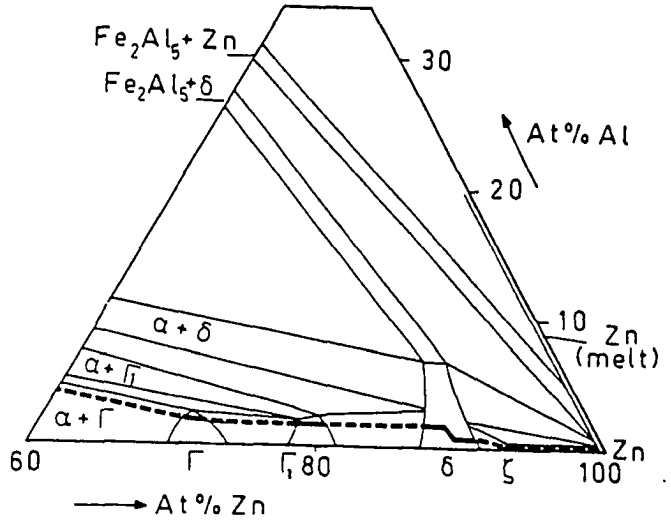

Figure 17. Diffusion path of an Fe_9Al-Zn(Fe) diffusion couple (19 hours, 450°C) on the zinc corner of the 450°C isotherm of the Fe-Zn-Al system [8].

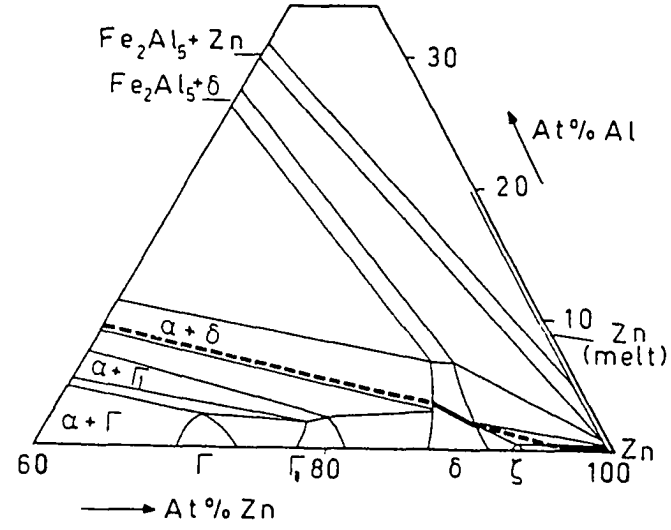

Figure 18. Diffusion path of an Fe_3Al-Zn diffusion couple (21 hours, 450°C) on the zinc corner of the 450°C isothermal section of the Fe-Zn-Al system [8].

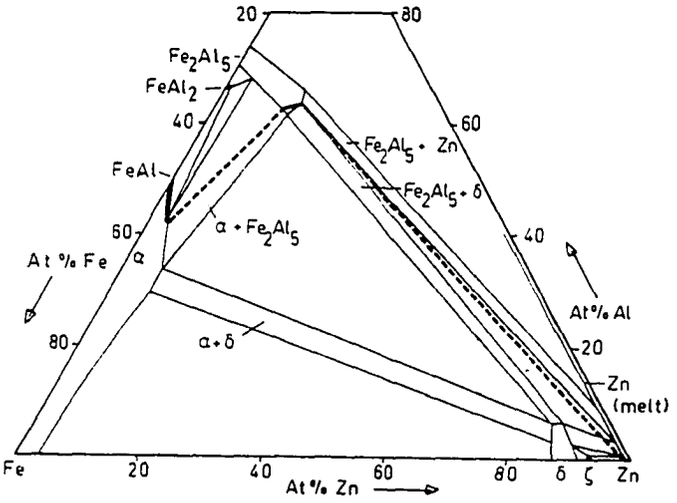

Figure 19. Schematic course of the diffusion path of an FeAl-Zn(Fe) diffusion couple, dipped for 74 hours, on the 450°C isotherm of the Fe-Zn-Al system [8].

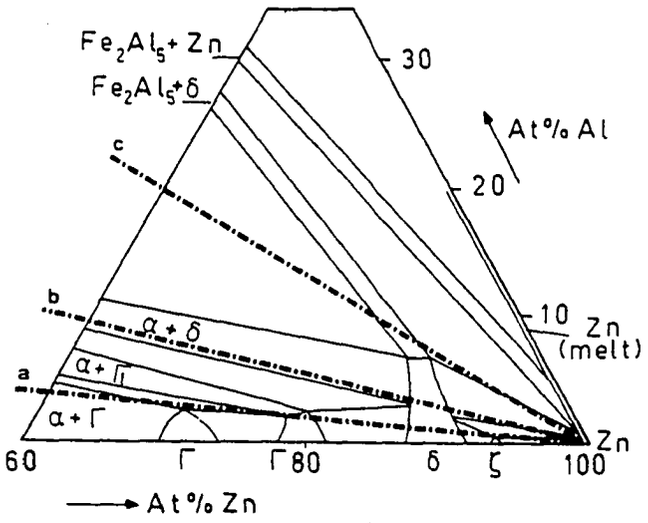

Figure 20. Zinc corner of the 450°C isotherm of the Fe-Zn-Al system. Lines a , b, c are the straight lines (mass balance lines) joining the terminal compositions of Fe_9Al-, Fe_3Al-, and FeAl-Zn(Fe) diffusion couples respectively [8].

If the reaction starts with iron being dipped into a molten bath of zinc containing 1.2 at% (1.4 wt%) aluminum, then according to the phase diagram the formation of several compounds is possible. Because the phase Fe_2Al_5 is the most thermodynamically stable, it will form first. The aluminum necessary for this formation is supplied by the bath, and near the iron substrate the bath will become depleted in aluminum.

Starting at point A in Figure 21 the diffusion path will drop to a lower aluminum concentration, and bend into the Fe_2Al_5 + Zn two phase region. If the aluminum could be continuously supplied then this path would be a stable one, and it would obey the mass balance rule, and only cross line a once. However, in time, the aluminum supply becomes retarded, and a depletion of aluminum in the melt occurs near the iron dipped specimens. Hence the bath will move to lower aluminum concentrations. When point A reaches A' in Figure 21 the formation of Fe-Zn phases cannot be delayed any longer. The time for the bath to change from chemistry A to A' is the incubation period for Fe-Zn phase formation. In comparing the above described reaction with the diffusion couples studied, it was found that the Fe_2Al_5 layer formed during the Fe-Zn (Al) reaction, also formed in the Fe_9Al and Fe_3Al diffusion couples. For the Fe-Zn (Al) reaction, the necessary aluminum flux to the surface is possible due to the high mobility of aluminum atoms in the melt. In the reaction between FeAl and Zn (Fe), however, Fe_2Al_5 enrichment occurs from a retarded aluminum enrichment of the substrate [8].

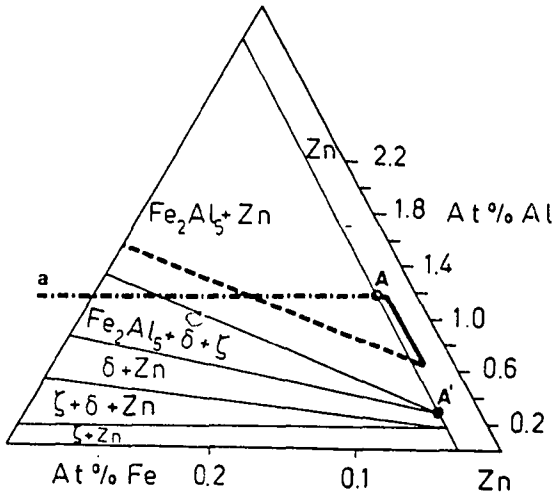

Figure 21. Zinc corner of the 450°C isotherm of the Fe-Zn-Al system (12) with schematic diffusion path and mass balance line (a) of a hypothetical diffusion couple Fe-Zn (1.2 at% Al), 450°C (note: Fe and Al axes are not drawn to the same scale) [8].

Kirkaldy et al [12] hot-dip galvanized specimens of FeAl, $FeAl_2$, $FeAl_3$ and Fe_2Al_5 into iron saturated zinc baths containing 0.0%, and 1.7 wt% Al. The results indicated that at 450°C Zn attack on the Fe_2Al_5 phase was much faster than that for the $FeAl_3$ phase. After annealing the couples for 800 hours at 450°C, the Fe_2Al_5, $FeAl_3$, and FeAl compounds were found to equilibrate with zinc by dissolving 14, 7, and 12 wt% zinc, respectively. The observed rapid attack of the $FeAl_2$ phase suggested the stability range of this phase is limited to very low zinc values.

The principal tie lines of the two phase regions, as well as the three phase equilibria between Fe_2Al_5, Fe-Zn delta phase and Zn, and between Fe_2Al_5, delta, and alpha FeAl (Zn) were determined quantitatively (represented in at% in Figure 2a). The results are in disagreement with the existence of a ternary Fe-Zn-Al compound as suggested by Ghuman and Goldstein [9], who most likely had actually analyzed Fe_2Al_5 which contained substantial amounts of zinc, and the solubility of Zn in Fe_2Al_5 to that extent is not represented on the equilibrium Fe-Zn-Al isotherm at 450°C.

The corner of the three phase triangle zeta-delta-Zn was determined to be at 0.07 wt% Al, and that for the three phase triangle Fe_2Al_5 (Zn)-delta-Zn, at 0.11 wt% Al. The upper limiting tie line of the two phase region Fe_2Al_5-Zn was not defined, but the couple Fe_2Al_5-Zn (1.7 wt% Al) showed equilibrium conditions that indicated that this aluminum value is a lower limit for the tie lines of this two phase field. The limiting tie line for the two phase field in contact with $FeAl_3$ can be estimated to be that predicted from the Zn-Al binary diagram as 16 wt% Al.

2. Iron-Zinc Diffusion

A variety of diffusion mechanisms may occur during hot-dip galvanizing and galvannealing. One investigation studied galvanized coatings that were annealed and analyzed for the possibility of diffusion induced grain boundary migration, DIGM, of zinc diffusion into alpha iron or ferrite [30]. It was determined that the penetration of zinc in

ferrite for the hot-dip galvanized coatings was negligible (less than one micron) at some points, while it reached up to ten microns at other locations on the same surface. In the galvanized condition penetration also varied with the side of the sheet analyzed. If volume diffusion had occurred little penetration of zinc into the ferrite would have occurred, and the zinc concentration in the steel itself would be uniform at a given depth.

After annealing the galvanized samples for long times the zinc concentration in ferrite was nonuniform and suggested that DIGM took place instead of volume diffusion [30]. Discontinuities in zinc concentration were observed to occur across grain boundaries, such that two adjacent ferrite grains, for example, contained zero and nine weight percent zinc respectively, indicating the presence of DIGM. The depth of penetration of zinc was two orders of magnitude greater than that expected for volume diffusion and effective zinc diffusivity was four orders of magnitude greater than that expected for volume diffusion. The zinc diffusivity value varied with temperature and the concentration of zinc, as is shown in Table IV [30]. Zinc penetration was found to take place in an initial surge with a maximum penetration reached after annealing at 400°C for 48 hours. It is assumed that ferrite gains additional zinc because the Fe-Zn gamma phase which forms after some incubation time in galvanized and galvannealed coatings was not present as a uniform layer at the beginning of annealing. DIGM stopped after the gamma phase grew to a uniform layer. Grain boundary motion lead to a doubling of zinc penetration depth in 48 hours. Beyond that time no further penetration was observed. It is unclear from the results why after a given reaction time DIGM was not time dependent.

Table IV. Observed Penetration Depths (μm) and Calculated Diffusivity of Zinc in Alpha Iron [30].

	t (Hours)			
	0	12	48	192
450 °C				
obs.	1 to 3	7	40	45, 50 45
$2(Dt)^{0.5}$	0.00006	0.004		0.017
550 °C				
obs.	1 to 3	10, 170 20, 15 22, 22 21	45, 35	45, 50 55
$2(Dt)^{0.5}$	0.00006	0.22		0.87

Diffusion data extrapolated from those in Reference 13.
D (8 pct Zn) = 2.8×10^{-15} cm²/s at 550 °C. D (4 pct Zn) = 1.1×10^{-16} cm²/s at 450 °C.

Another theory proposed on the diffusion mechanism between iron and zinc is that a pronounced Kirkendall effect occurs at the start of annealing with iron atoms diffusing into zinc and zinc atoms diffusing into iron. Shortly thereafter, the diffusion becomes "one-sided", and zinc atoms diffuse by a vacancy mechanism [31]. In the equation, $Y = Kt^n$ where Y is the width of the alloy phase, t the time of the reaction, and K a growth constant, the value of n determines how rapidly the phase grows with time. If the rate of growth of the alloy phase is controlled by diffusion, n = 0.5, and a parabolic growth law is followed. The values of n for all of the Fe-Zn phases did not adhere to this value, therefore volume diffusion is not the rate determining process for all iron-zinc alloy phase growth [16]. A parabolic law did not hold if a later formed phase in the growing intermetallic layer had a higher diffusivity of zinc than the previous layer formed. The newly formed phase with the higher diffusivity consumed the initial phase, causing its width to decrease with time, thus deviating its growth from parabolic law. Essentially,

phase boundary movement occurs over time, and this movement can be different from one iron-zinc phase to another as is shown in Figure 22 [16].

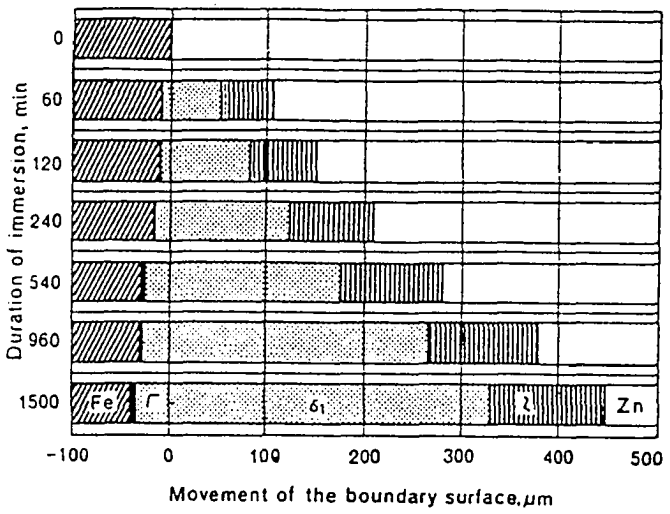

Figure 22. Displacement of phase boundaries during the reaction between Fe and Zn [16].

The gamma/iron and delta/gamma boundaries move toward the substrate iron while the delta/zeta and the zeta/eta boundaries move in a direction toward the surface of the coating as shown in Figure 22. The delta phase layer moves in two opposite directions. Therefore while a new gamma phase layer forms at the steel/coating interface, on the other side of the gamma phase layer the delta phase consumes the gamma phase. Similarly, zeta forms at the zeta/eta phase boundary while the delta phase consumes the zeta phase at the delta/zeta phase interface [16].

In an iron-zinc diffusion couple that was annealed, zeta formed first followed by delta and then gamma phase. Molybdenum powder markers were used to observe the Kirkendall effect. The markers remained between the zeta phase and the free zinc eta phase during annealing, supporting the mechanism that one-sided diffusion of zinc occurs. Generally in a diffusion couple, the element with the lower melting point will have the greater diffusion coefficient (though this is not always the case) and for the iron-zinc system this is true. The melting point for zinc is 419.58°C, and for iron it is 1538°C [32], therefore the higher diffusivity of zinc in iron-zinc phases is not unusual, and it can be assumed that the diffusion of zinc predominates over that of iron. In a multiphase binary system the thickness of each alloy layer is a function of the weighted differences of the interdiffusion coefficients of not only the phase in question, but also of the interdiffusion coefficients of the adjacent phase layers. Diffusion relationships in multicomponent metallic systems that involve the motion of planar phase interfaces are complex and encompass many variables [33].

E. Factors Affecting Alloy Layer Formation

1. Surface Characteristics

a. Surface Oxides

In a continuous galvanizing line, the sheet steel is annealed in a reducing N_2/H_2 atmosphere before it is immersed in the molten zinc bath. The pre-annealing treatment serves to clean the steel surface of oxides just prior to hot-dipping. The pre-annealing stage of the process is also used to recrystallize the cold rolled structure of the sheet steel. Some researchers [34 - 39] have found that selective surface oxidation of manganese, silicon, aluminum, vanadium, chromium, and titanium occurs under temperature and dew point pre-annealing conditions that are used in commercial galvanizing lines. Most authors agree that the oxide formation is concentrated at grain boundaries [40]. The formation of surface oxides may affect zinc wetting of the substrate by posing as a nonuniform barrier. Substrate steel chemistry has been found to cause different surface chemistries to develop during continuous annealing steel sheet prior to hot-dip galvanizing. Analysis by secondary ion mass spectroscopy (SIMS) found [41] that a Ti IF steel surface contained more Al_2O_3 than an ULC steel annealed under the same conditions in a 5% H_2-N_2 reducing environment (dew point -28°C). Surface oxides may also play a role in both the development of the galvanized coating layer, and in the subsequent

diffusional growth of iron-zinc phases during galvannealing. The role of surface oxides on coating formation has not yet been studied in detail.

b. Surface Microstructure

The effect of substrate microstructure on the growth of as galvanized iron-zinc coating morphology was examined in a study by Nishimoto et al [26]. The morphology of Fe-Zn compounds that form at the steel interface during continuous galvanizing were classified into three types, outburst structure (Type-l), fine granular structure (Type-2), and pillar-like structure (Type-3). Good correspondence was found between the Fe-Zn coating and underlying steel sheet surface microstructure. By comparing substrate grain structure to coating microstructure it was determined that the outburst structure (Type-1) formed at substrate grain boundaries, and the fine granular Fe-Zn structure (Type-2) was found at locations within the substrate grain interior.

Microstructures of Type-2 and Type-l are shown with accompanying Mossbauer spectroscopy in Figure 23 [26]. According to Graham et al [42] a singlet in the Mossbauer spectroscopy represents the zeta phase and an asymmetric doublet indicates the presence of the delta phase. Therefore Figure 23a shows a fine granular structure that consists of mostly delta phase, while the pillar-like structure on the surface of the outburst structure in Figure 23b is almost entirely zeta phase. A separate microstructure and Mossbauer spectroscopy for pillar-like structure, Type-3, was difficult to distinguish from

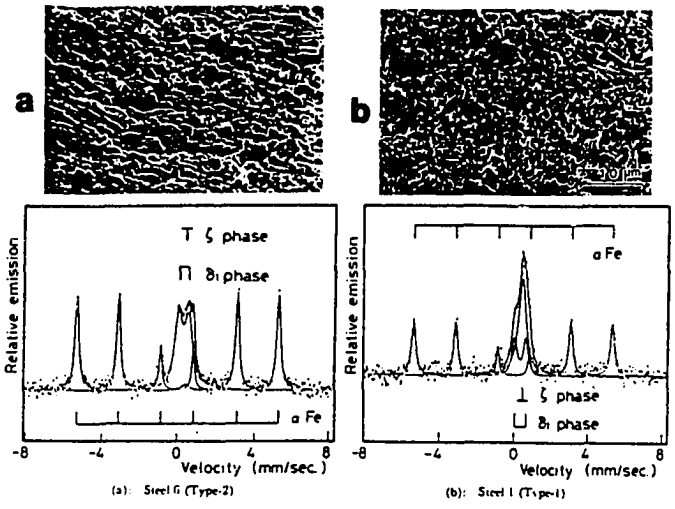

Figure 23. Micrographs of Fe-Zn microstructures (a) Type-2 structure and accompanying Mossbauer spectrum (b) Type-1 structure and accompanying Mossbauer spectrum [26].

the Type-1 outburst structure so it was not analyzed as a separate entity. From the above-mentioned study it was concluded that iron-zinc morphology Types 1 and 3 consist mainly of zeta phase and Type-2 is mostly composed of delta phase.

Substrate grain size is thought to also play a role in Fe-Zn reaction rates. Recent investigators [43, 44] have shown that as the grain size of a Ti stabilized interstitial free (IF) steel decreases Fe-Zn reaction rates increase during post dip annealing. The same grain size effect was observed for Zn (0 wt% Al) coatings electrodeposited onto a Ti stabilized IF steel which was subsequently annealed [45]. Guttmann [44] proposes that the Fe_2Al_5 layer that forms upon the substrate during galvanizing forms epitaxially so that Fe_2Al_5 crystals form colonies of the same orientation as the underlying substrate steel

grain. The colonies form low angle boundaries when contained within an underlying substrate grain interior, and Fe and Zn diffusion follow volume diffusion rates at the low angle boundaries. At the substrate grain boundary, however, two adjacent Fe_2Al_5 colonies of different orientations form a random high angle boundary. This high angle boundary is a short circuit diffusion path for Zn and Fe interdiffusion. The short circuit diffusion paths give rise to Fe-Zn outburst formation at substrate grain boundary locations. Therefore the steel substrate grain boundary is indirectly related to outburst formation, because the steel grain boundary fixes the location of short circuit diffusion paths in the Fe_2Al_5 layer [44].

2. Zinc Bath and Substrate Steel Chemistry

a. Zinc Bath Aluminum Additions

Aluminum has commonly been used in commercial hot-dip zinc galvanizing baths because of its ability to improve the luster of the coating and to reduce atmospheric oxidation of the bath [9]. Aluminum also enhances the formability characteristics of the galvanneal coating by forming iron-aluminum alloy layers that inhibit the growth of the inherently brittle intermetallic Fe-Zn phases such as the gamma and $gamma_1$ phases which form at the steel/coating interface. At aluminum additions of 0.1 - 0.3 weight percent and bath temperatures of 450°C, the inhibiting action of the transient iron-aluminum phases aid in the production of a ductile alloyed Fe-Zn coating.

Smith and Batz [46] found that aluminum levels above 0.15 weight percent in the zinc bath retarded the formation of a fully alloyed iron-zinc coating. The increased effectiveness of the Fe-Al barrier at the interface was found to be directly related to the aluminum content in the bath. For better formability of the coating, it was suggested that the growth of the iron-zinc phases during annealing outside of the galvanizing bath should be halted as soon as the eta or free zinc phase (formed adjacent to the Fe-Zn phases at the surface of the coating) has been consumed by the growing Fe-Zn alloy layer, referred to as marginal Fe-Zn alloying [46]. At bath aluminum contents between 0.15 and 0.16 weight percent, an anomaly was observed for the time needed to reach marginal alloying. At higher aluminum contents greater than 0.16 wt% suppression of the delta phase occurred and the time necessary for marginal alloying increased at certain reaction temperatures. The change in the kinetics of the Fe-Zn reaction was believed to be related to the change in the growth rate of the delta phase, as is indicated by anomalies occurring in Figure 24 at a bath temperature of 540°C and for bath aluminum contents of 0.16 and 0.17 weight percent [46]. It is well known that aluminum additions to the zinc bath inhibit iron-zinc alloy layer growth, but it is not yet specifically understood how the kinetics are affected.

Tang [11] has shown that full inhibition does not occur until the bath Al content is equal to 0.15 wt% (at 450°C). Below 0.14 wt% Al, Fe-Zn zeta and delta phases are in equilibrium with the melt while above 0.14 wt% Al, Fe_2Al_5 is in equilibrium with the melt which results in inhibition of the Fe-Zn reactions for a sustained period of time.

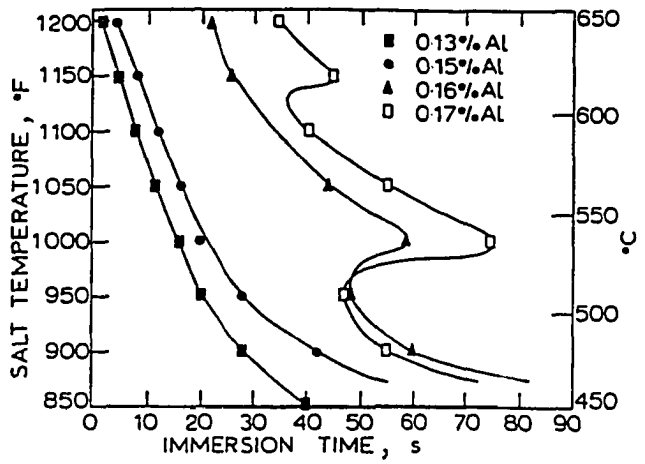

Figure 24. Effect of Zn bath Al content on the time required for marginal alloying (coating thickness 22.9-25.4 μm/side) [46].

As the temperature of the steel at the point of entry into the molten bath is increased, the thickness of the Fe-Zn alloy layer formed in the as-galvanized condition increases [16]. Higher aluminum contents in the bath counteract this steel temperature effect and reduce the thickness of the as-galvanized iron-zinc alloy layer. One explanation for this anomaly could be the role of the initial Fe-Al and ternary Fe-Al-Zn compounds on the steel surface that inhibit Fe-Zn layer growth. It is believed that if the steel enters the bath at a temperature higher than that of the bath itself, a more effective inhibition layer forms. For IF and low carbon steels as sheet entry temperature into the Al containing Zn bath increases the amount of Fe-Al-Zn compound was also found to increase [47, 48]. The amount of Fe-Al-Zn compound formed was also found to be a strong function of bath Al content as well [47].

b. Substrate Steel Chemistry

(i). Interstitial Free Steels

Interstitial free steels are steels that contain low levels of the interstitial elements, carbon and nitrogen. Titanium, niobium, and aluminum are added to these steels as stabilizers to form stable compounds with carbon and nitrogen that remain present in an interstitial solid solution. Nitrogen levels are low in IF steels and are effectively removed from solid solution by AlN and TiN formation, thus most attention is focused at carbon removal for enhanced formability. Typical alloy composition ranges for IF steels are shown in Table V [49]. Although carbon levels are extremely low, residual carbon can give rise to an undesirable sheet texture for forming operations. Because of the low solubility of carbon in bcc alpha-iron (Figure 25), residual carbon can cause strain or quench aging in annealed structures.

Table V. Composition (wt%) of IF Deep Drawing Quality Steels [49].

C	Si	Mn	P	Al	N	Nb	Ti	S
0.002- 0.008	0.01- 0.03	0.10- 0.34	0.01- 0.02	0.03- 0.07	0.001- 0.005	0.005- 0.040	0.01- 0.11	0.004 0.01

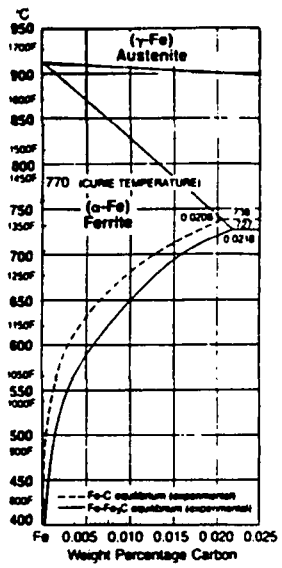

Figure 25. Fe-rich side of the Fe-C equilibrium diagram, showing extent of ferrite phase field and decrease of carbon solubility with decreasing temperature [49].

The stabilizing additions also promote a cube-on-corner recrystallization texture ((111}/<110>) that is favorable for severe forming operations, such as deep drawing [49]. The {111}/<110> texture results in a high normal anisotropic plastic strain ratio, r_m. Microstructures with high r values resist thinning, which can lead to fracture of sheet subjected to severe forming deformation. The resulting steel microstructure consists of ferrite with a fine precipitate dispersion.

Stabilizers in IF steels remove interstitial solid solution elements to improve formability at the cost of strength. This lack of strength can cause the sheet used in automotive body applications to be sensitive to denting. One method to improve strength in IF steels is through the addition of phosphorus as a solid solution strengthener. One drawback of

alloying with phosphorous is that cold work embrittlement can occur if too much phosphorous is added to the steel. Phosphorous segregates to ferrite grain boundaries during and after annealing of the cold rolled sheet, especially in the presence of a carbide former [40]. Boron can be added with phosphorous to avoid embrittlement because boron will segregate at grain boundaries and prevent phosphorous segregation. When boron was not added to a phosphorous containing IF steel, the phosphorous content at grain boundaries was found to be ten times that of the bulk phosphorous content of the steel [50]. The decrease in phosphorous enrichment at grain boundaries due to the addition of boron is dependent upon the composition of the IF steel. Ti-Nb IF steels show the greatest reduction in embrittlement upon the addition of boron [50].

(ii) carbon

The effect of carbon content in the sheet steel on galvannealing has been examined in past studies. In one particular experiment, bath composition was maintained at 0.16 weight percent aluminum while the substrate carbon content was varied [26]. The hot-dip galvanized low carbon steel microstructure consisted of a fine granular structure, while an ultra low carbon steel formed a combination microstructure of outburst structure and fine granular structure. The surface coating microstructure results [26] indicate that as the carbon content in the base steel is increased, the formation of outburst iron-zinc structures decreases [26]. After heat treating and upon subsequent cooling, carbon segregates to the grain boundaries in the substrate steel and reduces the thermodynamic activity at the grain

boundaries. The reduction in activity at the grain boundary leads to a more thermodynamically stable Fe_2Al_5 structure which inhibits the formation of the outburst structure. The effect of carbon on the finished galvannealed coating product with respect to alloying period and hardness was also investigated. For galvanized specimens reheated in an infrared furnace at 450°C, the hardness of the coating increased with a longer alloying period. The relationship between hardness and alloying period is shown in Figure 26 [26]. Also evident from this figure is that as the carbon content in the steel decreases (from line a to d in Figure 26) , the rate of hardening of the coating increases. Most likely low carbon compositions in the steel allow for the faster development of the brittle intermetallic iron-zinc phases, thus resulting in the observed increased rate of hardening of the alloyed Fe-Zn coating. Therefore during galvannealing carbon acts as an inhibitor for the formation of Fe-Zn phases due to its segregation to the substrate steel grain boundaries.

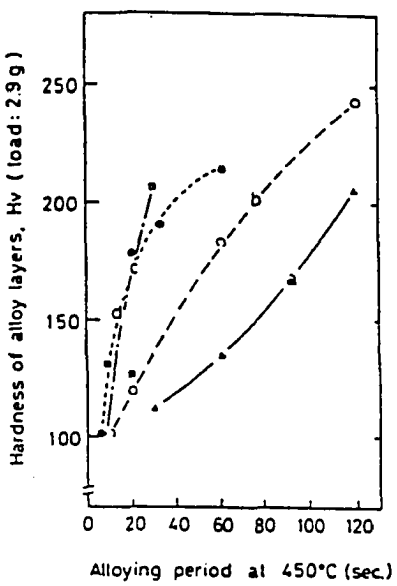

Figure 26. Relationship between alloying period and average hardness of alloy layers, with carbon content decreasing from plot a to plot d [26].

(iii) titanium

In low carbon steels (100 ppm) containing titanium, carbon forms titanium carbides and the inhibition effect of substrate steel carbon on Fe-Zn reactions discussed above is reduced. The decline in the inhibition effect of substrate steel carbon is due to carbide formation, thus solute carbon, not total carbon content, inhibits outburst structure formation for Fe-Zn reactions occurring in zinc baths containing aluminum. Titanium stabilized low and ultra low carbon steels would therefore be expected to have more outburst structures associated with their coating morphology.

Steels with additions of titanium are known to have good drawability characteristics but little is known about the rate of Fe-Zn reactions during hot-dip galvanizing and galvannealing of the substrate. In a study by Fukuzuka [51], titanium (0.11 and 0.20 wt%) and titanium-chromium (Ti 0.20, Cr 0.36 wt%) steel sheets were galvanized and tested in conjunction with a low carbon steel. The coating of the hot-dip galvanized low carbon steel tended to have aluminum concentrated at the interface between the coating layer and the substrate. The titanium and titanium-chromium added sheet did not exhibit this aluminum concentration behavior. Titanium was not found in the zeta or delta phases formed on titanium and titanium-chromium steels, however, slight amounts of chromium were found in both phases of the coated titanium chromium added sheet. During annealing, considerable growth of the iron-zinc alloy phases was observed on the titanium and titanium-chromium containing steels as compared to the low carbon steel and this is

shown in Figure 27 [51]. The rapid growth of the iron-zinc phases is most likely due to the absence of, or only a thin film of, an iron-aluminum inhibition layer. The suppression effect of the iron-aluminum layer on titanium and titanium-chromium containing steels was not as effective a barrier to iron-zinc phase growth as it was on the low carbon steel substrate.

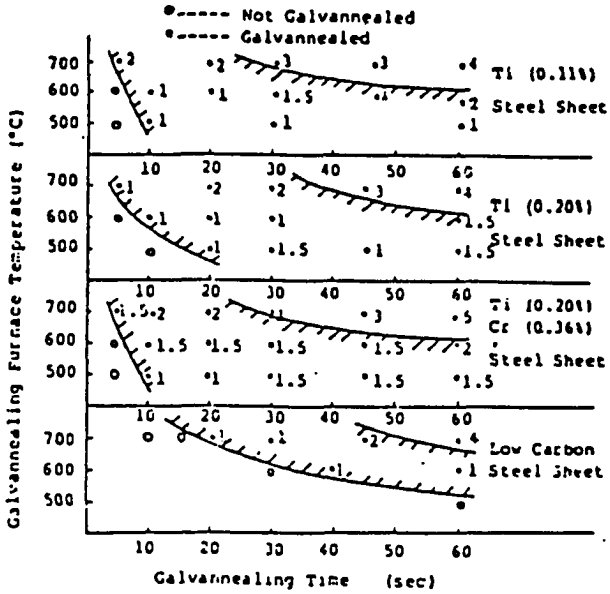

Figure 27. Galvannealing behavior of Ti, Ti-Cr and low carbon steel sheets [51].

To understand more clearly the effect substrate steel Ti may have on Fe-Zn reactions an excess Ti (Ti*) equation was developed [43] and is shown below:

$$Ti^* = \text{total Ti} - 3.99C - 1.49S - 3.42N.$$

C, S, and N represent carbon, sulphur, and nitrogen content of the steel in wt% respectively. The excess Ti equation accounts for Ti that forms precipitates of TiC, TiS, and TiN. The excess Ti is that which is left over after precipitate formation. Toki found that for a positive excess Ti value and a low coating bath Al content (0.11 wt%) Fe-Zn reaction rates were accelerated most likely because TiC formation lead to clean grain boundaries (no segregation of carbon) which provided fast diffusion paths for Fe and Zn diffusion. For coatings containing 0.2 wt% Al, no significant effect of excess Ti was observed on Fe-Zn reaction rates [43]. However, when Zn(Al) coated Ti IF steels were compared to low carbon steels [47, 52] Fe concentration gradient development was found to be slower for the low carbon steel, which indicates that excess substrate Ti may be related to increased reactivity in the substrate. Faderl [47] found more iron in the coating for the Ti IF steel as compared to the low carbon steel even though both had approximately the same Al concentration in the inhibition layer. Zn (0 wt% Al) electrodeposited onto Ti IF and TiNb IF steels showed that upon annealing the total Fe content in the coating increased with excess Ti in the tested substrate steel, indicating excess Ti may increase Fe-Zn reaction rates [45]. Guttmann, however, studied two levels of excess Ti in a Ti IF steel and determined there was no significant effect of excess Ti on Fe-Zn reaction rates [53].

(iv) phosphorus

According to Abe et al [54] the phosphorus content in the steel substrate behaves much like aluminum in the zinc bath in that it retards the growth rate of the iron-zinc alloy phases. By measuring the iron content of the iron-zinc alloy phases, Abe determined the extent of alloying. He found that as phosphorus levels in the base steel increased the iron content in the coating decreased, leading to the conclusion that increased phosphorus levels inhibit Fe-Zn alloy growth. The relationship between phosphorus and iron content in a galvanneal coating is shown in Figure 28 [54]. The same retarding effect was also observed for phosphorus-silicon containing sheet steels. It is thought that phosphorus and phosphorus-silicon added steels form Fe-Al and Fe-Zn-Al compounds that have greater stability at substrate grain boundaries. Phosphorus inhibits formation of the Fe-Zn outburst structure by behaving much like carbon. It migrates to grain boundaries especially in the presence of carbide formers such as titanium or niobium. Allegra [55] also found phosphorus to segregate to ferrite grain boundaries in low carbon steels (0.02-0.06 wt% C) containing at least 0.04 wt% P when heated for approximately 100 hours at 482°C. The migration of phosphorus to the ferrite grain boundary blocks the diffusion of Zn along the grain boundary and lowers the thermodynamic activity at the boundaries. Therefore phosphorus in the base steel acts as an inhibitor to Fe-Zn alloy growth primarily due to grain boundary segregation of phosphorus [27, 55].

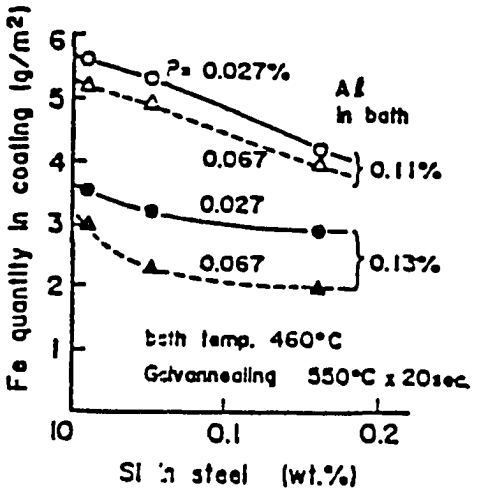

Figure 28. Iron content in the coating decreases with increased levels of phosphorous in the base steel [54].

Phosphorus additions to IF steels and their influence on galvanizing and galvannealing reaction kinetics have been studied [38,39,43,47-50]. Toki [43] modified the excess Ti (Ti*) equation to account for FeTiP precipitates that form in P containing IF steels. The modified excess Ti (Ti**) equation is shown below:

$$Ti^{**} = \text{total Ti} - 3.99C - 1.49S - 3.42N - 1.55P.$$

C, S, N, and P represent carbon, sulphur, nitrogen, and phosphorus amounts in the steel in wt% . Toki (43) found that for P contents equal to or greater than 0.05 wt%, and when Ti** was negative in value, FeTiP precipitates were located within the ferrite grain interior as well as along ferrite grain boundaries. The FeTiP precipitates act as a physical barrier

to Fe and Zn interdiffusion, thus reducing Fe-Zn phase growth rates. As the phosphorus content of the steel increased Fe-Zn phase growth was found to be retarded [43]. Because FeTiP formation also consumes Ti, Toki proposes that more solute carbon remains in solid solution and most likely segregates to substrate steel grain boundaries further inhibiting Fe-Zn reactions. Therefore for Ti IF steels containing phosphorus, substrate steel grain size does not have a strong influence on Fe-Zn reactions. Lin et al (56) found that P containing IF steel inhibited delta formation during galvanizing when compared to a non P containing IF steel. Lin et al [56] propose that P segregates to the steel surface during recrystallization annealing and galvanizing and this results in stabilizing the inhibition layer and retarding Fe-Zn growth reactions.

Mercer [52] found rephosphorized steel to contain the least amount of Fe after galvanizing when compared to low carbon and Ti IF steels processed similarly. Fe-Zn growth reactions were dramatically retarded on the rephosphorized steel coated in Zn baths containing Al greater than 0.14 wt% and then annealed at 560°C. Mercer proposes that there exists phosphorus enrichment at grain boundaries which impede Fe and Zn interdiffusion at ferrite grain boundaries. Coffin [57] studied the galvannealing behavior of 0.2 wt% Al-Zn coated TiNb and TiNb-P IF steels galvannealed at 460°C, and determined that P delayed delta and gamma phase formation and slow delta and gamma phase layer growth rates.

E. Summary

Upon reviewing the current literature on zinc hot-dip coatings, it was apparent that many processing variables influence the Fe-Zn reactions that occur galvanizing and galvannealing. Of particular importance to many of these studies was the investigation of how processing variables affected Fe-Zn phase growth. Specifically, substrate interstitial free (IF) steel variables such as surface oxide, substrate solute additions, and substrate surface chemistry affects on the rate of Fe-Zn phase reactions are not well understood.

III. Research Objectives

Owing to great demand from automotive manufacturers, steel coating facilities have significantly increased their production of Zn coated IF steel in recent years. One serious drawback associated with this development is the fact that it is much more difficult to control the coating Fe-Zn alloying rate during hot-dip galvanizing when IF steels are employed as substrates, as compared to the use of traditional low carbon steel substrates. In the interest of optimizing the properties of Zn coated IF steels, an understanding of steel substrate reactivity during hot-dip galvanizing and galvannealing of IF steels must be developed. The present research project was formulated in an effort to address some of the outstanding questions relating to the kinetics of Fe-Zn phase growth on IF steels.

The present work specifically focuses on the galvanizing portion of the coating process, in an attempt to understand reaction kinetics that occur in the Zn bath prior to post-dip annealing. The study was conducted to investigate the effects of both substrate solute composition and substrate surface conditions such as grain size and surface phosphorus segregation on the kinetics of Fe-Zn phase growth during galvanizing. Another goal of the work was to evaluate the effect of surface oxide on Fe-Zn reaction kinetics.

A. Substrate Solute Effects

Much of the work to date on the study of galvanizing reaction kinetics has been conducted

on pure iron substrates, and little data exist in the literature regarding the role of substrate solute additions on galvanizing reaction kinetics. As a result, one objective of the present work was to study the effect of steel solute additions of Ti, Nb, and P on the kinetics of the Fe-Zn reaction during hot-dip galvanizing. Two IF steels, a Ti stabilized (Ti IF), and a Ti and Nb stabilized (TiNb IF) were compared to an ULC steel in order to evaluate the role of Ti and Nb additions on galvanizing reaction kinetics. P was also studied as a solute addition to the IF steels. All six of the steels studied (ULC, ULC-P, Ti IF, Ti-P IF, TiNb IF, TiNb-P IF) are currently used to produce hot-dip coatings for the automotive industry.

B. Grain Size Effects

According to a mechanism proposed by Hisamatsu [1], greater reactivity exists at the grain boundaries of IF steels than at the grain boundaries of typical low carbon steels, and IF steels are thus believed to be more reactive in the formation and growth of Fe-Zn phases than are low carbon steels. This mechanism has been proposed to explain the difficulty in controlling the coating alloying process on IF steel substrates. A second objective of the study was to produce (and galvanize) samples with markedly different grain sizes to address the role of substrate grain boundary reactivity during galvanizing.

C. Phosphorus Surface Segregation Effects

A mechanism proposed by Lin and Meshii [58] suggests that P segregation to the steel

surface during recrystallization annealing (prior to galvanizing) causes a reduction in the rate of Fe-Zn phase growth in P containing ULC and IF steel substrates. A third objective of the present work was thus to evaluate the effect of P as a surface segregation element. In this portion of the research program, P was ion implanted to a controlled concentration level in order to produce a phosphorus surface segregation layer. The implantation procedure was used to directly place P at the surface of the steel, in order to investigate the role of P as a surface segregant.

D. Surface Oxide Effects

Some discrepancy exists in the literature as to the role that discrete oxide particles present on the steel surface have on Fe-Zn reactions during hot-dip galvanizing [53, 59]. An objective of the present work was to model the oxide as an inhibition layer. A continuous iron oxide layer was produced at the surface of an ULC steel by deliberate oxidation in air, and the effect of the oxide on Fe-Zn reactions during hot-dip galvanizing was subsequently evaluated.

E. Summary of Research Objectives

In summary, the overall objective of the research program was to evaluate substrate steel conditions, such as bulk chemistry, grain size, and surface chemistry effects on Fe-Zn reaction kinetics and phase growth during hot-dip galvanizing.

IV. Experimental Procedure

A. Materials

The following section describes the characteristics of both the substrate steels and the Zn, Al, and Fe used to prepare the hot-dip galvanizing baths.

1. Low Carbon Steel Substrates

One objective of the present research work was to compare the galvanizing reaction kinetics for substrate materials with similar chemistry but with widely varying grain size. The substrate material used to study the effect of substrate grain size on galvanizing reaction kinetics was a low carbon steel alloy initially produced in ingot form by BHP Steel in Port Kembla, Australia. This material was produced in a laboratory, and its chemistry is given as alloy LC in Table VI. The ingot was rolled to final sheet thicknesses of 2.0 and 0.4 mm, which correspond to 20 and 84% cold worked conditions, respectively. Samples of both thicknesses were decarburization annealed and were then subjected to either a recrystallization anneal or a strain anneal, as described below.

Table VI. BHP Sheet Steel Chemical Analysis (10^{-4} wt%, or parts per million).

Steel Alloy	C	Si	S	N	Al	Mn	P	Ti	Nb	B
LC	90	30	40	12	380	2580	20	80	<50	<3
LC-P	50	20	40	9	340	2690	600	60	<50	<3
Ti IF	80	20	30	12	310	2590	30	750	<50	<3
Ti-P IF	60	50	20	10	390	2670	750	610	<50	<3
Ti-Nb IF	70	30	30	8	310	2470	40	330	210	<3
Ti-Nb-P IF	60	50	30	9	330	2740	700	370	220	<3

The 0.4 mm thickness material was recrystallization annealed according to the IF steel annealing procedure outlined in the next section. The recrystallization annealed material ultimately attained a grain size of approximately 15 μm. In order to fulfill the stated objective of testing two materials with widely varying grain size, it was necessary to modify some of the steel samples using a strain annealing technique to produce a relatively large grain size. Since a lower degree of cold work is beneficial in producing material with a large grain size, the 2.0 mm thick sheet (20% cold worked) material was selected as the starting material for strain annealing. The strain annealed material ultimately attained an average grain size of 85 μm, which served as a comparison to the 15 μm grain size material produced by the recrystallization annealing process.

2. BHP Steel Interstitial Free (IF) Substrate Alloys

Six interstitial free (IF) steel alloys were chosen to study the effect of substrate solute additions on galvanizing reaction kinetics. All of the IF steels were cold rolled to a final thickness of 0.4 mm (84% cold work). The as-received substrate sheet steel chemistries are listed in Table VI. These chemistry values were determined at Cockerill Sambre, and confirmed earlier ingot chemical analysis conducted at BHP Steel. The six IF steels studied were: (1) a low carbon steel (LC), (2) a rephosphorized low carbon steel (LC-P), (3) a titanium stabilized steel (Ti IF), (4) a rephosphorized titanium stabilized steel (Ti-P IF), (5) a titanium and niobium stabilized steel (Ti Nb IF), and (6) a rephosphorized titanium and niobium stabilized steel (Ti Nb-P IF). Without further modification, the LC steel cannot be technically classified as an IF steel, owing to the abundance of free carbon in this material. However, the LC samples were decarburization annealed prior to galvanizing, in order to approximate the low carbon content possessed by the IF steels. At that point, the carbon content of the LC steels was sufficiently low that these steels could be classified as ULC (ultra low carbon) steels. ULC steels are often referred to as unstabilized IF steels, since these steels are essentially interstitial free (i.e. carbon free), even though this state is achieved by decarburization rather than by the addition of stabilizing solutes such as Ti or Nb. The 0.4 mm thick ULC material was used as a baseline to which IF steels were compared. This comparison was used to investigate the effects of solute additions (Ti, Nb, and P) on the galvanizing reaction kinetics of IF steels.

3. Phosphorus Ion Implanted Low Carbon Steel Substrates

The substrate material used for P-ion implantation was a low carbon steel in which extremely large grains (10-20 mm) had been produced using a strain-anneal technique. Since it was not possible to procure an adequate number of samples with identical chemistry for use in ion implantation, three alloys with similar chemistries were used as implantation substrates. The substrate chemistries are listed in Table VII, and were determined by both wet chemical analysis and inert gas fusion analysis at an independent laboratory.

Table VII. Low Carbon Substrate Chemical Analysis (wt%).

Alloy	C	Si	S	N	Al	Mn	P	O
1	0.015	0.037	0.012	0.0076	0.019	0.119	0.010	0.0424
2	0.032	0.029	0.003	0.0003	0.001	0.006	0.003	0.0093
3	0.026	0.023	0.001	0.0006	<0.001	0.01	0.004	0.0094

The extremely large grain size possessed by the P-ion implanted samples also allowed these specimens to be included in the previously mentioned evaluation of grain size effects. One limitation to the use of these samples in the grain size investigation, however, is the fact that the alloy chemistry is not identical to the chemistry of the 15 μm or 85 μm steels described earlier in this section. The P-ion implanted substrates could thus not be used to make *direct* conclusions about the effect of grain size on galvanizing reaction kinetics.

4. Surface Oxide Gleeble-Annealed Substrate Samples

The LC 0.4 mm sheet material was the substrate steel used for the Gleeble-anneal surface oxide phase of this study (the LC substrate chemistry is listed in Table VI).

5. 0.00 wt% Al-Zn Bath Materials

The zinc used in producing the hot-dip galvanizing baths was obtained in ingot form and had a chemistry of 99.997 wt% Zn, and 0.0012 wt% Pb. Other elements such as Cd, Sn, Al, Cu, and Fe were present in trace amounts (< 0.0003 wt% each). Once molten, the zinc bath was saturated with iron (0.03 wt% Fe at 450°C), based on the solubility determinations of Kirkaldy et al [7, 12] and Tang [11, 13]. The iron used to saturate the zinc bath was obtained from Johnson-Matthey in rod form, and had an extremely pure chemistry of 99.999 wt% Fe. All Zn baths were iron-saturated because previous work has shown steel reactivity to be enhanced if the zinc bath is undersaturated in iron, due to rapid dissolution of the steel during initial immersion in the bath.

6. 0.20 wt% Al-Zn Bath Materials

The zinc and iron raw materials discussed above were also used to produce the aluminum-containing zinc bath. The 0.20 wt% aluminum added to the melt was obtained from Johnson-Matthey in ingot form, and had a chemistry of 99.9985 wt% Al. Since the

presence of Al reduces the solubility of Fe in molten zinc, a lower amount of Fe was used than in the Al-free bath. The solubility of Fe in a zinc bath containing 0.20 wt% Al at 450°C was recently established as 0.008 wt% Fe [13]; this is the Fe concentration utilized to saturate the zinc bath in the tests employing Al as a bath constituent.

B. Substrate Sample Preparation

Substrates were prepared in several different ways prior to galvanizing, as described below.

1. Low Carbon Steel Substrates

Prior to galvanizing, both the 0.4 mm thickness and the 2.0 mm thickness LC steel sheet samples were subjected to a decarburization anneal in order to produce ultra low carbon (ULC) steel, which has a carbon content similar to that of IF steels. After the decarburization anneal, the 2.0 mm thick ULC sheet was subjected to a strain anneal in order to produce large grain size material, and the 0.4 mm thick steel was subjected to a recrystallization anneal. The 2.0 mm thick ULC sheet ultimately attained a grain size of approximately 85 μm, and is thus referred to as 85 μm ULC steel in the remainder of this document. The 0.4 mm thick ULC sheet ultimately attained a grain size of approximately 15 μm. Since the 15 μm ULC steel was treated in an identical manner to the IF steels once the decarburization process was completed, it will be categorized as an IF steel from

this point forward. Details of the annealing methods used (decarburization annealing, strain annealing, and recrystallization annealing) are provided in the following sections.

a. Decarburization Annealing

Decarburization annealing was performed in a tube furnace at 815°C for 6.5 hours by placing the LC steel sample in an alumina tube (inner diameter 5 cm) which had screw-tightened end caps to provide an airtight seal. The stated annealing hold time (6.5 hours) does not include the 15-30 minutes necessary for the tube furnace to reach the set temperature. The tube furnace was flushed at the beginning and end of each anneal with ultra high purity argon gas to remove oxygen. Annealing was conducted under a reducing 18% H_2/N_2 gaseous environment. The H_2/N_2 gas was bubbled through water prior to being introduced into the furnace, since moisture is generally present in the reducing atmospheres used in commercial galvanizing lines. After annealing, samples were immediately water-quenched and then pickled in a 10% HCl solution to remove the thin surface oxide film which formed during the quenching process.

b. Strain Annealing

A strain annealing technique was used to generate the very large substrate grains required to study the effect of grain size on galvanizing reaction. It was anticipated that adequately large grains could not be produced in the Ti and Ti-Nb stabilized IF steels, since these

alloys contain fine precipitates of TiC, TiCN, and NbCN which act to prevent the growth of large grains by pinning grain boundaries during annealing. The ULC steel was thus selected to study the effect of substrate grain size on Fe-Zn reaction kinetics, since this steel does not contain such precipitates which can act to pin growing grain boundaries.

Low carbon steel sheet (2.0 mm thickness) was first machined to the dimensions of a reduced-section flat tensile specimen according to ASTM standard E8 - 89 (60). The total length of the specimen was 76.2 mm (3 inches). The machined specimens were pickled in an acid solution (10% HCl), ground on both flat surfaces using 120 grit SiC grinding paper, and pickled once again in 10% HCl in order to remove surface dirt and scale due to rolling. The samples were then decarburization annealed according to the procedure described in the previous section. The carbon content of the LC steel was significantly reduced by the decarburization process described above (final carbon content of 0.005 wt%), and the decarburized LC samples thus are referred to as ULC material.

Previous investigators have observed significant grain growth in ultra low carbon and low carbon steel alloys which had been strained by 2-5% [61, 62]. The decarburized, reduced-section samples were thus strained (at a rate of 2.54 mm per minute) on a Model 4206 Instron to a final gauge length elongation of 5%. The strained samples were then recrystallization annealed at 875°C in the tube furnace under a reducing 18% H_2/N_2 gaseous atmosphere. The annealing hold time was set to 4000 minutes (66.67 hours) to promote grain growth in the ULC steel substrate [61, 62]. The samples were then

machined from 2.0 mm thickness down to a thickness of 0.7-0.8 mm in order that the final sample thickness after chemical polishing (which is described below) would approximate the sheet thickness of the other samples used in the study (0.4 mm thickness). The machined samples were subsequently decarburization annealed once again at 815°C for 35 minutes, water quenched, and cleaned in a 10% HCl acid solution.

Finally, the samples were chemically polished to remove unwanted surface structure such as small recrystallized grains at the substrate surface, which can result from machining and subsequent annealing. Samples were chemically polished in a freshly prepared solution containing 7 ml HF, 50 ml of 50% concentrate H_2O_2, and 50 ml H_2O at 15°C (63). Each sample was immersed for 3 minutes in the solution, rinsed in 50% concentrate H_2O_2, rinsed in water, flushed with ethyl alcohol, and dried. The final thickness of the sample after chemical polishing was 0.3-0.5 mm, which is approximately the same thickness as both the non-strain annealed 15 μm ULC steel and the IF steel material (0.4 mm thick). As stated previously, the final average grain size of the strain annealed, ultra low carbon steel was determined to be 85 μm.

2. BHP IF Steel Recrystallization Annealing

Each of the six IF steels was initially obtained from BHP Steel in a cold rolled condition (0.4 mm in thickness, 84% cold worked). Recrystallization annealing of these samples was performed because rolled sheet is subjected to a recrystallization anneal on a typical

commercial galvanizing line. Samples were first sectioned to a dimension of 37 x 254 x 0.4 mm. The samples were then recrystallization annealed in a tube furnace using the following procedure. The tube furnace (while cool) was first purged of oxygen using a steady flow of ultra high purity argon for 30 minutes. The samples were then recrystallization annealed in a reducing 18% H_2/N_2 gaseous atmosphere at 815°C for 15 minutes (note that the hold time of the anneal did not include the time necessary for the furnace to reach temperature). Following the 15 minute hold, the furnace was purged with ultra high purity argon for 30 minutes, after which the samples were removed and water quenched. Cross sectional light optical microscopy was used to confirm that all of the samples were fully recrystallized after the above recrystallization anneal procedure. The final carbon content and the calculated excess Ti (Ti**) content of the alloys after recrystallization annealing are listed in Table VIII. As stated previously, the average grain size of the recrystallization annealed ULC steel was determined to be 15 μm. All of the remaining IF steel alloys were found to have grain sizes in the range of 10-20 μm.

Table VIII. Carbon and Excess Ti (Ti**) Content of IF Steels After Recrystallization Annealing (wt%).

Sample	carbon content (wt%)	Ti**
LC (ULC)	0.003	-0.025
LC-P (ULC-P)	0.003	-0.117
Ti IF	0.006	+0.011
Ti-P IF	0.004	-0.086
TiNb IF	0.003	-0.004
TiNb-P IF	0.004	-0.112

Ti** = Total Ti - 3.99C - 1.49S - 3.42N - 1.55P

3. Phosphorus Ion Implantation Sample Preparation

a. Substrate Preparation Prior to Implantation

Prior to P-ion implantation, the extremely large grain size (10-20 mm) substrate were cleaned in a 3% EDTA solution, rinsed in water, and then rinsed in ethyl alcohol. EDTA was used to remove a protective lacquer which had previously been applied to the test samples. After cleaning with EDTA, the samples were chemically polished in a solution of 14 ml HF, 100 ml of 30% concentrate H_2O_2, and 100 ml H_2O at 15°C. Samples were immersed in the solution for approximately 3 minutes then rinsed in 30% concentrate H_2O_2, and flushed with ethyl alcohol [63, 64]. After chemical polishing, samples were etched using an aqueous 11 wt% ammonium persulfate solution in order to reveal grain structure; etching was performed by swabbing both flat surfaces of the sample with the etching solution. The samples were then rinsed in water and flushed with ethyl alcohol. Samples were sectioned to 25.4 x 25.4 x 0.3 mm and photographed on both flat surfaces. Because the grain structure of this material was extremely large and the sheet thickness small, all of the grain boundaries are continuous through the thickness of the material. Therefore, the grains on opposite flat sides of the sample are actually mirror images of one another (see Figure 29). The approximate grain size of this material was determined to be 10-20 mm (10,000 to 20,000 μm).

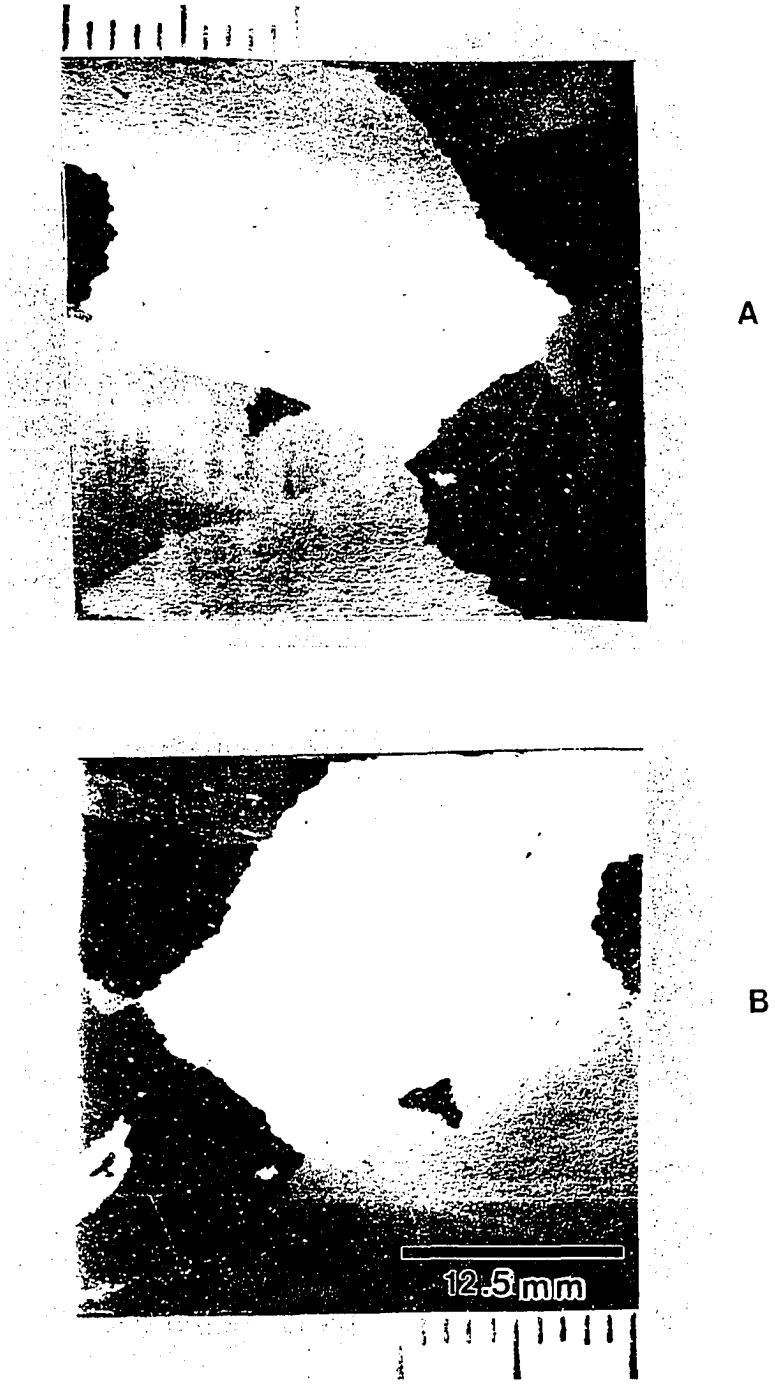

Figure 29. Grain structure of the (a) P ion implanted and (b) Non P ion implanted surfaces of a single low carbon steel substrate (note that the due to the large grain size and thin cross section of the substrate, opposite side surfaces show a mirror image of another indicating the grains are through thickness grains).

b. Ion Implantation

In the semiconductor industry, ion implantation of relatively heavy elements (dopants) into light target materials (Si wafers) is routinely accomplished. The ion implantation of a light element (such as P) into a heavy target (such as Fe), however, is much less common. Fortunately, some previous work does exist on this topic, as Clayton et al [65, 66] studied the ion implanting of phosphorous into stainless steel. The general ion implantation parameters used in the present study were adapted from this previous work. The objective of the present ion implantation procedure was to implant 1×10^{17} P atoms/cm^2 into each target steel sample, since Clayton et al [65, 66] were able to achieve this level of doping in the case of a stainless steel substrate.

Phosphorus ion implantation was conducted at the Accelerator Laboratory of the Solid State Division of Oak Ridge National Laboratory in Oak Ridge, Tennessee. A Varian Extrion Accelerator Model 200-1000 High Current Implanter was used to ion implant the samples. Samples were clipped to a holder so that they were flush with the holder surface and positioned perpendicular to the incoming ion beam. The center 20 mm diameter of the sample was exposed to the ion beam, and the sample holder was kept at 0°C to prevent heating of the sample during implantation. Gallium phosphine (GaP) was used as the source material and HCl as the carrier ion gas. The beam of P ions was focused and accelerated at the target at an energy of 40 KeV. All implantation was performed under high vacuum conditions ($1.0 - 2.0 \times 10^{-7}$ torr). A schematic representation of the Extrion

Accelerator Model 200-1000 is shown in Figure 30.

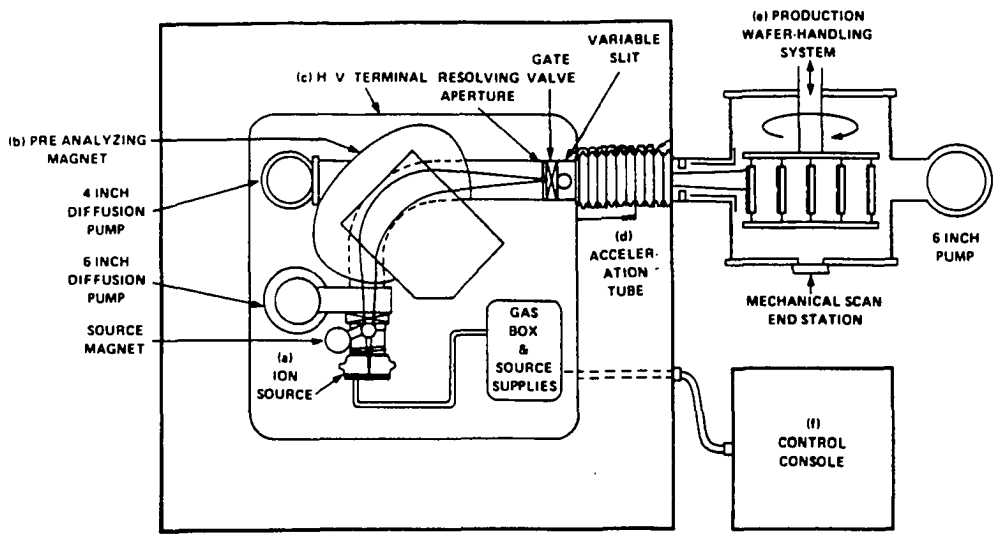

Figure 30. Schematic of the Extrion Model 200-1000 high current implanter (a) ion source system (35KeV) (b) analyzing magnet (c) high voltage terminal (d) post analysis acceleration (35-200 KeV) (e) production wafer handling system ,and (f) control system.

Ion implantation was performed on only one side of each specimen, in order that a phosphorus-containing and a phosphorus-free surface would be produced on each sample. This procedure allowed the effect of phosphorous on galvanizing reaction kinetics to be studied directly, without the need to account for such complicating effects as differences in substrate grain size or chemistry.

c. Rutherford Backscattering Spectroscopy (RBS)

Rutherford backscattering spectroscopy was used to analyze the surface chemistry of the ion implanted samples in a non-destructive manner. This analysis was conducted at the Accelerator Lab of the Solid State Division of Oak Ridge National Laboratory [67]. Rutherford backscattering utilizes accelerated helium alpha particles (He^{+} or He^{++}) with an energy of approximately 1 MeV to determine the concentration profile of the implanted species in the target. Alpha particles interact *only* with other ions, and these particles are thus repelled by phosphorus ions but do not interact with the Fe substrate atoms. The repelled (backscattered) alpha particles can be collected in order to quantify the amount of phosphorus present. A Van de Graff accelerator source was used for the RBS analysis with an accelerated beam energy of 1 MeV [67].

4. Surface Oxide Sample Preparation

Low carbon steel (0.4 mm thickness) was chosen as the substrate for the surface oxide portion of this study. These samples were not subjected to a decarburization process, since it was judged that carbon content would not influence the effect of surface oxides on galvanizing reaction kinetics. LC sheet samples were sectioned to 50.8 x 228.6 x 0.4 mm and cleaned in acetone. A set of thermocouple wires was attached to the center of each specimen to monitor thermal processing while the sample was heat treated in the Gleeble

HAZ 1000. Using electric resistance heating, each sample was heated up to 650°C at a rate of 500°C/s. Samples were then held at 650°C for either 1, 5, 10, 30 or 60 seconds. After the isothermal hold was complete, the samples were cooled at 25°C/s using an air and water mist spray. The entire heat treatment procedure was performed under atmospheric conditions to allow the steel substrate surface to oxidize. The samples were then sectioned to remove the 50.8 mm x 50.8 mm center portion of the sample from the remainder of the specimen. The center portion of the Gleeble annealed sample was previously determined [68] to be the region of the sheet sample which experienced a uniform heat cycle; this section of the sample would thus be expected to form a uniform oxide. This 50.8 x 50.8 mm center section was further sectioned to produce four samples, each 25.4 x 25.4 mm in dimension. The average thickness of the oxide formed for each hold time was determined by both cross-sectional light optical microscopy and a LECO 2001 image analysis system.

C. Hot-Dip Galvanizing

1. Precleaning and Fluxing

A precleaning and fluxing procedure was employed prior to galvanizing, in order to generate a clean, reproducible substrate surface which could be readily wetted by the molten zinc in the bath. Samples were precleaned and fluxed under a benchtop chemical

fume hood adjacent to the galvanizing simulator. The process is described below for each of the four types of steel substrates utilized.

a. 85 μm grain size ULC Steel

The 85 μm ULC steel samples had been previously chemically polished and thus did not require an initial cleaning step. Due to the relatively small length of the 85 μm grain size ULC material (approximately 75 mm), samples were clamped to a section of sheet material (37 x 216 x 0.4 mm), which served as an extender arm to accommodate the fixed dimensions of the hot-dip galvanizing simulator.

The ULC sample was immersed in an alkaline (caustic) cleaning solution (18 g/l NaOH, 2.5 g/l sodium pyrophosphate, 0.5 g/l Na_2CO_3, and 1ml/l Tergitol) at 80°C for 2 minutes. The sample was brushed clean while still immersed in the caustic solution using a soft nylon bristle brush, and was subsequently rinsed under running tap water. The sample was then pickled in 10% HCl at room temperature for 20-30 seconds, and was again rinsed under running tap water. Finally, the sample was immersed in a 75°C fluxing solution (20 g/l $ZnCl_2$, 7 g/l NH_4Cl, and 3 drops/200ml Merapol HCS) for 5 minutes [69].

b. BHP Steel IF Steel Alloys

The six IF steel alloys were cleaned according to the procedure outlined above for the 85 μm ULC steel with one minor exception. Prior to caustic cleaning, each IF sample was first immersed in a 10% HCl solution to remove the thin surface oxide which had formed during the water quenching step which followed recrystallization annealing. After pickling, the samples were rinsed under running tap water and cleaned in the same manner as the 85 μm grain size ULC steel.

c. Phosphorus Ion Implanted Samples

As with the 85 μm grain size ULC steel samples, the P-ion implanted samples (25.4 x 25.4 x 0.3 mm) had to be attached to an extender arm of scrap sheet material (37 x 216 x 0.4 mm) in order to fit into the fixed dimensions of the simulator. In order to maintain the surface integrity of the P-ion implanted material (i.e. to prevent removal of the material which contained implanted phosphorus ions), these samples were not precleaned after ion implantation. Prior to being run on the hot-dip galvanizing simulator, the samples were immersed in the flux solution (75°C) for 5 minutes.

d. Surface Oxide Samples

Due to their size (25.4 x 25.4 x 0.4mm) the surface oxide samples were attached to an extender arm (37 x 216 x 0.4 mm) so as to fit to the fixed dimensions of the simulator. In order to prevent chemical removal of the oxide which had been deliberately formed on the Gleeble annealed material, these samples were not precleaned and were only immersed in the flux solution (75°C) for 5 minutes.

2. Hot-Dip Galvanizing Simulator

A significant aspect of the present research work involved the construction and assembly of a facility designed to automate the galvanizing process within the laboratory. A brief summary of the essential characteristics of the galvanizing simulator appears below.

The simulator consists of an automated delivery system and three associated processing stations, which were situated below the delivery system. The delivery system was designed to allow for horizontal motion, in order that the substrate specimen could be aligned directly over each of the processing stations. Once the sample was placed above a given processing station by the horizontal delivery motion, the automated vertical delivery unit was used to insert the substrate specimen into the processing station. Each processing station was aligned so that the sample to be hot-dip galvanized could be inserted and removed vertically from each station. The horizontal traverse was

accomplished via a motor-driven cam mechanism and the vertical stroke was controlled by a pneumatic piston. All samples were galvanized using the same insertion and removal rate at each of the three stations (10 cm/s). The simulator processing stations were arranged in the following order: (1) a preheat/drying furnace, (2) a Zn melt furnace and (3) a water quench tank (Figure 31). Prior to a production run, the delivery system was programmed for a given dwell time (i.e. residence time) at each of the simulator stations, and thus only one sample at a time could be processed. The dwell time at each station was computer controlled, and sample processing was thus fully automated and reproducible.

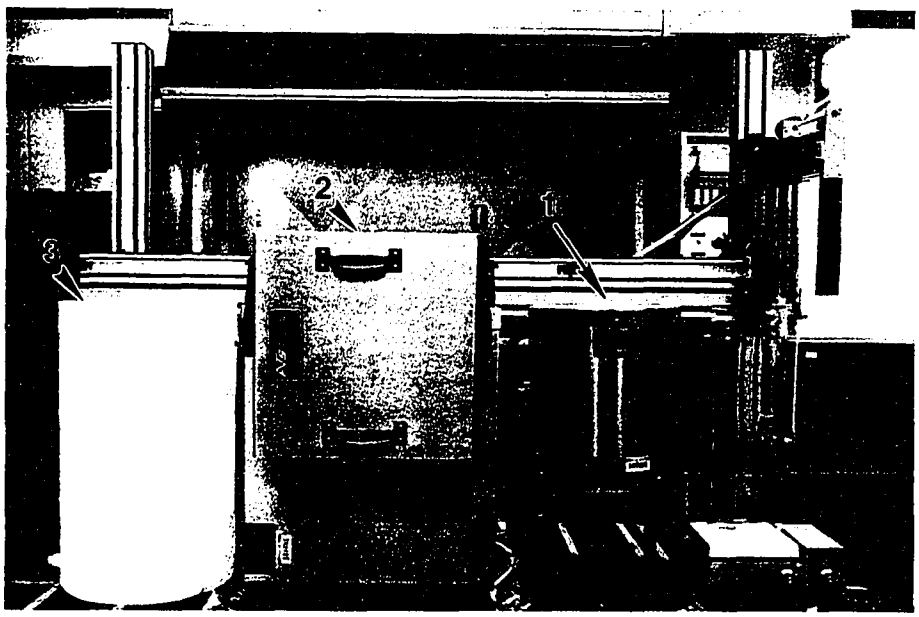

Figure 31. Automated laboratory hot-dip galvanizing simulator with a specimen loading station and (1) drying furnace, (2) melt furnace, and (3) water quench tank.

After fluxing, all samples were attached to the automated delivery system using a pneumatically controlled gripper mechanism (Figure 32).

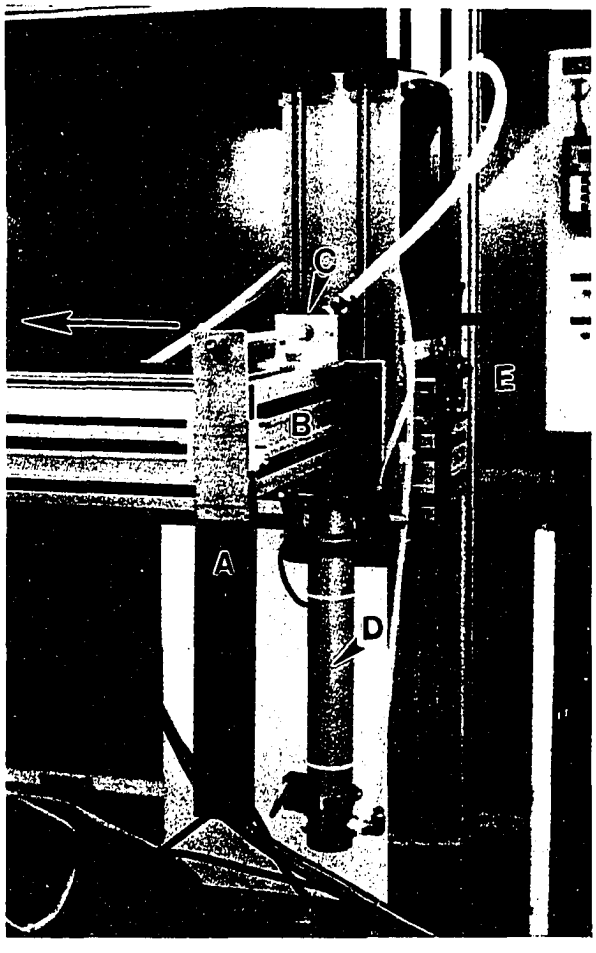

Figure 32. (a) specimen and (b) specimen holder arm of the automated laboratory hot-dip galvanizing simulator. The pneumatically controlled piston (c) served to grip the specimen, while piston (d) vertically transported the sample in and out of each processing station, respectively. The horizontal traverse of the specimen holder arm (in a direction shown by the arrow) was controlled by a motor and cam shaft assembly (e).

At the first station of the simulator (station (1) in Figure 31, the preheat/drying furnace), samples were dried at 120°C for 5 minutes. This procedure allows the film of flux solution on the surface of the sample to completely dry, thus providing a clean and highly

wetable substrate surface to the zinc bath. Because the simulator was not encased in a controlled environment, higher temperatures of drying were not utilized, as preheat temperatures greater than 120°C would have led to surface oxidation prior to immersion in the bath. Samples were therefore not produced in exactly the same manner as commercially-produced sheet, since the commercial product is manufactured by heating the strip in a reducing gaseous environment (which prevents surface oxidation) to a temperature of approximately 460°C.

Before the sample was immersed into the molten zinc bath (station (2) in Figure 31), the surface of the bath was skimmed in order to remove surface drosses. The zinc bath was contained in a 12.7 cm inner diameter SiC crucible. The crucible was charged with approximately 17 kg of zinc. The bath temperature was held at 450 ± 2°C, and was monitored using a thermocouple probe which was immersed into the bath prior to sample production. A refractory plate with a 6 cm hole cut in its center was positioned over the crucible. This plate covered the opening of the melt furnace and most of the opening of the SiC crucible, in order that the bath temperature could be maintained while the top of the melt furnace was removed during a galvanizing production run. A small 8 mm hole was drilled in the plate and used as a port for the bath thermocouple probe. Samples were individually inserted into the bath (at a downstroke rate of 10 cm/s) for the preset programmed time and then vertically removed at a rate of 10 cm/s. Finally, the samples were delivered to the water quench tank (station (3) in Figure 31). Less than 2.5 seconds elapsed between the time of removal from the zinc melt and the time of immersion in the

quench tank. Prior to water quenching, the zinc on the surface of the sample had not yet solidified (i.e. was still molten). The samples were deliberately processed in this manner, in order that only growth reactions that occurred in the bath would be studied. In other words, the water quenching step was utilized in an attempt to avoid phase growth that would have inevitably occurred upon slow cooling. Samples were immersed in the water quench tank for 2 minutes to allow the samples to fully cool to room temperature before handling.

3. Test Matrix

The test matrix of galvanized samples for each set of substrate material immersed in the 0.00 wt% Al (iron-saturated) and 0.20 wt% Al (iron-saturated) zinc baths is given in Table IX. In most cases, identical time of immersion samples were produced from both zinc baths in order to study the effect of bath aluminum on galvanizing kinetics. In the case of the 85 μm grain size ULC and phosphorus ion implanted samples, an additional set of extended immersion time samples were produced from the 0.20 wt% Al-Zn bath.

Table IX. Test Matrix of Substrate Steel Specimens Prepared on the Hot-Dip Galvanizing Simulator.

Substrate Sample / Zn Bath Chemistry	Time of Immersion in the Zn Bath (seconds)
85 μm ULC steel / 0.00 wt% Al-Zn	5, 10, 30, 60, 120, and 300
85 μm ULC steel / 0.20 wt% Al-Zn	5, 10, 30, 60, 120, and 300
85 μm ULC steel / 0.20 wt% Al-Zn	1200 and 1800
BHP IF and ULC steel / 0.00 wt% Al-Zn	5, 10, 30, 60, 120, and 300
BHP IF and ULC steel / 0.20 wt% Al-Zn	5, 10, 30, 60, 120, and 300
P Ion Implanted and non P Ion Implanted LC steel / 0.00 wt% Al-Zn	5, 30, 60, 120, and 300
P Ion Implanted and non P Ion Implanted LC steel / 0.20 wt% Al-Zn	5, 30, 60, 120, and 300
P Ion Implanted and non P Ion Implanted LC steel / 0.20 wt% Al-Zn	1800, 2700, and 3600
Surface Oxide / 0.00 wt% Al-Zn	10, 60, 100, and 300
Surface Oxide / 0.20 wt% Al-Zn	10, 60, 100, and 300

4. Zinc Bath Sampling

Bath samples were taken both before and after each set of substrates in the test matrix were galvanized, in order to check that the bath chemistry was at the desired composition. Molten zinc was extracted using a quartz pipette tube inserted approximately 6 cm below the surface of the bath. The 6 cm depth was chosen to match the location at which all of the coated samples were analyzed in cross section. After molten zinc was withdrawn from the bath, the quartz tube was water quenched and then broken to remove the solidified cylindrical bath sample. The sample was sent to an independent laboratory for chemical

analysis. The chemical analysis for Fe, Al, and Zn content was obtained for each bath sample, and the data are listed in Appendix A.

D. Coating Chemistry

The IF steel alloys which were coated on the galvanizing simulator were sectioned in order to measure the total Fe, Zn and Al contents in the galvanized coating. Individual samples were sectioned from the center of the coated sheet (15 x 50 x 0.4 mm) and analyzed at Cockerill Sambre in Liege, Belgium using inductively coupled plasma (ICP) analysis. The chemical analysis of the coatings are listed in Appendices B and C (70).

E. Light Optical Microscopy

1. Substrate Grain Structure

Uncoated substrate steel samples were mounted and analyzed in cross section, transverse to the rolling direction of the sheet. The procedure used to section, mount, and grind the sheet sample has been previously described [71]. Sample mounts were polished on a cloth charged with 6 μm diamond paste, followed by polishing steps using 1.0 μm and 0.3 μm alumina slurry solutions. Final polishing was performed on a polishing cloth charged with a 0.05 μm colloidal SiO_2 solution. Etching of the interstitial free steel substrates was initially performed using a Beraha etchant (a color tint etchant) which consisted of 10 gm

sodium thiosulfate and 3 gm potassium metabisulfate in 100 ml H_2O [63, 64]. Sample mounts were immersed with the polished sample surface face-up (with no agitation) in Beraha's etchant for 1 minute and 45 seconds. The 15 and 85 μm grain size ULC alloy samples were etched in a 2% nital solution (2 ml nitric acid in 98 ml H_2O) for approximately 30 seconds.

2. Coating Structure

Zinc coated samples were prepared for light optical microscopy (LOM) according to a previously documented procedure [71]. No modifications to the referenced sample preparation procedure [71] for galvanneal coatings were necessary to properly prepare the significantly thicker hot-dip galvanized coatings. Bright field light optical micrographs for both substrate and coating structure were recorded on a Reichert-Jung MeF3 metallograph.

Only faint grain boundary relief was visible on these samples after they had been etched for coating structure and observed in bright field. Since grain boundaries often show stronger contrast in dark field than in bright field, photomicrographs were taken using dark field imaging for both the 85 μm grain size ULC and the low carbon 10 - 20 mm grain size P-ion implanted material. Dark field photomicrographs were also recorded on the Reichert-Jung MeF3 metallograph.

F. Quantitative Image Analysis (QIA)

1. Grain Size Determination

The procedure outlined here closely follows ASTM standard E112 - 84 for grain size determination [72]. Grain size was determined using a linear intercept count method. The sample was positioned such that a horizontal line etched into the microscope eyepiece was aligned parallel to the sample surface. Sample positioning was further controlled such that the grain boundaries at the outermost surface of the sample were bisected by the horizontal line. The number of bisected grain boundaries was counted for an entire field, and the procedure was repeated across the complete edge length of the sample. A magnification was chosen so that 30-50 counts per field were obtained. This procedure was repeated for the parallel edge on the opposite side of the same sample in order to improve the statistics of the grain size data. All grain size analysis was conducted on samples transverse to the rolling direction of the sheet.

2. Coating Characterization

a. Total Alloy Layer Thickness

Once the light optical microscopy (LOM) observations of the Zn-coated samples had been completed, the samples were measured for total Fe-Zn alloy layer thickness on the LECO

2001 Image Analysis System. Based on gray level contrast, the computer software within the LECO 2001 System isolated the total Fe-Zn alloy layer, distinguishing it from the steel substrate and the unalloyed zinc eta phase overlay. The same program then assigned a pseudo color to the gray level of the Fe-Zn alloy layer and inserted a vertical grid capable of performing 50 thickness measurements of the isolated layer. A total of 10 fields (50 measurements per field) were taken for each coated sample to measure the thickness of the entire Fe-Zn alloy layer (Figure 33). A magnification of 1000X was necessary for short immersion times (5 and 10 seconds), while other samples studied were analyzed at a magnification of 400X so that the total Fe-Zn alloy layer could be imaged within the field of view of the image analysis system.

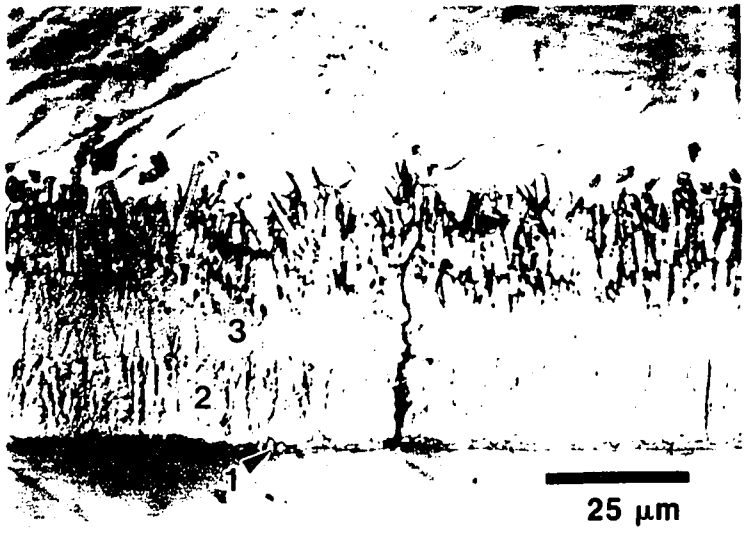

Figure 33. Cross sectional microstructure of a 0.00 wt% Al-Zn coating formed after 300 seconds of immersion in the bath on the ULC steel substrate. Three Fe-Zn phase layers were found to develop over the reaction times studied: (1) gamma phase (2) delta phase and (3) zeta phase.

b. Individual Alloy Layer Thickness

As expected, an increased time of immersion in the bath led to the formation of a number of sequential growth layers within the coating. In order to quantify the growth rate of the individual layers, the individual layer thicknesses were measured over time. Because the LECO 2001 system could not isolate the individual layers based on gray level contrast, the layers had to be directly (manually) measured using the digitized image. The image analysis system was calibrated at each magnification employed so as to accurately quantify the manually inserted vertical lines denoting individual layer thickness. These individual layer measurements were performed at a magnification of 1000X. Five fields of data (with 10 measurements per field) were obtained for each layer measured. Each individual layer in the field of view was measured using the basic procedure described above.

G. Electron Probe Microanalysis

A JEOL 733 Superprobe was used for compositional microanalysis of the hot-dip galvanized coatings via electron probe microanalysis (EPMA). Linescans were conducted across the transverse cross section of the coated sample so that the EPMA analysis began on the steel substrate and progressed at 1 μm intervals across the steel/coating interface and the entire Fe-Zn alloy layer. The linescan was terminated once 5 consecutive readings of the same composition were obtained from the zinc eta phase overlay layer. X-ray microanalysis was conducted for Fe, Zn, and (when applicable) Al, at each point along the

linescan. The beam voltage used for analysis was 20 kV at a beam current of 16.3-16.8 nA. Additional parameters used in the EPMA analysis are shown in Table X.

Table X. Electron Microprobe Conditions used for Fe, Zn and Al Analysis.

WDS Crystal and Spectrometer Conditions	Fe	Zn	Al
Crystal	LiF	LiF	TAP
Bias (volts)	1700	1650	1700
Baseline	1.84	1.20	1.90
Window	10	10	5
Background Count Location*	± 2 mm	± 3 mm	± 6 mm

*distance off K_α peak used for analysis

After Fe, Zn, and Al x-rays had been collected at each position along the linescan, peak count information was analyzed by the Tracor Northern 8500 system integrated with the JEOL 733 Superprobe. The software unit of the Tracor Northern system transformed peak count data into quantitative compositional data using relative peak count information on standards and known correction equations. The correction procedure used for all of the microprobe data presented here is known as a $\phi(\rho z)$ method. This method was chosen primarily because it allows for more accurate analysis of light element detection (Al) when simultaneously analyzing for heavier elements such as Fe and Zn [73]. Although aluminum was not analyzed for in all of the coatings, all x-ray data were quantified using the same $\phi(\rho z)$ correction method, in order that data for non-aluminum and aluminum-containing coatings could be effectively compared.

The standards used for iron and zinc detection were both of 99.999 wt% purity. The standards were prepared according to the polishing procedure outlined for the coated steel samples. Carbon coating of the standards was performed in the same batch as the carbon coating of the coated steel sample mounts, in order that differences in carbon coating thickness would not be a source of error in the analysis. The aluminum standard used for analysis was of purity > 99.9 wt%.

For the beam conditions and the standards utilized, minimum detectability limits were calculated by the Tracor Northern 8500 system. Using a conservative count time of 20 seconds (although typical count times were about 40 seconds at each spot location, this count time would occasionally decrease to values as low as 20 seconds), the minimum detectability limits were calculated to be 0.035 wt% for Fe, 0.055 wt% for Zn, and 0.006 wt% for Al. The estimated error in the microanalysis measurements was approximately ± 10 percent of the absolute value of the composition determined.

1. Hot-Dip Galvanized 85 μm Grain Size ULC Steel Alloy

In order to prepare flat polished samples for microprobe analysis, the 0.00 wt% Al-Zn coatings on the 85 μm grain size ULC steel were ground on 8 μm and 3 μm SiC grinding papers once LOM and QIA were completed. The mounts were then polished according to a previously outlined procedure [71], through a final polishing step of 0.25 μm using a

diamond paste on a Struers nap cloth. Sample mounts were then carbon coated to reduce charging of the sample during the EPMA analysis.

One complete linescan was conducted on each of the 85 μm ULC - 0.00 wt% Al-Zn coated samples immersed for 5, 10, 30, 60, 120, and 300 seconds. Corresponding linescan analysis for the 0.20 wt% Al-Zn coated samples could not be conducted for the short-time immersion samples, due to the fact that little measurable growth was observed on those samples (phase layer ~ 1 μm thick). Since small crystals were observed on some of the 0.20 wt% Al-Zn coated samples, spot analysis was conducted on isolated crystals when possible (using the same microanalysis conditions described above). Longer time immersion samples from the 0.20 wt% Al-Zn bath showed large crystal growths, and many spot analyses were obtained from the same crystal on each of the longer time immersion samples.

2. Hot-Dip Galvanized BHP Steel Interstitial Free Steel Alloys

Similar microprobe conditions (beam voltage, current, spectrometer settings) to those described above were used for the analysis of the six 10-20 μm grain size interstitial free (IF) steel alloys which had been hot-dip galvanized in 0.00 and 0.20 wt% Al-Zn baths. The same Fe, Zn and Al standards were used for the analysis, as well as the same $\phi(\rho z)$ correction and quantification software. For each IF substrate, three times of immersion were chosen for study: 10, 60 and 300 seconds. These individual time of immersion

samples were analyzed from both 0.00 and 0.20 wt% Al-Zn baths. Linescan analysis was conducted on all of the above-mentioned samples according to the procedure discussed in the previous section.

3. Hot-Dip Galvanized Phosphorus Ion Implanted Samples

In the case of the P-ion implanted samples, linescans were conducted on each side of the sample so that the coating compositional data for the P-ion implanted and non P-ion implanted surfaces could be compared. For the 0.00 wt% Al coatings, linescans were conducted on all of the samples galvanized: 5, 30, 60, 120, and 300 seconds of immersion. The linescan analysis was conducted according to the procedures previously described for the 85 μm ULC steel and IF steel alloy substrates. Because the phosphorus ion implanted 0.20 wt% Al-Zn coated material showed little or no growth over 5-300 seconds of immersion, it was not possible to perform linescan analyses of these samples. Selected spot analysis was conducted where small crystals of growth were observed during the holds which lasted for less than 300 seconds. For the 1800, 2700, and 3600 second samples (0.20 wt% Al-Zn coatings), one single large growth layer formed and selected spot analysis for three separate locations within the growth layer were obtained: (1) the substrate/growth layer interface area, (2) the central portion of the growth layer and (3) the outer portion of the growth layer near the growth layer/Zn eta phase overlay interface. Both the phosphorus ion implanted and non phosphorus ion implanted sides of the coated sample were analyzed.

After linescan or spot analysis was completed for each zinc coated sample, a backscattered electron (BSE) and a secondary electron (SE) image was recorded of the area in which the analysis was conducted. The images were recorded at the same beam conditions (voltage, current) which had been used for microanalysis.

H. Scanning Electron Microscopy

Because the BSE images from the JEOL microprobe showed greater atomic number contrast than anticipated (based upon contrast calculations as a function of atomic number differences between adjacent Fe-Zn layers), further imaging work was conducted on the SEM. Selected 0.00 wt% Al-Zn coated samples (immersion time of 300 seconds) were imaged in the SEM at a beam voltage of 20 kV and a condenser lens current of 1.6 A with the objective aperture set to 200 μm. These conditions resulted in good contrast BSE images with improved resolution over that of the JEOL 733 Superprobe images.

Similar beam conditions were used in an attempt to image the 0.20 wt% Al-Zn coated samples, with the exception that the condenser lens current was set to 1.7 A. However, the quality of the resulting BSE image contrast was very low. Varying the beam conditions did not improve the atomic number contrast of the samples.

SEM imaging (BSE) was also performed on selected 300 second time of immersion IF steel samples, because a significantly thick total alloy layer growth was found to form

from both zinc bath chemistries. The same SEM operating conditions were used to image selected 85 μm grain size ULC steel and P-ion implanted samples hot-dip galvanized in a 0.20 wt% Al-Zn bath.

I. Microhardness Testing

A limited number of microhardness indentations were performed on the 15 μm grain size ULC steel alloy hot-dip galvanized for 300 seconds in a 0.0 wt% Al-Zn bath. A LECO model M-400 FT microhardness tester was used for Vickers microhardness testing. A load of 25 g was used to form the indent. The diagonals of the indent were measured, and the Vickers hardness number computed. 10 indents were measured in the substrate steel, and zinc overlay layer as well as in each of the individual layers observed in a lightly etched sample cross section. The gamma phase layer was not sufficiently thick to be measured by an indent at a 25 gm load.

V. Results and Discussion

A. Effect of Substrate Steel Solute Additions

1. Morphology of Fe-Zn Phase Formation in a 0.00 wt% Al-Zn Bath

a. Formation and Growth of Fe-Zn Phases

The sequential nucleation of Fe-Zn phases occurs at the steel/coating interface in the following order; (1) zeta phase (2) delta phase and after some incubation time (3) gamma phase, as shown in Figure 34. The Fe-Zn phase layer development is also shown schematically in Figure 35, where the sequence of reaction is represented chronologically. t_0 corresponds to zero time, and development occurs according to time such that $t_0 < t_1 < t_2 < t_3 < t_4$.

Zeta, the most Zn rich Fe-Zn phase to form at the steel/coating interface, nucleates first (t_1 in Figure 35). The zeta layer nucleation is immediately followed by delta phase

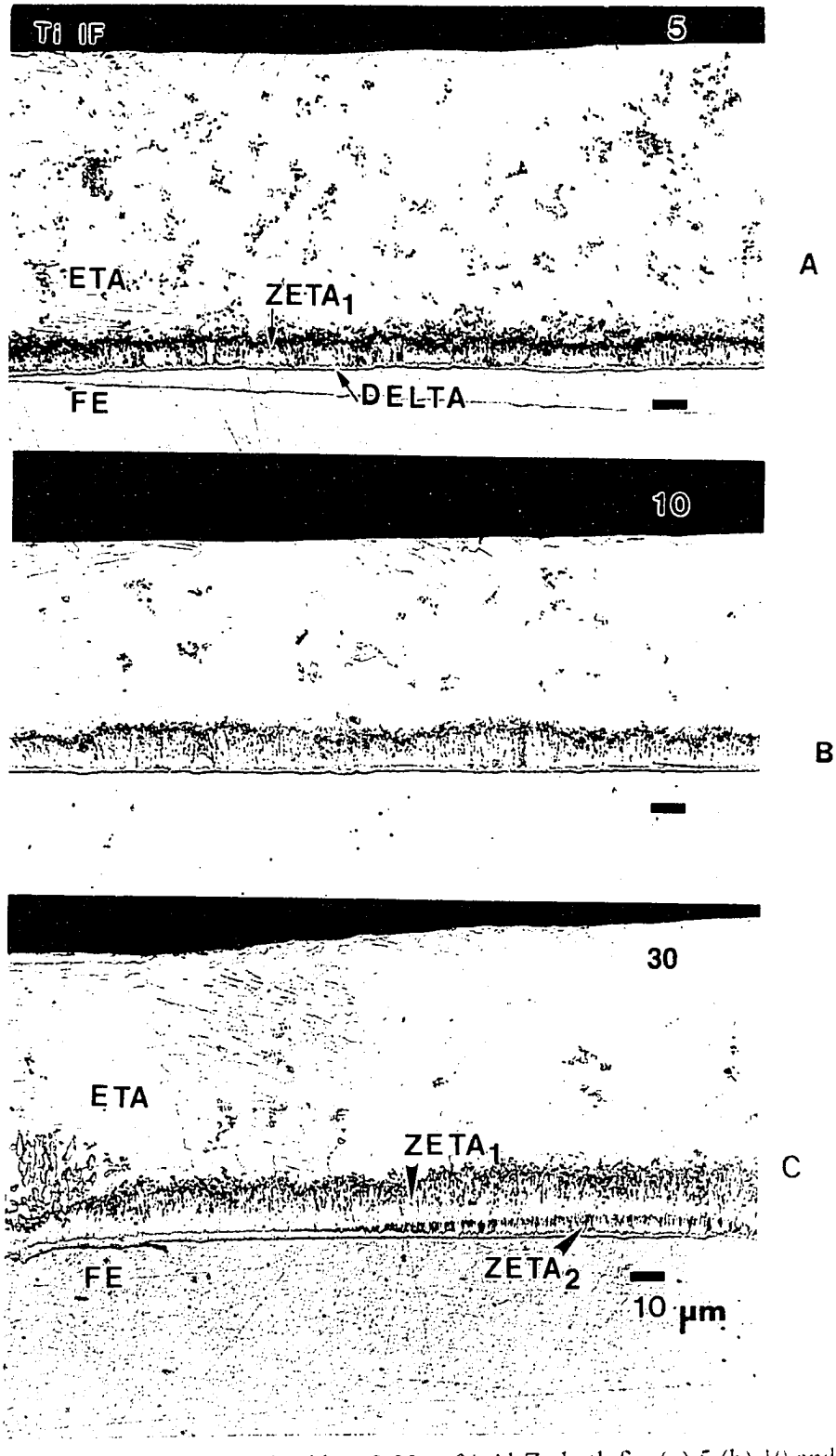

Figure 34. Ti IF steel hot-dip galvanized in a 0.00 wt% Al-Zn bath for (a) 5 (b) 10 and (c) 30 seconds of immersion.

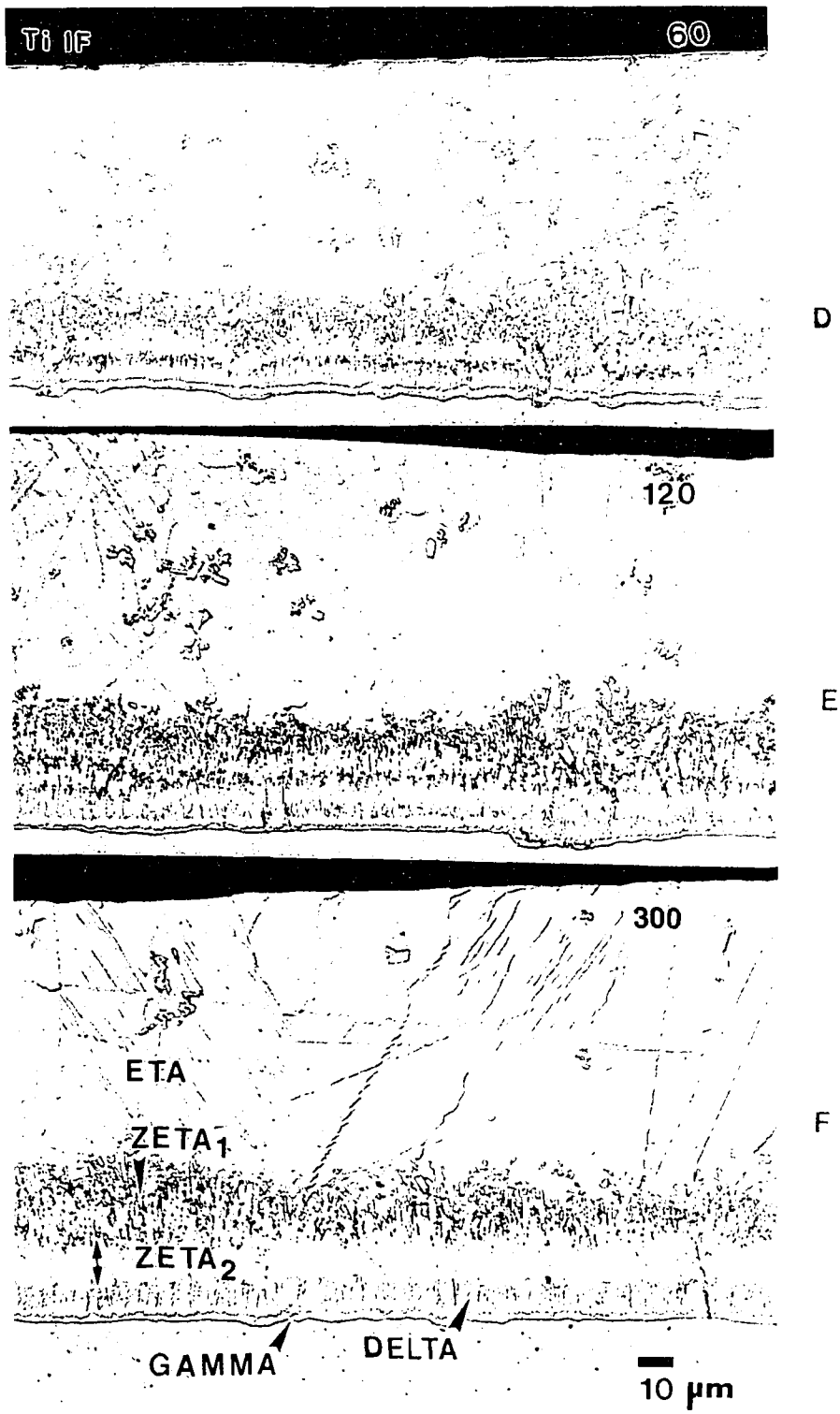

Figure 34. Ti IF steel hot-dip galvanized in a 0.00 wt% Al-Zn bath for (d) 60 (e) 120 and (f) 300 seconds of immersion.

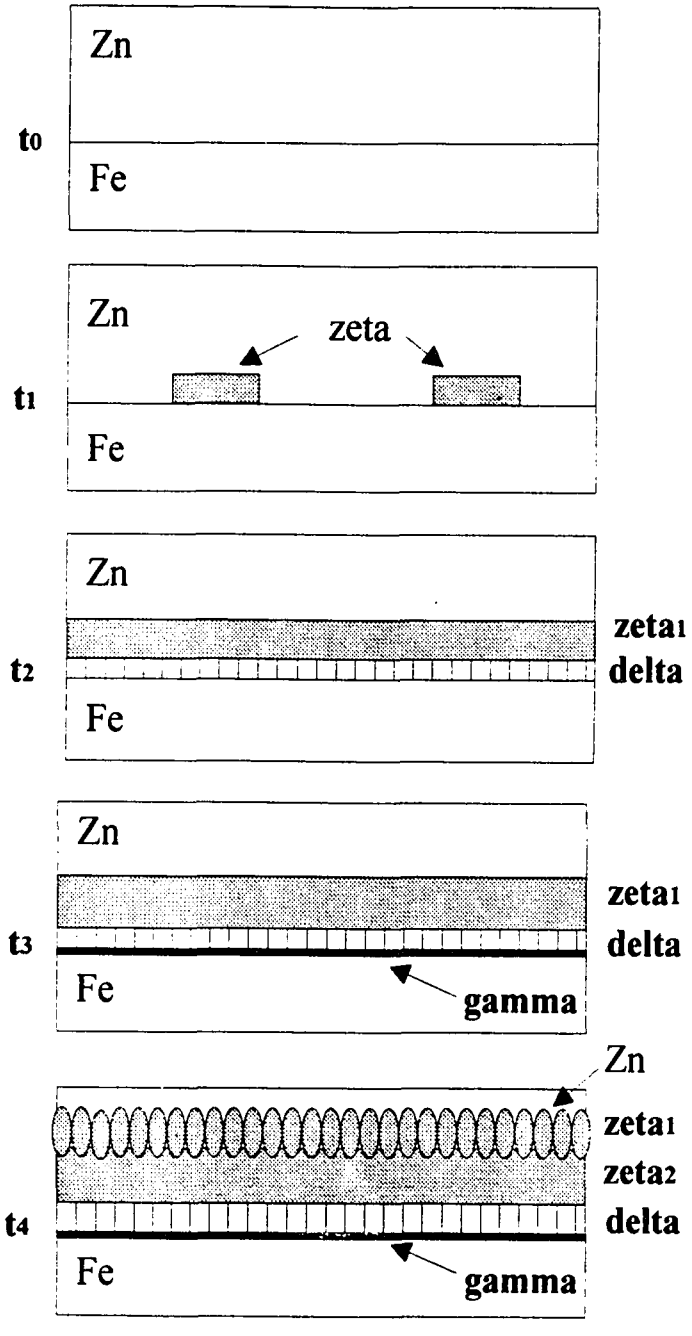

Figure 35. A schematic representation of Fe-Zn phase layer formation in a 0.00 wt% Al-Zn galvanizing bath. t_0 corresponds to zero time, and development occurs according to time, such that $t_1 < t_2 < t_3 < t_4$.

formation (t_2 in Figure 35) at the alpha Fe/zeta interface. There was no apparent delay in the formation of zeta or delta phases as both were found to form a continuous layer at the lowest reaction times, that is after 5 seconds of reaction time. The gamma phase was found to form (t_3 in Figure 35) after an incubation time of 30 seconds. The last morphological feature to develop in the 0.00 wt% Al-Zn bath was the formation of a second zeta layer ($zeta_2$) between 30 and 60 seconds of reaction time (t_4 in Figure 35) at the $zeta_1$/delta interface.

X-ray diffraction analysis of the gamma, delta and zeta phase layers results in severe peak overlap [74], especially for the delta and zeta phases, thus this type of analysis was not conducted for phase identification purposes. In order to confirm individual phase layer identification initially characterized by morphology in light optical microscopy (LOM), electron probe microanalysis for Fe and Zn composition was determined at 1.0 μm increments across the total Fe-Zn alloy layer for the 10, 60 and 300 second immersion samples. The Fe concentration profile data are plotted in Figures 36-41. The iron composition data were found to correspond to what was observed morphologically, with gamma, delta and zeta phase layer compositions (based upon metastable Fe-Zn equilibrium [24]) corresponding to the measured individual layer thickness data in Figure 42. No significant differences in the Fe composition profiles were observed for the substrates studied. The P containing substrates which showed the disappearance of the gamma phase at 300 seconds of reaction had Fe compositions at the steel/coating interface which

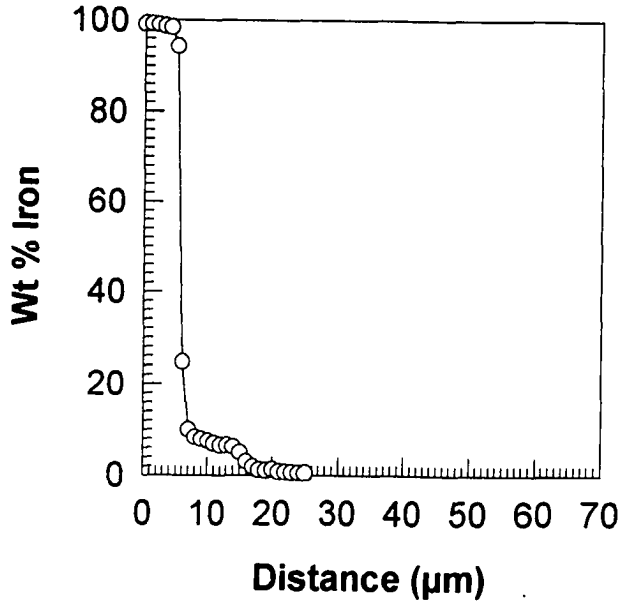

A

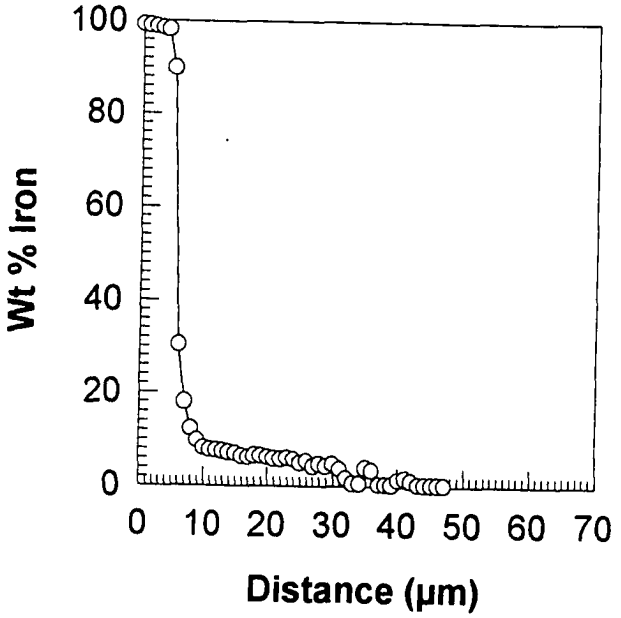

B

Figure 36. Iron concentration profile for the total Fe-Zn alloy layer formed on the 15 μm grain size ULC steel hot-dip galvanized in a 0.00 wt% Al-Zn bath for (a) 10 and (b) 60 seconds of immersion.

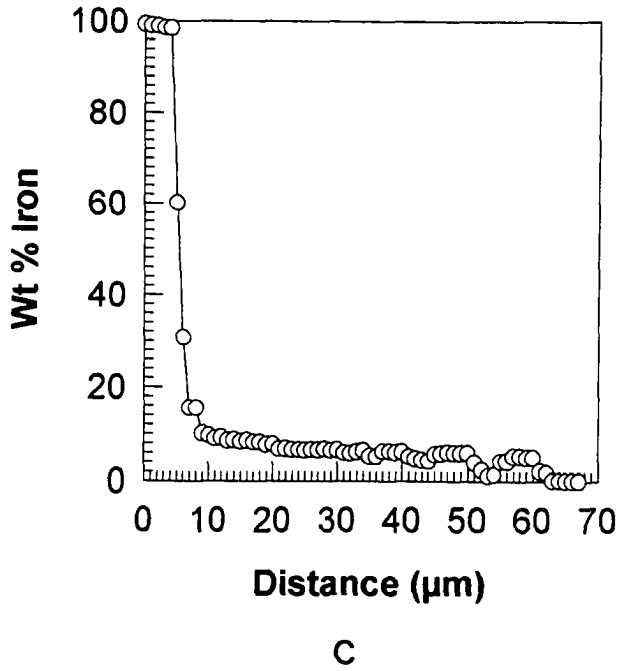

Figure 36. Iron concentration profile for the total Fe-Zn alloy layer formed on the 15 μm grain size ULC steel hot-dip galvanized in a 0.00 wt% Al-Zn bath for (c) 300 seconds of immersion.

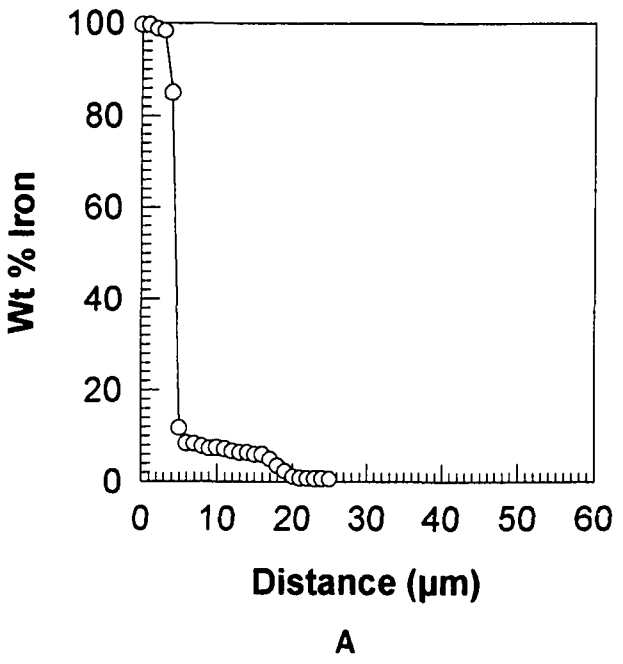

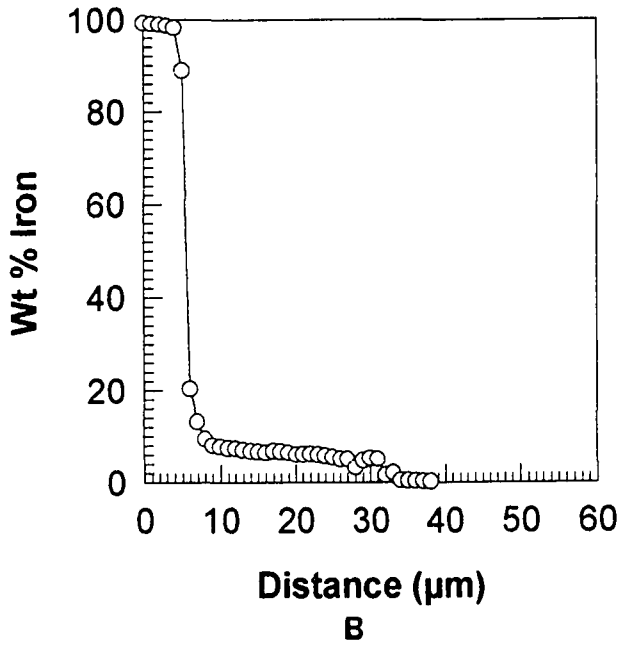

Figure 37. Iron concentration profile for the total Fe-Zn alloy layer formed on the ULC-P steel hot-dip galvanized in a 0.00 wt% Al-Zn bath for (a) 10 and (b) 60 seconds of immersion.

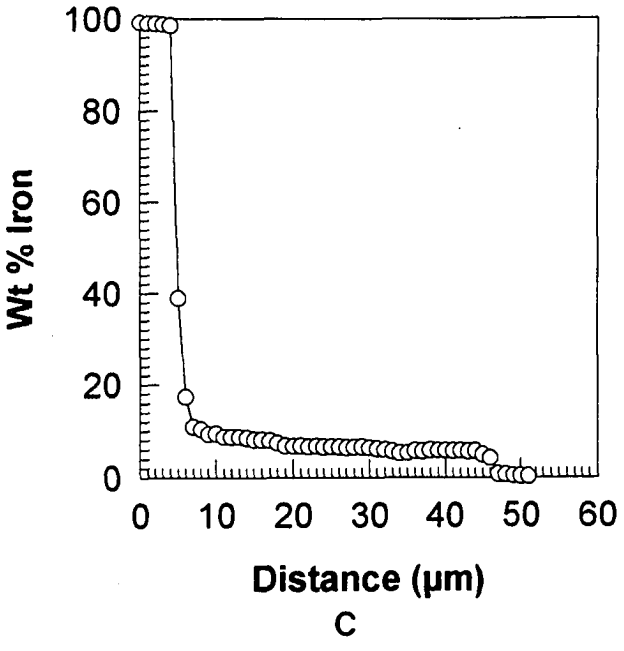

Figure 37. Iron concentration profile for the total Fe-Zn alloy layer formed on the ULC-P steel hot-dip galvanized in a 0.00 wt% Al-Zn bath for (c) 300 seconds of immersion.

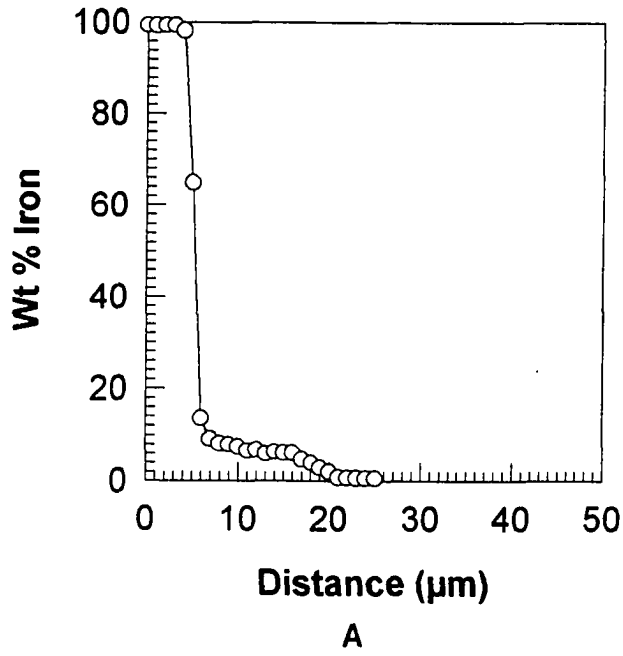

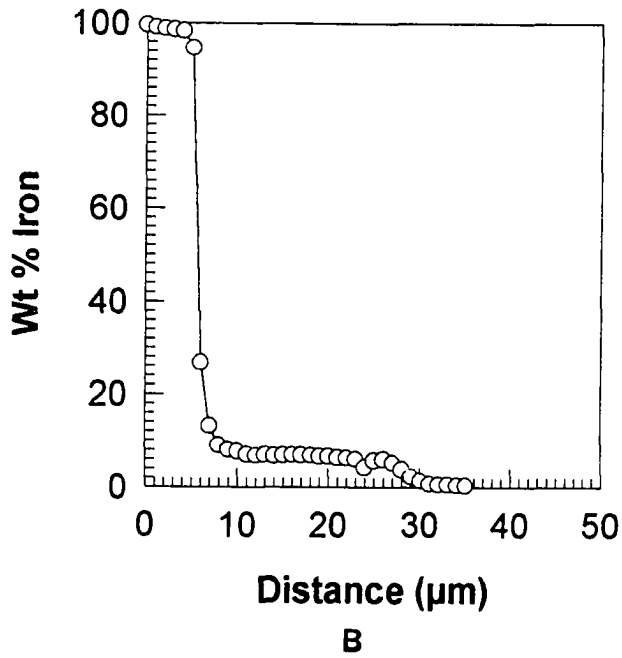

Figure 38. Iron concentration profile for the total Fe-Zn alloy layer formed on the Ti IF steel hot-dip galvanized in a 0.00 wt% Al-Zn bath for (a) 10 and (b) 60 seconds of immersion.

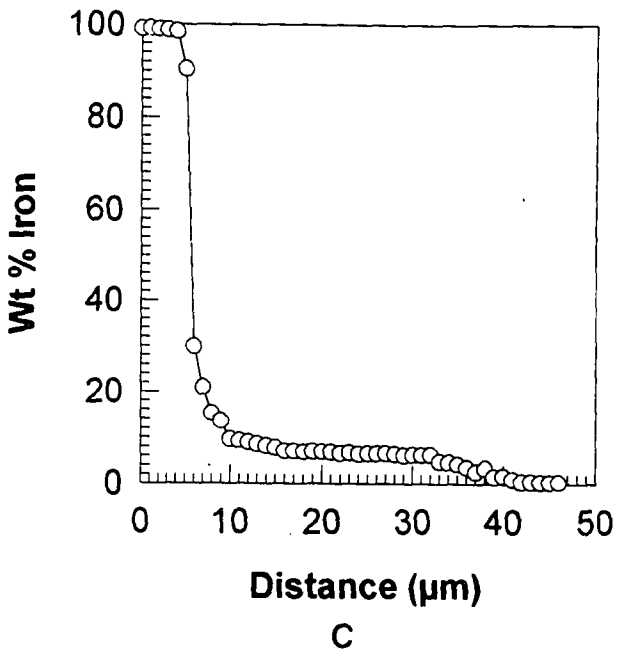

Figure 38. Iron concentration profile for the total Fe-Zn alloy layer formed on the Ti IF steel hot-dip galvanized in a 0.00 wt% Al-Zn bath for (c) 300 seconds of immersion.

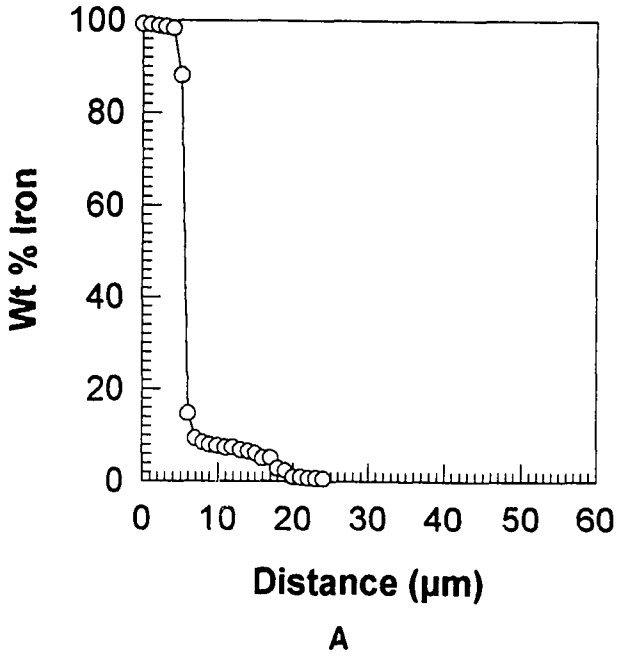

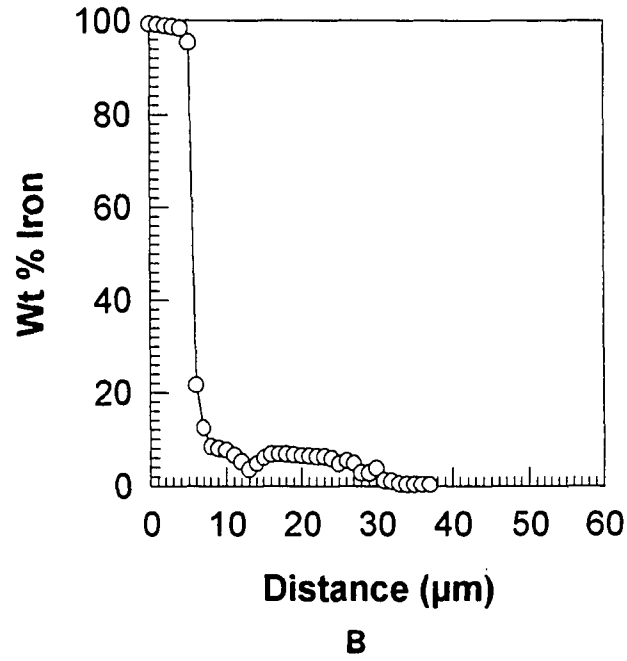

Figure 39. Iron concentration profile for the total Fe-Zn alloy layer formed on the Ti-P IF steel hot-dip galvanized in a 0.00 wt% Al-Zn bath for (a) 10 and (b) 60 seconds of immersion.

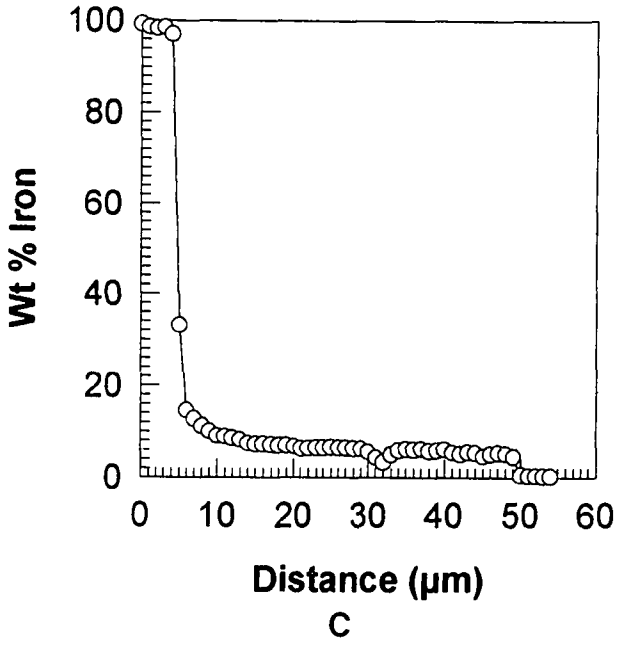

Figure 39. Iron concentration profile for the total Fe-Zn alloy layer formed on the Ti-P IF steel hot-dip galvanized in a 0.00 wt% Al-Zn bath for (c) 300 seconds of immersion.

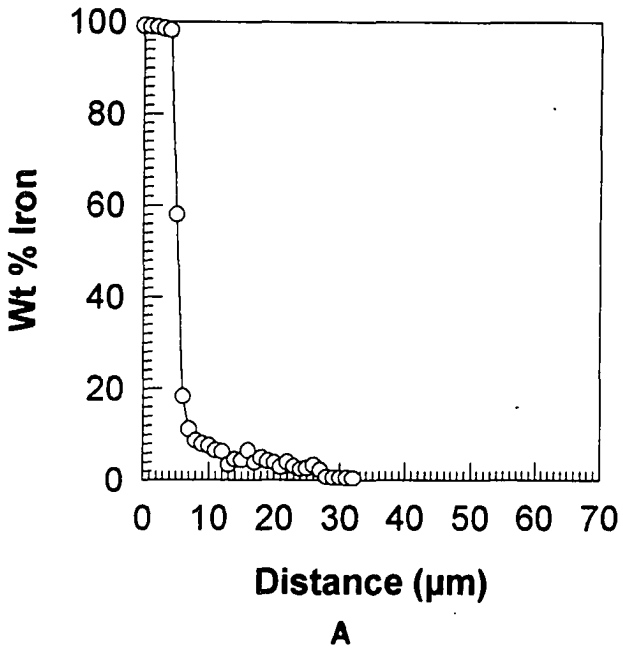

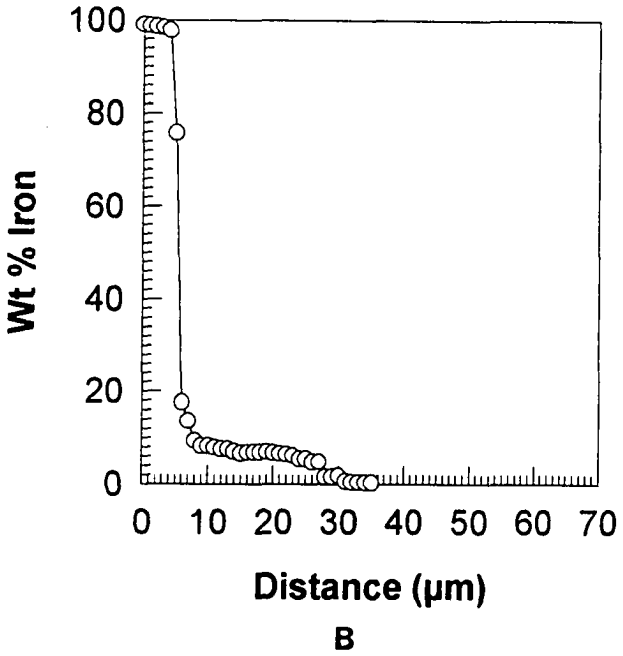

Figure 40. Iron concentration profile for the total Fe-Zn alloy layer formed on the TiNb IF steel hot-dip galvanized in a 0.00 wt% Al-Zn bath for (a) 10 and (b) 60 seconds of immersion.

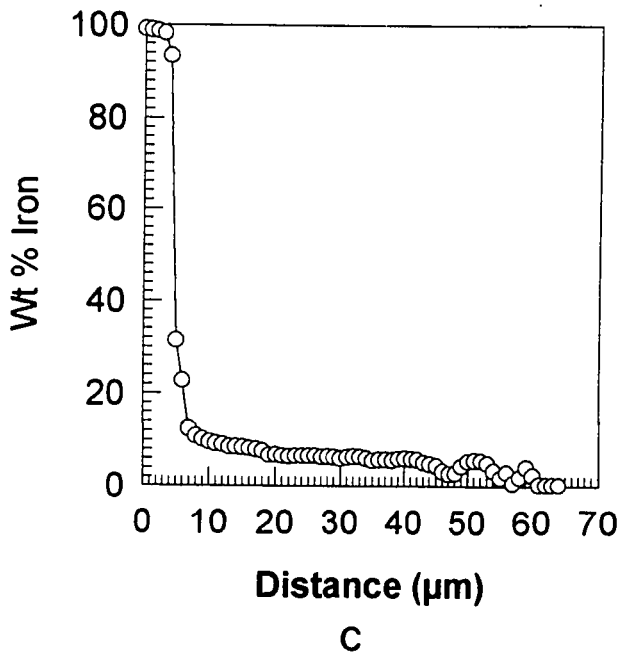

Figure 40. Iron concentration profile for the total Fe-Zn alloy layer formed on the TiNb IF steel hot-dip galvanized in a 0.00 wt% Al-Zn bath for (c) 300 seconds of immersion.

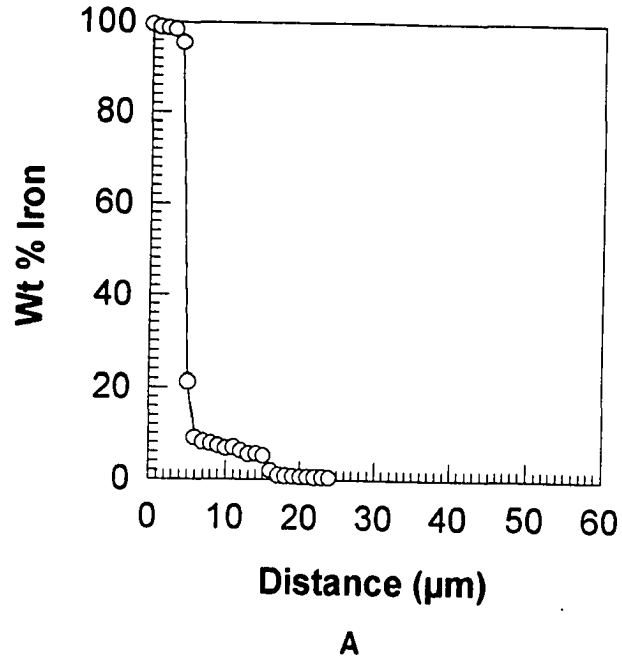

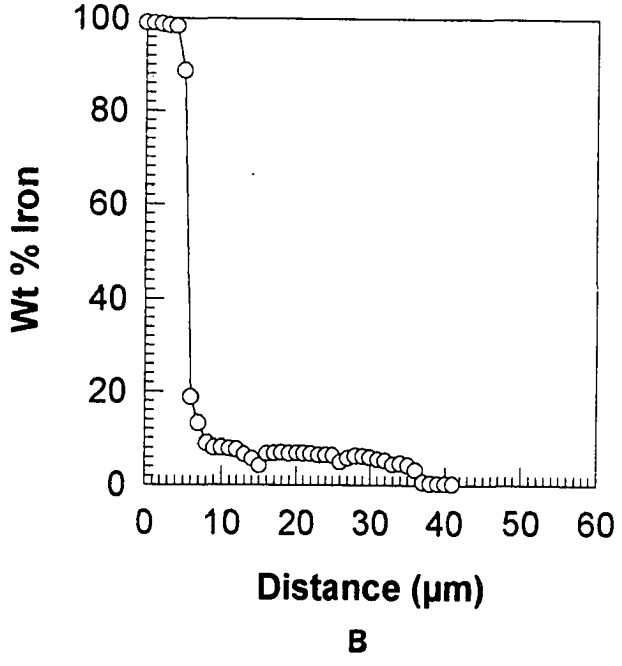

Figure 41. Iron concentration profile for the total Fe-Zn alloy layer formed on the TiNb-P IF steel hot-dip galvanized in a 0.00 wt% Al-Zn bath for (a) 10 and (b) 60 seconds of immersion.

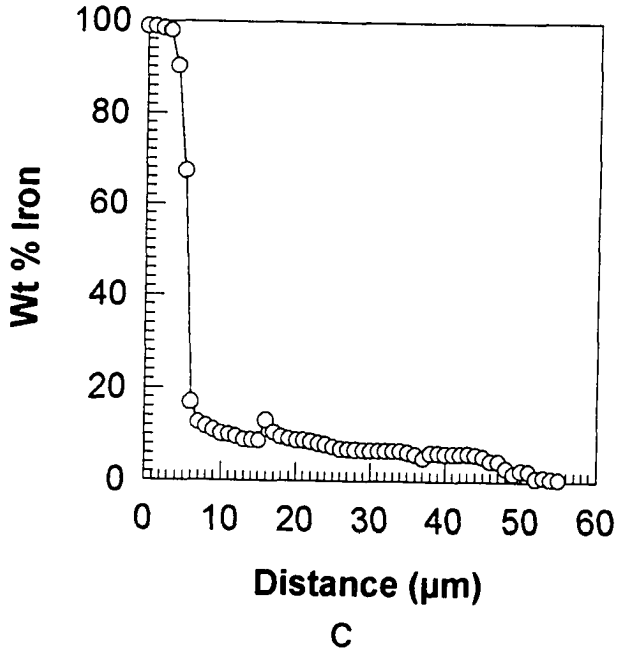

Figure 41. Iron concentration profile for the total Fe-Zn alloy layer formed on the TiNb-P IF steel hot-dip galvanized in a 0.00 wt% Al-Zn bath for (c) 300 seconds of immersion.

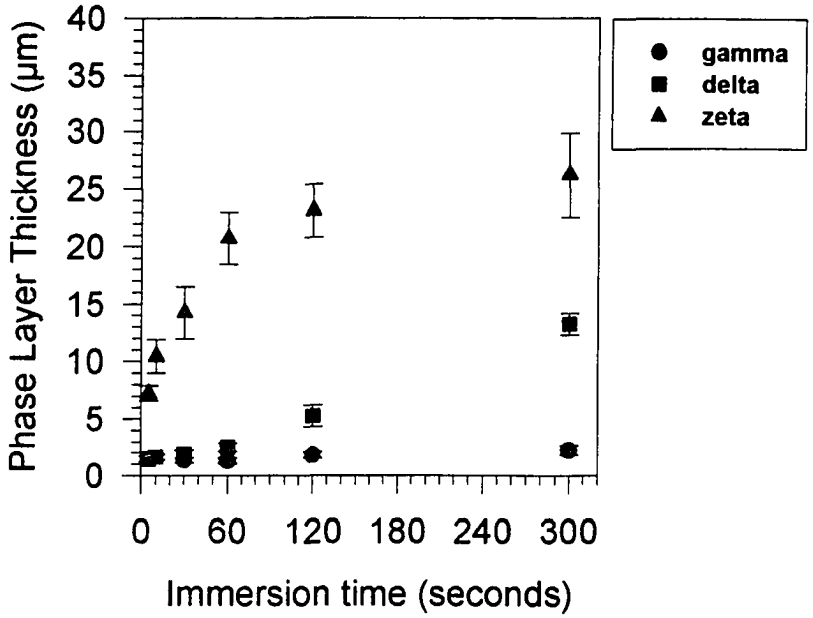

A

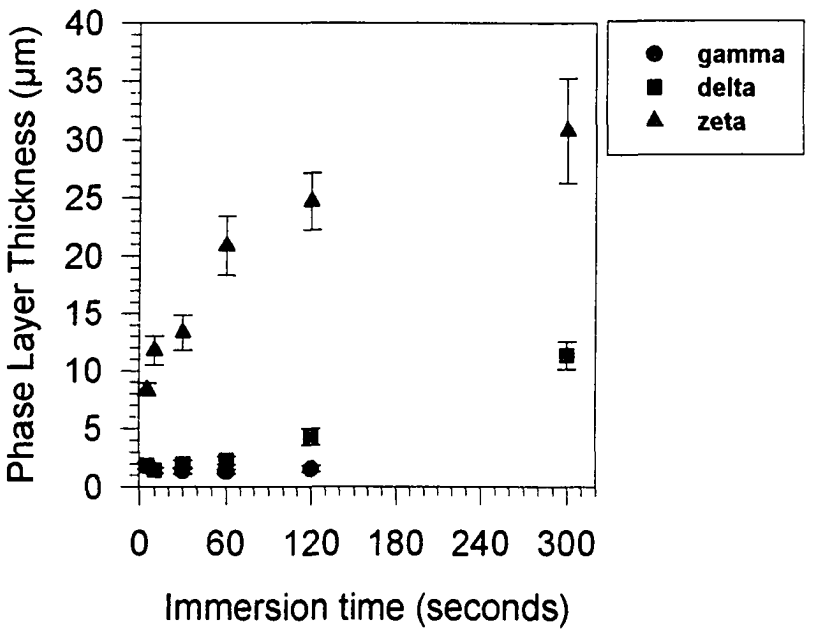

B

Figure 42. Individual Fe-Zn gamma, delta, and zeta phase layer growth for the (a) ULC (b) ULC-P steel substrates hot-dip galvanized in a 0.00 wt% Al-Zn bath.

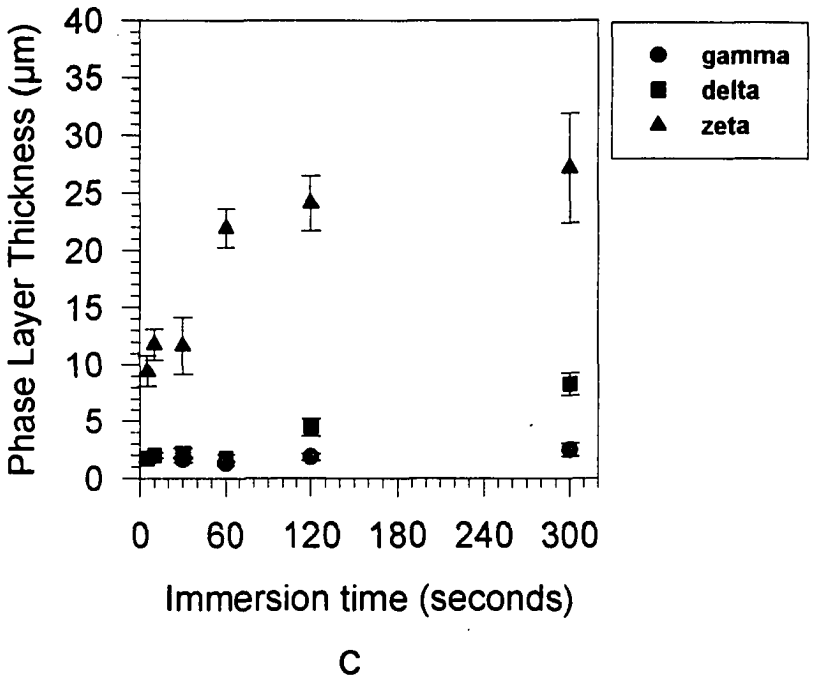

C

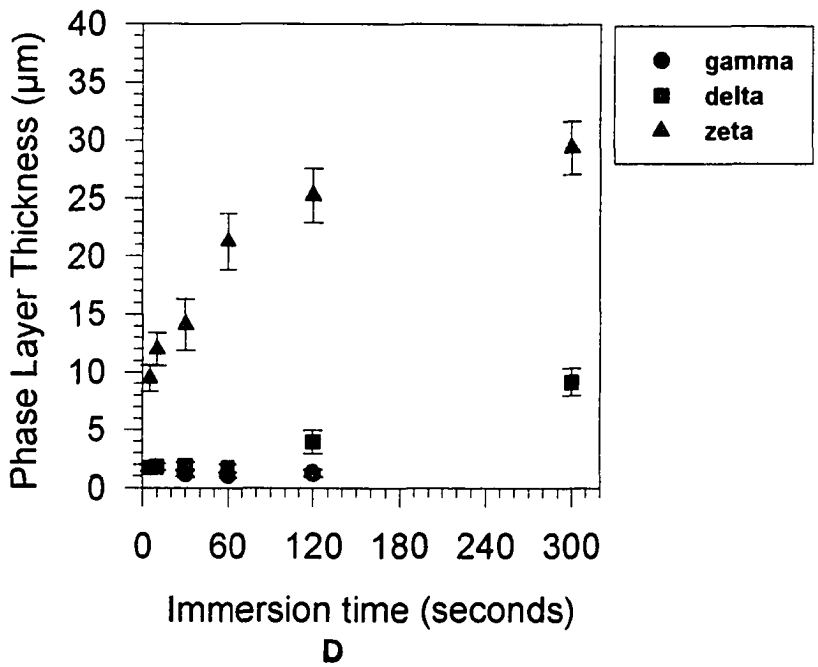

D

Figure 42. Individual Fe-Zn gamma, delta, and zeta phase layer growth for the (c) Ti IF (d) Ti-P steel substrates hot-dip galvanized in a 0.00 wt% Al-Zn bath.

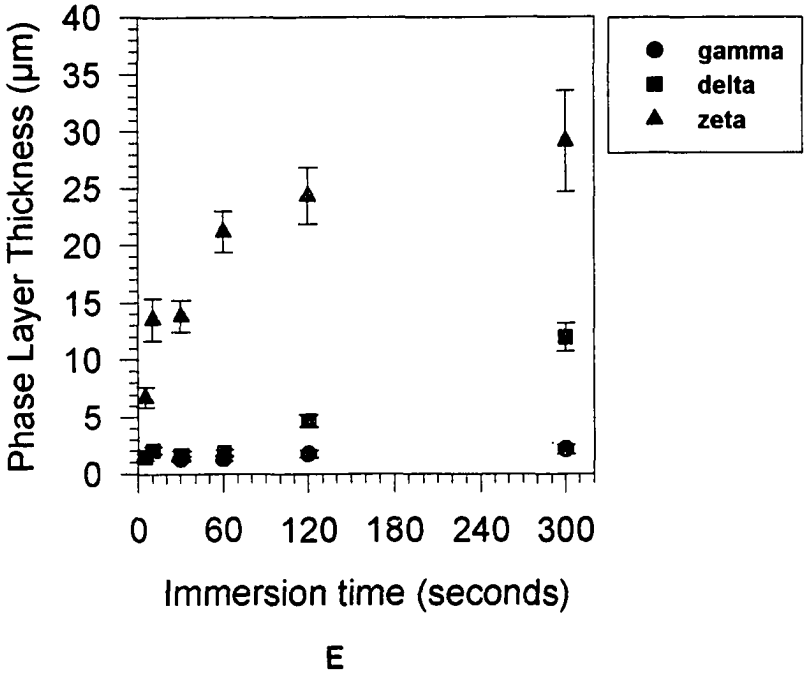

E

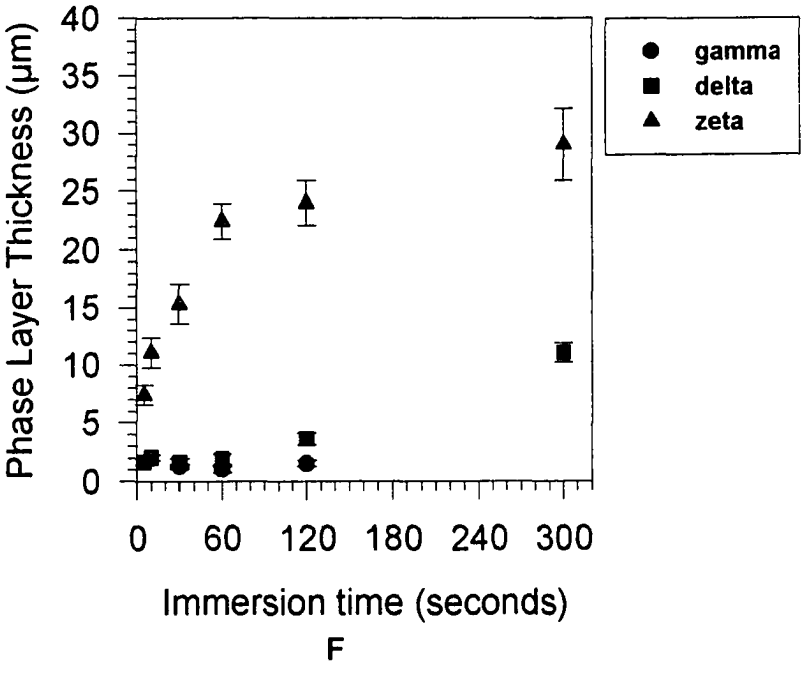

F

Figure 42. Individual Fe-Zn gamma, delta, and zeta phase layer growth for the (e) TiNb IF and (f) TiNb-P IF steel substrates hot-dip galvanized in a 0.00 wt% Al-Zn bath.

corresponded to a delta phase supersaturated in Fe, according to metastable Fe-Zn phase equilibria [24]. An example back scattered electron (BSE) image (which shows atomic number contrast in a polished and unetched sample) of a total Fe-Zn alloy layer formed in a 0.00 wt% Al-Zn bath is shown in Figure 43. The atomic number contrast visible in Figure 43 confirmed the development of a three phase Fe-Zn layer structure which was observed morphologically and identified by composition in the electron microprobe.

Microhardness testing was conducted on the individual Fe-Zn phase layers formed on the ULC steel sample immersed for 300 seconds to further confirm the Fe-Zn phase identification, especially between the delta and zeta phase layers. The 300 second immersion sample was chosen because relatively thick layers of delta and zeta phases could be analyzed. The Vickers microhardness data are reported in Table XI, and are in general agreement the with trends reported for ferrite, and the Fe-Zn delta, zeta, and eta phases [22, 44]. The gamma phase layer could not be evaluated because its layer thickness was too thin to be adequately tested at the smallest load (25g) available on the microhardness tester.

Initially the zeta phase layer grows rapidly up until 60 seconds of reaction time, while the delta and gamma phase layers showed little or no growth during the same time of reaction (Figure 42). However, from 60 to 300 seconds of reaction time zeta and gamma layer growth rates slowed, and delta layer growth accelerated. The zeta and gamma phase layers for all substrates were found to have growth kinetics following $t^{1/3}$ and $t^{1/4}$

Table XI. Vickers Microhardness Data of Individual Fe-Zn Phase Layers and ULC Substrate Steel (25 g load, 15 second dwell time).

Layer	Average Vickers microhardness number
ULC steel	85.7 ± 1.6
Delta Phase	273.2 ± 20.5
Zeta Phase	117.9 ± 9.0
Eta Phase	40.6 ± 4.7

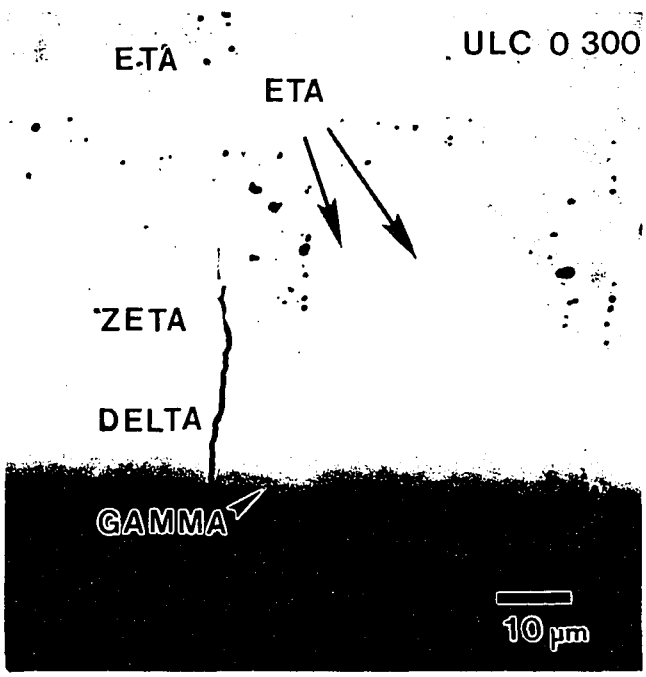

Figure 43. BSE image of the three distinct Fe-Zn phase layers formed on the 15 µm grain size ULC steel hot-dip galvanized in a 0.00 wt% Al-Zn bath for 300 seconds of immersion.

relationships, respectively, (see following section V. A. 2) indicating their growth may follow grain boundary diffusion controlled growth. That both zeta and gamma phase layers show growth-time relationships less than $t^{1/2}$ indicates that the supply of Zn to these growth layers is reduced as a function of time.

The reduction of Zn supply through the zeta layer could be due to coarsening of the zeta phase columnar structure during diffusional growth. As the width of the zeta phase columnar structure increases during the reaction less columnar boundary area is available for fast diffusion of liquid Zn, and the Zn supply becomes limited as liquid channels of Zn in contact with the zeta layer become narrower and are eventually blocked by the growth and coarsening of the zeta phase layer itself. The zeta phase has a columnar needle-like morphology (Figure 34) indicative of a type of morphology found for grain boundary diffusion controlled kinetics [75], as shown in Figure 44b.

The gamma phase layer also may have had a morphology indicative of grain boundary diffusion controlled growth similar to that shown in Figure 44e and f. The limiting mechanism of the grain boundary diffusion of Zn for gamma phase growth could be due the recrystallization of the gamma layer during the galvanizing reaction at 450°C. Because recrystallization can occur at about 0.75 T_m, (T_m = melting temperature in Kelvin) recrystallization of the gamma phase can then possibly occur at 791 K, or 518°C (T_m = 782°C). For the $gamma_1$ phase recrystallization can occur at a temperature of 344°C (T_m = 550°C). In this study it was not possible to distinguish between gamma and $gamma_1$

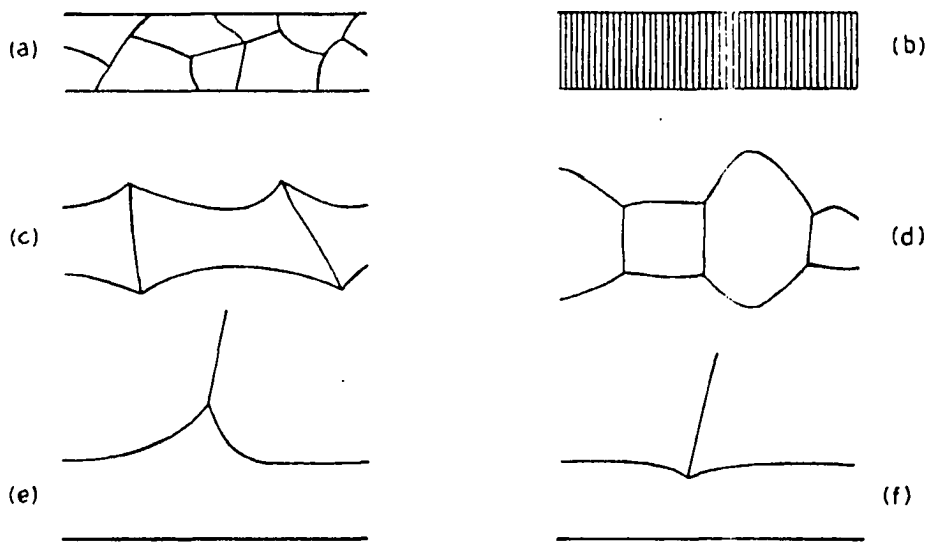

Figure 44. Various morphologies of a reaction layer in a binary diffusion couple (a) volume diffusion, (b)-(c) and (e)-(f) grain boundary diffusion, and (d) growth along a preferred crystallographic direction, controlled processes [75].

phases at the interface, however, the gamma$_1$ phase has typically been found to form as a distinct layer between the delta and gamma phases after long time annealing in solid Fe-Zn diffusion couples [22] or at elevated temperatures of annealing, such as 500-550°C [56, 76], thus the gamma phase layer studied here is most likely not gamma$_1$ phase, and the temperature of galvanizing (450°C) was then not sufficient to cause recrystallization of the gamma phase layer. Adachi [77] found that grain growth did not occur in the gamma phase during annealing at 500°C, therefore it most likely did not occur in this study during galvanizing at 450°C. Therefore recrystallization and grain growth of the gamma layer do not account for the observed $t^{1/4}$ kinetics of growth of the gamma phase layer during galvanizing. Possibly the growth of the delta phase layer also influences the growth of the gamma phase. The migration of the delta phase has been found to occur in two directions, both toward the Zn melt and zeta phase layer, as well as toward the substrate steel and gamma phase layer (Figure 22). The consumption of the gamma phase by the rapidly growing delta phase layer may best explain the non-parabolic growth behavior of the gamma phase layer.

The delta layer, like the zeta phase layer, showed a two stage growth development for all substrates, with a transition in growth occurring at 60 seconds of reaction time (Figure 42). After formation the delta layer had little or no growth up to 60 seconds, and thereafter delta layer growth was rapid. At 60 seconds of immersion time liquid Zn was able to penetrate the zeta phase layer and react with the delta phase layer, thus resulting in an increased rate of growth of the delta phase. The delta phase layer appeared to grow at

the expense of the zeta phase layer because 60 seconds of reaction time was also the point at which voids were found to develop within the zeta phase layer, and its growth rate slowed.

b. Void Formation in the Zeta Phase

Based upon light optical microscopy (LOM), at 30-60 seconds of reaction a horizontal array of voids were found to form within the zeta layer (see Figure 34d-f). The voids distinguishing the two zeta phase layers were found upon repolishing and back scattered electron (BSE) imaging analysis of the unetched structure to be entrapped eta phase (solidified Zn) (Figure 43). The growth of the zeta layer was analyzed as two separate layers: (1) $zeta_1$ which was defined as the layer adjacent to the delta layer before void formation, and (2) $zeta_2$ which formed at the $zeta_1$/delta interface at 60 seconds of reaction time. The growth of the two zeta layers is presented in Figure 45. The $zeta_1$ layer showed rapid growth from 5 - 30 seconds, then at 60 seconds the formation of the $zeta_2$ layer occurred and the $zeta_1$ layer then showed essentially no growth from 60 - 300 seconds of reaction and the entrapped eta phase remained at a constant distance from the Zn/$zeta_1$ interface.

Channels of liquid Zn were found to reach the $zeta_1$/delta phase by transport along the columnar structure of the $zeta_1$ phase layer. Therefore the initial rapid growth (< 30 seconds) of the $zeta_1$ layer could occur according to linear interface controlled kinetics.

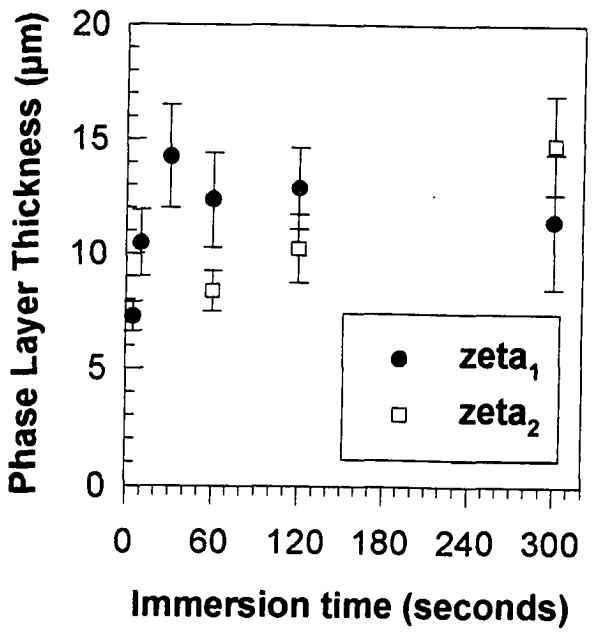

Figure 45. Separate $zeta_1$ and $zeta_2$ phase layer growth for the ULC steel hot-dip galvanized in a 0.00 wt% Al-Zn bath.

The growth of the $zeta_1$ layer changes over from linear to parabolic growth at approximately 60 seconds. Sixty seconds of reaction time corresponds to the time of $zeta_2$ layer formation at the $zeta_1$/delta interface, and also to the point at which voids are found to form. Van Loo [78] found a similar reaction layer morphology in a $TiAl_3$ growth layer formed between Ti and Al in a solid Ti-Al diffusion couple, where Al was the dominant diffusing species. The $TiAl_3$ layer developed an internal horizontal array of pores which remained at a constant distance from the Al/$TiAl_3$ interface. Van Loo also found the initial linear reaction to be difficult to determine due to the short time of duration (a few hours). In the Fe-Zn system the possible observed linear growth duration for the $zeta_1$ phase layer is approximately 5-60 seconds, and its kinetics were also difficult to define as linear according to the growth data.

In the case of the liquid-solid diffusion couple analyzed here, the zeta layer grows linearly up to a critical thickness (10-15 μm) which occurred after 30-60 seconds of reaction time. After this initial growth, further growth of the zeta phase layer may become unstable due to growth stresses that have developed within the zeta layer. The surface contact of the zeta layer with the liquid Zn may keep the outermost columnar structure of the zeta phase in tension and thus allows for liquid Zn penetration along the columnar zeta layer and reaction at the zeta/delta phase interface. After liquid Zn reaches the zeta/delta interface a new zeta layer ($zeta_2$) formed. The first zeta layer that formed ($zeta_1$) did not show growth after 60 seconds. As stated earlier 60 seconds of reaction was the time at which both the formation of entrapped eta occurred and the delta layer growth accelerated as the

total zeta layer growth slowed. In the Fe-Zn system gamma and delta phase layers are formed in addition to the zeta phase layer and the rapid growth of the adjacent delta layer must also be considered in how it affects the zeta layer growth pattern.

c. Disappearance of Gamma Phase

The gamma phase layer was found to disappear on all of the P containing substrates (galvanized in 0.00 and 0.20 wt% Al-Zn baths) after 300 seconds of reaction. According to Horstmann [16] the gamma phase should form at the substrate alpha Fe/gamma interface during the reaction between Fe and Zn. The gamma layer formation and growth appears to occur for reaction times between 30 and 300 seconds on the ULC, Ti IF and TiNb IF steels, however, for the P containing steels the growth of gamma layer occurs only up to 120 seconds of reaction. After 120 seconds the rapidly growing delta phase consumes the gamma phase on the P containing alloys as shown in Figure 46.

The observed disappearance of the gamma phase may be due to the supply of Fe from the substrate steel being eliminated. If the chemical potential of Fe at the substrate/gamma interface were to become negligible, the driving force for Fe diffusion would be eliminated. For the P containing substrates it appears as though the supply of Fe from the substrate has been significantly reduced, thus the gamma phase would then serve as the source of Fe atoms for delta layer growth occurring at the gamma/delta interface.

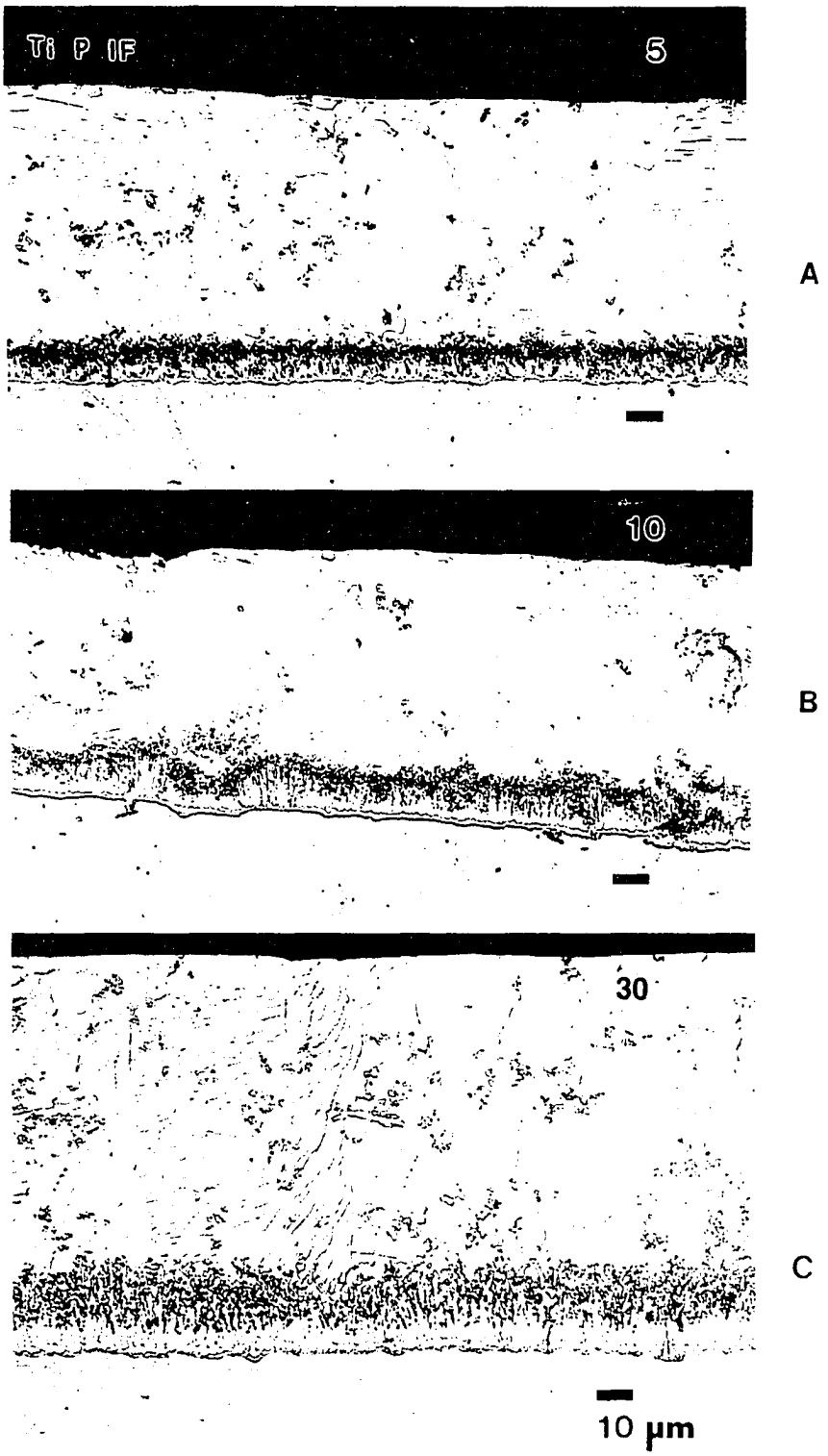

Figure 46. Ti-P IF steel hot-dip galvanized in a 0.00 wt% Al-Zn bath for (a) 5 (b) 10 and (c) 30 seconds of immersion.

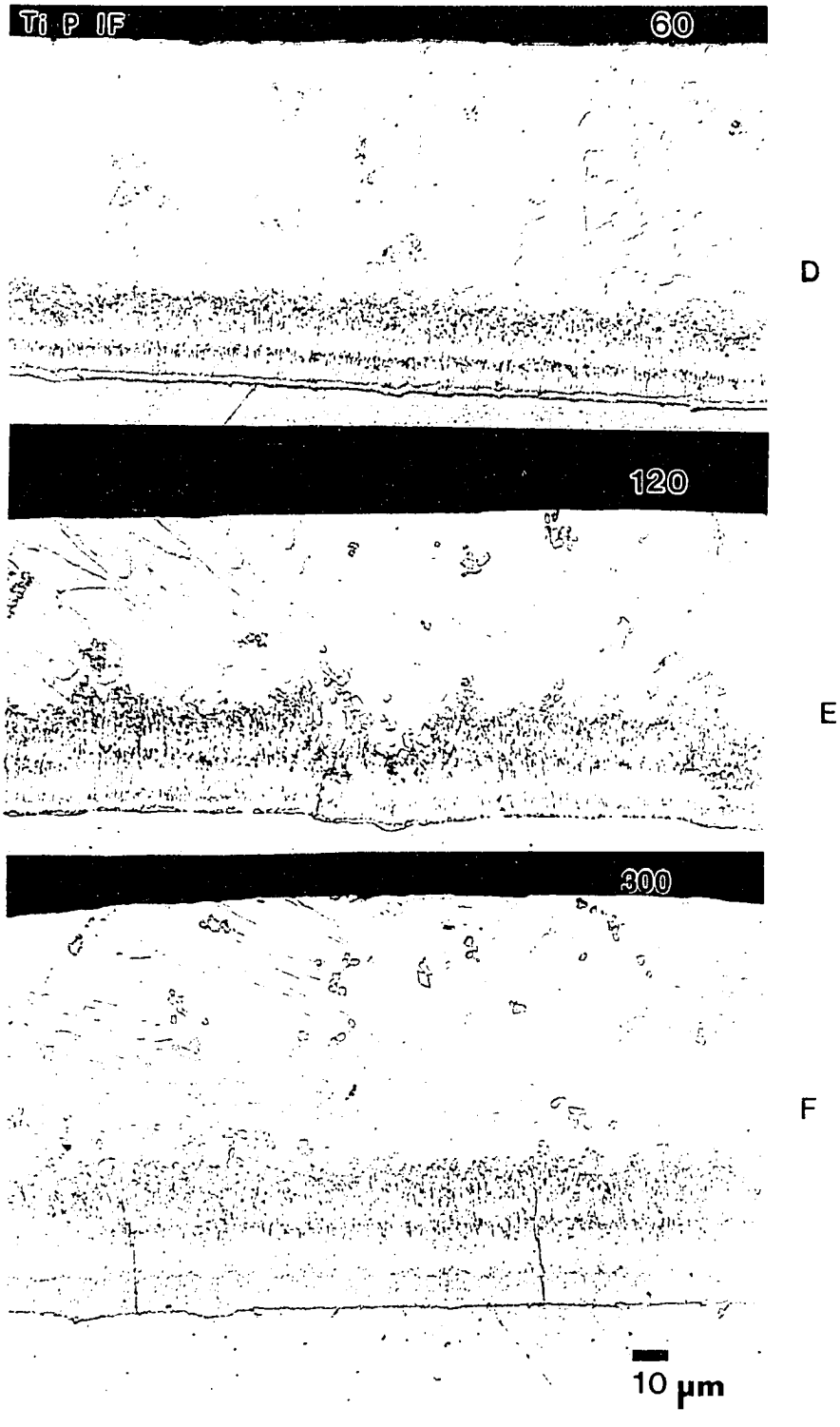

Figure 46. Ti-P IF steel hot-dip galvanized in a 0.00 wt% Al-Zn bath for (d) 60 (e) 120 and (f) 300 seconds of immersion.

A well documented mechanism about the role of P in low and ultra low carbon substrate steel is that P segregates to substrate grain boundaries during recrystallization annealing [55] and thus blocks the diffusion of Zn along these fast diffusion paths during hot-dip galvanizing. Allegra found that P in excess of 0.04 wt% in low carbon steels (0.04-0.05 wt % C), segregated to ferrite grain boundaries, thus preventing grain boundary Zn diffusion during galvanizing in a 55 wt% Al-Zn bath. The ULC-P, Ti-P IF, and TiNb-P IF steels discussed here contained 0.06-0.07 wt % P and 0.003-0.006 wt% C, a chemistry similar to that studied by Allegra, therefore P segregation to ferrite grain boundaries in IF steels most likely influences Fe-Zn reactions.

2. Kinetics of Fe-Zn Phase Growth in a 0.00 wt% Al-Zn Bath

Six interstitial free steels (with grain sizes of approximately 10-20 μm) were analyzed to determine reaction kinetics during hot-dip galvanizing in a 0.00 wt % Al-Zn bath for 5-300 seconds of immersion. The total Fe-Zn alloy layer or reaction layer was typically of a uniform thickness and its coverage at the steel/coating interface was complete. Fe-Zn total alloy layer development was similar on all of the steel substrates, and an example of Fe-Zn alloy layer development on the Ti IF steel substrate is shown in Figure 34. The total Fe-Zn alloy layer thickness was measured for each reaction time studied, and the growth data for the six steel substrates studied are shown in Figure 47.

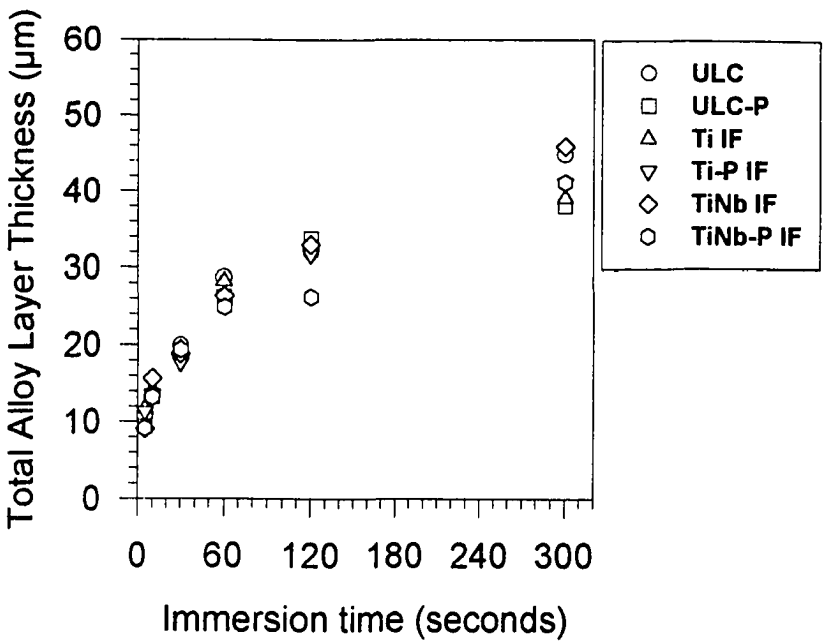

Figure 47. Total Fe-Zn alloy layer growth for substrate steels hot-dip galvanized in a 0.00 wt% Al-Zn bath.

a. Total Alloy Layer Growth

To evaluate the kinetics of total Fe-Zn alloy layer growth, a power law growth equation

$$Y = Kt^n \qquad (1)$$

was used to interpret the growth data where Y is the growth layer thickness, t is reaction time, K is a growth rate constant, and n is the growth rate time constant. By applying a logarithmic function on either side of equation (1),

$$\log Y = \log K + n \log (t) \qquad (2)$$

and plotting the log value of the total alloy layer thickness (Y) as a function of the log value of immersion time in the bath (t) a line can be fitted to the data whose slope is n, the growth rate time constant value [16], and whose y-intercept is log K, a log value of the growth rate constant. The growth rate time constant value is an indication of the type of kinetics controlling the growth of the layer under study. An n value of 0.5 is indicative of parabolic diffusion controlled growth, while an n value of 1.0 is representative of linear kinetics in which growth is interface controlled.

The total Fe-Zn alloy layer was analyzed to determine growth rate time constant values. The n values were determined from a linear regression analysis in the software program Sigma Plot (copyright Jandel Scientific) and are shown in Table XII. The n values were found to range from 0.31 to 0.37, and do not match a 0.50 value expected for parabolic volume diffusion controlled growth. The total alloy layer growth instead followed a $t^{1/3}$ ($n \sim 0.33$) relationship. As discussed previously on the morphology of individual Fe-Zn phase layer growth, liquid Zn was found to penetrate along the columnar structure of the zeta phase (the thickest phase layer in the total alloy layer and the phase layer in direct contact with the Zn melt during immersion). Zeta phase layer growth was also found to follow $t^{1/3}$ kinetics, therefore it appears as though the kinetics of growth of the Fe-Zn phase layer in contact with the Zn melt controlled the overall growth rate of the total alloy layer.

Table XII. Total Fe-Zn Alloy Layer Growth Rate Time Constant (n) Values for Steels Hot-Dip Galvanized in a 0.00 wt% Al-Zn Bath.

Sample	Growth Rate Time Constant, n
ULC	0.35 ± 0.02
ULC-P	0.35 ± 0.03
Ti IF	0.31 ± 0.02
Ti-P IF	0.33 ± 0.02
TiNb IF	0.37 ± 0.03
TiNb-P IF	0.34 ± 0.03

Although the growth of the total Fe-Zn alloy layer did not follow a $t^{1/2}$ relationship, its growth was controlled by a steady state diffusion process. For a steady state diffusional growth process, plotting the concentration of Fe in the total Fe-Zn alloy layer as a function of $x/t^{1/2}$ (where x is a distance parameter, and t is reaction time) an invariant penetration plot over the reaction times studied should result. As shown in Figure 48, the penetration curve was invariant for the Fe-Zn reaction layer formed at 10, 60 and 300 seconds of reaction time on the ULC steel hot-dip galvanized in the 0.00 wt % Al-Zn bath. The penetration curves for the other steel substrates studied in this bath were also invariant over 10-300 seconds of reaction time in the Zn bath. Onishi [31] has previously shown that in solid Fe-Zn diffusion couples annealed at 410°C in which molybdenum markers were placed at the original Fe/Zn interface, the markers were always found at the Zn/zeta phase interface for reactions studied up to 100 hours of annealing time. Onishi's results indicate that one sided diffusion of Zn through the Fe-Zn phases dominates the

total alloy layer growth rate, and the penetration curve in Figure 48 shows a steady state diffusion process controls the total Fe-Zn growth reaction.

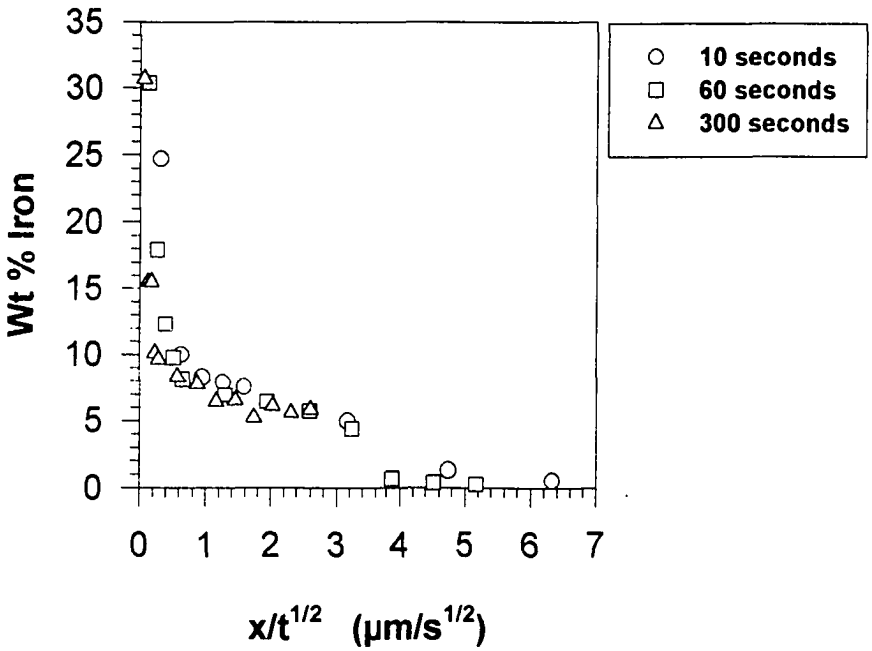

Figure 48. Iron concentration penetration curve for the 15 µm grain size ULC steel substrate hot-dip galvanized in a 0.00 wt % Al-Zn bath.

Because the kinetics of the total Fe-Zn alloy layer did not follow the expected parabolic kinetics, an attempt was made to evaluate total alloy layer growth according to linear parabolic kinetics as proposed by Dybkov [79], and later shown to exist in the Au-In system by Millares [80]. However, the total alloy layer growth data (as well as individual Fe-Zn phase layer growth data) for the Fe-Zn system were found not to follow linear-parabolic reaction kinetics, as is shown in Appendix D. One explanation for the observed $t^{1/3}$ growth kinetics is that the total alloy layer growth is controlled by diffusion along

intermetallic Fe-Zn phase layer grain boundaries (perhaps during coarsening of the zeta phase layer) instead of by bulk Fe and Zn interdiffusion.

In the Fe-Zn system discussed here the total alloy layer did not follow parabolic or linear parabolic kinetics. Similar results have been found in thin film reaction layer growth analysis. The initial nucleation and growth to coalescence of a product phase as determined by calorimetry (prior to the formation of a contiguous layer) can cause analysis of the growth data to not follow parabolic or linear-parabolic kinetics [81]. Analysis of just the growth of the reaction based on linear, parabolic, or linear-parabolic kinetics assumes that a contiguous layer exists at t = 0, and that nucleation is irrelevant to the kinetic analysis. In the Fe-Zn system studied here, the shortest time of reaction studied (5 seconds) resulted in the formation of a continuous layer of both zeta and delta phases. Although the initial nucleation of zeta (t_1 in Figure 35) was not directly observed, phase nucleation may have significantly affected the kinetics of phase growth.

If the nucleation site density for the first phase to form (zeta phase) was high then the growth data should have followed linear parabolic growth, however the zeta phase layer did not follow this growth behavior, as shown in Appendix D. Because the zeta phase layer had already grown to a thickness of 5-10 μm after 5 seconds of reaction, the product layer in the Fe-Zn system formed under the galvanizing conditions used in this study is many orders of magnitude larger than the nm scale reaction layers studied in thin films by [81]. The nucleation sites for the zeta phase may therefore have been separate by

distances in the range of 0.1-10 μm. The lower bound of 0.1 μm can be estimated based upon the fact that in thin film reactions the scale of localized nucleation and growth events prior to coalescence is on the nm scale (approximately 15 nm in the Nb/Al system [81]), and at least 1 or 2 orders of magnitude increase in the average nucleation site distance must have been present in the Fe-Zn reactions analyzed here in order to observe the non-linear-parabolic growth of the zeta phase. The upper bound of nucleation site distance was estimated based upon the total thickness of the zeta phase layer formed at the shortest reaction time studied because in thin film reactions the nucleation site distance is typically less than the thickness of the reaction layer formed. If these assumptions are valid then the upper bound of the estimated distance between nucleation sites approaches the grain size of the steel (10-20 μm). Preferential nucleation sites for zeta phase may have existed at substrate grain boundary sites, and the nucleation at these sites therefore may explain the non-parabolic and non-linear-parabolic growth behavior of the zeta phase and total Fe-Zn reaction layer.

b. Individual Phase Layer Growth

All of the substrate steels showed the development of a three layer morphology of gamma, delta and zeta phases, as shown in Figures 34 and 35. Zeta the most Zn rich Fe-Zn phase formed first followed sequentially by delta and gamma phase layers. The delta and zeta phase layers were present at all of the reaction times studied (5-300 seconds), whereas the gamma phase often had an incubation time of 30 seconds associated with its formation.

Individual phase layer growth data for gamma, delta, and zeta phase layers formed on each of the substrate steels studied are shown in Figure 42.

(i). Gamma Phase Layer Growth

The gamma phase was first observed at 30 seconds of reaction time on all of the substrate steels studied. Phosphorus containing substrates showed a disappearance of the gamma layer at 300 seconds of reaction time, after exhibiting gamma layer growth at 30, 60, and 120 seconds of immersion in the bath, as shown in Figure 46 for Fe-Zn alloy layer development on the surface of the Ti-P IF steel substrate.

The gamma layer thickness data were first fit to determine n values over the corresponding reaction time ranges over which an interfacial gamma layer was observed on each individual substrate steel. The n values are listed in Table XIII. Growth rate time constant (n) values for the ULC, Ti IF and Ti Nb IF steel alloys were between 0.22 - 0.24, and were within the error values of one another, indicating gamma layer growth followed a $t^{1/4}$ relationship. The n values for the P containing alloys ranged from 0.035 - 0.13 and had a large error associated with their values due to the disappearance of the gamma phase at 300 seconds, and to the reduced number of data points over which the data could be fitted. Although the error was large for the growth rate time constant (n) values determined for the P containing alloys, P substrate solute additions were found to significantly retard the kinetics of gamma phase layer growth.

Table XIII. Individual Fe-Zn Phase Layer Growth Rate Time Constant (n) Values for the Steels Hot-Dip Galvanized in a 0.00 wt% Al-Zn Bath.

Sample / Layer	Growth Rate Time Constant, n
Gamma Phase Layer	
ULC	0.24 ± 0.06
ULC-P	0.10 ± 0.08
Ti IF	0.22 ± 0.11
Ti-P IF	0.035 ± 0.080
TiNbIF	0.23 ± 0.05
TiNb-P IF	0.13 ± 0.28
Delta Phase Layer	
ULC	0.51 ± 0.11
ULC-P	0.44 ± 0.12
Ti IF	0.34 ± 0.12
Ti-P IF	0.37 ± 0.13
TiNbIF	0.44 ± 0.15
TiNb-P IF	0.39 ± 0.15
Zeta Phase Layer	
ULC	0.32 ± 0.03
ULC-P	0.32 ± 0.03
Ti IF	0.28 ± 0.05
Ti-P IF	0.29 ± 0.03
TiNbIF	0.33 ± 0.05
TiNb-P IF	0.33 ± 0.03

(ii). Delta Phase Layer Growth

The delta phase layer growth data were also analyzed for growth rate time constant, n, values according to a power law growth relationship and the values are listed in Table XIII. The n values range from 0.35 - 0.51 but have a large error associated with their values. The large error was associated with the two stage growth of the delta phase layer. Initially (5-30 seconds of reaction) the delta layer shows little or no growth, however, at 60 seconds of immersion and thereafter delta layer growth is rapid (Figure 42). Overall the delta layer growth followed a $t^{1/3}$ to $t^{1/2}$ relationship, and this growth was similar on all of the substrate steel alloys studied.

(iii). Zeta Phase Layer Growth

In evaluating the development and growth of the zeta phase layer it was observed that a horizontal array of entrapped regions of eta phase formed within the zeta phase layer after 60 seconds of reaction time, as shown in Figure 46d-f. Electron probe microanalysis and BSE imaging confirmed that both layers on either side of the entrapped eta phase were of a composition corresponding to zeta phase. The individual $zeta_1$ and $zeta_2$ growth layers (discussed previously in section V. A. 1.) could not be analyzed to determine the growth rate time constant (n value) of each layer due to a lack of data on either side of the 60 second transition point. Therefore more data before and after 60 seconds of reaction time is needed to accurately fit the two stage growth of the zeta phase layer. It was found that

the zeta phase layer could be more accurately evaluated for its growth behavior as one layer, thus zeta phase layer growth analysis was conducted on the total zeta layer ($zeta_1$ + $zeta_2$, including the voids in the layer thickness measurements). Initially the total zeta layer ($zeta_1$ + $zeta_2$) growth was evaluated based upon linear-parabolic kinetics, however, the total zeta layer growth data did not show linearity for this type of analysis (shown in Appendix D). The zeta phase layer thickness data were then fit to determine a growth rate time constant n value, which are listed in Table XIII. Growth rate time constant values ranged from 0.28 - 0.33, thus the total zeta layer kinetics followed a $t^{1/3}$ relationship.

Coarsening of the zeta phase could account for the observed $t^{1/3}$ growth followed by the total zeta layer. Coarsening and grain growth during phase layer growth where grain boundary diffusion occurs has been shown to follow $t^{1/3}$ kinetics as shown by Tu [82] on the growth of the Cu_6Sn_5 phase formed between a molten Pb/Sn solder and a thin Cu_3Sn phase formed on a Cu substrate. In that work [82] Cu was the dominant diffusing species, and the Cu_6Sn_5 phase was able to grow due to (1) Cu diffusing into the liquid channels of the solder, and (2) Cu diffusing into the growing Cu_6Sn_5 grains. The flux of Cu atoms also resulted in a coarsening of the Cu_6Sn_5 phase, thus causing a reduction in the liquid solder channel area, and the kinetics of growth for the Cu_6Sn_5 phase followed a $t^{1/3}$ relationship. A similar mechanism of Zn diffusion and a flux of Zn atoms supplying the growing zeta phase layer may have resulted in a coarsening of the zeta phase layer structure. Figure 34d-f shows that the width of the columnar features of the zeta phase have increased, indicating some coarsening may have occurred during growth.

For grain boundary diffusion in the presence of a compound layer enough material must be delivered to the growth interface along grain boundaries [83]. If the grain size of the reaction layer increases than growth can occur according to less than parabolic ($n < 0.5$) kinetics. Any mechanism that results in appreciable loss of a material from a growing layer or a time dependent reduction of the flux of material to the growth interface can also result in non-parabolic growth behavior. Material from a reaction layer could be lost due to dissolution. In the Fe-Zn system, the dissolution or consumption of the zeta phase by the delta phase layer is possible. For grain boundary diffusion non-parabolic behavior can also result from a time dependent reduction in the flux to the growth interface, due to an increase in grain size of the reaction layer or to reduction in the number of high diffusivity paths between the source and the growth interface. The reduction in the number of high diffusivity paths can occur in the absence of grain growth if the grain boundaries become blocked.

Phosphorus and other solute additions to the substrate steel would generally be thought not to have a significant influence on zeta phase layer growth because substrate steel solute additions should not affect the diffusion of Zn across the zeta phase layer. Due the fact that the zeta layer is located at a distance of approximately 2-20 μm from the steel/coating interface and that it is not in direct contact with the substrate steel, its growth rate should not be directly affected by substrate chemistry. Only dramatic changes in delta phase layer growth rate on one side of the zeta phase layer, and/or changes in the ability of

liquid Zn to penetrate the zeta phase layer (for example coarsening of the zeta phase columnar structure) should be the only significant factors affecting zeta layer growth.

Summarizing the kinetics observed for the Fe-Zn phase layers formed in the 0.00 wt% Al-Zn coatings, the total Fe-Zn alloy layer as well as the individual phase layers did not follow parabolic or linear parabolic kinetics. Most likely the observed total Fe-Zn alloy layer growth kinetics were due to a grain boundary diffusional growth mechanism, or to nucleation at preferential sites (such as substrate grain boundaries). The total Fe-Zn alloy layer had a growth rate time constant (n) value of 0.33 while the gamma layer had an average n value (for the non P containing substrates) of 0.25, the delta phase layer n value was approximately 0.33-0.50, and the zeta layer had the same growth time relationship as the total Fe-Zn alloy layer with an average n value of 0.33. The n values determined from the individual phase layers are in agreement with the n values reported previously in the literature of 0.25, 0.50, and 0.35 for the gamma, delta, and zeta phase layers, respectively [17]. P solute additions were found to retard gamma phase layer kinetics only, and showed no effect on delta and zeta phase growth. Ti and Nb solute additions showed no significant effect on the kinetics and rate of Fe-Zn phase layer growth in the 0.00 wt% Al bath. The growth kinetics of the zeta phase layer dominated the kinetics of the total Fe-Zn alloy layer as both were found to follow a $t^{1/3}$ growth relationship.

3. Morphology of Fe-Zn Phase Formation in a 0.20 wt% Al-Zn Bath

Fe-Zn phase growth was morphologically similar on all of the substrate steels studied, and a representative example of Fe-Zn alloy layer development on the Ti IF steel is shown in Figure 49. The Fe-Zn phase layer development is also shown schematically in Figure 50, where the sequence of reaction is represented chronologically. t_0 corresponds to zero time, and development occurs according to time such that $t_0 < t_1 < t_2 < t_3 < t_4$. Unlike the 0.00 wt% Al-Zn bath, total Fe-Zn alloy layer growth in the 0.20 wt% Al-Zn bath was inhibited by the initial formation of an Fe-Al intermetallic layer at the steel/coating interface (t_1 in Figure 50), documented by other investigators to be either an Fe_2Al_5 phase [7] or an Fe-Zn-Al ternary compound [9]. The nature of this inhibiting layer is a transient one, and it is eventually penetrated by liquid Zn to form Fe-Zn delta phase (t_2 in Figure 50) and after some incubation time gamma phase forms (t_3 in Figure 50). The localized growths eventually coalesce to form regions of a continuous Fe-Zn alloy layer, however areas of Fe_2Al_5 phase remain undisturbed up to 300 seconds of reaction time (t_4 in Figure 50). Therefore the localized Fe-Zn growth reaction is due to the inhibiting effect of an Fe_2Al_5 or $Fe_2Al_5(Zn)$ layer that first forms at the steel/coating interface and acts as a physical barrier to Zn diffusion, resulting in discontinuous Fe-Zn alloy phase growth in a 0.20 wt% Al-Zn bath. Localized regions of Fe-Zn growth (outbursts) at the steel/coating interface were found to form on all of the steel substrates studied. The localized regions of Fe-Zn growth showed a 2 phase layer morphology within the total Fe-Zn alloy reaction layer, with delta phase layer forming first at the steel/coating interface, followed by gamma

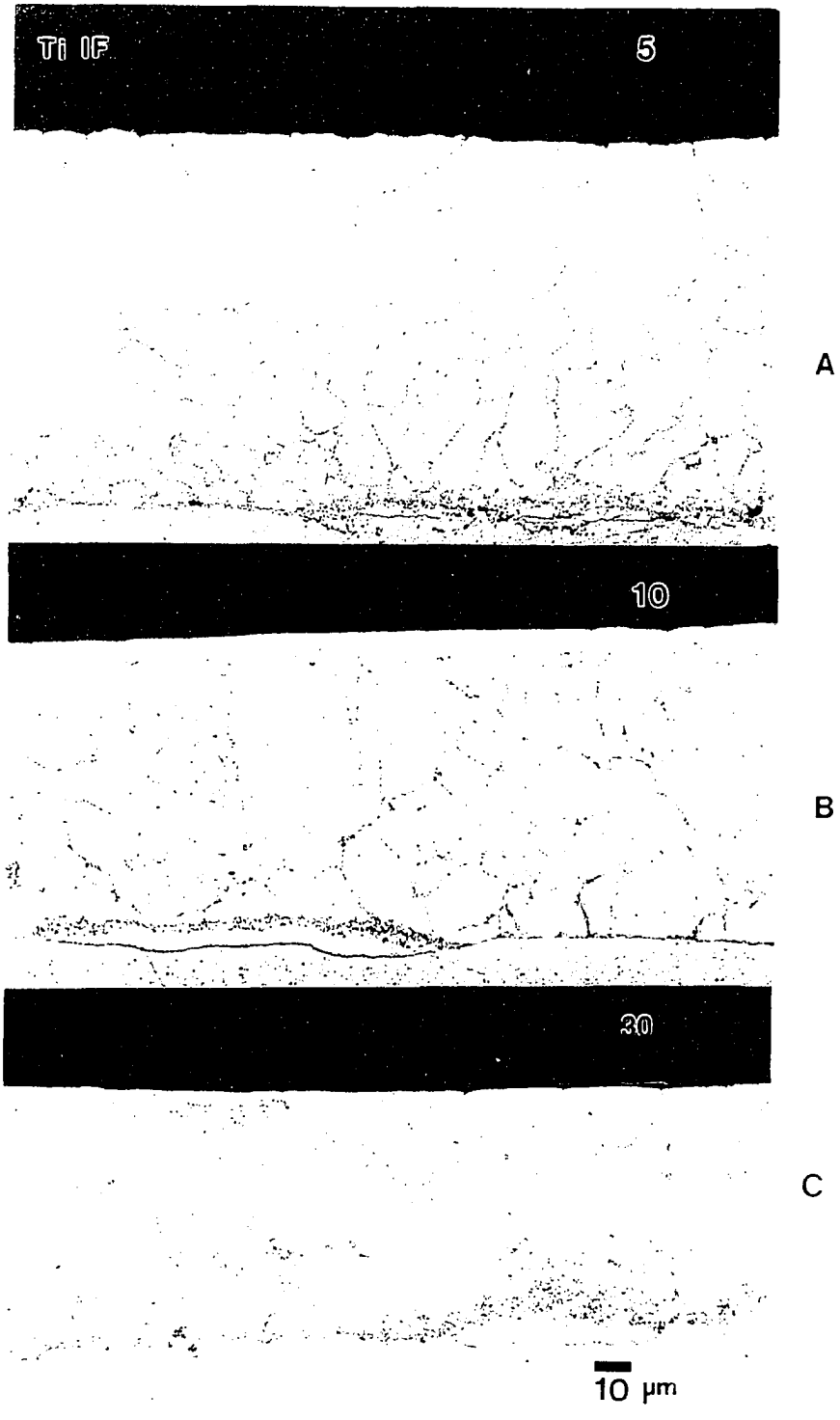

Figure 49. Ti IF steel hot-dip galvanized in a 0.20 wt% Al-Zn bath for (a) 5 (b) 10 and (c) 30 seconds of immersion.

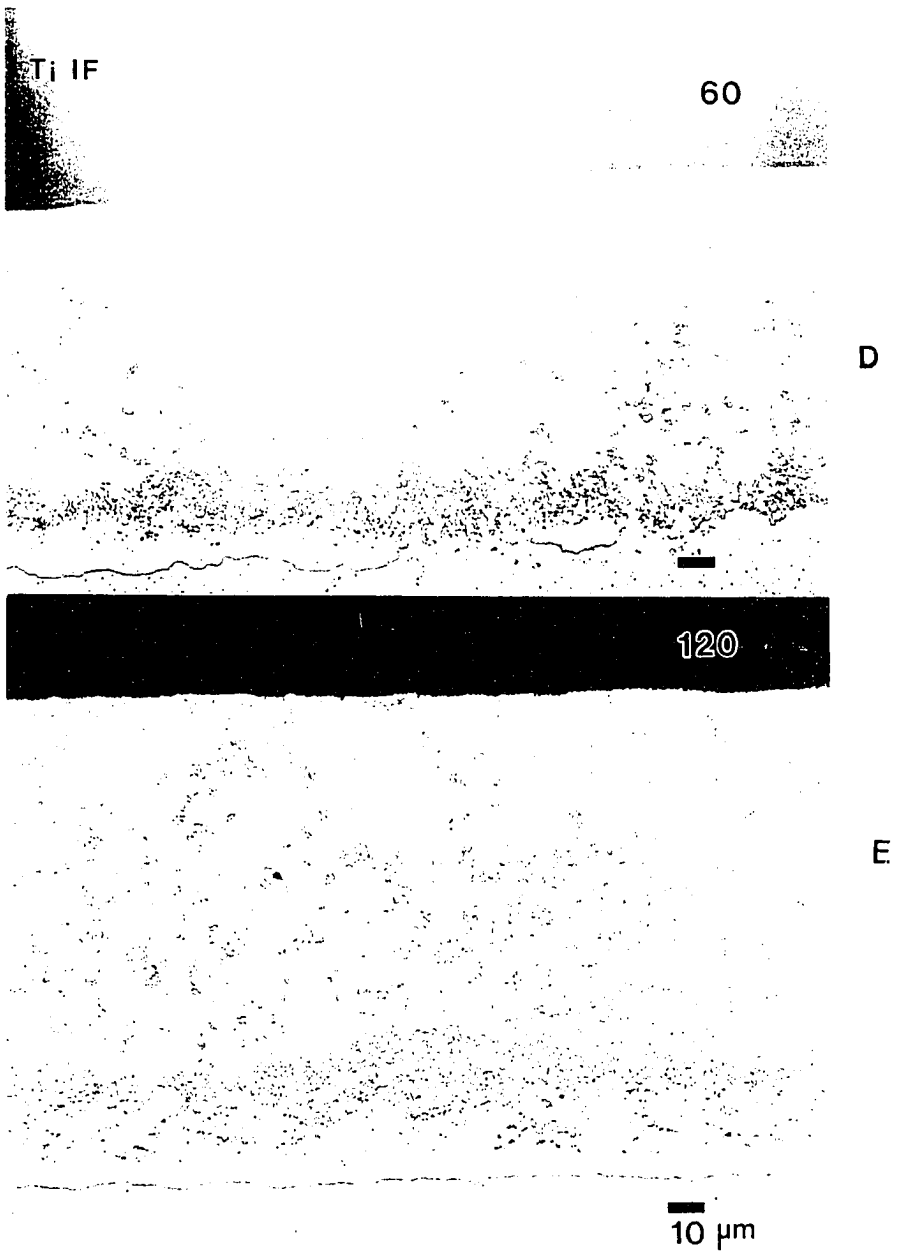

Figure 49. Ti IF steel hot-dip galvanized in a 0.20 wt% Al-Zn bath for (d) 60 and (e) 120 seconds of immersion.

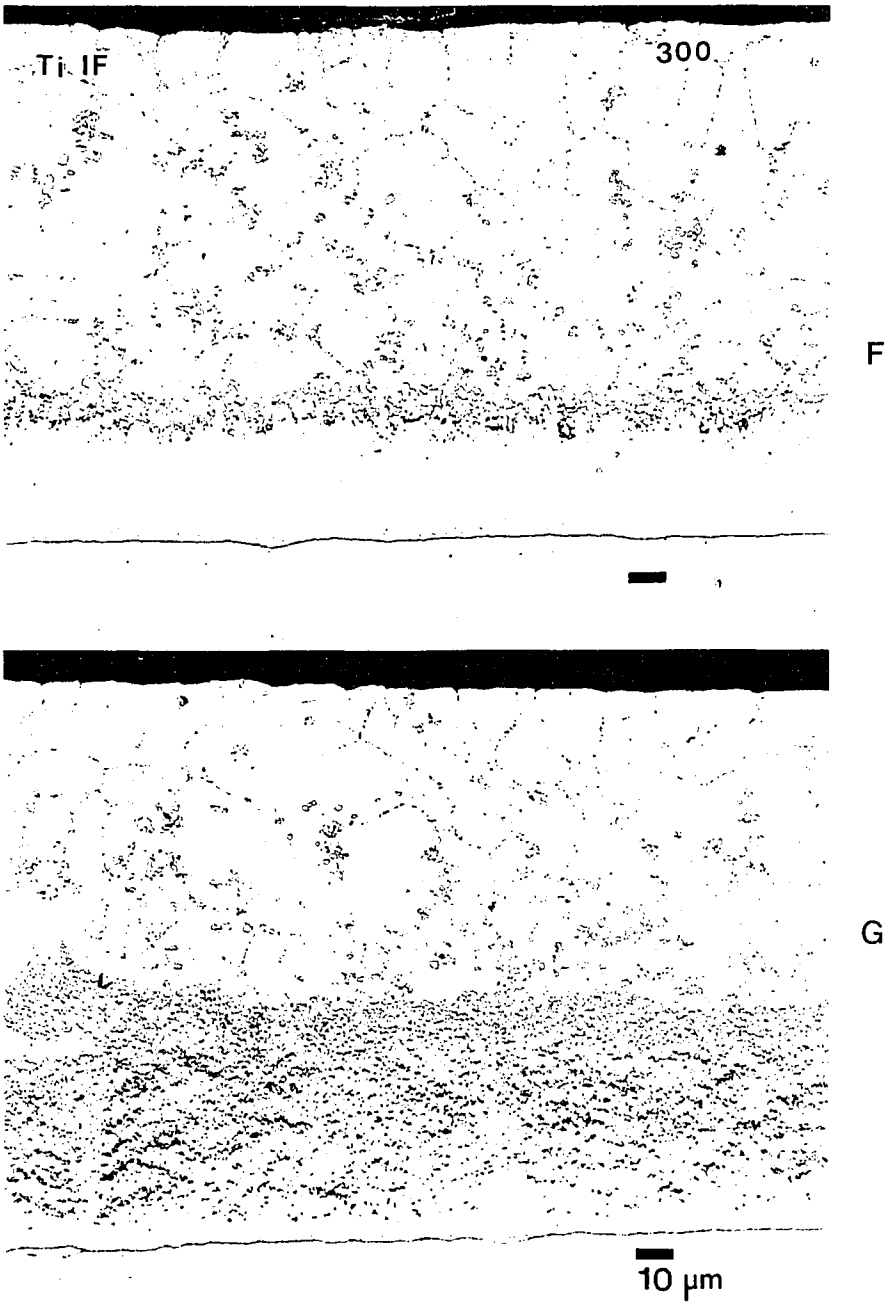

Figure 49. Ti IF steel hot-dip galvanized in a 0.20 wt% Al-Zn bath for 300 seconds of immersion, (f) and (g).

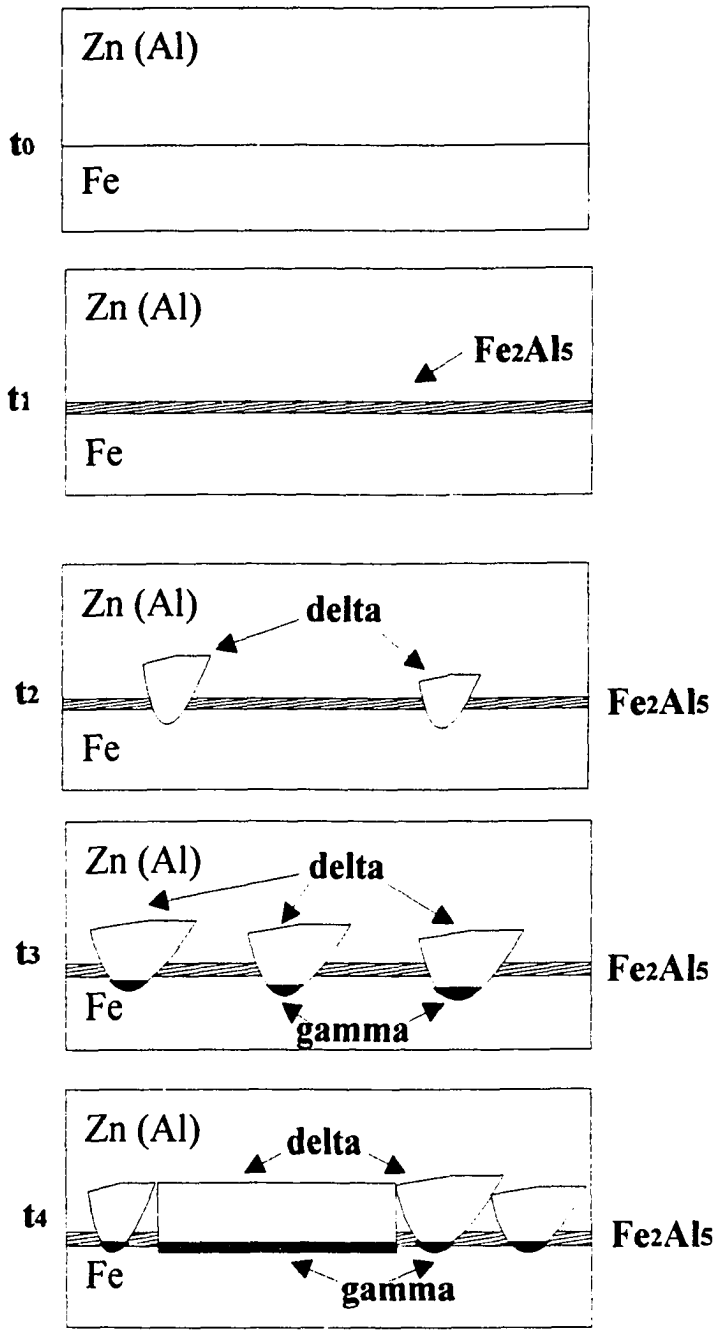

Figure 50. A schematic representation of Fe-Zn phase layer formation in a 0.20 wt% Al-Zn galvanizing bath. t_0 corresponds to zero time, and development occurs according to time, such that $t_1 < t_2 < t_3 < t_4$.

phase layer formation at the alpha Fe/delta phase interface. The delta phase was found to form at the shortest reaction time of 5 seconds, and was the dominant growth layer within the total Fe-Zn alloy layer at all of the reaction times studied.

In order to confirm individual phase layer identification initially characterized by morphology in light optical microscopy (LOM), electron probe microanalysis for Fe, Zn, and Al composition was determined at 1.0 μm increments across the total Fe-Zn alloy layer perpendicular to the steel/coating interface (parallel to the direction of diffusion) for the 10, 60 and 300 second immersion samples. The Fe and Al concentration profile data are plotted in Figures 51-56, and support the gamma and delta phase identification determined by morphology in LOM. Because delta phase has a high solubility for Al (see Figure 9b), Al present at the steel/coating interface becomes distributed throughout the delta phase layer. All of the substrate steels showed similar Fe and Al concentration profiles, thus the composition analysis determined in this study did not support the work of Fukuzuka et al [51] who had previously reported that IF steels galvanized in Al containing baths had lower amounts of Al located at the steel/coating interface, and this lack of Al resulted in the observed higher reactivity of IF steels. An example back scattered electron (BSE) image of an 0.20 wt% Al-Zn coating is shown in Figure 57. The atomic number contrast in the image also indicates a two phase layer morphology in the localized Fe-Zn growth regions. The BSE images confirmed that no zeta phase layer formed as was observed in LOM, and determined from compositional data analysis of the Fe-Zn alloy layer.

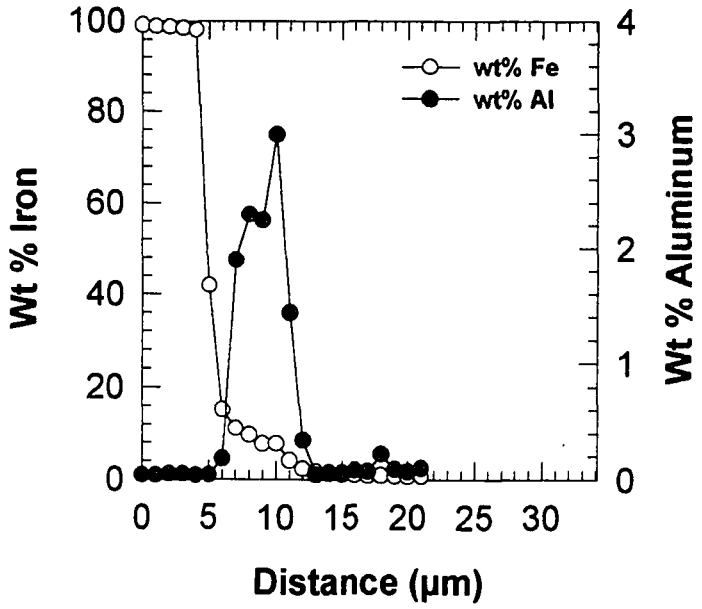

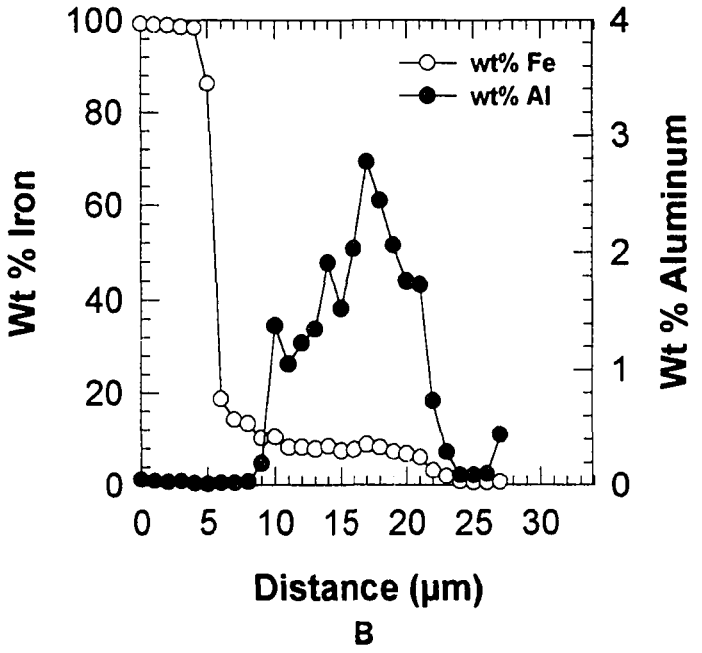

Figure 51. Iron and aluminum concentration profiles for the total Fe-Zn alloy layer formed on the 15 μm grain size ULC steel hot-dip galvanized in a 0.20 wt% Al-Zn bath for (a) 10 and (b) 60 seconds of immersion.

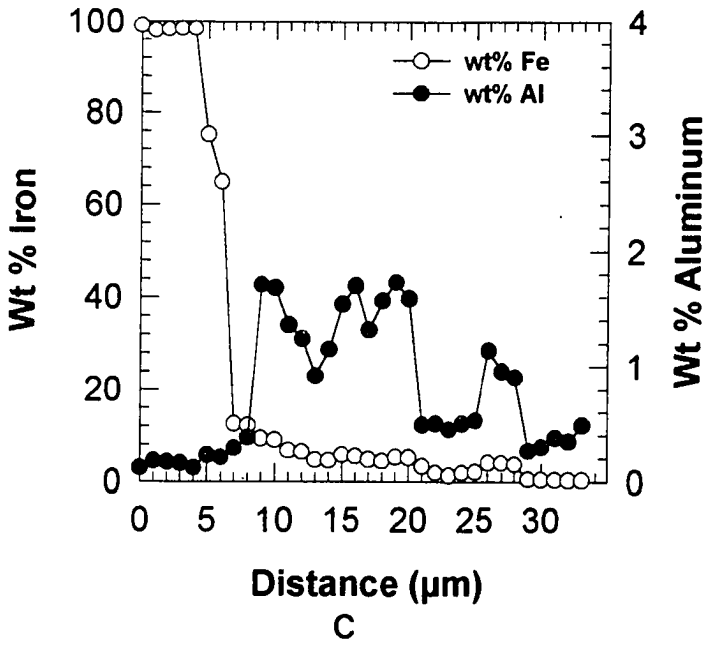

Figure 51. Iron and aluminum concentration profiles for the total Fe-Zn alloy layer formed on the 15 μm grain size ULC steel hot-dip galvanized in a 0.20 wt% Al-Zn bath for (c) 300 seconds of immersion.

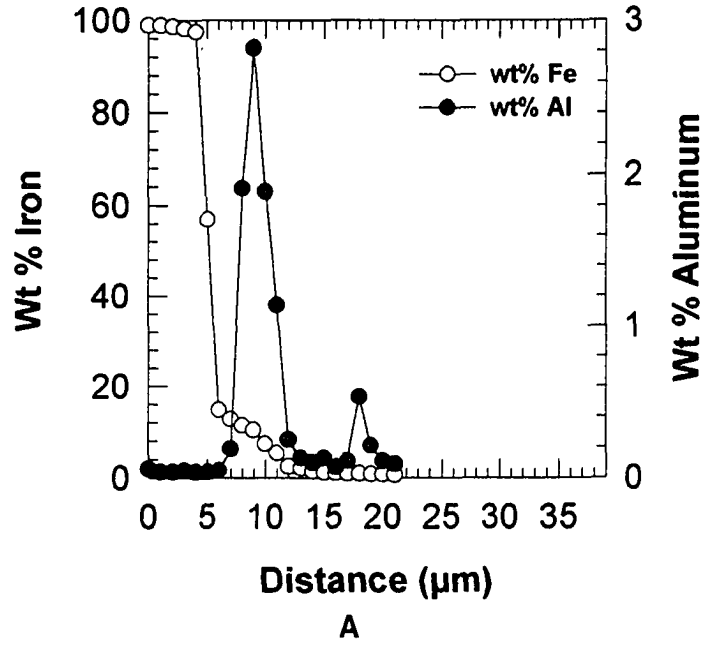

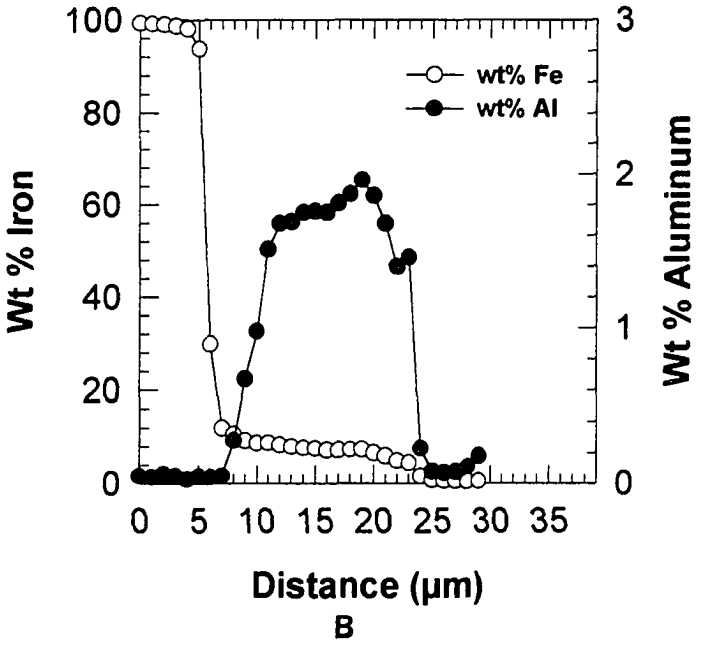

Figure 52. Iron and aluminum concentration profiles for the total Fe-Zn alloy layer formed on the ULC-P steel hot-dip galvanized in a 0.20 wt% Al-Zn bath for (a) 10 and (b) 60 seconds of immersion.

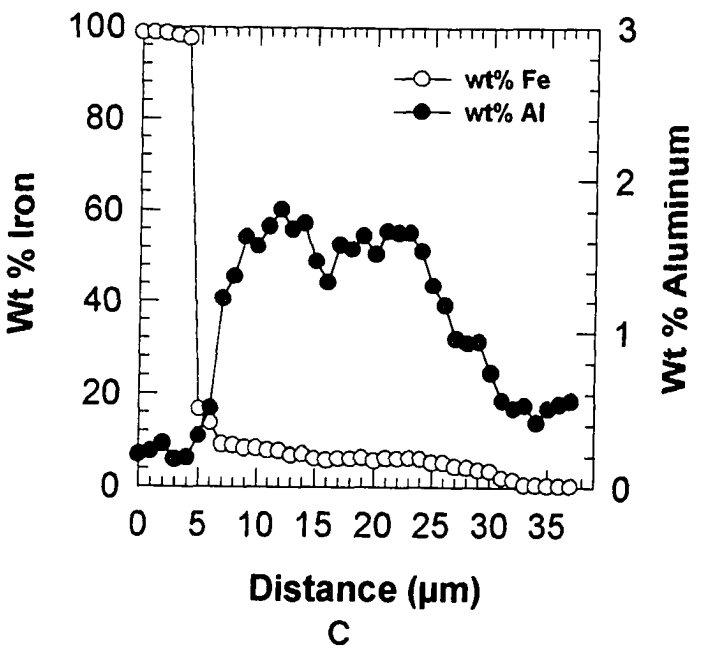

Figure 52. Iron and aluminum concentration profiles for the total Fe-Zn alloy layer formed on the ULC-P steel hot-dip galvanized in a 0.20 wt% Al-Zn bath for (c) 300 seconds of immersion.

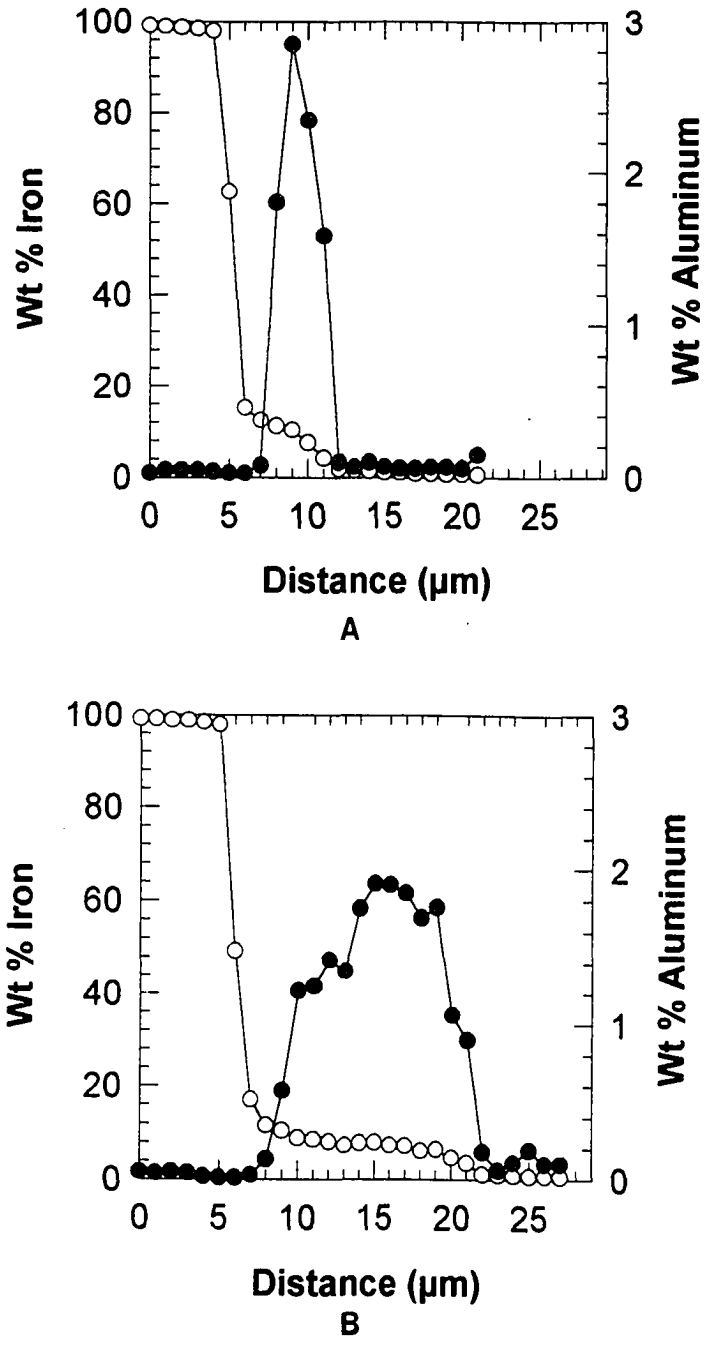

Figure 53. Iron and aluminum concentration profiles for the total Fe-Zn alloy layer formed on the Ti IF steel hot-dip galvanized in a 0.20 wt% Al-Zn bath for (a) 10 and (b) 60 seconds of immersion.

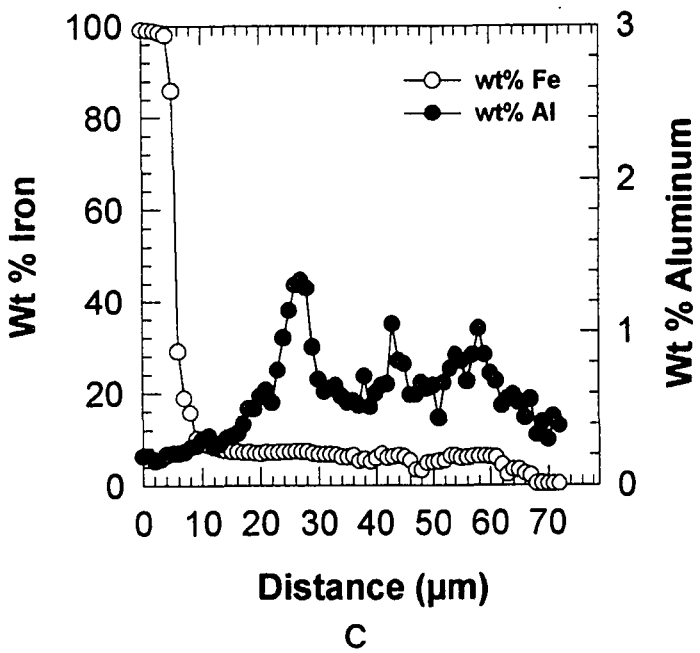

Figure 53. Iron and aluminum concentration profiles for the total Fe-Zn alloy layer formed on the Ti IF steel hot-dip galvanized in a 0.20 wt% Al-Zn bath for (c) 300 seconds of immersion.

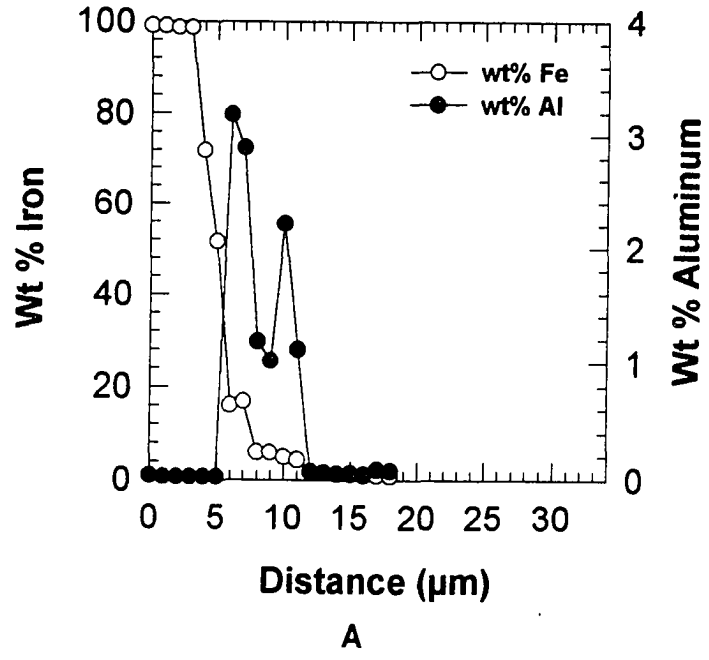

A

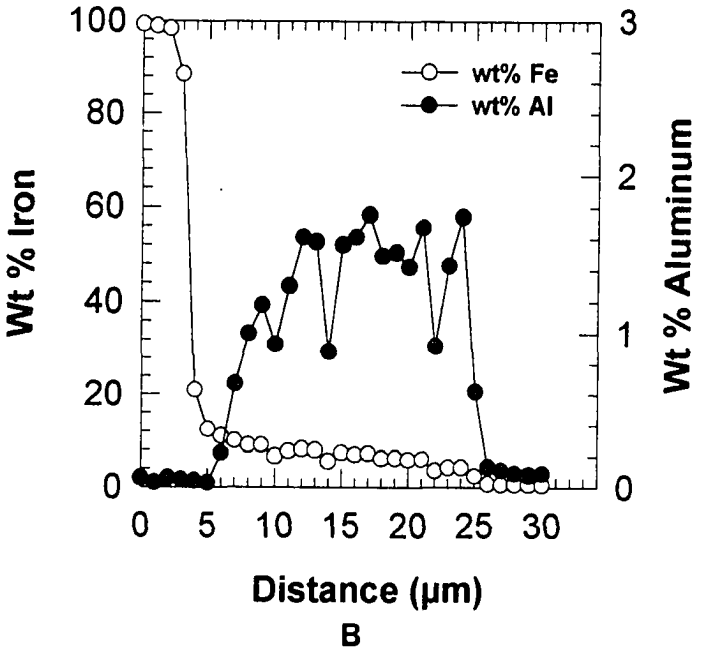

B

Figure 54. Iron and aluminum concentration profiles for the total Fe-Zn alloy layer formed on the Ti-P IF steel hot-dip galvanized in a 0.20 wt% Al-Zn bath for (a) 10 and (b) 60 seconds of immersion.

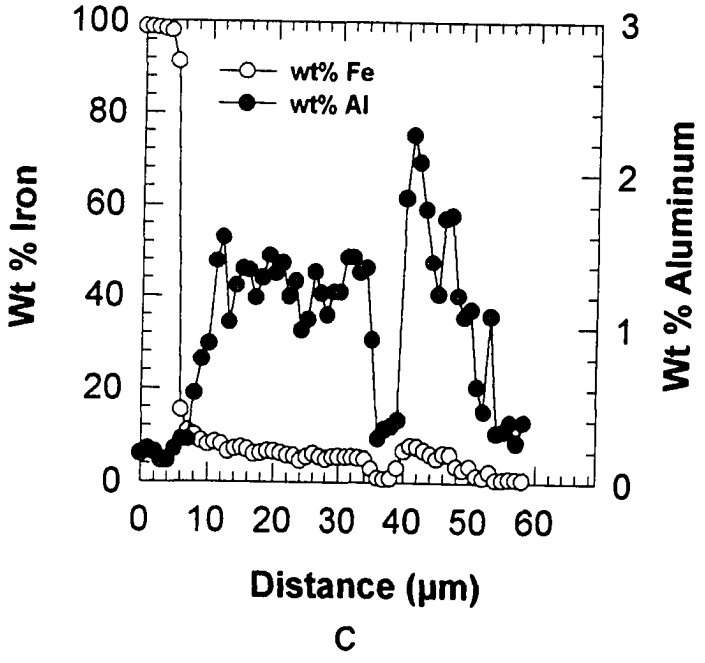

Figure 54. Iron and aluminum concentration profiles for the total Fe-Zn alloy layer formed on the Ti-P IF steel hot-dip galvanized in a 0.20 wt% Al-Zn bath for (c) 300 seconds of immersion.

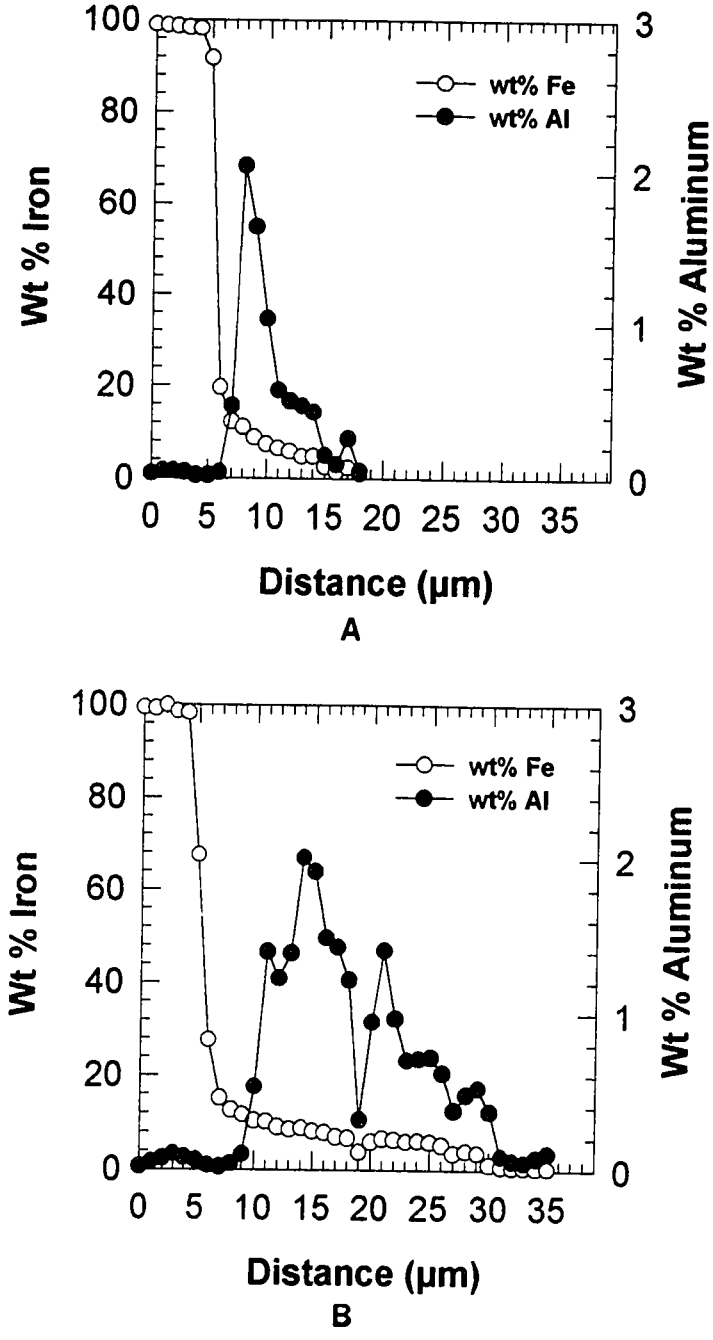

Figure 55. Iron and aluminum concentration profiles for the total Fe-Zn alloy layer formed on the TiNb IF steel hot-dip galvanized in a 0.20 wt% Al-Zn bath for (a) 10 and (b) 60 seconds of immersion.

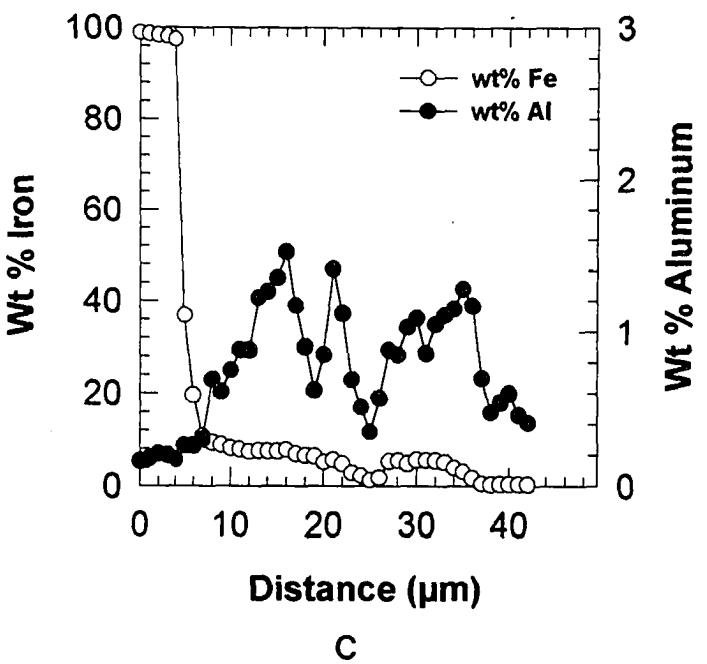

Figure 55. Iron and aluminum concentration profiles for the total Fe-Zn alloy layer formed on the TiNb IF steel hot-dip galvanized in a 0.20 wt% Al-Zn bath for (c) 300 seconds of immersion.

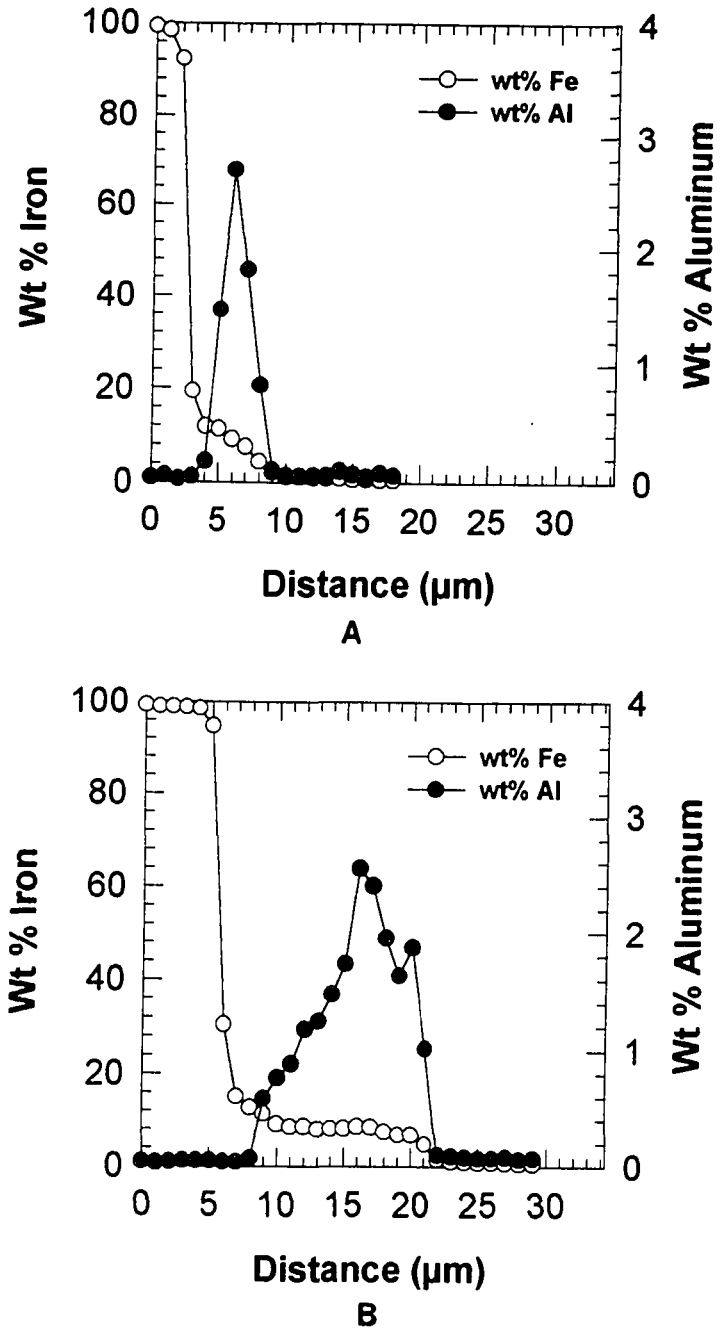

Figure 56. Iron and aluminum concentration profiles for the total Fe-Zn alloy layer formed on the TiNb-P IF steel hot-dip galvanized in a 0.20 wt% Al-Zn bath for (a) 10 and (b) 60 seconds of immersion.

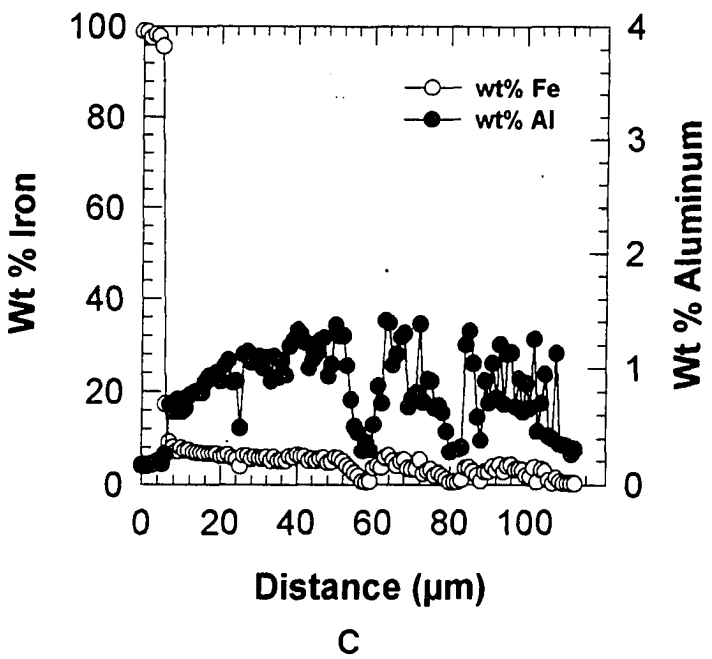

Figure 56. Iron and aluminum concentration profiles for the total Fe-Zn alloy layer formed on the TiNb-P IF steel hot-dip galvanized in a 0.20 wt% Al-Zn bath for (c) 300 seconds of immersion.

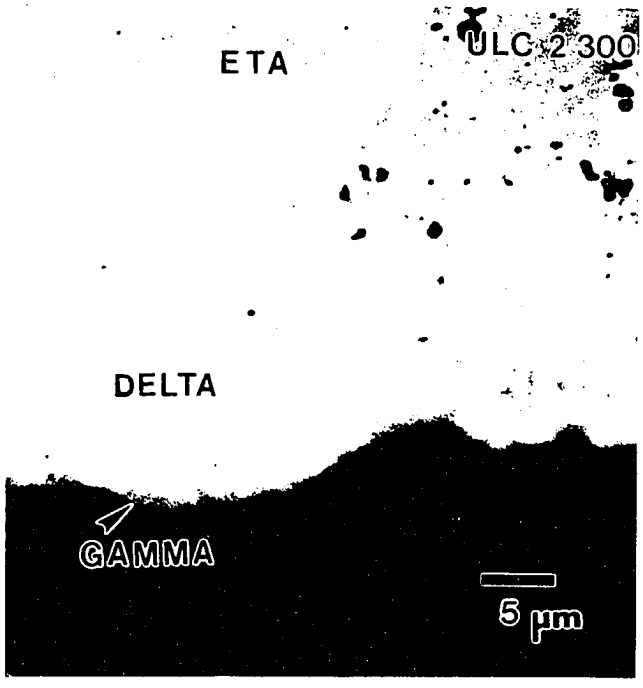

Figure 57. BSE image of the two distinct Fe-Zn phase layers formed on the 15 µm grain size ULC steel hot-dip galvanized in a 0.20 wt% Al-Zn bath for 300 seconds of immersion.

In contrast to the 0.00 wt% Al-Zn bath, zeta phase was not detected in the coatings formed in the 0.20 wt% Al-Zn bath because the diffusion path for the Fe-Zn reaction layer through the metastable ternary Fe-Zn-Al isotherm at 450°C [24] indicates that the delta phase is in equilibrium with eta phase, the solid solution of Fe in Zn. The equilibrium ternary phase diagram like that shown in Figure 2a could have led to the incorrect identification of delta and zeta phases within the total Fe-Zn alloy layer. The metastable ternary diagram (shown in Figure 9a) is a more accurate guide to the identification of phase layers that form after short time reactions (< 30 minutes). The diffusion path through the ternary isotherm (determined from composition analysis of the total Fe-Zn alloy layer after 300 seconds of immersion in a 0.20 wt% Al-Zn bath) follows a path that does not allow for the formation of the zeta phase. The diffusion path for the Fe-Zn reaction layer remained the same over 10-300 seconds of reaction time indicating diffusional growth of the Fe-Zn phases during immersion in the 0.20 wt% Al-Zn bath. The Fe-Al inhibition layer was too thin to be evaluated by electron microprobe analysis for composition and therefore its diffusion path through the metastable ternary phase diagram could not be determined. The diffusion path for the Fe-Zn reaction layer (starting from the Fe corner of the ternary diagram) was determined to follow an $\alpha/(\alpha + \Gamma)/\Gamma/(\Gamma + \delta)/\delta/(\delta + \eta)/\eta$ path, as shown in Figure 58a, and the $(\Gamma + \delta)/\delta/(\delta + \eta)/\eta$ portion of the path is shown in Figure 58b.

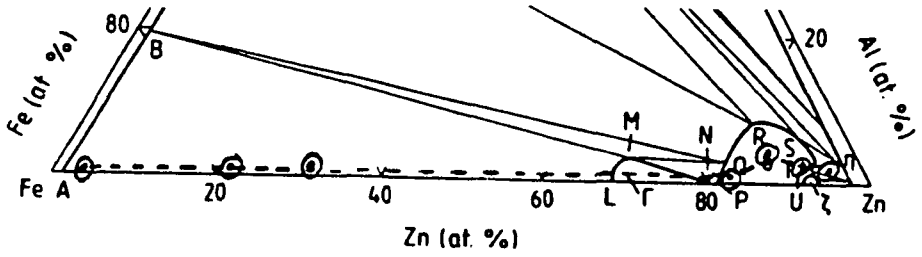

Figure 58a. Diffusion path of the Fe-Zn alloy layer formed in the 0.20 wt% Al-Zn bath shown on the enlarged Fe-Zn binary portion of the metastable Fe-Zn-Al isotherm at 450 °C [24].

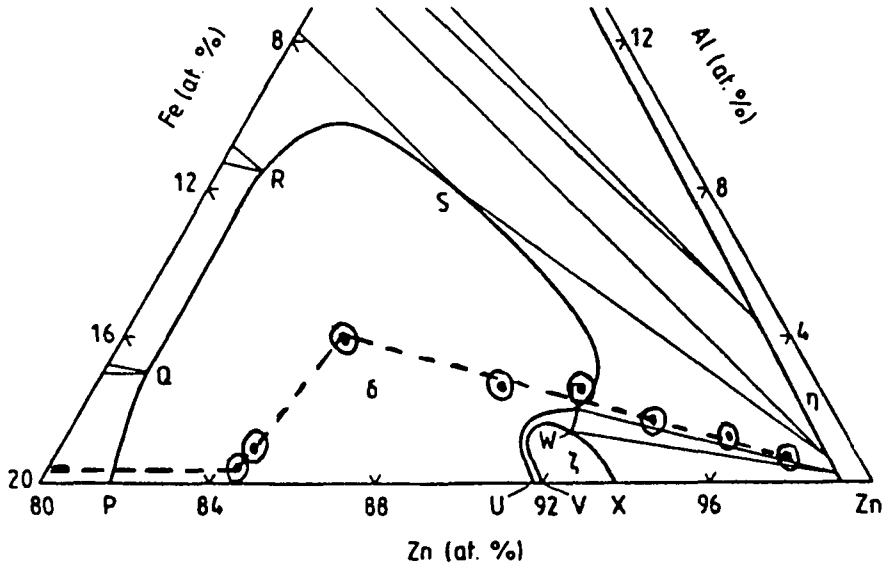

Figure 58b. Diffusion path of the Fe-Zn alloy layer formed in the 0.20 wt% Al-Zn bath through the Zn rich corner of the metastable Fe-Zn-Al isotherm at 450 °C [24].

The morphology of the localized Fe-Zn growths also supports the finding that delta phase is in metastable equilibrium with eta phase. Figure 49g shows a morphology referred to in the literature as a breakaway morphology. The breakaway morphology has a mottled appearance because it has been penetrated by liquid Zn and contains regions of entrapped eta phase, therefore the delta phase layer is in a state of metastable equilibrium with liquid Zn during immersion, and zeta phase did not form during immersion or upon solidification of the Zn to form eta phase. The penetration of Zn through the Fe-Zn phase in contact with the melt was also found to occur for the zeta phase layer in 0.00 wt% Al-Zn bath. The zeta layer also showed regions of entrapped eta phase, representative of liquid Zn penetration and subsequent solidification. In the 0.00 wt% Al-Zn bath zeta phase was in a state of metastable equilibrium with the Zn melt during immersion.

The growth of the delta phase was rapid and was most likely due to liquid Zn penetration of the delta phase which resulted in a porous structure (or breakaway morphology) when observed in cross section (Figure 49g). After an incubation time, gamma phase formed at the alpha Fe/delta phase interface. The incubation time of the formation of gamma phase varied for the different substrate steels, and may be due to steel solute addition effects on the breakdown of the inhibition Fe_2Al_5 layer. The gamma phase kinetics were difficult to define according to a growth-time relationship due to little or no growth, and on some substrates the disappearance of the gamma layer at extended reaction times. As in the case of the 0.00 wt% Al-Zn coatings, the gamma phase was found to disappear on the P containing steels after 300 seconds of reaction (discussed previously in section V.A.1).

4. Kinetics of Fe-Zn Phase Growth in a 0.20 wt% Al-Zn Bath

The same substrate steel substrate alloys studied in the 0.00 wt% Al-Zn bath were also analyzed for galvanizing reaction kinetics for 5-300 seconds of reaction time in a 0.20 wt% Al-Zn bath. Total alloy layer growth, and individual gamma and delta phase layer growth were characterized at localized regions of Fe-Zn phase growth along the steel/coating interface.

a. Total Alloy Layer Growth

Total alloy layer thickness data for all of the substrate steels studied are shown in Figure 59. The total alloy layer thickness data were first analyzed to determine growth rate time constant (n) values. The total alloy layer n values are reported in Table XIV. The n values range from 0.47-0.60, corresponding to parabolic kinetics, where n = 0.50. Up to 120 seconds of reaction time all of the substrates followed the same outburst growth behavior and only at 300 seconds of reaction were large differences in total growth of the outbursts observed between the substrates (Figure 59). The breakaway morphology of the outburst was extremely pronounced on the Ti/Ti-P and TiNb/TiNb-P IF steel substrates at 300 seconds of reaction indicating a rapid change in the growth rate of the outburst. Because data was not available for reaction times longer than 300 seconds, this rapid growth of the outbursts observed on the IF steels could not be quantified.

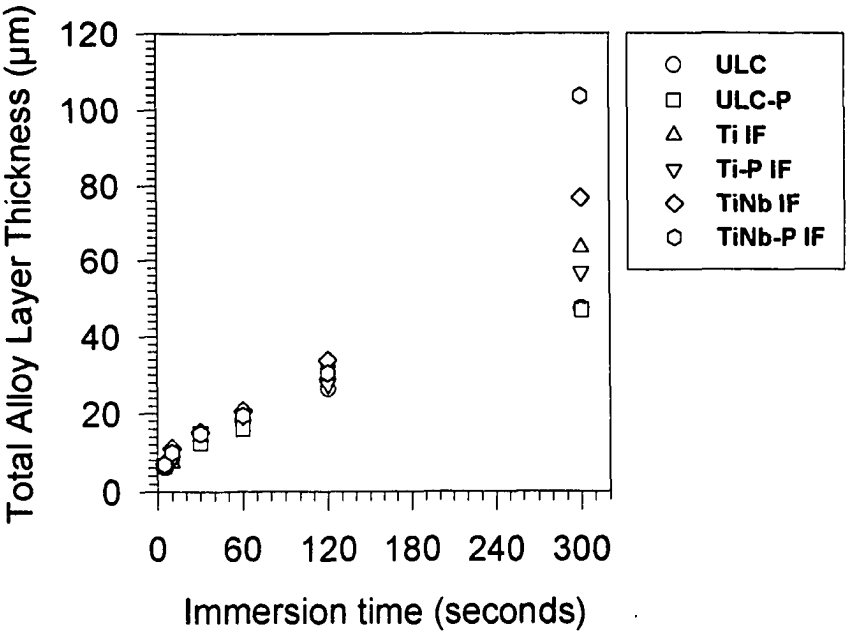

Figure 59. Total Fe-Zn alloy layer growth for substrate steels hot-dip galvanized in a 0.20 wt% Al-Zn bath.

Table XIV. Total Fe-Zn Alloy Layer Growth Rate Time Constant (n) Values for the Steels Hot-Dip Galvanized in a 0.20 wt% Al-Zn Bath.

Sample	Growth Rate Time Constant, n
ULC	0.48 ± 0.02
ULC-P	0.47 ± 0.05
Ti IF	0.55 ± 0.04
Ti-P IF	0.50 ± 0.04
TiNbIF	0.54 ± 0.06
TiNb-P IF	0.60 ± 0.09

b. Individual Phase Layer Growth

Individual phase layers of gamma and delta phases were observed to develop for all of the steels hot-dip galvanized in the 0.20 wt% Al-Zn bath. Individual phase layer growth data for the separate substrate steel alloys are shown in Figure 60.

(i). Gamma Phase Layer Growth

The gamma phase layer was observed to first form at different reaction times, depending upon substrate chemistry (see Table XV). P solute additions to the substrate steel delayed gamma layer formation, except in the case of TiNb IF steels, which appeared to be the most reactive, with the shortest incubation times for gamma phase formation.

Table XV. Reaction time at which the Fe-Zn Gamma Phase Layer was first observed to form and grow on Steels Hot-Dip Galvanized in a 0.20 wt% Al-Zn Bath.

Sample	reaction time(seconds)
ULC	10
ULC-P	30
Ti IF	30
Ti-P IF	60
TiNb IF	10
TiNb-P IF	10

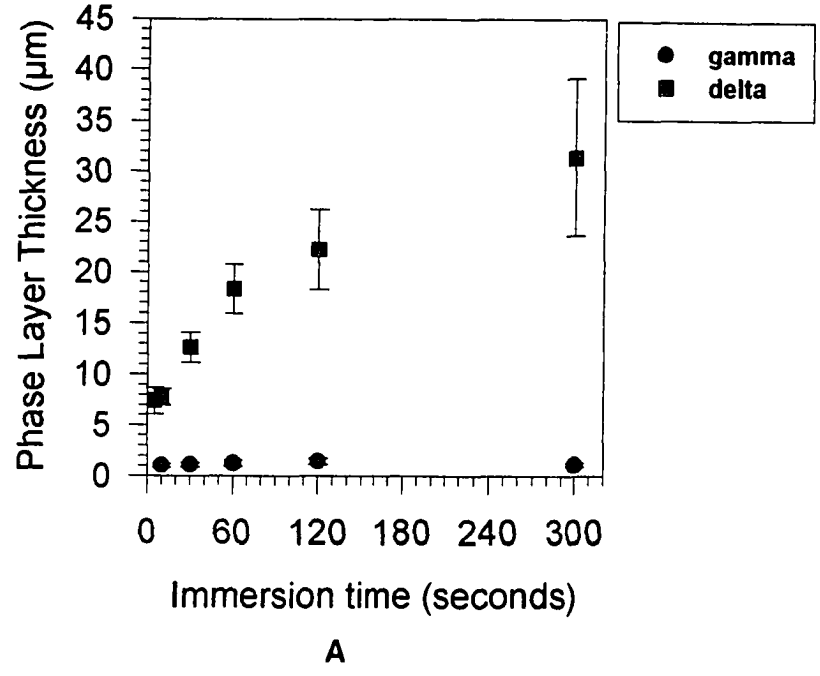

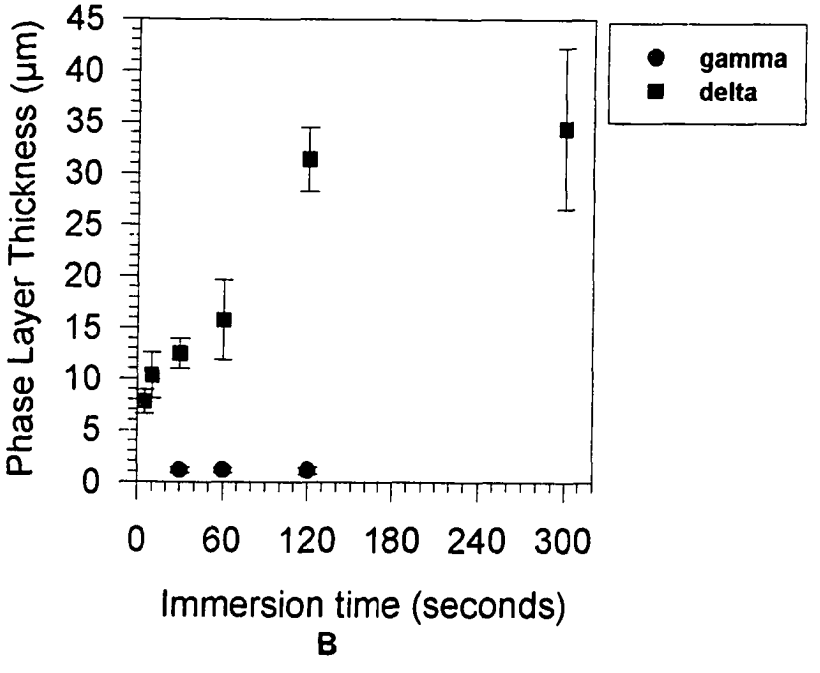

Figure 60. Individual Fe-Zn gamma and delta phase layer growth for the (a) ULC and (b) ULC-P steel substrates hot-dip galvanized in a 0.20 wt% Al-Zn bath.

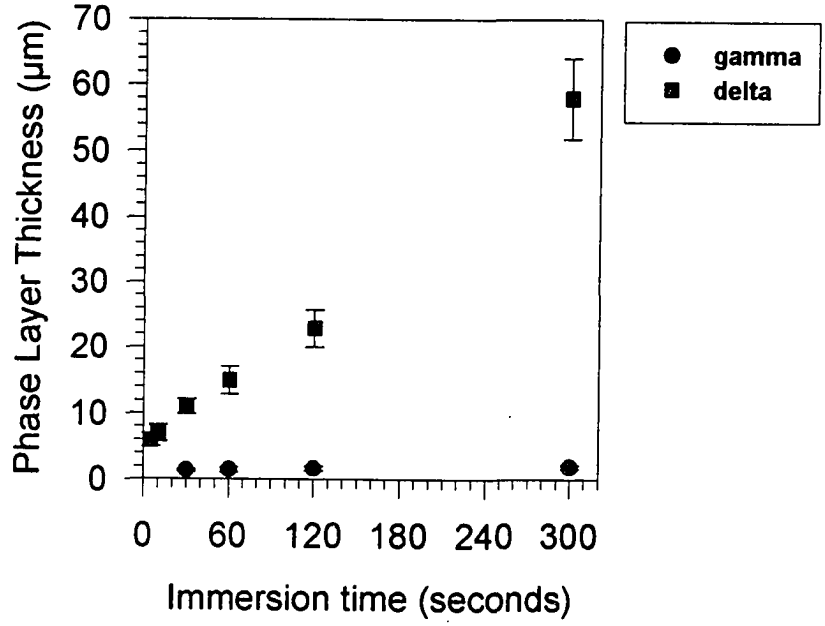

C

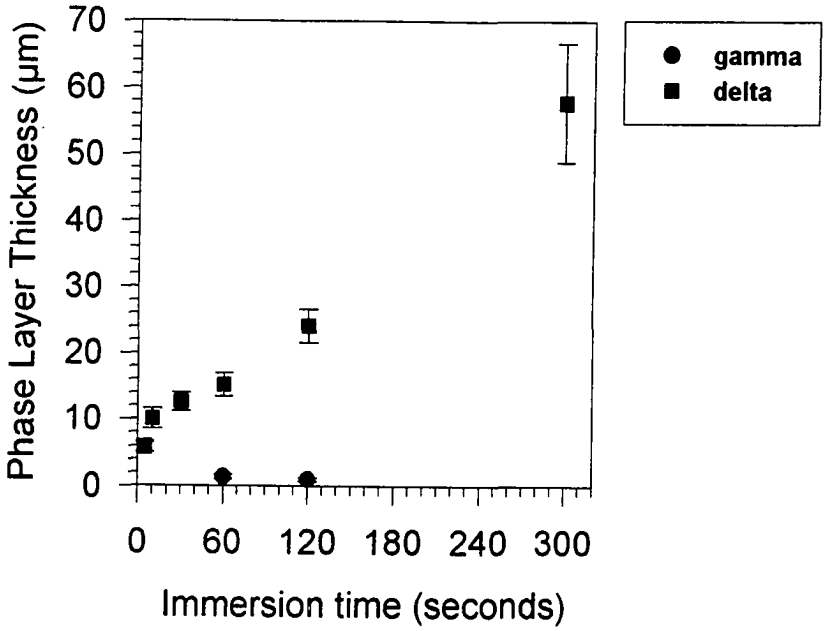

D

Figure 60. Individual Fe-Zn gamma and delta phase layer growth for the (c) Ti IF and (d) Ti-P IF steel substrates hot-dip galvanized in a 0.20 wt% Al-Zn bath.

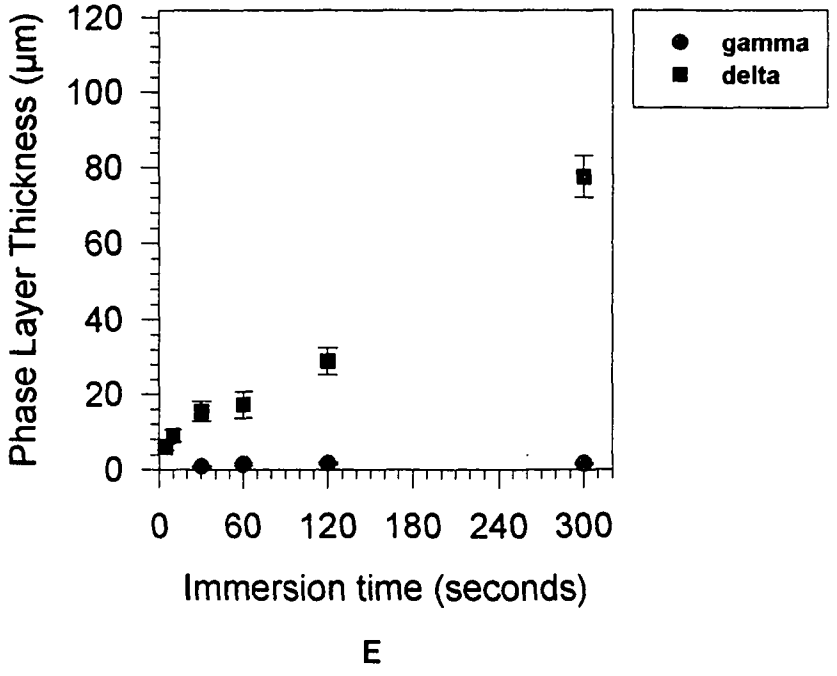

E

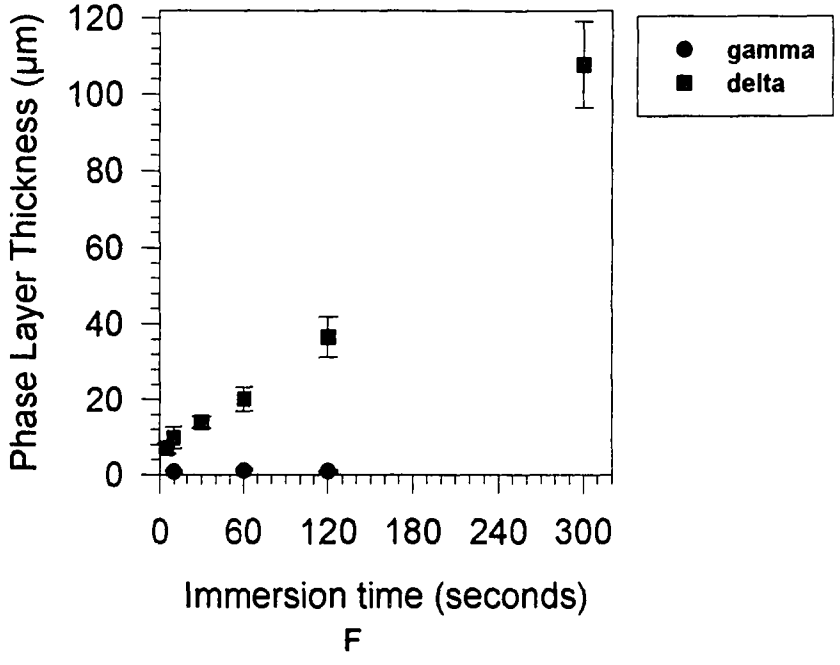

F

Figure 60. Individual Fe-Zn gamma and delta phase layer growth for the (e) TiNb IF and (f) TiNb-P IF steel substrates hot-dip galvanized in a 0.20 wt% Al-Zn bath.

To best evaluate the gamma phase layer data, growth rate time constant values were determined over the associated time frame at which gamma phase was found to form and grow on the different steel substrates. The n values for the gamma layer are reported in Table XVI, and a large degree of error was found to be associated with some of the values. Generally the gamma layer was found to show little or no growth in the 0.20 wt% Al-Zn bath. The observed lack of growth of the gamma phase has been previously reported for galvanized coatings formed in a bath containing 0.10 wt% Al-Zn which were then annealed at temperatures of 450°C-550°C [84]. Comparison of the non P containing substrates (ULC, Ti IF, and TiNb IF) indicates that Ti, and Ti and Nb solute additions enhanced the growth kinetics (n value) of the gamma phase layer.

Because all of the P containing alloys did show the disappearance of the gamma phase layer after 300 seconds of reaction, a negative n value was determined for the growth rate time constant on the ULC-P and Ti-P steel substrates (Table XVI). The negative n values are not physically possible, however, they do indicate a situation of no growth of the gamma phase layer, and its consumption over time by the delta phase layer. P additions to the substrate steel appeared to eventually over time destabilize the interfacial gamma layer, as was found to occur in 0.00 wt % Al-Zn baths.

Table XVI. Individual Fe-Zn Phase Layer Growth Rate Time Constant (n) Values for the Steels Hot-Dip Galvanized in a 0.20 wt% Al-Zn Bath.

Sample / Layer	Growth Rate Time Constant, n
Gamma Phase Layer	
ULC	0.050 ± 0.049
ULC-P	- 0.032 ± 0.003
Ti IF	0.16 ± 0.01
Ti-P IF	- 0.528*
TiNbIF	0.19 ± 0.05
TiNb-P IF	0.036 ± 0.158
Delta Phase Layer	
ULC	0.38 ± 0.02
ULC-P	0.38 ± 0.05
Ti IF	0.53 ± 0.07
Ti-P IF	0.50 ± 0.07
TiNbIF	0.57 ± 0.07
TiNb-P IF	0.62 ± 0.09

* no error determined due to fit over just 2 data points

(ii). Delta Phase Layer Growth

According to Figure 60a and b, the delta layer formed on the ULC/ULC-P substrates followed parabolic growth up to 300 seconds, while the Ti/Ti-P and TiNb/TiNb-P steels showed parabolic growth up to 120 seconds (Figures 60c-f). The observed growth behavior was related to the accelerated rate of outburst growth which occurred on the Ti and TiNb IF steel substrates. Delta phase layer growth was first fit to determine growth rate time constant values. The Ti/Ti-P and TiNb/TiNb-P steel data were fit up to 120 seconds of reaction time as growth at 300 seconds did not follow the growth behavior which occurred at earlier reaction times. The n values are reported in Table XVI. The n values range from 0.38 - 0.62, indicating that the ULC/ULC-P steels showed n values (0.38) lower than those for the Ti and Ti and Nb containing steels (n = 0.5-0.62). Therefore delta layer growth followed more rapid kinetics on the Ti IF/Ti-P IF and TiNb IF/TiNb-P IF steels. As was found to occur for the gamma phase layer growth, solute additions of Ti and Ti and Nb resulted in more rapid growth kinetics of the delta phase layer. Additions of phosphorus were found not to influence the kinetics of delta layer growth for any of the steels studied.

Summarizing the Fe-Zn phase growth kinetics that occurred in the 0.20 wt% Al-Zn bath, the total Fe-Zn alloy that formed was a localized growth, due to the initial formation of an Fe-Al inhibition layer (Fe_2Al_5) upon immersion of the substrate into the Zn bath. The total Fe-Zn alloy or outburst followed $t^{1/2}$ growth kinetics, as was generally found for the delta

phase layer growth which was in contact with the liquid Zn melt during immersion. Similarly, in the 0.00 wt% Al-Zn bath total Fe-Zn alloy layer growth followed a $t^{1/3}$ relationship as did the zeta phase layer which was in contact with the liquid Zn during immersion in that bath. Thus the supply of Zn through the Fe-Zn phase in contact with the liquid Zn dominates the overall total Fe-Zn alloy layer growth reaction. The fact that the n values for the total alloy layer are not the same for the 0.00 and 0.20 wt% Al-Zn baths is most likely related to the consumption of the zeta phase layer by the rapidly growing delta layer in 0.00 wt% Al-Zn coatings. The $t^{1/3}$ kinetics of the zeta phase layer in 0.00 wt% Al-Zn baths may also be related to a nucleation and growth mechanism, with preferential nucleation sites occurring at substrate grain boundaries.

The gamma phase layer in the 0.20 wt% Al-Zn bath showed little or no growth, therefore its growth kinetics were difficult to define. Solute additions of Ti and Ti and Nb were found to cause more rapid growth of both the gamma and delta phase layers in 0.20 wt% Al-Zn baths, while P solute additions resulted in negative growth kinetics of the gamma phase layer, which led to the eventual disappearance of the layer at the longest time of reaction studied.

5. Summary

The previously reported effects of substrate solute additions on galvanizing have concentrated on reactions in Zn baths containing Al due to the fact that these baths are

commonly used in the steel industry to produce high quality automotive Zn coatings. It is generally thought that P solute additions reduce steel reactivity while Ti additions increase steel reactivity during hot-dip galvanizing and galvannealing, thus affecting process control of an optimally alloyed Fe-Zn coating. The findings of this study show that P retards gamma layer growth in both 0.00 and 0.20 wt% Al-Zn baths and has no effect on total Fe-Zn alloy layer growth. Ti and Nb additions to the substrate steel accelerated the growth kinetics of both the gamma and delta phase layers in the 0.20 wt% Al-Zn bath only.

To better understand substrate effects on the galvanizing reaction further study was needed on how the nucleation of Fe-Zn phases could be influenced by substrate/coating interface reactions. Based upon the findings of this study and mechanisms proposed in the literature, three interface reactions were chosen for further investigation, and they were: (1) the role of a surface oxide, (2) the role of substrate grain size, and (3) the role of P surface segregation. The investigation of substrate/coating interface reactions are discussed in the following section.

B. Substrate/Coating Interface Reactions

1. Effect of Substrate Iron Oxide

The annealing conditions prior to hot-dip galvanizing are conducted in atmospheres reducing for Fe, but which are usually oxidizing for elements such as Mn, P, Ti and Al which may be present in the steel. The oxidation of these elements leads to the formation of internal oxides as well as surface oxide particles. The location of some of these oxide particles at substrate steel grain boundaries has lead some investigators [59] to conclude that oxide particles may cause Fe-Zn outburst growths to form. The proposed oxide mechanism relies on the fact that the oxide particles located at substrate steel grain boundaries can be reduced by Al in the Zn bath to form Al_2O_3, thereby causing a local depletion in Al concentration in the bath in the vicinity of the newly formed oxide. Because oxide particles are found to be concentrated at steel substrate grain boundaries, the Al depletion near the substrate steel grain boundaries is significant and leads to localized Zn attack and the formation of Fe-Zn growths or outbursts at the grain boundary [59]. Guttmann [53] proposes that Zn is able to diffuse along the oxide particle/Fe_2Al_5 interface (in Zn baths containing Al) and this interface provides a fast diffusion path for Zn. Because oxide particles are predominantly found at substrate grain boundaries, the rapid diffusion and accelerated attack of Zn results in outbursts of Fe-Zn growth occurring at the substrate steel grain boundaries. In order to evaluate the proposed liquid Zn/oxide mechanism, oxidized steel samples were prepared for galvanizing reaction studies.

The purpose of the substrate iron oxide experiments was to study the effect of oxide thickness on Fe-Zn reaction kinetics during hot-dip galvanizing in 0.00 and 0.20 wt% Al-Zn baths. In the experiments described here the oxide was present as a continuous layer, instead of discrete oxide particles, thus the effect of a uniform oxide layer on galvanizing reactions was studied. The oxide layer development on the 84% cold worked low carbon steel annealed at 650°C for various hold times is shown in Figure 61. The oxide layer was found to follow $t^{1.3}$ kinetics, with a growth rate constant of 1.07 ± 0.29 $\mu m^3/s$. The oxide which formed was identified by x-ray diffraction analysis to be magnetite, Fe_3O_4, Figure 62. Most of the d-spacing data could also be attributed to Fe_2O_3, but this oxide is usually formed at temperatures greater than 1400°C [85]. The steel samples with varying oxide layer thickness were then hot-dip galvanized for 10 to 300 seconds, in 0.00 and 0.20 wt% Al-Zn baths.

a. 0.00 wt% Al-Zn Bath

The oxide layer initially acted as a physical barrier to liquid Zn attack of the underlying steel. Prolonged immersion in the bath led to penetration of the oxide by liquid Zn and reaction with the substrate steel to form Fe-Zn phases, as shown in Figure 63 where an oxide layer of varying thickness was galvanized for 300 seconds in a 0.00 wt% Al-Zn bath. The localized Fe-Zn alloy growths or outbursts which formed were counted along the entire length of the specimen for each of the oxidized samples studied. As the oxide layer thickness on the steel surface increased from approximately 1 to 4.5 μm, the number

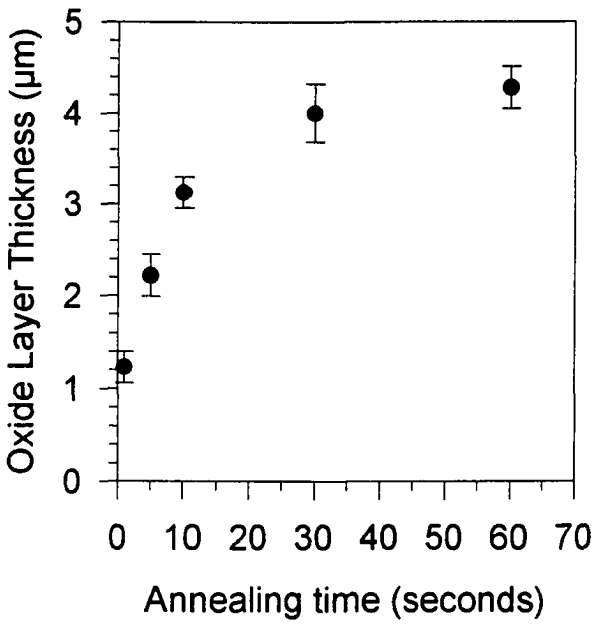

Figure 61. Surface oxide layer growth at 650°C.

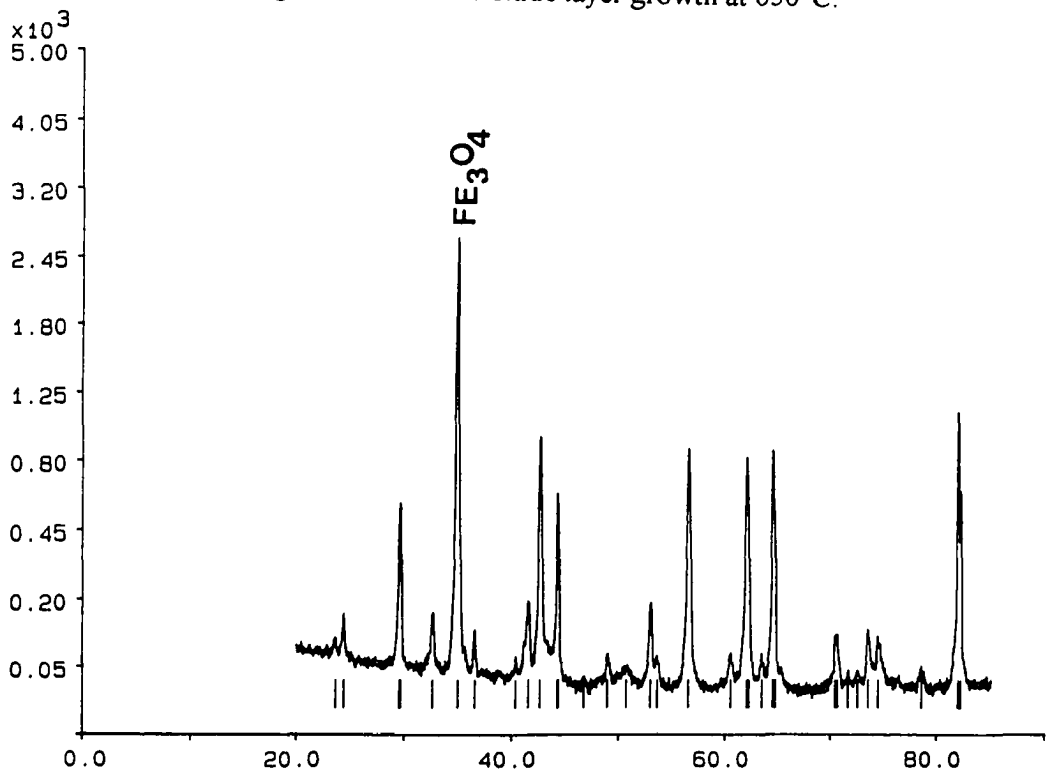

Figure 62. X-ray diffraction spectrum from an oxide layer formed after a 60 second anneal at 650°C.

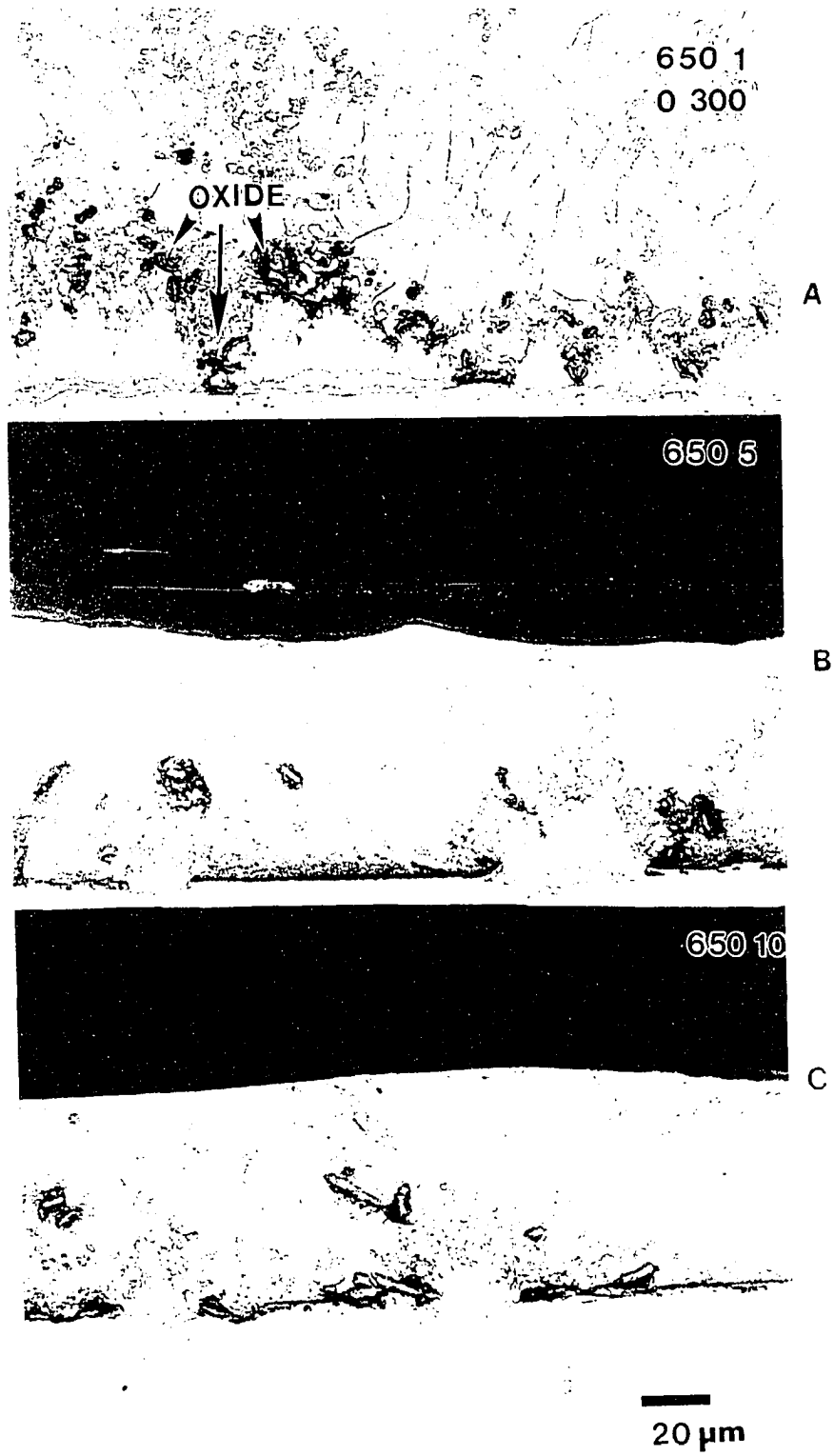

Figure 63. Fe_3O_4 oxide layer of (a) 1.23 µm (b) 2.22 µm and (c) 3.13 µm in thickness hot-dip galvanized in a 0.00 wt% Al-Zn bath for 300 seconds of immersion.

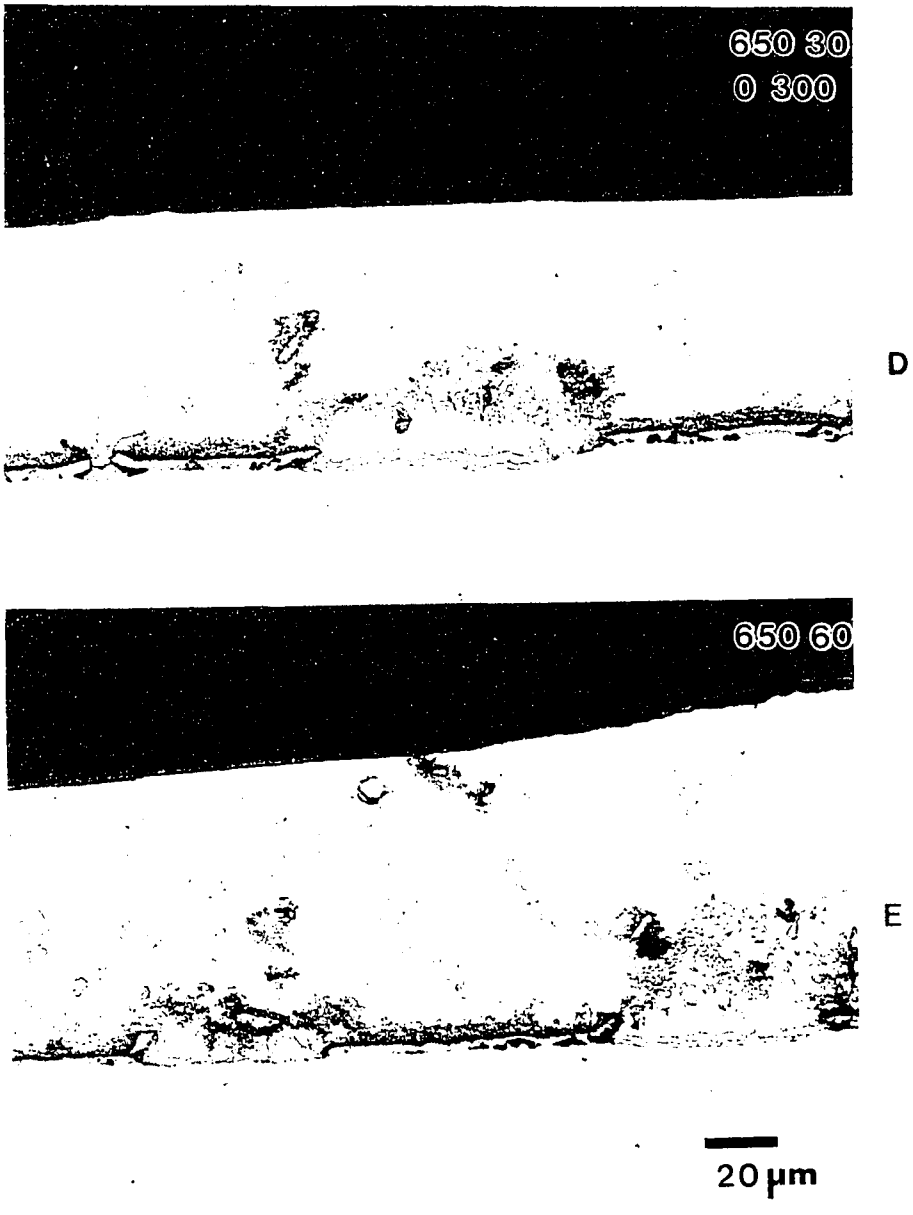

Figure 63. Fe_3O_4 oxide layer of (d) 4.00 µm and (e) 4.28 µm in thickness hot-dip galvanized in a 0.00 wt% Al-Zn bath for 300 seconds of immersion.

of localized Fe-Zn alloy growths decreased, as shown in the outburst count data in Figure 64. The Fe_3O_4 layer acts as a physical barrier thus a thick oxide layer provided a greater resistance to liquid Zn attack compared to thin oxide layers immersed for the same reaction time in the bath.

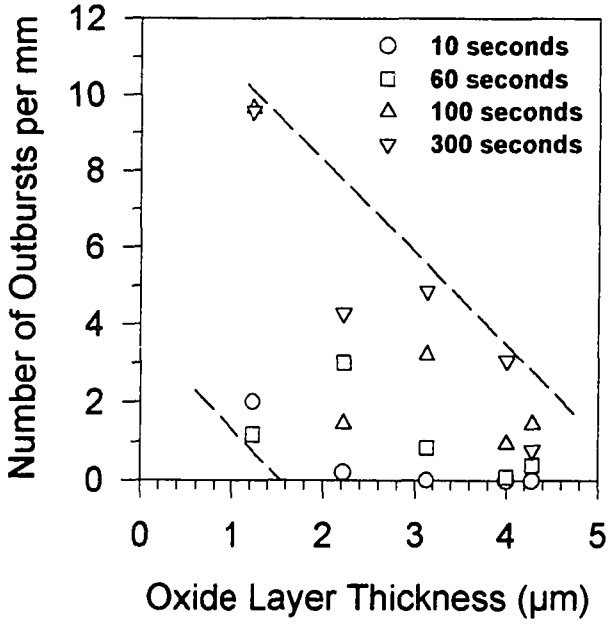

Figure 64. Number of localized Fe-Zn alloy growth events or outbursts formed on the oxidized steel surfaces hot-dip galvanized in a 0.00 wt% Al-Zn bath for 10, 60,100 and 300 seconds of immersion.

Immersion time in the Zn bath was varied to study the attack of an oxide layer of uniform thickness. Prolonged immersion in the bath led to penetration of the oxide by liquid Zn and reaction with the substrate steel to form Fe-Zn phases as shown in Figure 65 where an oxide of uniform thickness was galvanized for 10, 60, 100, and 300 seconds in a 0.00 wt% Al-Zn bath. After some incubation time weak points in the brittle oxide, such as cracks,

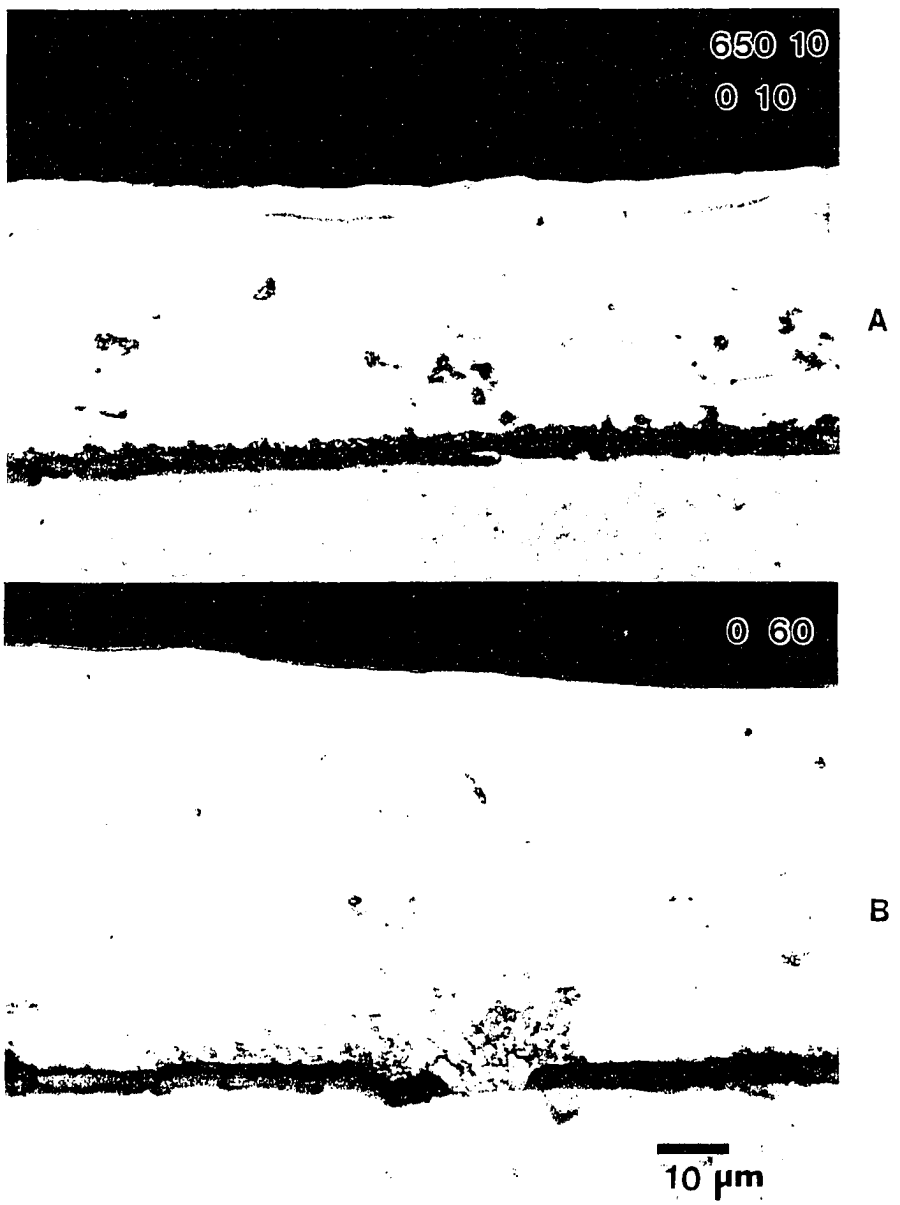

Figure 65. Cross sectional micrograph of Fe_3O_4 oxide layer formed after 10 second anneal at 650°C and hot-dip galvanized in a 0.00 wt% Al-Zn bath for (a) 10 and (b) 60 seconds of immersion.

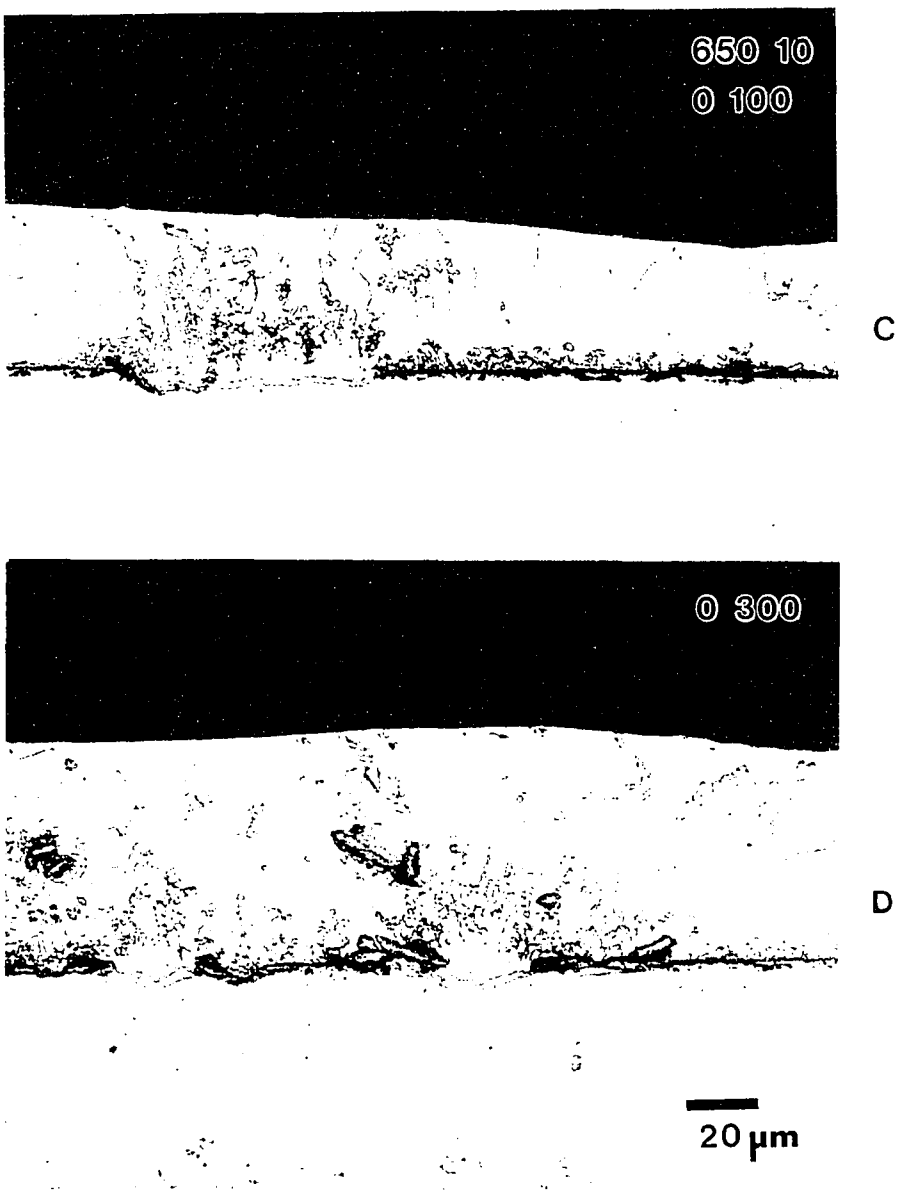

Figure 65. Cross sectional micrograph of Fe_3O_4 oxide layer formed after 10 second anneal at 650°C and hot-dip galvanized in a 0.00 wt% Al-Zn bath for (c) 100 and (d) 300 seconds of immersion.

allow for liquid Zn transport to the steel surface and the nucleation of Fe-Zn alloy growths at the steel/coating interface. As the immersion time in the bath increased the number of localized Fe-Zn growths increased. Figure 64 also indicates that as the time of immersion in the Zn bath was increased for an oxide layer of uniform thickness (i.e. a 3.13 μm oxide layer as shown in Figure 65) the trend was toward an increase in the number of Fe-Zn outbursts formed. As expected, the longer time of exposure of the oxide layer to liquid Zn resulted in increased attack and penetration of Zn to the substrate steel.

The localized Fe-Zn growth regions that formed due to Zn penetration of the oxide layer had a growth direction which was predominantly toward the Zn melt. However, if the oxide layer itself is used as a marker, some Fe-Zn phase growth into the steel substrate was also apparent, as shown in Figure 65c and d. Lateral growth of the Fe-Zn reaction layer also occurred along the steel/oxide interface. At longer times of immersion the localized Fe-Zn growths were observed to coalesce (see Figure 63a). The coalescence of Fe-Zn growths made it difficult to accurately quantify the number of independent growth events on thin oxide layers at long reaction times, however, the reaction generally progressed toward complete coverage of the steel/coating interface, and the exfoliated oxide became incorporated into the coalesced structure as distinct oxide particles (arrows) in the final alloy layer structure, as shown in Figure 63a.

Fe-Zn phases formed on the oxidized steel surface samples were compared morphologically to growths formed on non oxidized substrate steel samples galvanized in

the same 0.00 wt% Al-Zn bath. The Fe-Zn alloy layer growth formed on the non oxidized substrate steel samples (ULC, ULC-P, etc. discussed in section V.A.1.) were analyzed for compositional analysis, thus identification of the individual Fe-Zn phases formed was possible. Therefore based upon the known compositional analysis of the morphologically similar Fe-Zn phases, a qualitative identification of Fe-Zn phases formed on the oxidized steel samples was made. The progress of Zn attack through the oxide layer and the Fe-Zn reaction sequence that followed is proposed as follows. Once liquid Zn penetrated the oxide layer, zeta phase was the first phase to form at the steel surface, and its columnar growth was predominantly toward the Zn melt, however some limited growth into the steel substrate also occurred (Figure 66). As reaction time increased, delta phase, and then gamma phase layers formed within the localized Fe-Zn growth regions (Figure 65c and d.). Lateral growth of the Fe-Zn alloy layer growths along the steel/coating interface resulted in the exfoliation of the oxide at the interface. The retained Fe_3O_4 oxide became incorporated into the coating Fe-Zn alloy layer structure near the zeta/Zn interface after the long times of reaction. Notably entrapped eta phase which was found to form within the zeta phase layer (between the $zeta_1$ and $zeta_2$ layers) on non oxidized steel samples (Figure 34d-f), was absent in the coatings formed on the oxidized steel surface samples. The incorporated oxide particles most likely act as a barrier to liquid Zn diffusion along the boundaries of the columnar zeta phase, thus preventing the formation of entrapped of eta phase regions within the zeta phase layer.

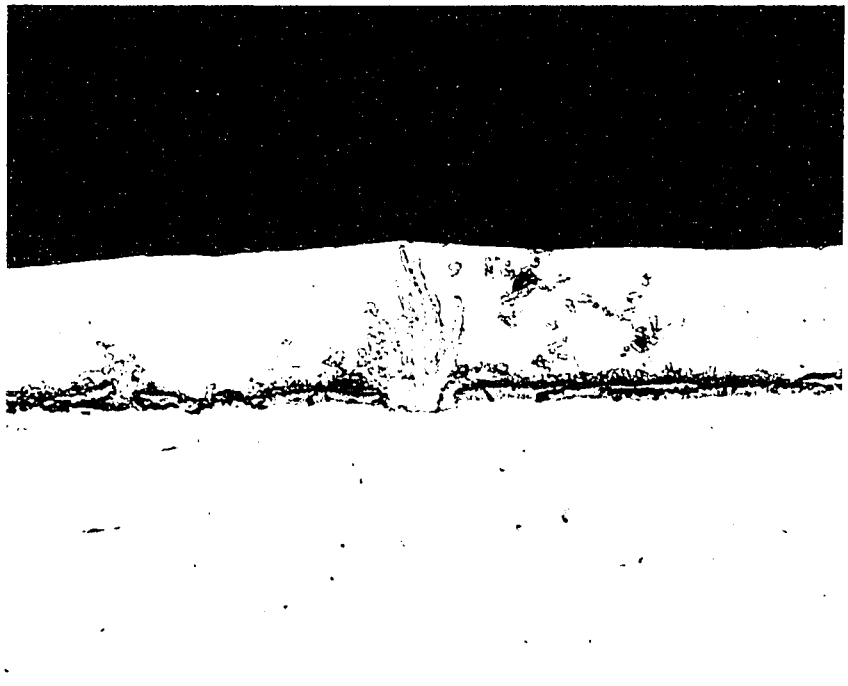

Figure 66. Columnar structure of the zeta phase layer first formed after Zn penetration of the oxide layer and reaction with the steel substrate (4.28 μm oxide layer, hot-dip galvanized in a 0.00 wt% Al-Zn bath for 100 seconds of immersion).

The oxidized steel samples with a 4.28 μm oxide layer had large areas of the oxide that were not attacked by Zn after 300 seconds of immersion in the bath. The apparent stability of the Fe_3O_4 oxide indicates that it is not immediately reduced thermodynamically by liquid Zn. The Ellingham diagram indicates that liquid Zn should reduce Fe_3O_4 at 450°C at oxygen partial pressures equal to or less than 10^{-14} atmospheres [85]. The partial pressure of oxygen in the Zn bath is unknown, however it can be considered to be extremely low as a Zn oxide forms as a dross on the surface of the bath due to exposure to standard room temperature and pressure conditions, and little if any oxygen remains

dissolved in the Zn bath. Discrete crystals of zeta or delta phase were found to form at the oxide/liquid Zn interface at all reaction times (Figure 65a-d), indicating that limited reduction of the oxide by liquid Zn may occur. Limited reduction of the oxide by liquid Zn may account for both the nucleation of zeta or delta phase on the oxide surface in contact with liquid Zn, as well as the attack of liquid Zn along defects in the oxide layer.

b. 0.20 wt% Al-Zn Bath

The wetting of the oxide surface by the Zn(Al) melt was poor, as evidenced by the extremely limited adherence of liquid Zn(Al) to the oxidized surface (Figure 67a). The liquid Zn(Al) melt appears not to reduce the Fe_3O_4 oxide layer even in a limited manner to allow for adhesion of the melt to the oxide.

Because of the absence of liquid Zn(Al) adhesion to the oxide and the lack of Fe-Zn reaction, no data could be collected on the effect of oxide thickness or bath immersion time on Fe-Zn growth which may occur on an oxidized steel surface in a 0.20 wt% Al-Zn bath. Only a few isolated growths were observed for the entire test matrix of samples, and generally these growths had a 2 layer morphology similar to that formed on non oxidized steel samples immersed in 0.20 wt% Al-Zn baths. The two layer morphology consisted of a gamma phase layer at the steel/coating interface, and an adjacent delta phase layer which constituted most of the localized Fe-Zn growth region (Figure 67b.).

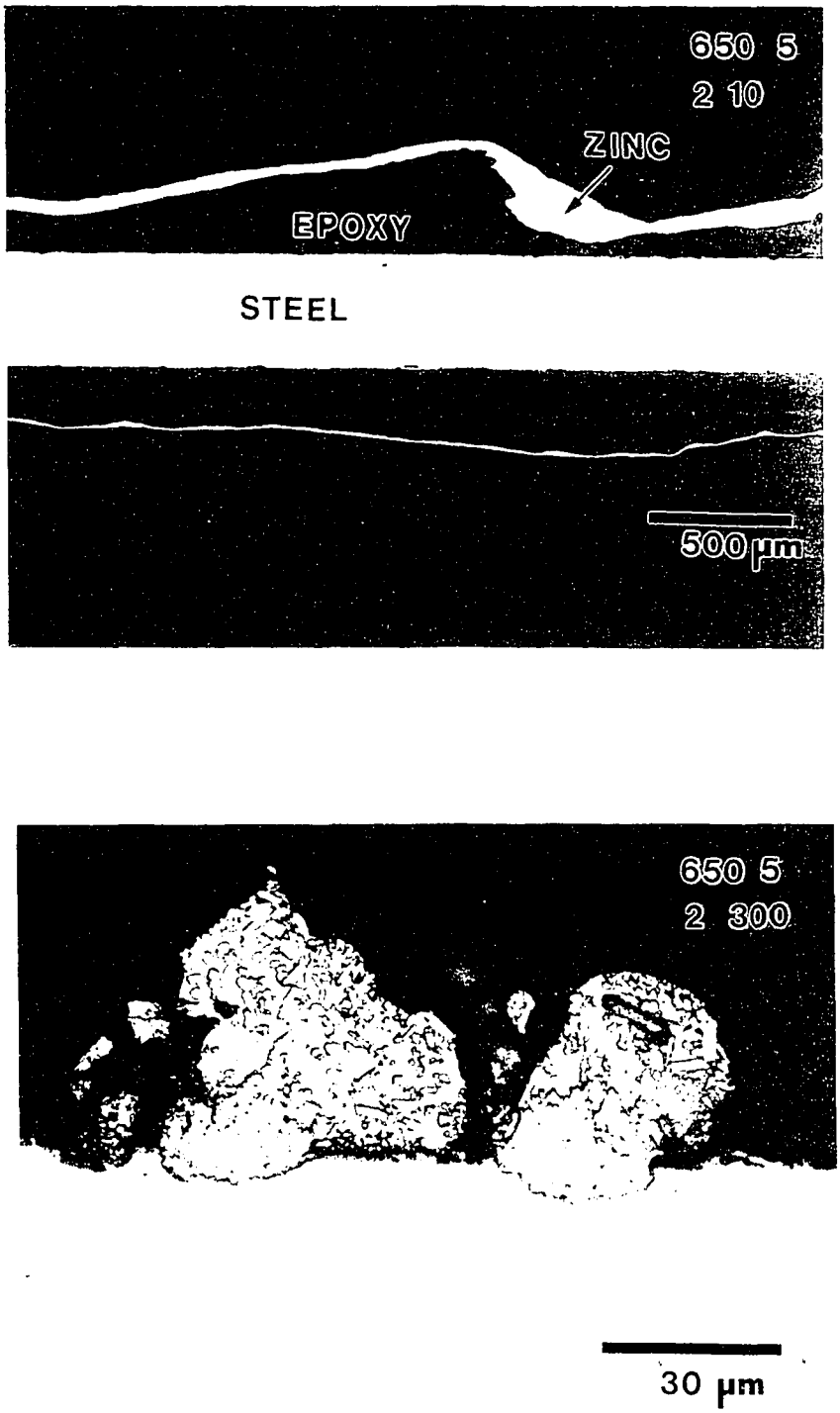

Figure 67. Poor wetting of the oxidized steel surface in a 0.20 wt% Al-Zn bath resulting in little adherence of the coating to the substrate (a), and a limited number of localized Fe-Zn alloy growth events (b).

For non oxidized steel samples, Fe-Zn outbursts that form in Zn(Al) baths often contain Fe and Al rich particles at the surface of the outbursts which are in contact with the liquid Zn [44], as though the Fe_2Al_5 inhibition compound has been pushed out into the Zn melt. On the same sample there exists no Fe-Al rich particles at the outburst/substrate steel interface where Fe-Zn growth has occurred, thus indicating an interruption in the Fe_2Al_5 layer inhibition. The Fe_3O_4 oxide layer formed on the oxidized steel surface samples was observed to be ejected into the Zn melt for the 0.00 wt% Al-Zn coatings, and was found to become incorporated into the surface structure of the Fe-Zn outbursts, at the zeta/Zn interface (Figure 63a). After outburst formation, no oxide remains at the outburst/substrate steel interface where this localized growth event occurred (Figures 63 and 65). The oxide layer attack by liquid Zn at the steel/coating interface also results in an interruption in the inhibition effect of the Fe_3O_4 oxide layer. Thus like the Fe_2Al_5 inhibition layer that forms at the steel/coating interface in Al containing Zn baths, the oxide layer at the steel surface acts as an inhibition layer for the Fe-Zn reaction. Similar to the Fe_2Al_5 layer which cannot remain thermodynamically stable under certain bath conditions, the Fe_3O_4 oxide layer contains defects along which liquid Zn is able to penetrate to the substrate steel surface and react to form Fe-Zn alloy phase growths. Thus the Fe_3O_4 oxide layer is similar to the Fe_2Al_5 layer in that it eventually becomes unstable. In the oxide layer fast diffusion paths for Zn are cracks, or other macroscopic defects whereas in the Fe_2Al_5 layer grain boundaries act as fast diffusion paths as recent experiments [86] have shown Zn to diffuse intergranularly in Fe_2Al_5 [86]. The Fe_3O_4 layer acts as a physical barrier to liquid Zn attack of the substrate steel much like the Fe_2Al_5

inhibition layer formed in Al containing Zn baths. Significant dissolution of the oxide did not occur, and thus the oxide layer alone did not cause Fe-Zn outbursts to form, rather localized Zn diffusion along defects (cracks) in the oxide result in outburst formation. The results discussed here support the liquid Zn/oxide mechanism of Guttmann [53] who postulated that Zn diffusion along oxide particle interfaces results in fast diffusion paths for Zn and the formation of Fe-Zn growths. Because the Al containing Zn bath had poor wetability of the oxidized surface the liquid Zn/oxide mechanism of Al in the bath reducing surface oxides [59] could not be evaluated in this study.

2. Effect of Substrate Grain Size

It has been proposed that IF steel substrate grain size influences Fe-Zn reaction kinetics and growth rate during hot-dip galvanizing [1]. It has been suggested [1] that a finer grain size substrate is more reactive because Fe-Zn phases are thought to first nucleate and grow at substrate steel grain boundaries, therefore as more grain boundary area is available for reaction with the liquid Zn bath on a fine grain size steel more rapid Fe-Zn phase growth results. Strain annealing experiments to produce large grain sizes for IF steels containing Ti ,and Ti + Nb additions were not successful due to the presence of fine precipitates of Ti and Nb carbides which act to pin grain boundaries and restrict grain growth. In order to evaluate the effect of substrate grain size two different grain sizes (15 μm and 85 μm) of the same chemistry ULC steel were hot-dip galvanized and their

relative Fe-Zn phase growth behavior was studied. Although the ULC steel did not contain stabilizing elements of Ti or Nb, it can be considered as an unstabilized interstitial free steel because it contains less carbon (0.003 wt%) than the solubility limit for C in ferrite (0.005 wt%), thus it contains small amounts of interstitial carbon yet some carbon remains in solid solution. Therefore the ULC steel can be considered as interstitial free, however, not all of the carbon is stabilized [49].

a. Total Fe-Zn Alloy Layer Growth - 0.00 wt% Al-Zn Bath

For both the 15 and 85 μm grain size ULC steel the entire steel/coating interface reacted with the liquid Zn to form a uniform reaction layer, hereafter referred to as a total alloy layer. Fe-Zn alloy layer development on the 15 and 85 μm grain size ULC steel substrates is shown in Figures 68 and 69, respectively. To determine the overall rate of reaction, the total Fe-Zn alloy layer thickness was measured for each sample and the data are plotted in Figures 70 and 71 for the coatings deposited on the 15μm and 85 μm grain size ULC steel substrates.

The total Fe-Zn alloy layer growth for both grain sizes of ULC steel showed the same behavior over the reaction times studied. Using the power law growth equation

$$Y = Kt^n \qquad (1)$$

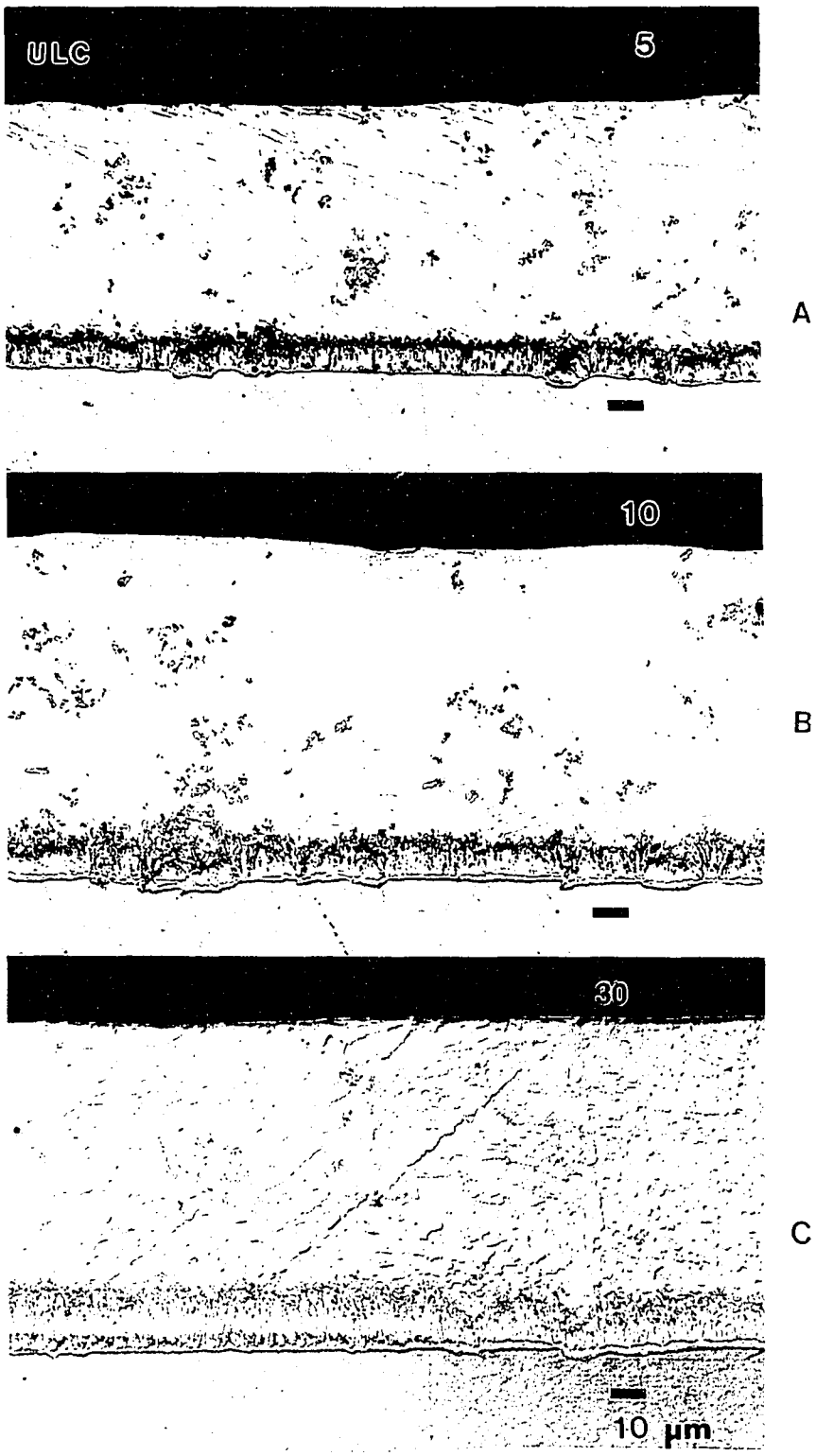

Figure 68. 15 µm grain size ULC steel hot-dip galvanized in a 0.00 wt% Al-Zn bath for (a) 5 (b) 10 and (c) 30 seconds of immersion.

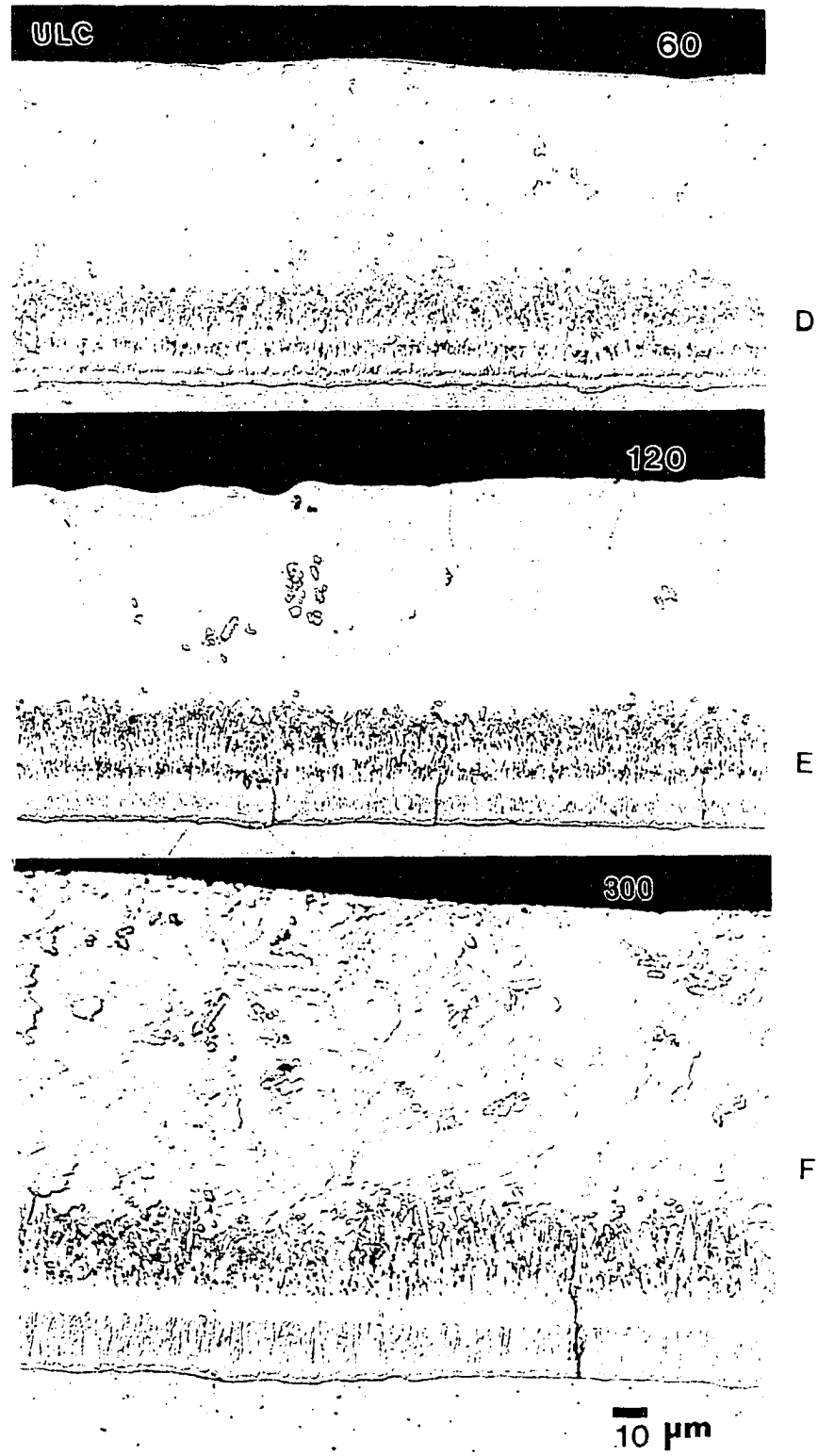

Figure 68. 15 µm grain size ULC steel hot-dip galvanized in a 0.00 wt% Al-Zn bath for (d) 60 (e) 120 and (f) 300 seconds of immersion

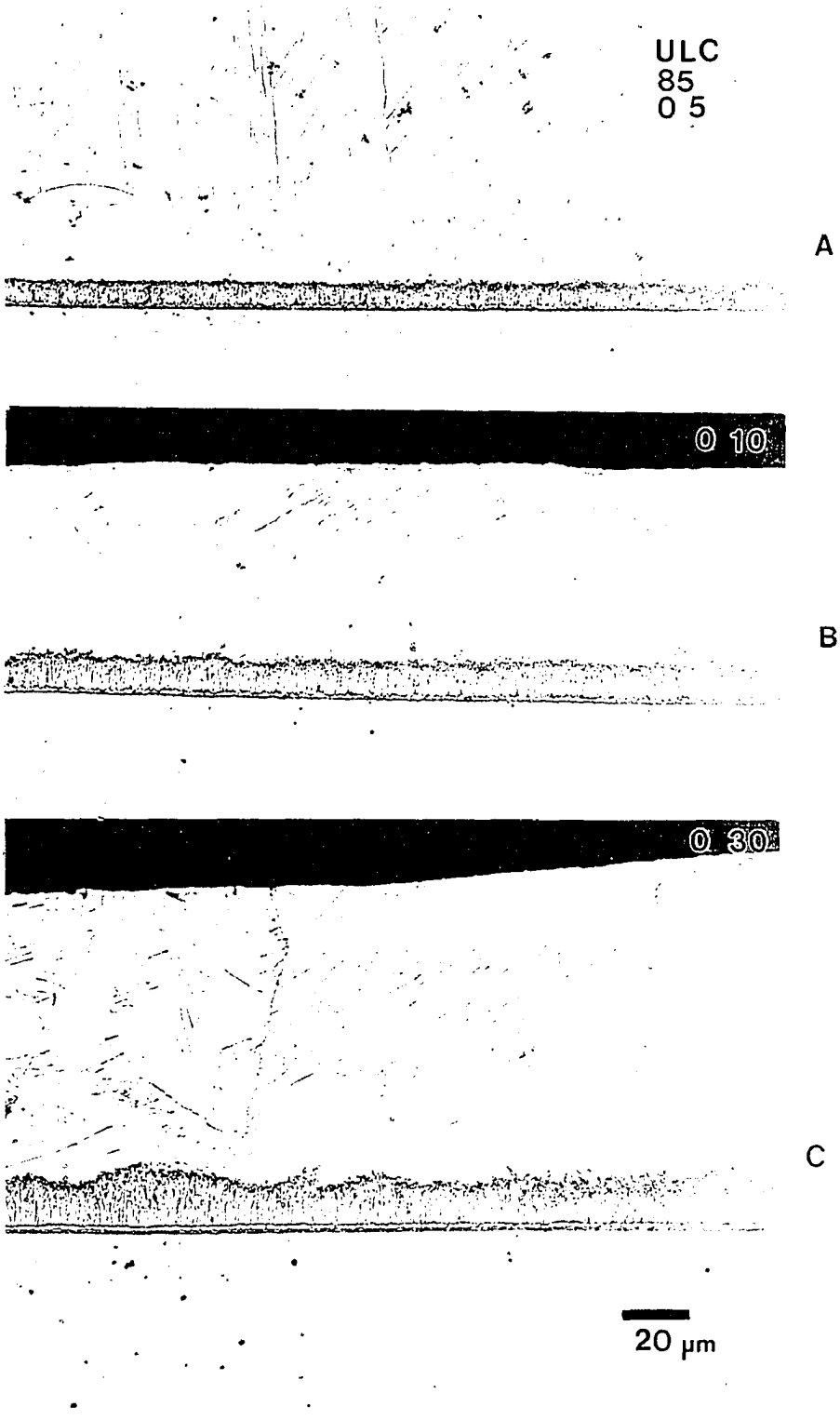

Figure 69. 85 µm grain size ULC steel hot-dip galvanized in a 0.00 wt% Al-Zn bath for (a) 5 (b) 10 and (c) 30 seconds of immersion.

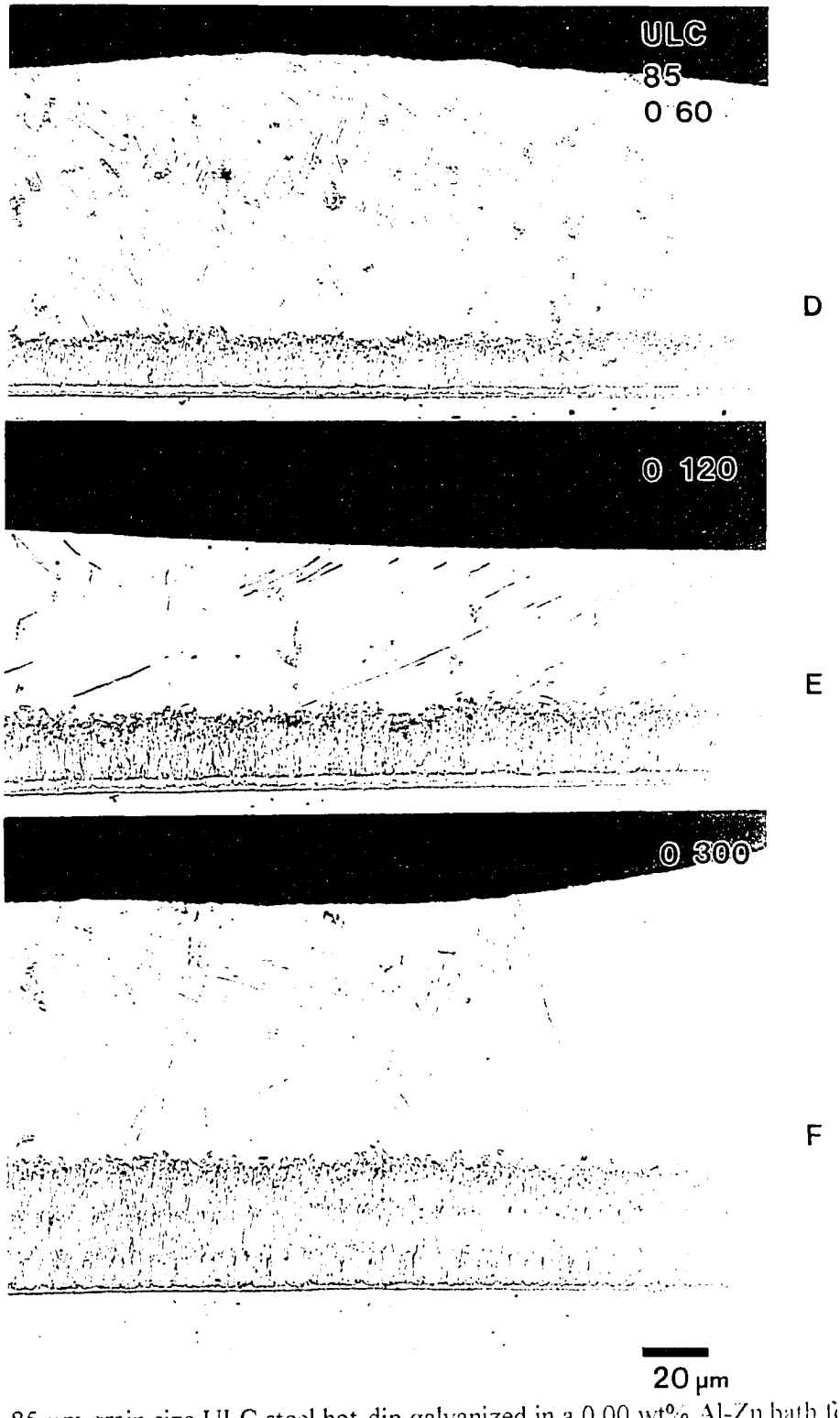

Figure 69. 85 µm grain size ULC steel hot-dip galvanized in a 0.00 wt% Al-Zn bath for (d) 60 (e) 120 and (f) 300 seconds of immersion.

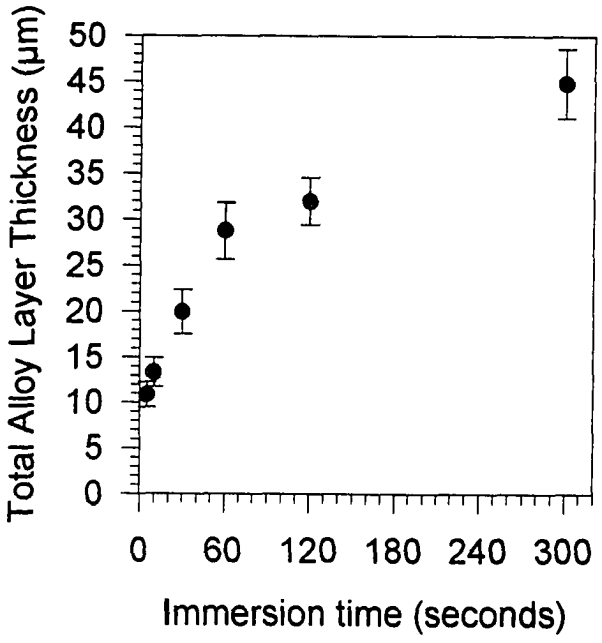

Figure 70. Total Fe-Zn alloy layer growth for the 15 µm grain size ULC steel hot-dip galvanized in a 0.00 wt% Al-Zn bath.

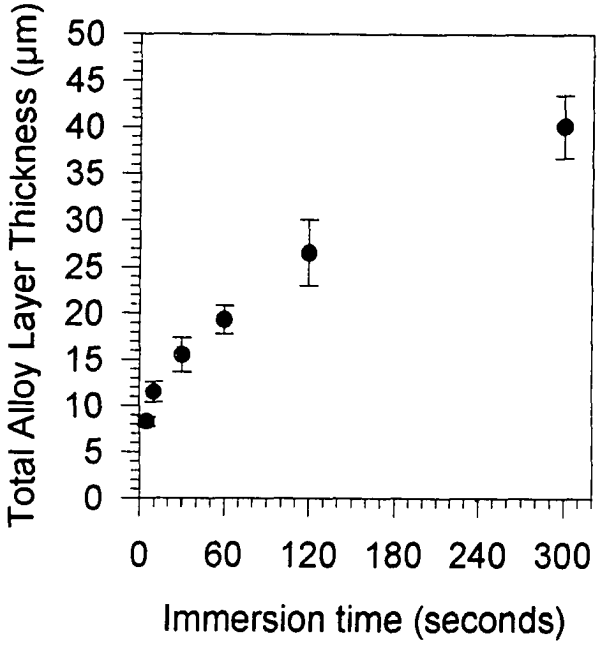

Figure 71. Total Fe-Zn alloy layer growth for the 85 µm grain size ULC steel hot-dip galvanized in a 0.00 wt% Al-Zn bath.

or applying a logarithmic function on either side of the equation,

$$\log Y = \log K + n \log (t) \qquad (2)$$

a plot of the log value of the total alloy layer thickness (Y) as a function of the log value of immersion time in the bath (t), can be fitted to the data to determine a line whose slope is defined as n, the growth rate time constant value [16]. The growth rate time constant value is an indication of the type of kinetics controlling the growth. An n value of 0.5 is indicative of parabolic diffusion controlled growth, while an n value of 1.0 is representative of linear kinetics in which growth is interface controlled. The total alloy layer n value was found by linear regression analysis to be 0.35 for the 15 μm grain size ULC steel, and 0.33 for the 85 μm grain size ULC steel, as shown in Table XVII. The regression analysis was conducted using the software program Sigma Plot and the error associated with the average thickness measurements could not be included in the fit of the data because logarithmic values of the error as fractions are negative on a log scale. The error reported in Table XVII is the error related to the linear regression of the data. Although there was a large error associated with the 85 μm ULC substrate, the total alloy layer growth behavior was observed to be similar to that for the 15 μm ULC. Therefore the following discussion will treat the two substrates as having total alloy layer growth that followed the same growth-time relationship.

Table XVII. Total Alloy Layer and Individual Fe-Zn Phase Layer Growth Rate Time Constant (n) Values for the 15 μm and 85 μm grain size ULC Steel Galvanized in a 0.00 wt% Al-Zn Bath.

Sample / Layer	Growth Rate Time Constant, n
15 μm ULC / total Fe-Zn alloy layer	0.35 ± 0.02
85 μm ULC / total Fe-Zn alloy layer	0.33 ± 0.21
15 μm ULC / gamma layer	0.24 ± 0.06
85 μm ULC / gamma layer	0.26 ± 0.02
15 μm ULC / delta layer	0.51 ± 0.11
85 μm ULC / delta layer	0.43 ± 0.18
15 μm ULC / zeta layer	0.32 ± 0.03
85 μm ULC / zeta layer	0.40 ± 0.08

The n values for total alloy layer growth indicate its growth follows a relationship which is slower than that expected for diffusion controlled kinetics. The data indicate a $t^{1/3}$ relationship, indicative of grain boundary diffusion or diffusion along grain boundaries during coarsening of the grain or grain growth [87]. Onishi [31] showed that the growth of the Fe-Zn phase layers in solid Fe-Zn diffusion couples (annealed at 410°C for up to 100 hours) were controlled by the dominant one sided diffusion of Zn through the phase layers toward the substrate Fe. Onishi found the total alloy layer in solid Fe-Zn diffusion couples to have an n value of 0.43. The n values determined here for total alloy layer

growth were determined over much shorter reaction times (5-300 seconds) and at a temperature of 450°C, above the melting point of Zn (419.58°C [14]). Therefore some discrepancy is expected between the growth rate time constant determined here for solid Fe-liquid Zn couples, and those of solid Fe-Zn couples analyzed previously [31]. The $t^{1/3}$ relationship determined for the growth of the total alloy layer together with the previously determined one sided diffusion of Zn [31], indicates that the supply of Zn to the growing total alloy layer becomes limited, otherwise growth would follow volume diffusion $t^{1/2}$ growth kinetics.

b. Individual Fe-Zn Phase Layer Growth - 0.00 wt % Al-Zn Bath

Three individual Fe-Zn phase layers were observed to form in the 15 and 85 μm grain size ULC 0.00 wt% Al-Zn coated steels; (1) gamma, (2) delta and (3) zeta phases. Zeta phase formed at the steel/coating interface first, followed in time by the formation of delta phase between the zeta phase and the steel/coating interface, and lastly a gamma phase layer formed between delta phase and the steel/coating interface (Figure 33). Therefore from the steel/coating interface, the final layered structure consisted of a uniform gamma phase at the steel/coating interface, a delta phase layer adjacent to the gamma phase, with zeta phase as a third distinct layer adjacent to the delta phase layer, and in direct contact with the liquid Zn melt.

The individual phase layer growth data is shown in Figures 72 and 73 for the 15 and 85 μm grain size ULC steel, respectively. To confirm the identity of the individual phase layers electron microprobe analysis for Fe and Zn analysis were conducted at 1.0 μm intervals along a line parallel to the diffusion direction (perpendicular to the steel/coating interface) on the 15 and 85 μm ULC steels immersed for 10, 60, and 300 seconds in the 0.00 wt% Al-Zn bath. The 15 μm ULC steel Fe-Zn alloy layer composition data was previously shown in Figure 36, and that for the 85 μm material is shown in Figure 74. The Fe composition analysis confirmed the identity of individual gamma, delta and zeta phase layers within the total Fe-Zn alloy layer (based upon metastable Fe-Zn phase equilibrium [24]). The Fe composition profiles for both the 15 and 85 μm grain size samples were similar, indicating that there was no significant differences in the chemistry of the alloy layer formed on the different grain size steel substrates. The region of the samples which were analyzed in the microprobe were photographed in a back scattered electron (BSE) imaging mode in an attempt to resolve atomic number contrast between individual phase layers. BSE images of the regions used for microprobe analysis for the 15 and 85 μm ULC steels are shown in Figures 75 and 76, respectively. The BSE images also show the development of a three phase layer morphology within the total Fe-Zn alloy layer.

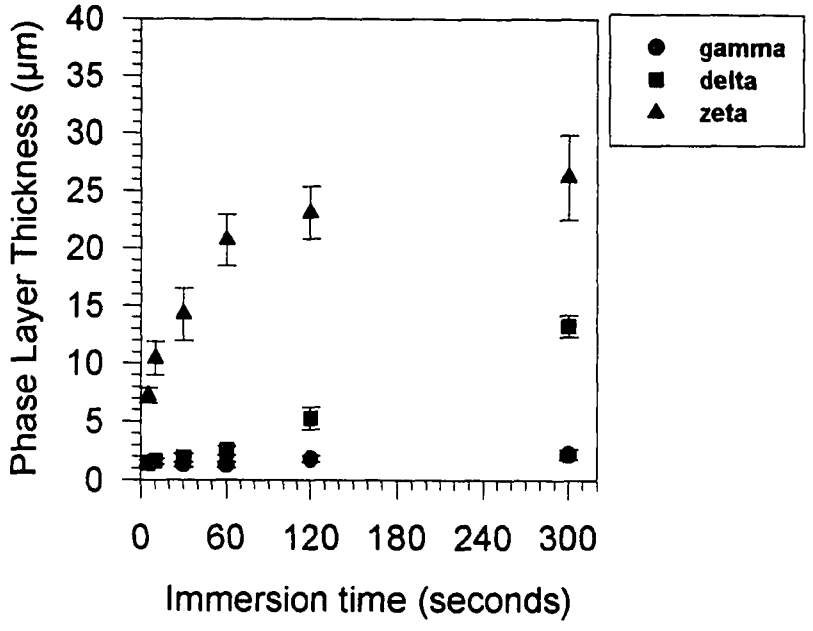

Figure 72. Individual Fe-Zn gamma, delta, and zeta phase layer growth for the 15 µm grain size ULC steel hot-dip galvanized in a 0.00 wt% Al-Zn bath.

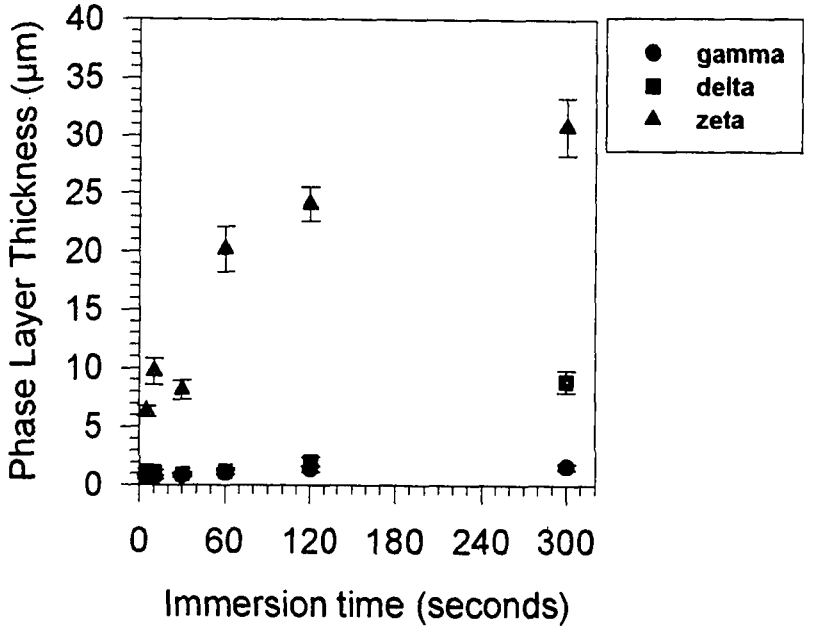

Figure 73. Individual Fe-Zn gamma, delta, and zeta phase layer growth for the 85 µm grain size ULC steel hot-dip galvanized in a 0.00 wt% Al-Zn bath.

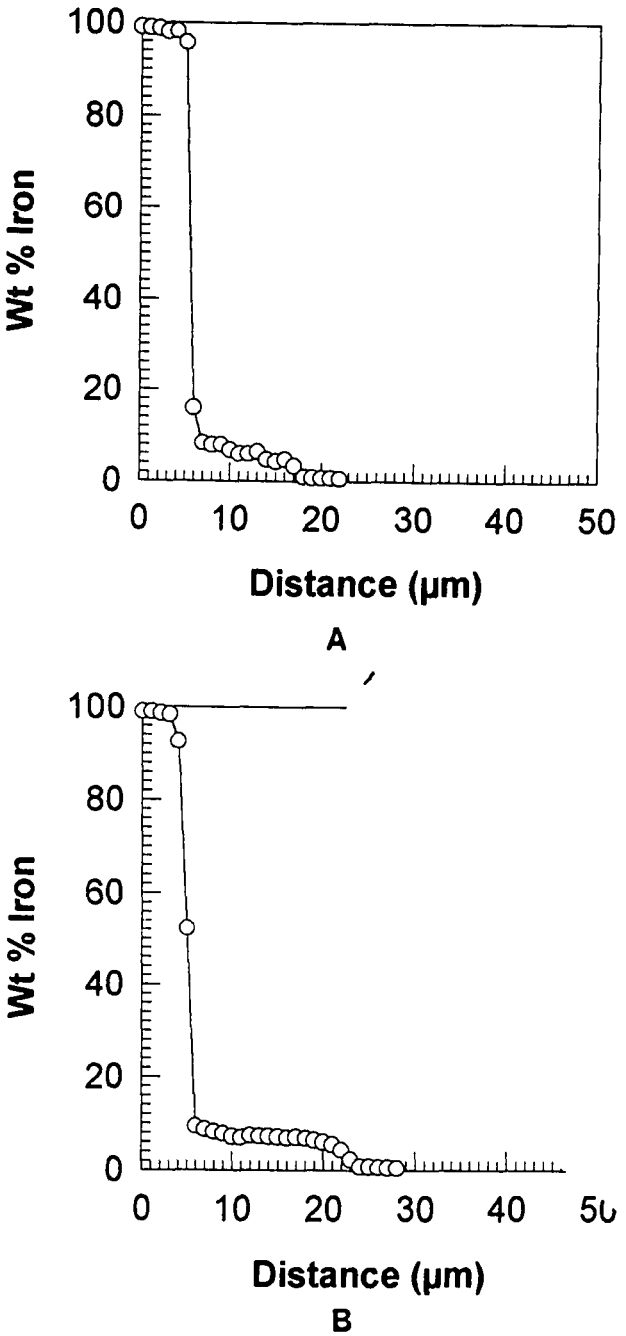

Figure 74. Iron concentration profile for the total Fe-Zn alloy layer formed on the 85 μm grain size ULC steel hot-dip galvanized in a 0.00 wt% Al-Zn bath for (a) 10 and (b) 60 seconds of immersion.

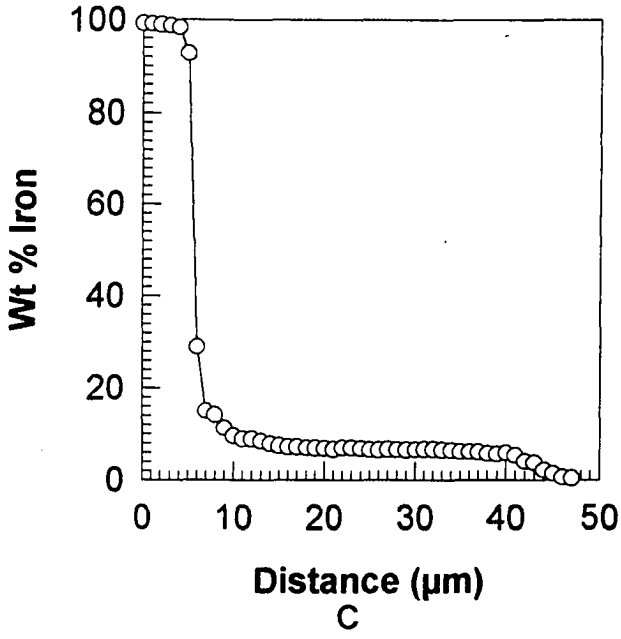

Figure 74. Iron concentration profile for the total Fe-Zn alloy layer formed on the 85 μm grain size ULC steel hot-dip galvanized in a 0.00 wt% Al-Zn bath for (c) 300 seconds of immersion.

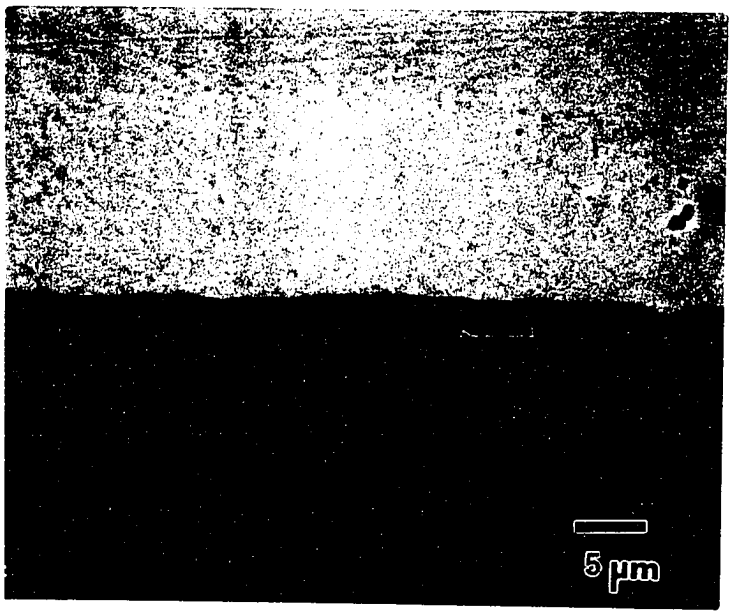

A

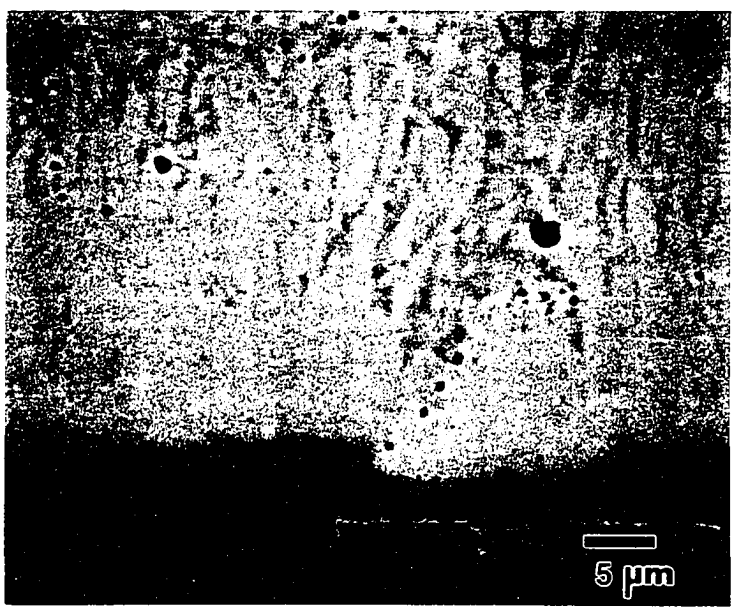

B

Figure 75. BSE images of the Fe-Zn phase layers formed on the 15 µm grain size ULC steel hot-dip galvanized in a 0.00 wt% Al-Zn bath for (a) 10 and (b) 60 seconds of immersion. The micrographs are the areas which were analyzed for compositional analysis presented in Figure 36a and b.

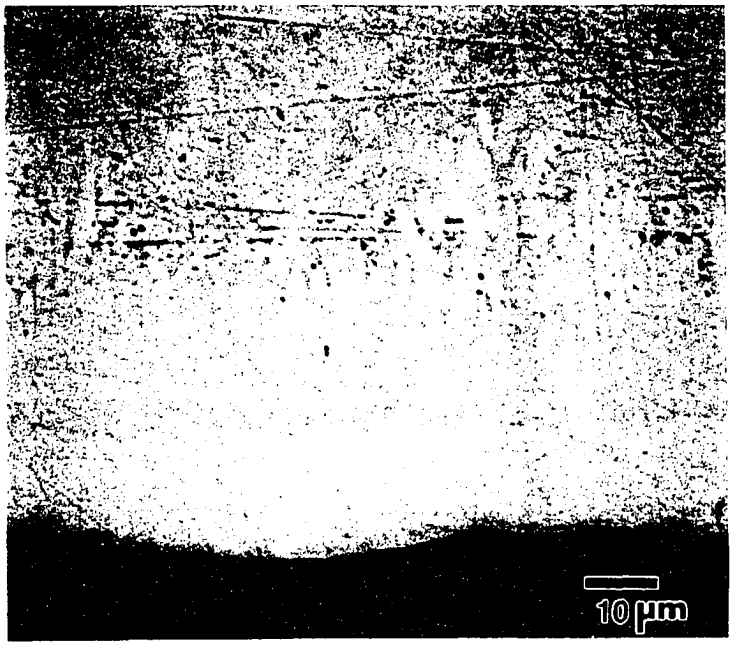

C

Figure 75. BSE images of the Fe-Zn phase layers formed on the 15 µm grain size ULC steel hot-dip galvanized in a 0.00 wt% Al-Zn bath for (c) 300 seconds of immersion. The micrograph is the area which was analyzed for compositional analysis presented in Figure 36c.

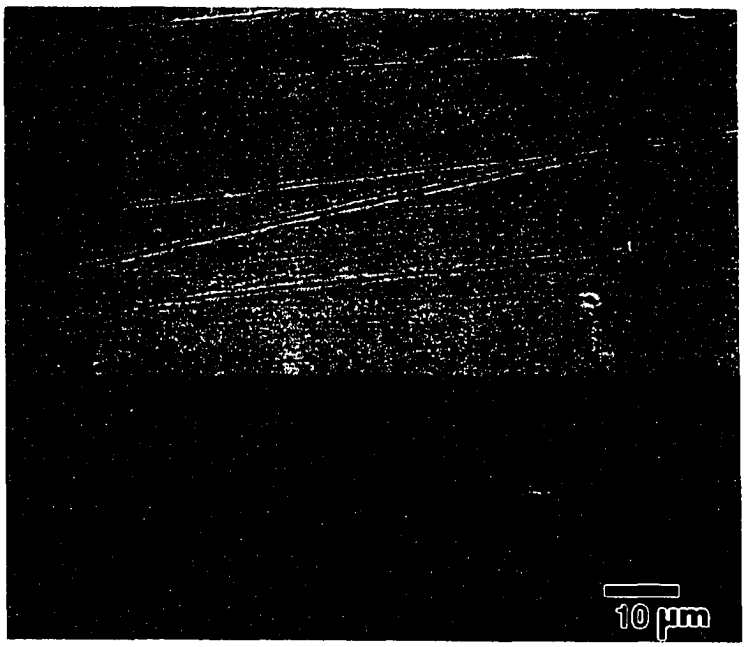

A

B

Figure 76. BSE images of the Fe-Zn phase layers formed on the 85 µm grain size ULC steel hot-dip galvanized in a 0.00 wt% Al-Zn bath for (a) 10 and (b) 60 seconds of immersion. The micrographs are the areas which were analyzed for compositional analysis presented in Figure 74a and b.

C

Figure 76. BSE images of the Fe-Zn phase layers formed on the 85 µm grain size ULC steel hot-dip galvanized in a 0.00 wt% Al-Zn bath for (a) 10 (b) 60 and (c) 300 seconds of immersion. The micrographs are the areas which were analyzed for compositional analysis presented in Figure 74c.

(i). Gamma Phase Layer Growth

The gamma layer growth discussed here and in following sections is for an interfacial gamma phase layer. The techniques used to evaluate layer composition could not resolve gamma from $gamma_1$ phase, therefore the entire layer is hereafter referred to as a gamma phase layer.

The 15 μm ULC steel first showed gamma layer formation after 30 seconds of reaction time. The gamma phase was observed to form and grow over the entire reaction time studied (5-300 seconds) for the 85 μm ULC steel. The gamma phase layer formed on the 15 μm ULC steel at times less than 30 seconds could have been present but then would have been too thin a layer to be resolved with the techniques used in this study. The growth rate time constant (n) values for gamma layer growth are reported in Table XVII. Both the 15 and 85 μm ULC steels showed similar n values (0.24 and 0.26, respectively). The n values determined for gamma layer growth are within the range of 0.10 - 0.50, which have been reported by other investigators for gamma layer growth [17].

Gamma layer growth followed a $t^{1/4}$ relationship, indicative of grain boundary diffusion growth kinetics or diffusion along grain boundaries of growing grains [87. The supply of Zn to the gamma phase layer may be limited due to the consumption of Zn atoms by the adjacent and more rapidly growing zeta and delta phase layers (discussed in the following section V.B.2).

(ii). Delta Phase Layer Growth

For both the 15 and 85 μm ULC samples the delta phase was observed to form and grow over the entire reaction time studied. The delta layer growth data were first analyzed to determine growth rate time constant values, and n values of 0.51 and 0.43 were calculated for the 15 and 85 μm ULC steels, respectively. The n values are in agreement with those reported by other investigators [17] of 0.49 - 0.65 for delta layer growth. The 85 μm steel had a large error associated with its n value (see Table XVII). Growth rate time constant values reported previously in the literature for individual Fe-Zn phase layer growth are not reported with their associated error in the regression analysis, therefore an error comparison of this data to previous work is not possible.

(iii). Zeta Phase Layer Growth

From 5 to 60 seconds of reaction time the zeta phase layer forms as a single layer, and it is adjacent to the delta phase layer and in contact with the liquid Zn bath. At 60 seconds of immersion and thereafter, the zeta phase layer has a two layer morphology which is defined by a horizontal array of voids (see Figure 68d-f). Upon further analysis of the unetched microstructure in the SEM the voids were found to contain solidified Zn (eta phase) as shown in Figure 77. Also evident in Figure 77 are pores which were found to form throughout the total Fe-Zn alloy layer, however, their formation occurred predominantly at the Zn/zeta phase interface. The pores are most likely shrinkage defects

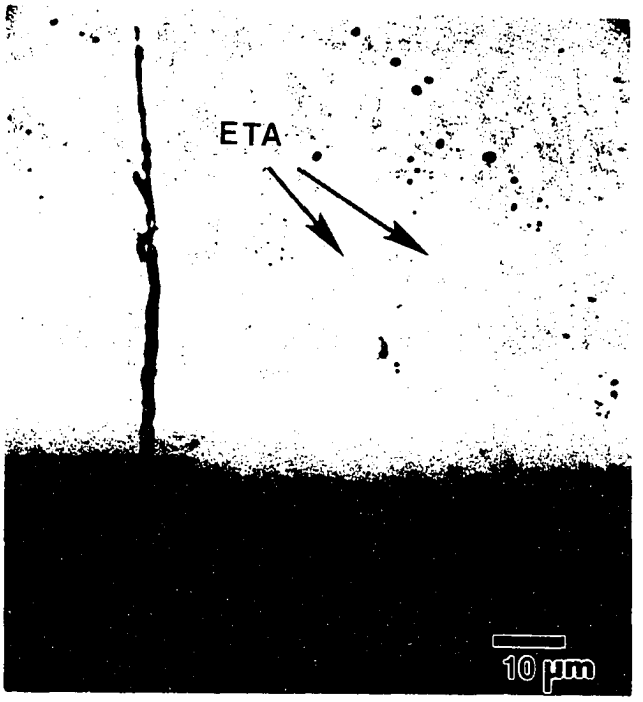

Figure 77. BSE images of the Fe-Zn phase layers formed on the 15 µm grain size ULC steel hot-dip galvanized in a 0.00 wt% Al-Zn bath for 300 seconds, showing areas of entrapped eta phase.

formed due to volume contraction during solidification of the melt to form eta phase. The mechanism describing the two layer morphology of zeta phase (and eta phase formation within the zeta phase) was previously discussed in section V. A. 1. The zeta phase was analyzed as one complete layer (with entrapped eta phase) and growth rate time constant values of 0.32 and 0.40 were calculated for the 15 and 85 µm ULC steels, respectively. The n values are near the range of 0.16 - 0.36 reported by other investigators for the growth time constant value of the zeta layer [17].

Zeta layer growth is most likely not affected by substrate grain size like the gamma and delta phase layers which are more closely associated with the substrate steel/coating interface. From the beginning of the reaction times studied (5 seconds) the zeta layer is in direct contact with liquid Zn. Limited Zn transport along the columnar boundaries of the zeta phase due to the possible coarsening of the zeta phase (discussed earlier in section V.A.2) may be responsible for the observed $t^{1/3}$ kinetics. The zeta phase is also affected by the rapid growth of the adjacent delta phase layer, and its apparent consumption of the zeta phase layer also affects the growth-time relationship determined for the zeta phase.

(iv). Summary

The total Fe-Zn alloy layer for the 0.00 wt% Al-Zn coatings followed $t^{1/3}$ kinetics, as was found for the zeta phase layer. The zeta layer was the thickest of the Fe-Zn phase layers formed in the 0.00 wt% Al-Zn bath, and constitutes the majority of the Fe-Zn total alloy layer. Therefore the kinetics of the zeta phase layer would be expected to dominate the total Fe-Zn alloy layer growth kinetics as well, and the same possible reaction mechanisms which control zeta layer growth most likely also control total alloy layer growth in 0.00 wt% Al-Zn coatings.

The individual phase layers had average growth rate time constant values such that n_{delta} (0.50) > n_{zeta} (0.33) > n_{gamma} (0.25). Delta layer growth appeared to be controlled by the bulk interdiffusion of Fe and Zn with Zn as the dominant diffusing specie [31]. Zeta layer

growth followed a $t^{1/3}$ relationship indicating that its supply of Zn was limited. Zeta layer growth is most likely affected by 2 factors (1) liquid Zn penetration along its columnar structure in contact with the Zn melt and (2) consumption of the zeta phase layer by the rapidly growing adjacent delta phase layer. Gamma phase followed the slowest growth kinetics ($t^{1/4}$), indicating its growth was also controlled by a limited supply of Zn diffusion along its grain boundaries. The gamma phase layer supply of Zn may have been limited by the rapidly growing delta phase layer and its consumption of the flux of Zn atoms from both the zeta phase layer and liquid Zn, thus a reduced flux of Zn atoms was available for gamma layer growth.

c. Total Fe-Zn Alloy Layer Growth - 0.20 wt% Al-Zn Bath

Unlike the 0.00 wt% Al-Zn coatings where a uniform Fe-Zn alloy layer formed, the 0.20 wt% Al-Zn coatings showed Fe-Zn alloy layer development which was discontinuous. Initially localized areas of Fe-Zn growth form, and over time these areas of growth grow laterally along the steel/coating interface and coalesce.

(i) 15 μm ULC Steel Substrate

The 15 μm ULC steel hot-dip galvanized in a 0.20 wt% Al-Zn bath showed localized regions of Fe-Zn growth, and the Fe-Zn phase layer development is shown in Figure 78. Unlike the 0.00 wt % Al-Zn coatings, there was not complete coverage of an alloy layer at

the steel/coating interface. Figure 78f and g are of the same sample surface that was galvanized for 300 seconds, which showed some areas of Fe-Zn growth (Figure 78f) while at other locations along the steel/coating interface no Fe-Zn phase growth was observed (Figure 78g). The growth behavior is related to the stability of the $Fe_2Al_5(Zn)$ layer which forms at the steel/coating interface during galvanizing in Zn baths containing Al. As previously described by Ghuman and Goldstein [9], Fe-Zn phases are able to grow in Al containing baths while at the same time $Fe_2Al_5(Zn)$ is stable and its growth occurs at locations where Fe-Zn phases do not form (Figure 16). Therefore in localized areas the $Fe_2Al_5(Zn)$ layer continues to act as an inhibition layer preventing Fe-Zn phase growth at the steel/coating interface. The Fe-Zn alloy layer structure that formed over the reaction times studied consisted of 2 distinct phase layers; gamma and delta phases. Delta phase formed first at the steel/coating interface followed by the formation of gamma at the steel/coating interface. The delta phase, adjacent to the gamma phase layer, constituted most of the total alloy layer. The delta phase boundary farthest from the steel/coating interface was in contact with the liquid Zn during immersion in the bath, and once solidified the liquid Zn formed solid eta phase. The kinetics of total alloy layer and individual gamma and delta phase layer growth for the 15 μm ULC steel galvanized in a 0.20 wt% Al-Zn bath was previously discussed in section V. A. 4. Zeta phase was not detected in the 0.20 wt% Al-Zn coatings and this is due to the fact that the diffusion path through the metastable ternary Fe-Zn-Al phase diagram at 450°C [24] for the 15 μm ULC steel immersed for 300 seconds in the 0.20 wt% Al-Zn bath (determined from experimentally obtained composition data of the Fe-Zn alloy layer), follows a path such

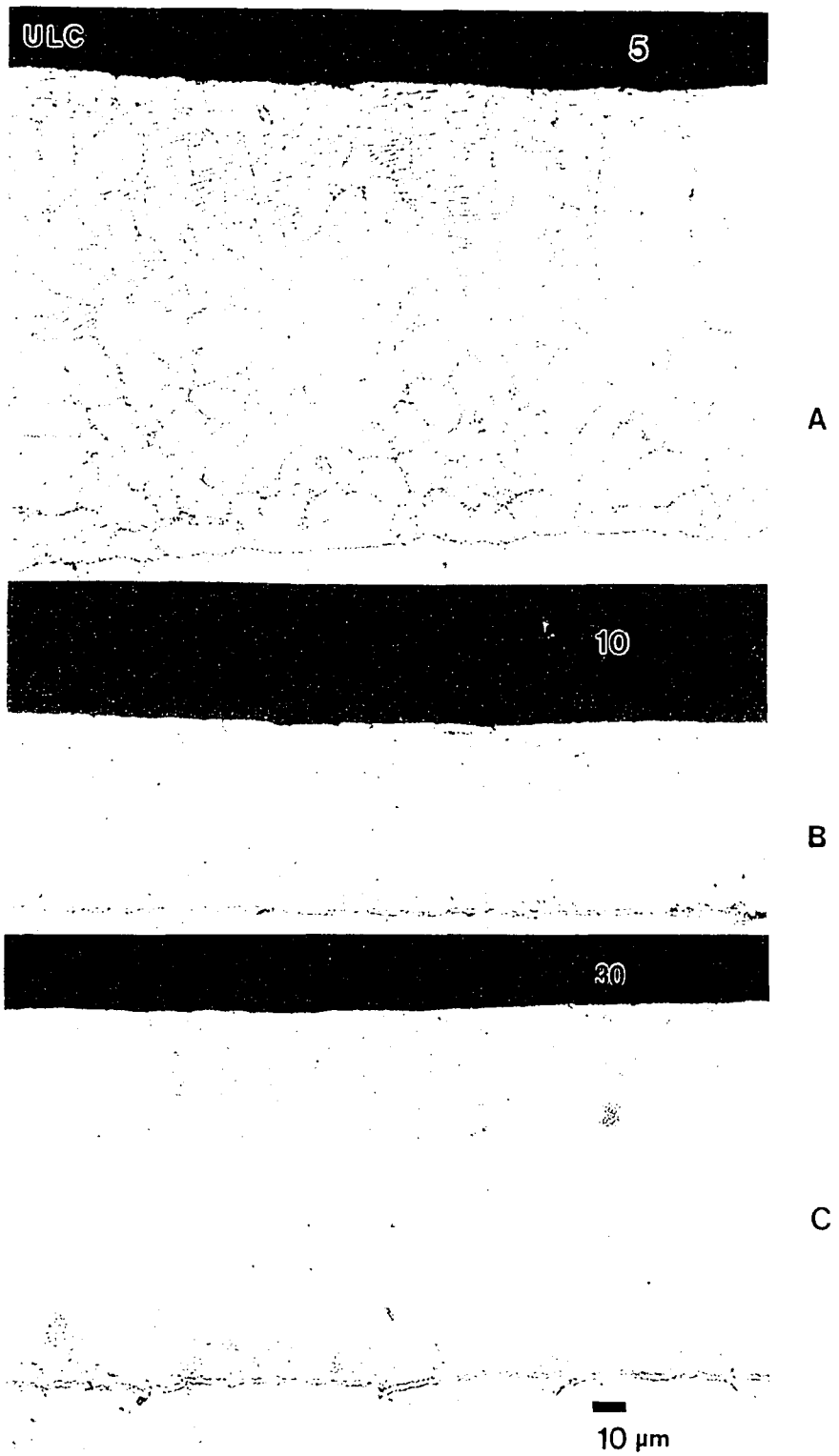

Figure 78. 15 µm grain size ULC steel hot-dip galvanized in a 0.20 wt% Al-Zn bath for (a) 5 (b) 10 and (c) 30 seconds of immersion.

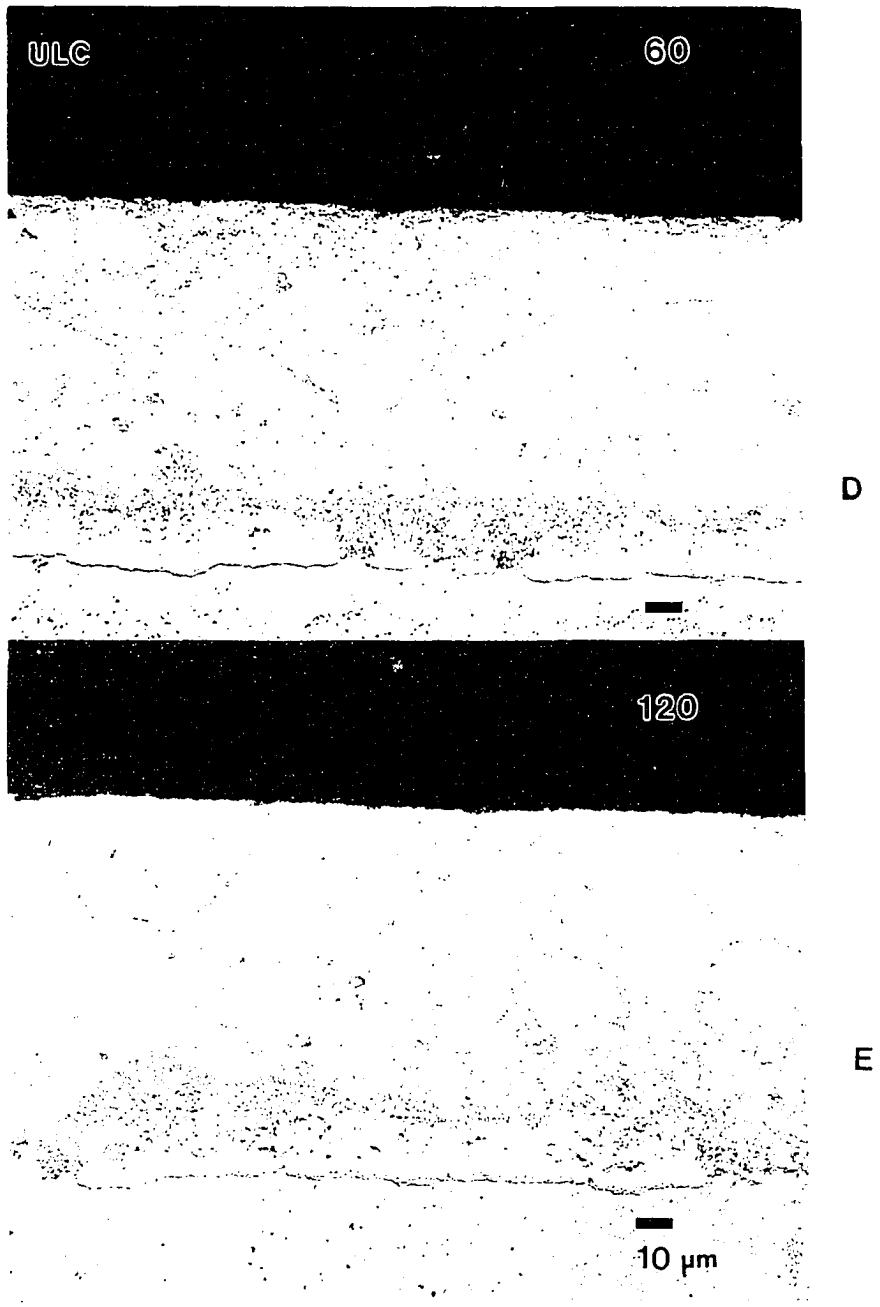

Figure 78. 15 µm grain size ULC steel hot-dip galvanized in a 0.20 wt% Al-Zn bath for (d) 60 and (e) 120 seconds of immersion.

Figure 78. 15 µm grain size ULC steel hot-dip galvanized in a 0.20 wt% Al-Zn bath for 300 seconds of immersion, (f) and (g).

that delta phase is in equilibrium with eta phase, Figure 51. The diffusion path through the metastable ternary isotherm was: $\alpha/\alpha+\Gamma/\Gamma/\Gamma+\delta/\delta+\eta/\eta$ for both short (10 second) and long (300 second) reaction times, therefore Fe-Zn growth in the Fe-Zn-Al system occurs by a diffusion mechanism that does not allow for the formation of the zeta phase.

(ii) 85 μm ULC Steel Substrate

The 85 μm ULC 0.20 wt% Al-Zn coatings showed no localized regions of Fe-Zn growth over the reaction times studied (5-300 seconds), as shown in Figure 79. The Fe-Al inhibition layer that formed initially upon immersion of the steel into the liquid Zn(Al) bath remained stable and did not appear to be penetrated by the liquid Zn even after 300 seconds of immersion time (Figure 79f and g). Because liquid Zn penetration to the steel surface did not occur, localized Fe-Zn phase growths did not nucleate, although in Figure 79f small crystals of a light colored phase are visible adjacent to the Fe-Al layer at the steel/coating interface.

Because little or no Fe-Zn phase growth was observed on the 85 μm ULC 0.20 wt% Al-Zn coated material, selected electron microprobe spot analyses near the steel/coating interface were conducted on the 5, 60, and 300 seconds of immersion samples in an attempt to identify the interfacial growths observed in Figure 79. The resulting composition data are shown in Table XVIII. Using the metastable 450°C Fe-Zn-Al isotherm [24], (Figure 9, and Table IIIA) the composition analyses listed in Table XVIII

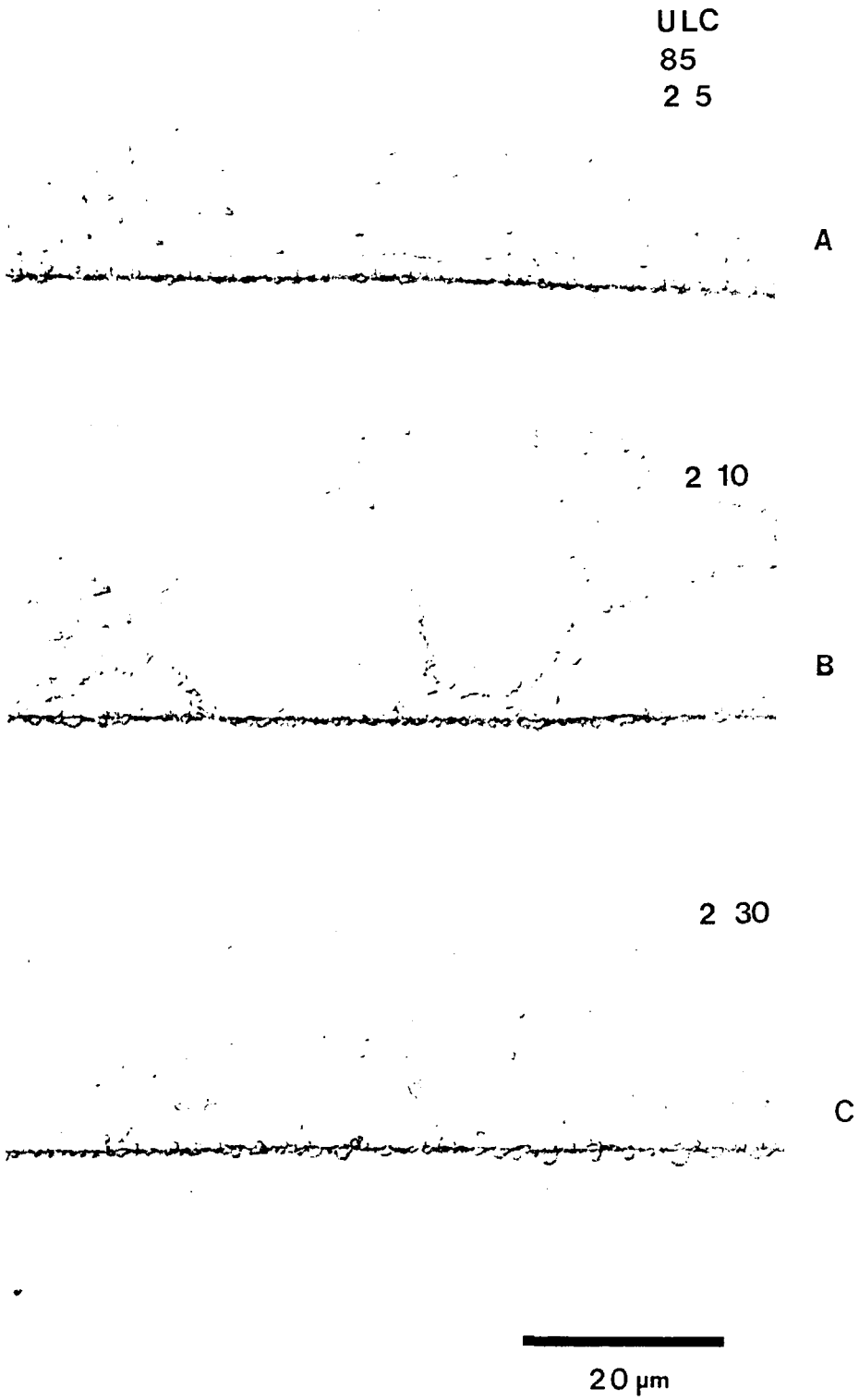

Figure 79. 85 µm grain size ULC steel hot-dip galvanized in a 0.20 wt% Al-Zn bath for (a) 5 (b) 10 and (c) 30 seconds of immersion.

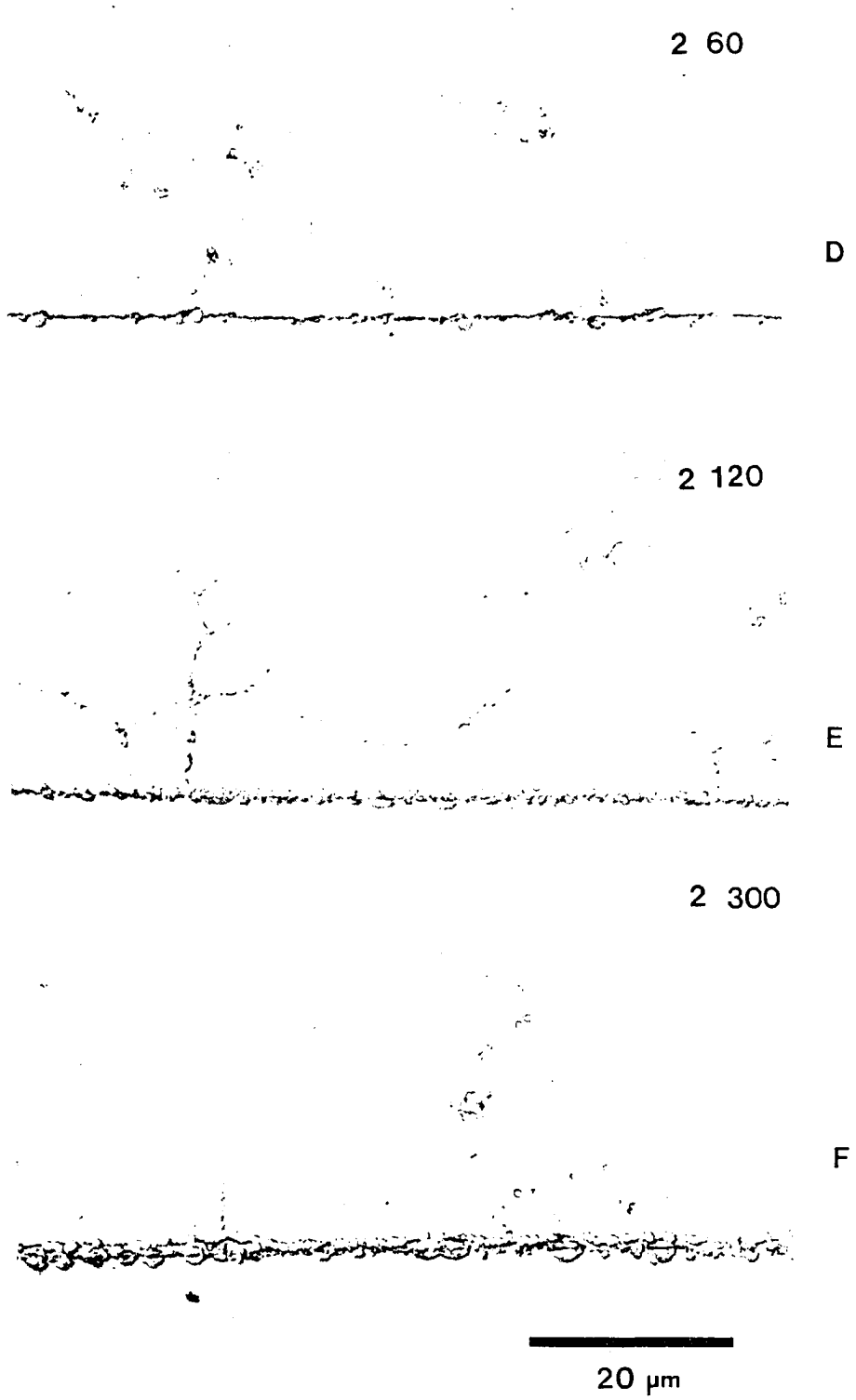

Figure 79. 85 µm grain size ULC steel hot-dip galvanized in a 0.20 wt% Al-Zn bath for (d) 60 (e) 120 and (f) 300 seconds of immersion.

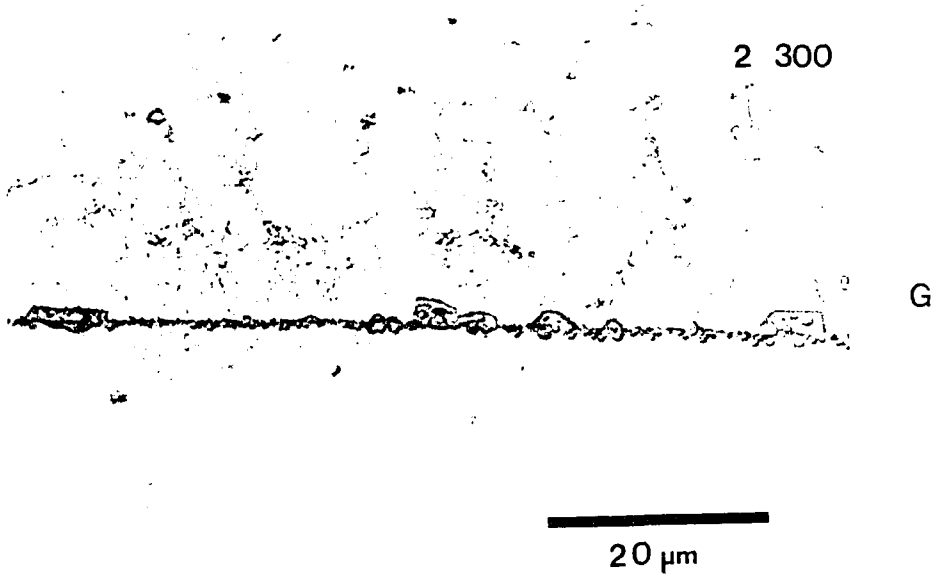

Figure 79. 85 µm grain size ULC steel hot-dip galvanized in a 0.20 wt% Al-Zn bath for (g) 300 seconds of immersion.

Table XVIII. Microprobe Spot Analysis of Interfacial Growths formed on 85 μm grain size ULC Steel Galvanized in a 0.20 wt% Al-Zn Bath for 5, 60, and 300 seconds of immersion.

Sample / Growth description	wt% Fe (at%)	wt% Zn (at%)	wt% Al (at%)	Phase ID*
5s / reaction layer ~ 1μm	15.27 (16.75)	81.86 (76.72)	2.88 (6.54)	$\alpha + \delta$
5s / reaction layer ~ 1μm	4.71 (5.41)	94.48 (92.68)	0.81 (1.91)	$\delta + \eta$
60s / reaction layer 2-3 μm	4.81 (5.50)	94.15 (92.04)	1.04 (2.46)	$\delta + \eta$
60s / reaction layer 2-3 μm	5.72 (6.52)	93.15 (90.80)	1.13 (2.68)	δ
60s / reaction layer 2-3 μm (near steel/coating interface)	8.36 (9.02)	86.70 (79.94)	4.94 (11.03)	$\delta + Fe_2Al_5$
300s / reaction layer ~ 3 μm	34.93 (24.77)	23.53 (14.25)	41.54 (60.98)	"
300s / reaction layer ~ 3 μm	33.90 (24.34)	25.90 (15.89)	40.21 (59.77)	"
300s / reaction layer ~3 μm	35.39 (25.80)	26.29 (16.37)	38.32 (57.83)	"
300s / reaction layer ~ 3 μm	46.32 (33.55)	15.94 (9.37)	37.74 (56.59)	$\alpha + \delta + Fe_2Al_5$
300s / reaction layer ~ 3 μm	42.96 (31.48)	20.19 (12.64)	36.85 (55.89)	$\alpha + \delta + Fe_2Al_5$
300s / reaction layer ~ 3 μm	36.04 (26.18)	25.32 (15.72)	38.64 (58.10)	$\delta + Fe_2Al_5$

* based upon the metastable Fe-Zn-Al ternary isotherm at 450°C[24].

were identified and attributed to the corresponding phase field in the metastable isotherm. At the short reaction times of 5 and 60 seconds in addition to the solid solution phases of α-Fe (ferrite) and Zn (Fe) eta phase, Fe-Zn delta phase, as well as an Fe-Al compound, Fe_2Al_5 phase form at the steel/coating interface. At longer times of reaction (300 seconds) the composition analysis of growths at the steel/coating interface correspond to Fe-Zn delta phase and Fe_2Al_5. It appears as though by 300 seconds the system has progressed to form an Fe_2Al_5 phase at the steel/coating interface. Microprobe spot analysis for the samples listed in Table XVIII were often conducted on areas of growth 1-5 μm in diameter, therefore some error is associated with the composition data due to the possible over sampling of the predominant surrounding eta phase, or of the Fe_2Al_5 layer previously shown [7, 9] to be present as a submicron layer at the steel/coating interface under these galvanizing conditions.

It was thought that the Fe_2Al_5 inhibition layer that formed during immersion of the 85 μm grain size ULC steel would eventually breakdown over some unknown reaction time and allow Fe-Zn growth to occur, thus longer times of immersion were chosen for study. Previous investigators [27] have shown that 0.20 wt% Al-Zn baths delay the formation of Fe-Zn phases for immersion times greater than 300 seconds. New samples of 85 μm ULC steel were subsequently studied at reaction times of 1200 and 1800 seconds in the 0.20 wt% Al-Zn bath. The extended time of reaction did result in the breakdown of the Fe_2Al_5 inhibition layer and the formation of a limited number of localized Fe-Zn phase growths, as shown in Figure 80.

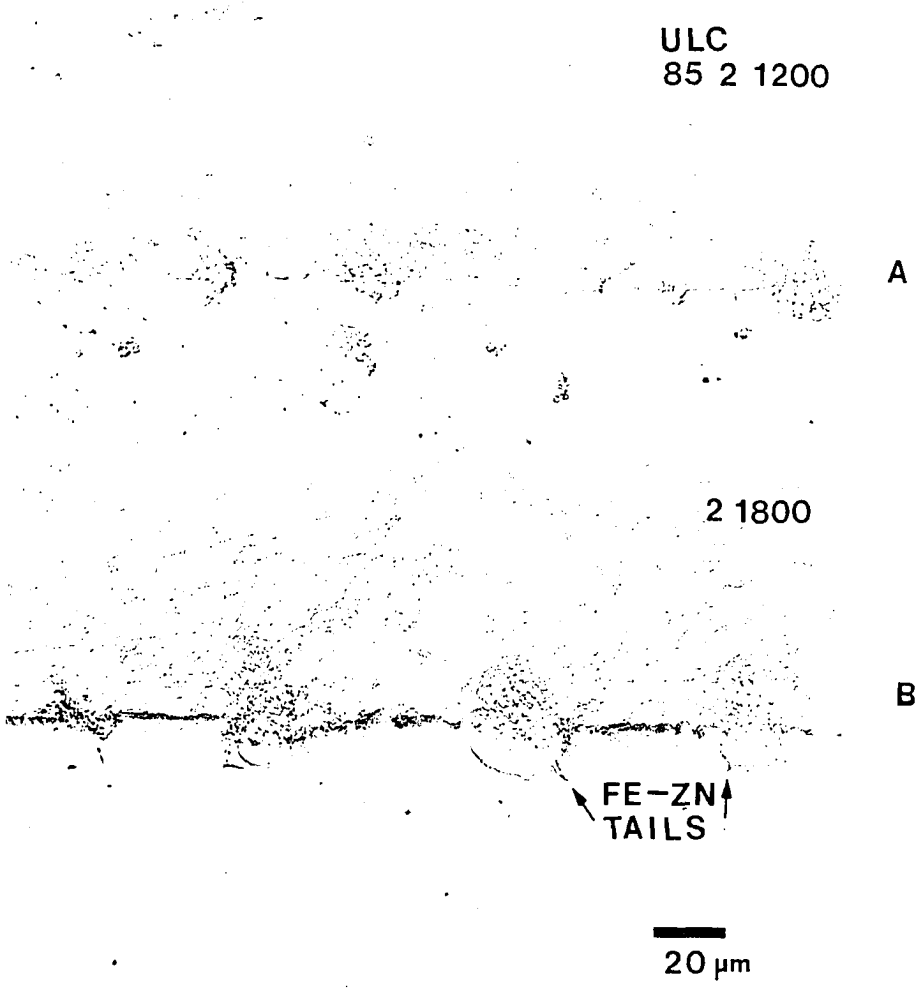

Figure 80. 85 µm grain size ULC steel hot-dip galvanized in a 0.20 wt% Al-Zn bath for (a) 1200 and (b) 1800 seconds of immersion.

Although limited Fe-Zn phase growth did occur, an insufficient number of Fe-Zn alloy growths formed which could be evaluated to yield statistically significant information on total or individual alloy layer phase growth at these extended reaction times. However, the localized Fe-Zn growths appeared to be associated with a substrate grain boundary when observed in dark field microscopy, Figure 81. The Fe-Zn outbursts typically had trailing elongated tails of Fe-Zn phase that extended Down along substrate grain boundaries. The Fe-Zn outbursts appear to consist of gamma and delta phase layers, based upon morphology comparisons to the Fe-Zn outbursts formed on the 15 μm ULC steel galvanized in a 0.20 wt% Al-Zn bath (Figure 78d and e). Further analysis of the long time immersion samples in the SEM (Figure 82) showed that the Fe-Al inhibition layer was faceted (arrows). Microprobe spot analysis was conducted on the Fe-Al inhibition layer which showed growth between the localized Fe-Zn growths during long time immersion, as shown in Figure 82. The composition data are shown in Table XIX, and indicate the Fe-Al compound formed at the steel/coating interface between the localized Fe-Zn growths is consistent with the composition of Fe_2Al_5 phase, based upon the metastable Fe-Zn-Al isotherm [24]. Therefore after 1200 and 1800 seconds of immersion localized areas of Fe-Zn alloy phase growths nucleate and grow, often at substrate steel grain boundaries, and an Fe_2Al_5 layer that formed at short times of 5 and 60 seconds of reaction is stabilized at the steel/coating interface and also grows between the localized Fe-Zn growths.

Figure 81. 85 µm grain size ULC steel hot-dip galvanized in a 0.20 wt% Al-Zn bath for 1800 seconds (a) bright field LOM image and (b) dark field LOM image.

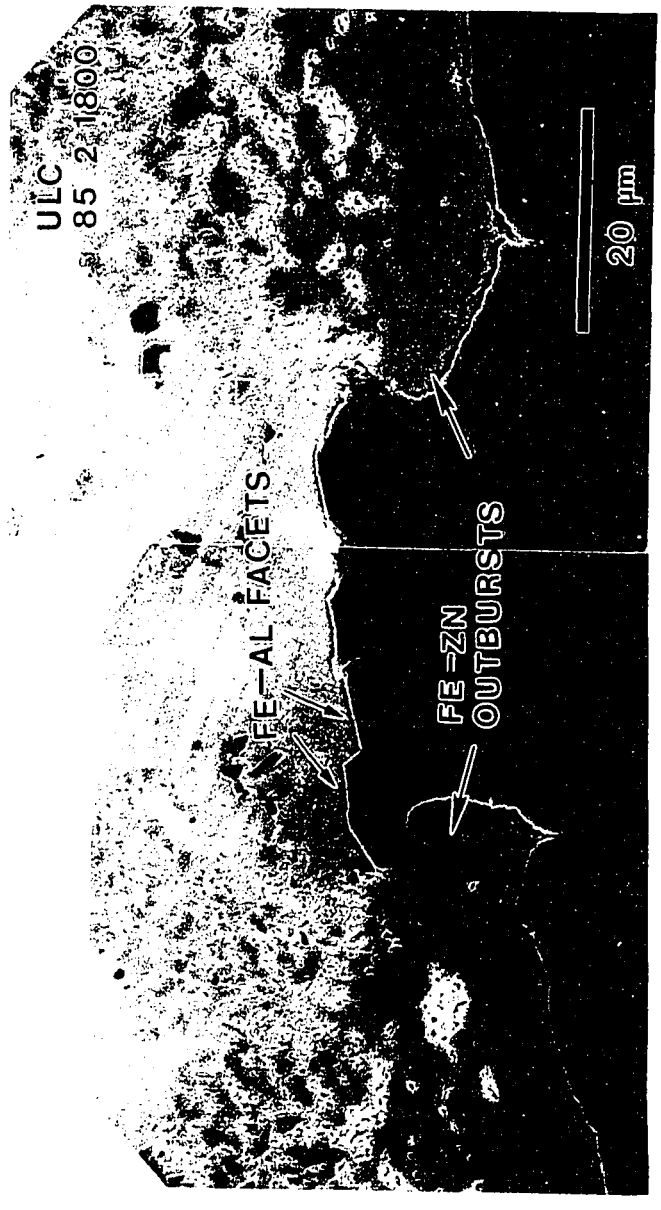

Figure 82. 85 µm grain size ULC steel hot-dip galvanized in a 0.20 wt% Al-Zn bath for 1800 seconds, secondary electron image.

Table XIX. Microprobe Spot Analysis of Interfacial Fe-Al Growths formed on the 85 μm grain size ULC Steel Galvanized in a 0.20 wt% Al-Zn Bath for 1200 and 1800 seconds of immersion.

Sample / Growth description	wt% Fe (At%)	wt% Zn (At%)	wt% Al (At%)	Phase ID*
1200s / burst like growth	38.03 (27.02)	21.03 (12.76)	40.94 (60.22)	Fe_2Al_5
1200s / burst like growth	39.46 (27.70)	18.36 (11.01)	42.18 (61.29)	Fe_2Al_5
1200s / facet growth	35.60 (25.19)	22.65 (13.69)	41.75 (61.13)	Fe_2Al_5
1200s / facet growth	30.49 (21.51)	26.81 (16.16)	42.70 (62.34)	Fe_2Al_5
1800s / facet growth	38.28 (26.61)	18.27 (10.85)	43.46 (62.54)	Fe_2Al_5
1800s / facet growth	37.73 (26.13)	18.29 (10.82)	43.97 (63.04)	Fe_2Al_5

* based upon the metastable Fe-Zn-Al ternary isotherm at 450°C [24].

Summarizing the effect of ULC substrate grain size hot-dip galvanized in the 0.20 wt% Al-Zn bath on total and individual phase layer kinetics, the major result was that no Fe-Zn phase growth was observed for the 85 μm grain size material at 5-300 seconds of reaction. The absence of Fe-Zn growth on the 85 μm ULC steel indicate that the Fe-Al inhibition layer remained stable during immersion in the bath for reaction times up to 300 seconds. After extended time in the bath (1200 and 1800 seconds) a limited number of localized Fe-Zn growths did occur, and the growths appeared in some cases to be associated with substrate grain boundaries. Substrate grain size is a more significant factor in Al containing baths than in the 0.00 wt% Al-Zn baths, specifically in the incubation time necessary for Fe-Zn phase nucleation and growth. A large grain sized ULC substrate

promoted the stability of the Fe-Al-Zn inhibition layer, and delayed the formation of Fe-Zn phases.

3. Effect of Phosphorus Surface Segregation

Very large grain size low carbon steel samples (Figure 29) were ion implanted with P to study the role P surface segregation may have on Fe-Zn reaction kinetics. After ion implantation the samples were analyzed for phosphorus concentration depth profiles using Rutherford Back Scattering (RBS) analysis. Figure 83 shows depth profiles for phosphorus obtained using RBS analysis on selected phosphorus ion implanted samples. The maximum phosphorus concentration was typically found at 10-20 nm below the sample surface and was 1400 - 1600 x 10^{19} atoms/cm^3 which is equivalent to 14-16 at% P (8.5-9.5 wt% P). The RBS depth resolution is broad (approximately 20 nm) therefore if material is implanted near the sample surface a concentration reading can appear at a negative depth, or above the surface [67]. The phosphorus can be considered as being implanted at a depth of 10-20 nm ± 20 nm, hence the maximum depth of phosphorus ion implantation was at approximately 40 nm.

Because the maximum depth of P concentration was located at approximately 40 nm from the surface of the sample, the ion implanted layer was completely consumed during galvanizing. Clayton et al [65] showed P-ion implantation in austenitic 304 stainless steel

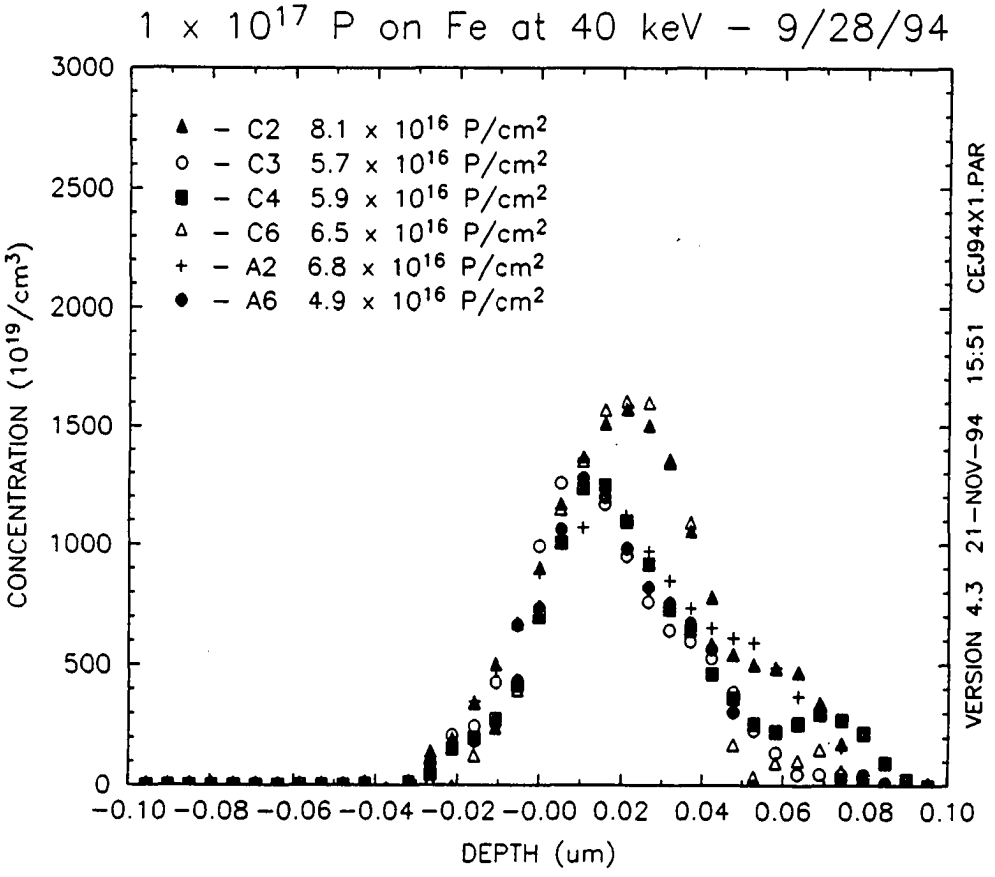

Figure 83. RBS phosphorous concentration depth profile for selected phosphorous ion implanted low carbon steel samples [67].

(under identical conditions to those described here) to form a microcrystalline 500 nm grain size surface layer with P in solid solution, at a concentration of 30 at%. The ion implanted layer studied here was not characterized beyond RBS, and analysis to study lattice defects due to ion implantation and how they may have affected the surface layer reaction were not the focus of this study.

The effect of one concentration distribution of phosphorus by ion implantation in an extremely large grain size low carbon steel was studied at 5 times of immersion; 5, 30, 60, 120, and 300 seconds. In order to evaluate the effect of P-ion implantation on Fe-Zn phase growth kinetics the P ion implanted and non phosphorus ion implanted surfaces of the same sample were compared. The chemistry of the steels used for this study, shown in Table VII, had an average grain size of approximately 10-20 mm. The Fe-Zn reaction layer which formed on the P and non P-ion implanted surfaces completely covered the entire steel/coating interface, and three Fe-Zn phase layers of gamma, delta, and zeta phases were observed to form sequentially and grow within this reaction layer on both sample surfaces, as shown in Figure 84. The Fe-Zn phase layer growth was similar to that observed on the 15 and 85 μm ULC steel described previously.

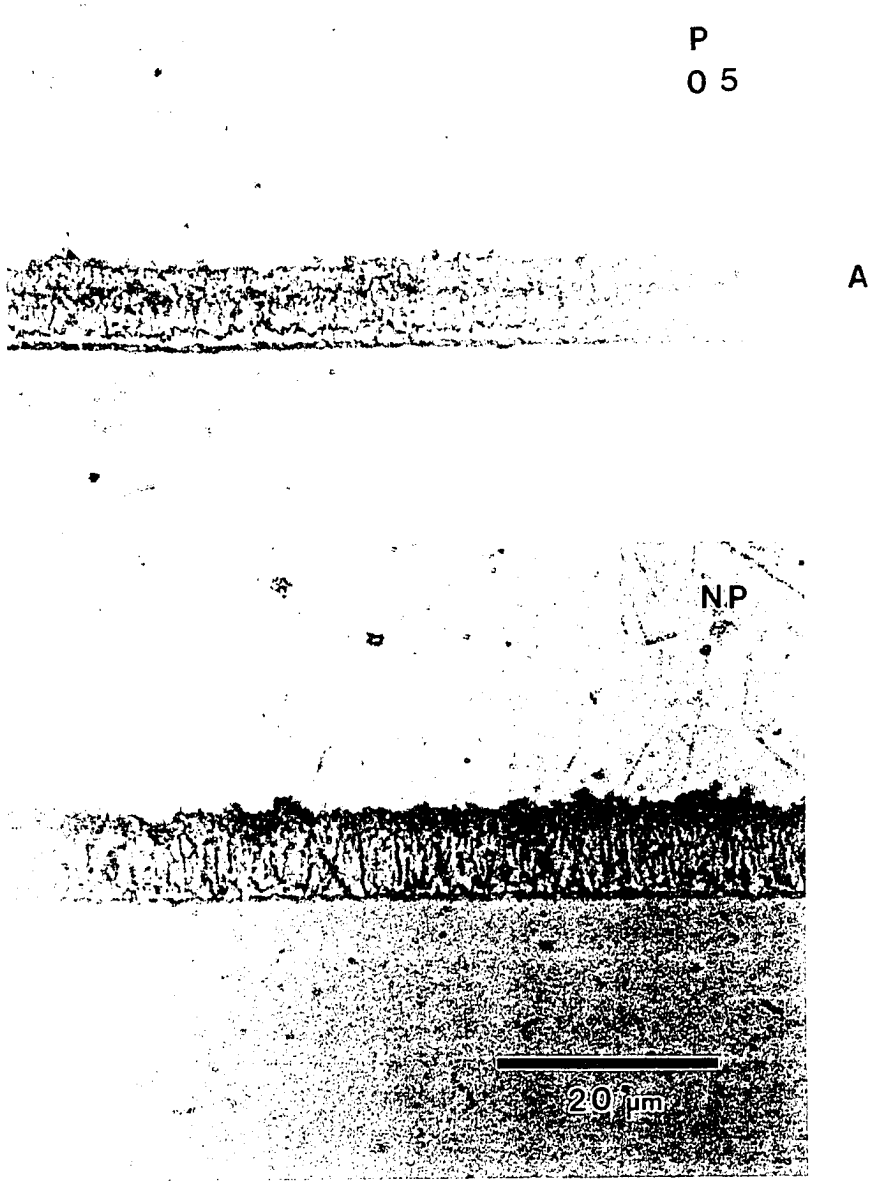

Figure 84. Phosphorous (P) and non phosphorous (NP) ion implanted low carbon steel surfaces hot-dip galvanized in a 0.00 wt% Al-Zn bath for (a) 5 seconds of immersion.

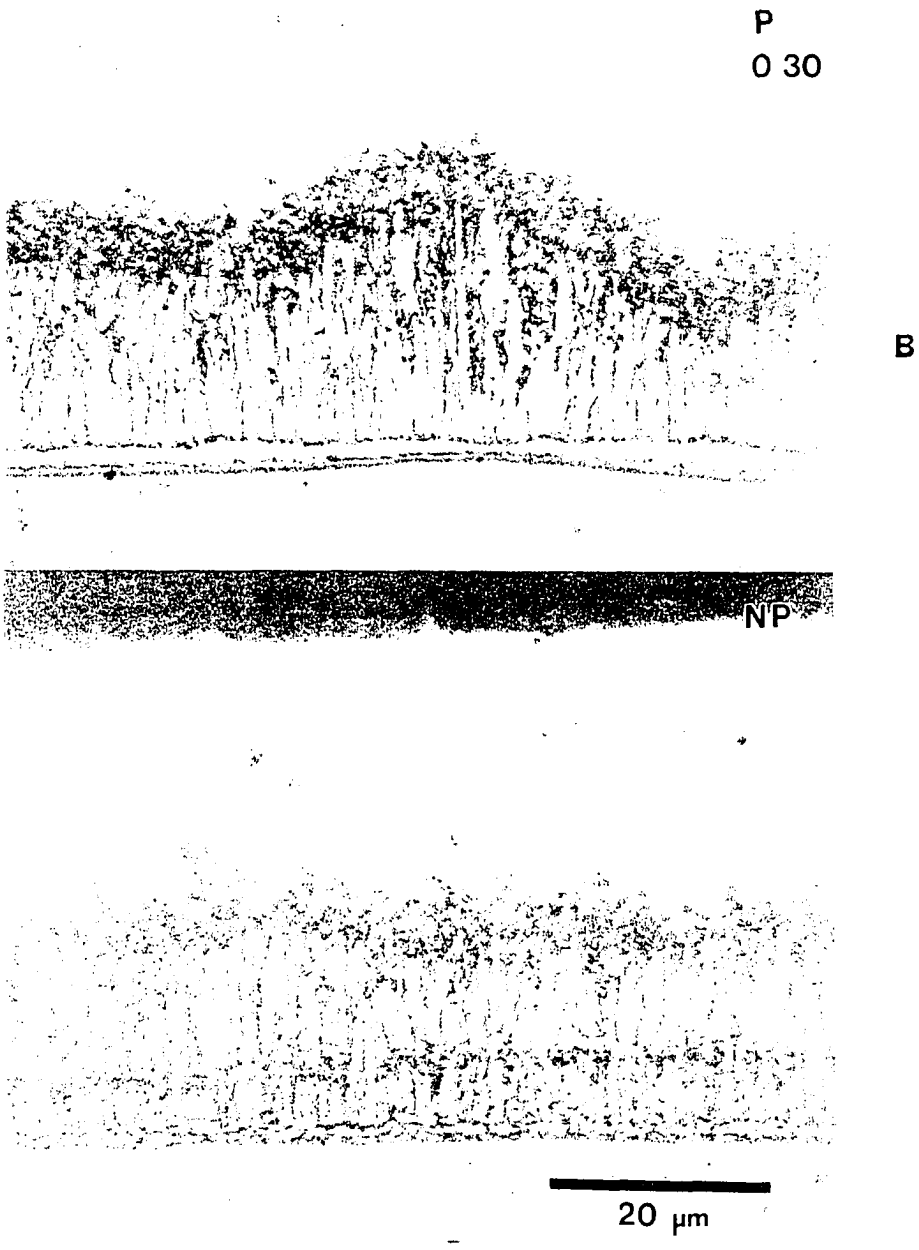

Figure 84. Phosphorous (P) and non phosphorous (NP) ion implanted low carbon steel surfaces hot-dip galvanized in a 0.00 wt% Al-Zn bath for (b) 30 seconds of immersion.

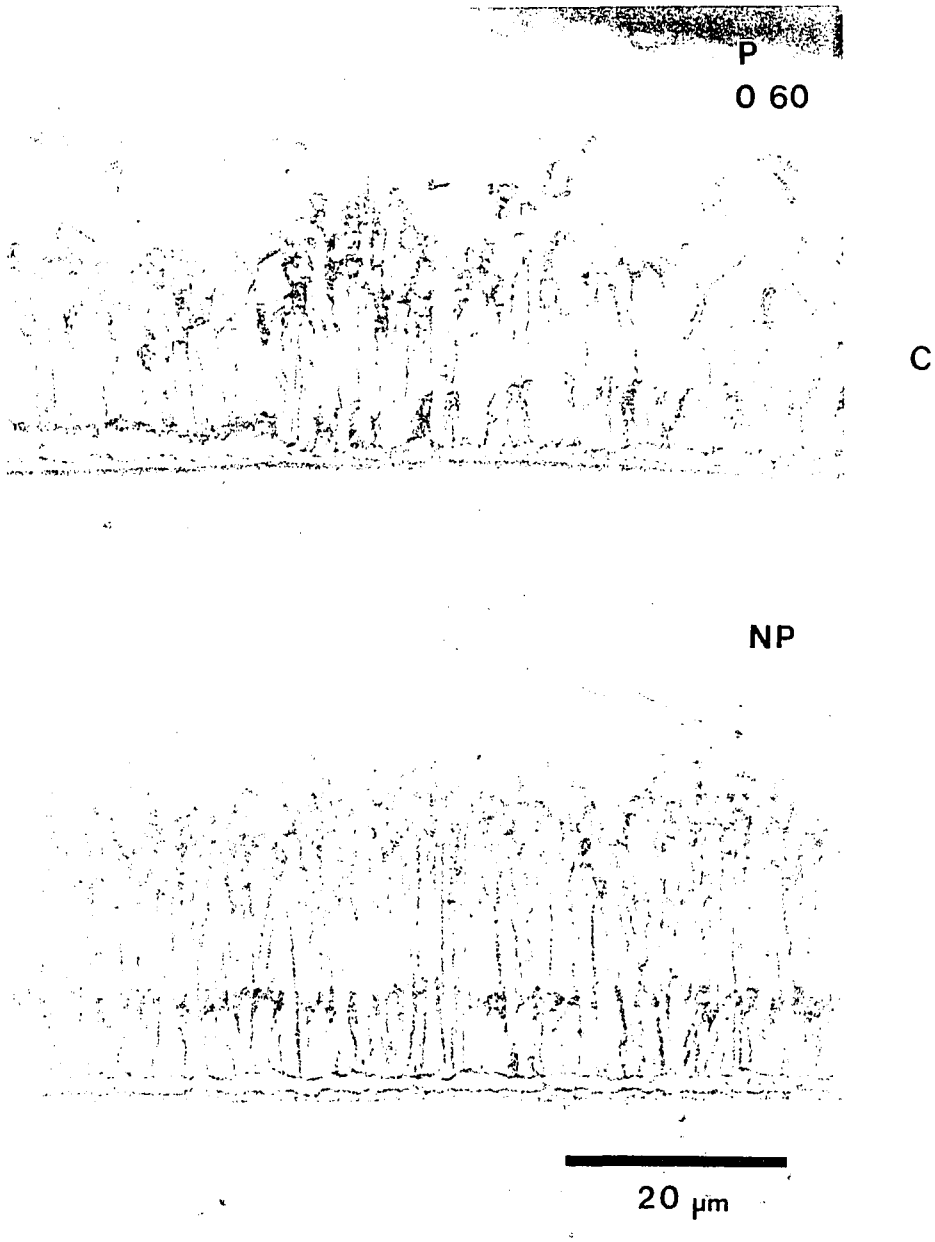

Figure 84. Phosphorous (P) and non phosphorous (NP) ion implanted low carbon steel surfaces hot-dip galvanized in a 0.00 wt% Al-Zn bath for (c) 60 seconds of immersion.

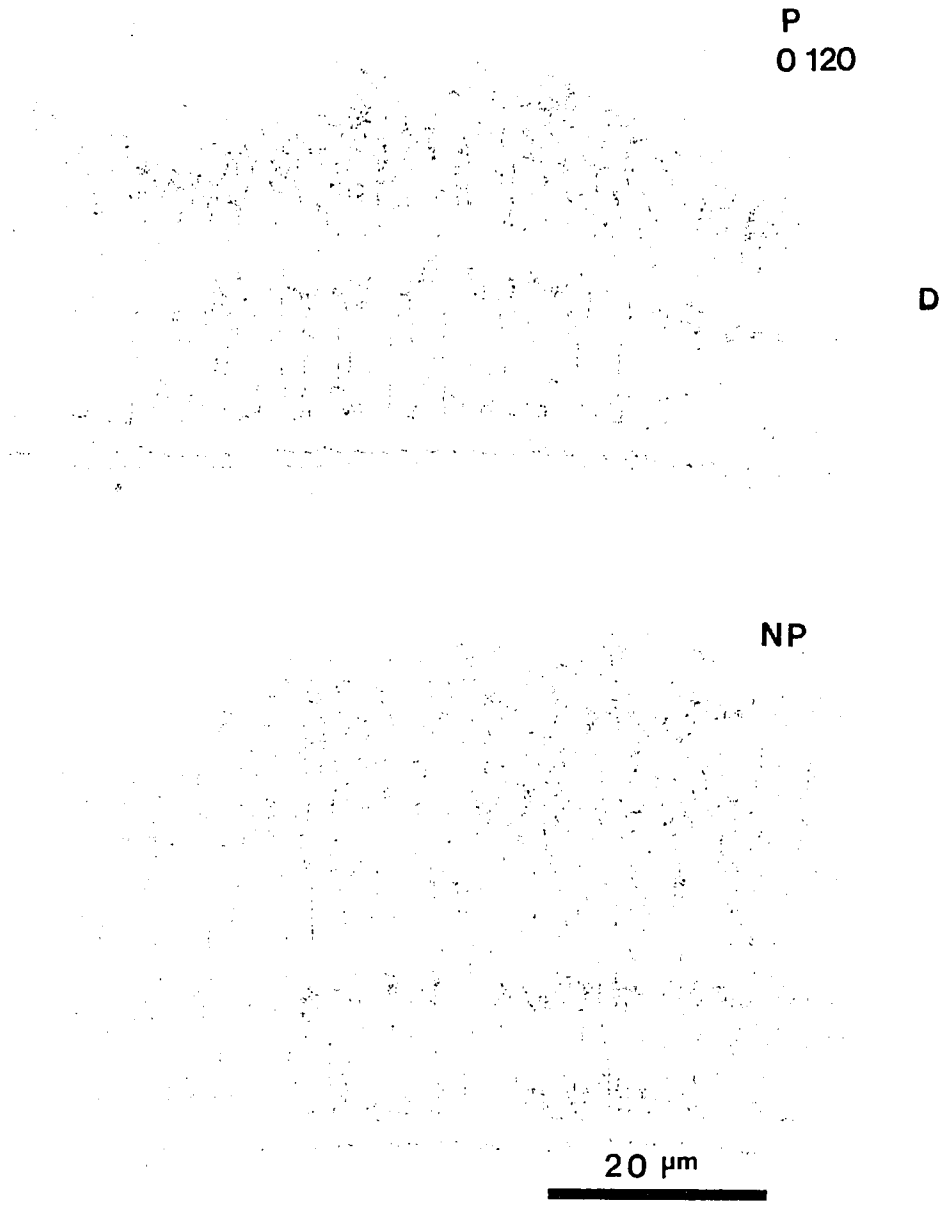

Figure 84. Phosphorous (P) and non phosphorous (NP) ion implanted low carbon steel surfaces hot-dip galvanized in a 0.00 wt% Al-Zn bath for (d) 120 seconds of immersion.

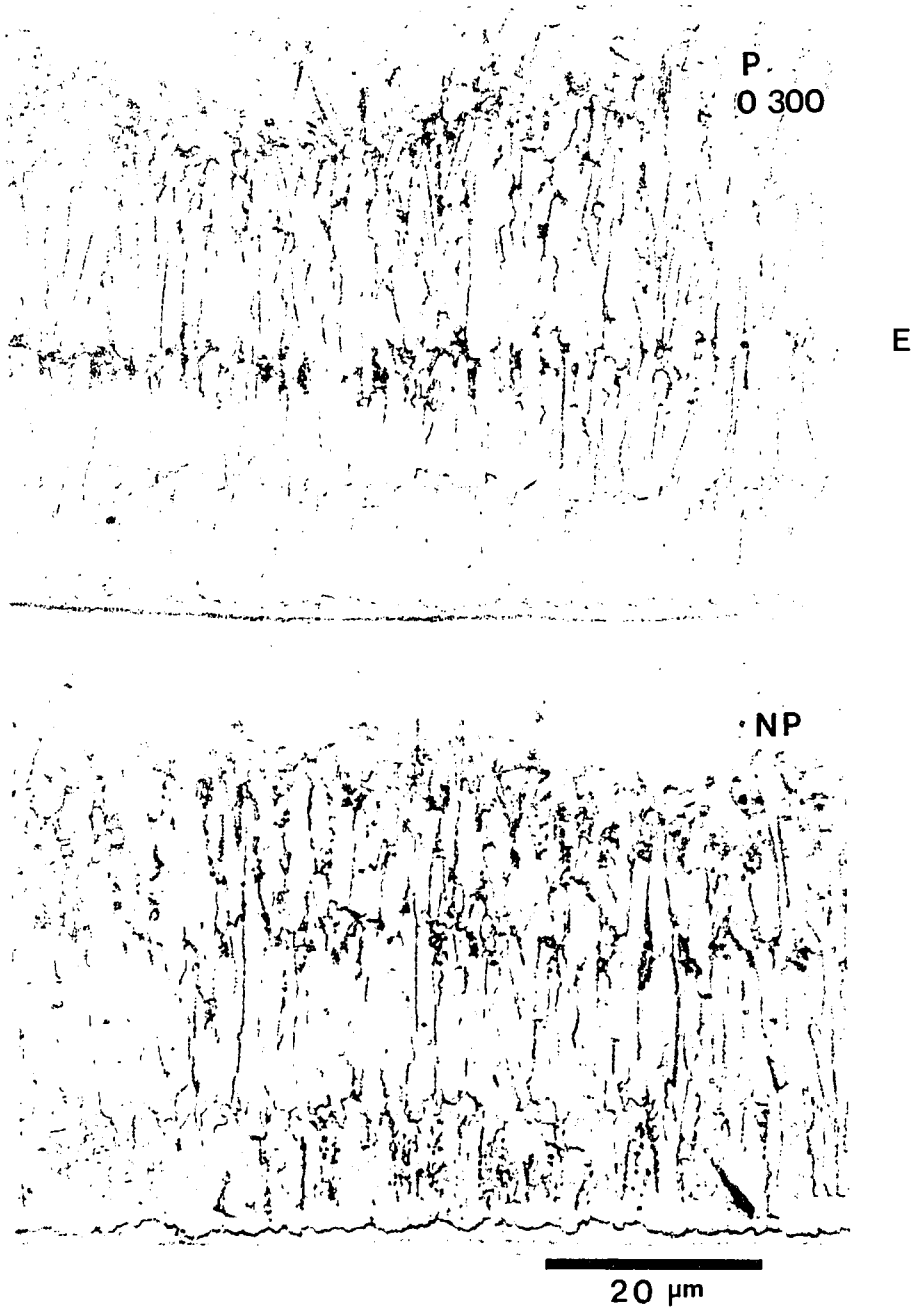

Figure 84. Phosphorous (P) and non phosphorous (NP) ion implanted low carbon steel surfaces hot-dip galvanized in a 0.00 wt% Al-Zn bath for (e) 300 seconds of immersion.

a. Total Fe-Zn Alloy Layer Growth - 0.00 wt% Al-Zn Bath

The entire P and non P-ion implanted steel surface reacted with liquid Zn to form an Fe-Zn alloy layer that completely covered the steel/coating interface. Ion implanted phosphorus had no effect on the nucleation and overall morphology of the Fe-Zn alloy layer. To study the overall rate of reaction, the total Fe-Zn alloy layer growth was measured for the P-ion implanted and non P-ion implanted surfaces. The total alloy growth data are shown in Figure 85. A fit of the total alloy layer thickness and time data using linear regression analysis in Sigma Plot to determine the growth rate time constant (n) value resulted in values of 0.42 and 0.38 for the P and non P-ion implanted surfaces, respectively (Table XX). Considering the error associated with each determined n value (0.04), the growth kinetics for the total alloy layer follow a similar function of time relationship for both the P and non P-ion implanted surfaces, hence the ion implantation of P had no effect on the growth kinetics of the total alloy layer.

The total alloy layer followed growth kinetics most closely approximating a $t^{1/3}$ to $t^{1/2}$ relationship. The total alloy layer growth followed a $t^{1/3}$ relationship on all other steel substrates (15 μm ULC, 85 μm ULC , ULC-P and Ti, and Ti+Nb stabilized IF steels) coated in the 0.00 wt% Al-Zn bath.

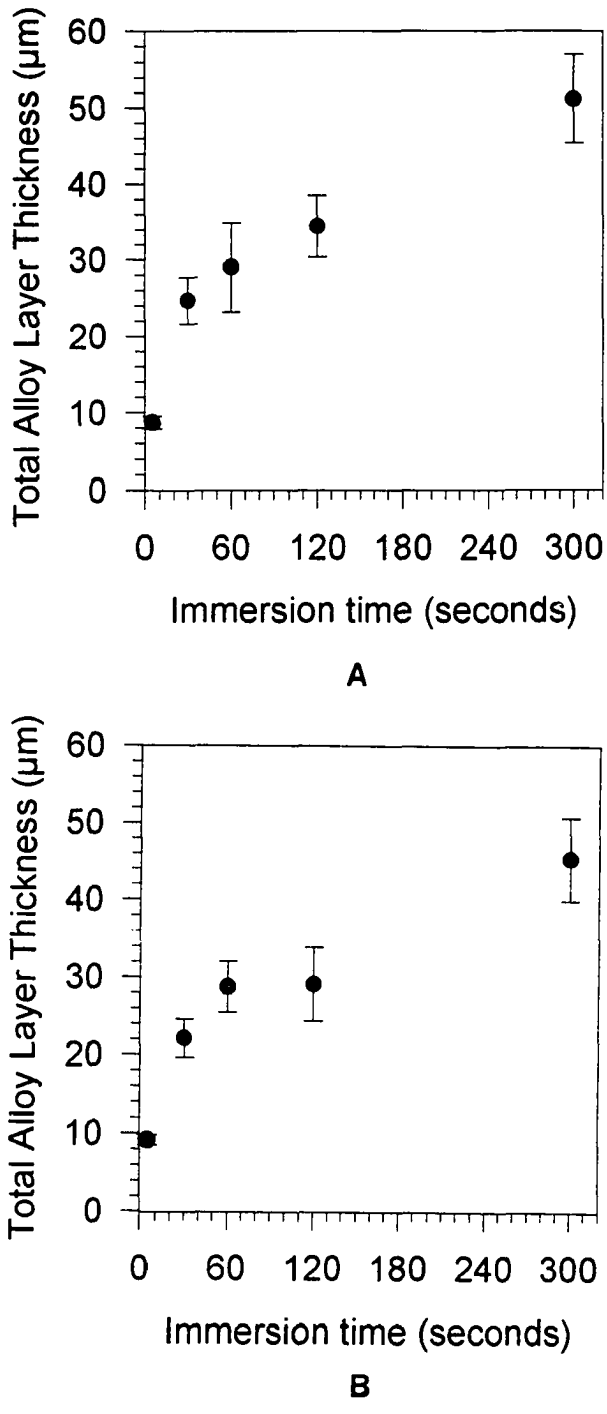

Figure 85. Total Fe-Zn alloy layer growth for the (a) P and (b) non P-ion implanted low carbon steel surfaces hot-dip galvanized in a 0.00 wt% Al-Zn bath.

Table XX. Total Alloy Layer and Individual Fe-Zn Phase Layer Growth Rate Time Constant (n)Values for the P and Non P-Ion Implanted Low Carbon Steel Galvanized in a 0.00 wt% Al-Zn Bath.

Sample / Layer	Growth Rate Time Constant (n)
P implanted / total FeZn alloy layer	0.42 ± 0.04
Non P implanted / total Fe-Zn alloy layer	0.38 ± 0.04
P implanted / gamma layer	0.25 ± 0.03
Non P implanted / gamma layer	0.31 ± 0.02
P implanted / delta layer	0.29 ± 0.11
Non P implanted / delta layer	0.49 ± 0.17
P implanted / zeta layer	0.43 ± 0.05
Non P implanted / zeta layer	0.36 ± 0.07

b. Individual Fe-Zn Phase Layer Growth - 0.00 wt% Al-Zn Bath

Three distinct Fe-Zn phase layers were observed on both the P and non P-ion implanted steel surfaces: gamma, delta, and zeta phases. Growth of individual Fe-Zn gamma, delta, and zeta phase layers were measured and the data are shown in Figure 86, and 87 for the P and non P-ion implanted surfaces, respectively. Electron microprobe analysis at 1.0 μm increments along a line parallel to the direction of diffusion was conducted for Fe and Zn

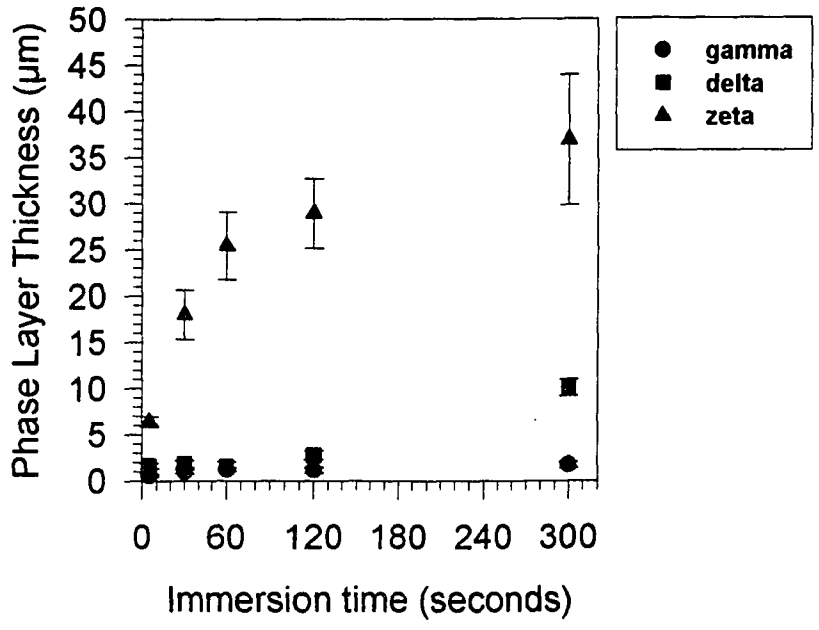

Figure 86. Individual Fe-Zn gamma, delta, and zeta phase layer growth for the P-ion implanted low carbon steel surface hot-dip galvanized in a 0.00 wt% Al-Zn bath.

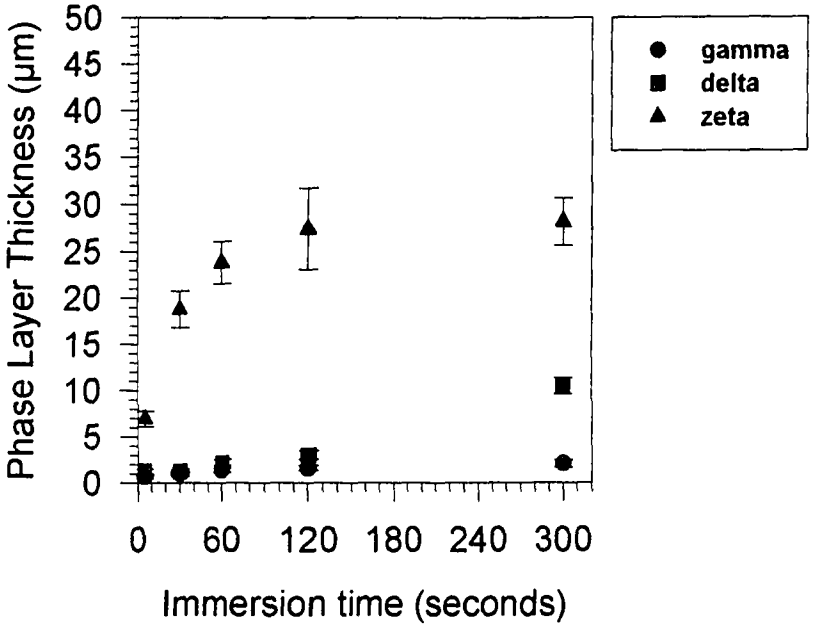

Figure 87. Individual Fe-Zn gamma, delta, and zeta phase layer growth for the non P-ion implanted low carbon steel surface hot-dip galvanized in a 0.00 wt% Al-Zn bath.

composition analysis on both the P-ion implanted and non P implanted surfaces for the 5, 60, and 300 second samples, and the data are shown in Figures 88 and 89 for the P-ion implanted and non P implanted surfaces, respectively. BSE images of the areas of the Fe-Zn alloy layer which were analyzed in the microprobe are shown in Figures 90 and 91, and correspond to the data represented in Figures 88 and 89, respectively. The BSE images in Figures 90c and 91c show the three phase layer morphology observed to form over the reaction studied in the 0.00 wt% Al-Zn bath. The Fe composition data and BSE images confirmed the identity of the Fe-Zn phase layers formed during immersion in the bath, previously identified by LOM.

(i). Gamma Phase Layer Growth

The gamma layer growth rate time constant values were determined from linear regression analysis to be 0.25 and 0.31 for the P and non P-ion implanted surfaces respectively. The error associated with n values indicates they were not significantly different for the two surfaces (see Table XX) hence the kinetics of growth for the gamma layer is the same for both surfaces. The n values are similar to those determined for 0.00 wt% Al-Zn coating gamma layer growth on the 15 μm (n = 0.24) and 85 μm (n = 0.26) ULC steel.

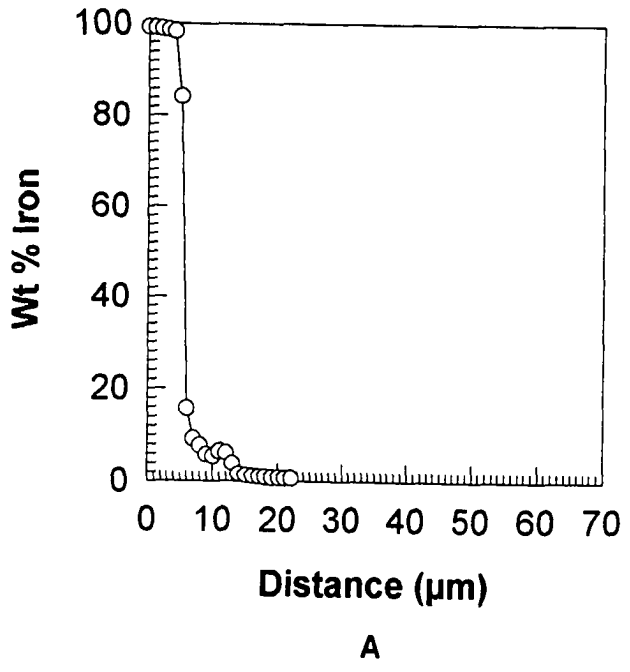

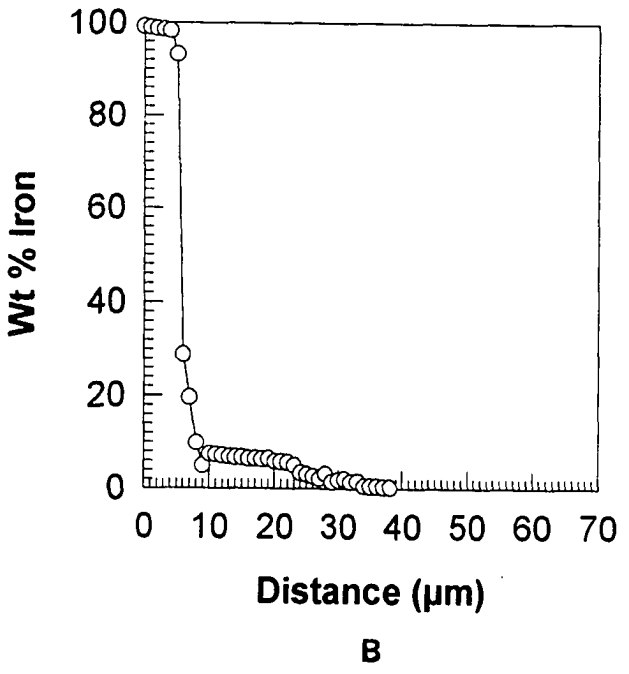

Figure 88. Iron concentration profile for the total Fe-Zn alloy layer formed on the P-ion implanted low carbon steel surface hot-dip galvanized in a 0.00 wt% Al-Zn bath for (a) 5 and (b) 60 seconds of immersion.

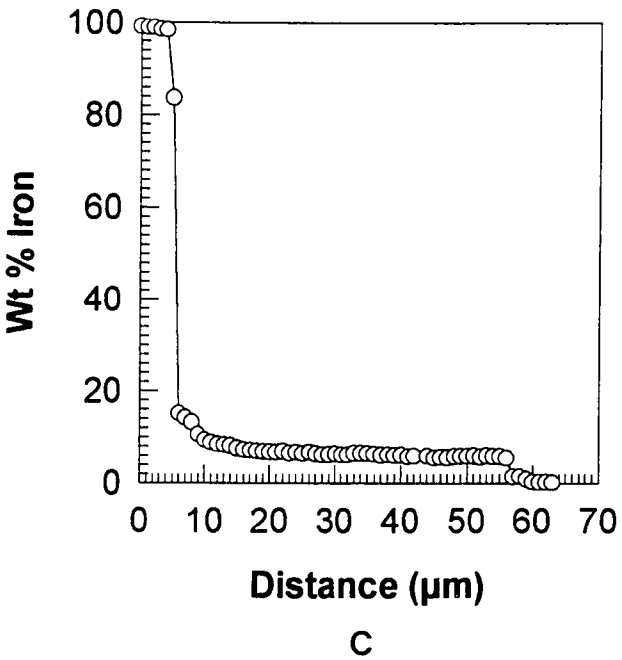

Figure 88. Iron concentration profile for the total Fe-Zn alloy layer formed on the P-ion implanted low carbon steel surface hot-dip galvanized in a 0.00 wt% Al-Zn bath for (c) 300 seconds of immersion.

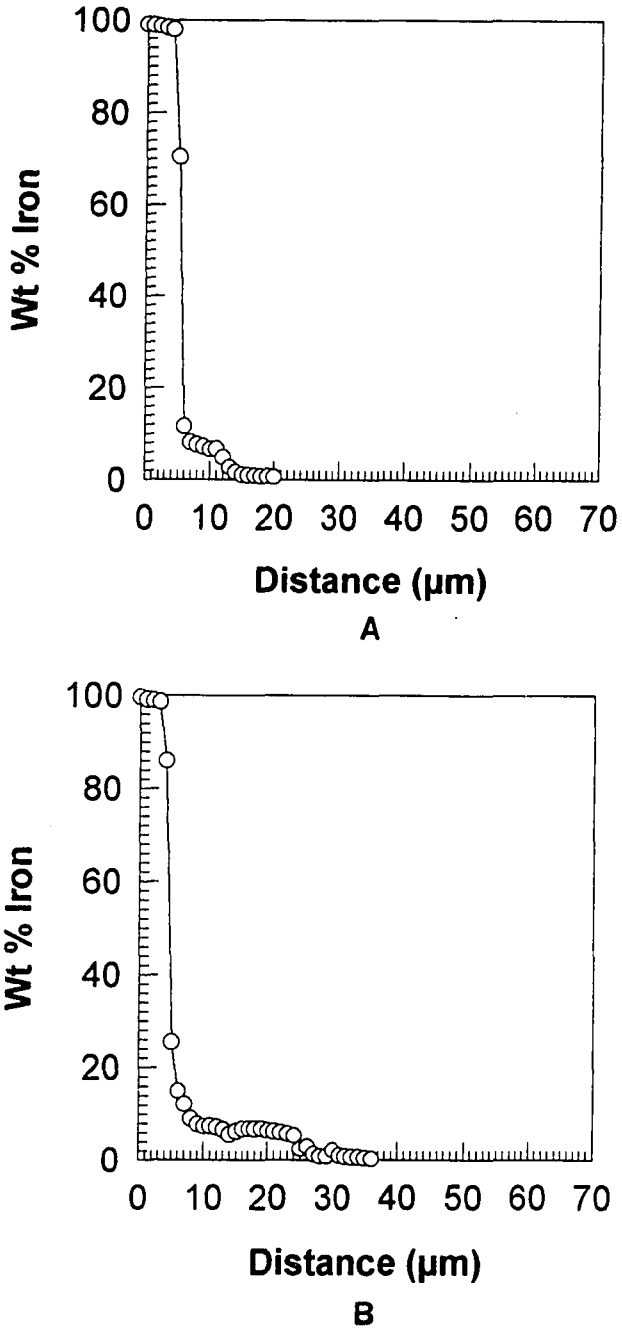

Figure 89. Iron concentration profile for the total Fe-Zn alloy layer formed on the non P-ion implanted low carbon steel surface hot-dip galvanized in a 0.00 wt% Al-Zn bath for (a) 5 and (b) 60 seconds of immersion.

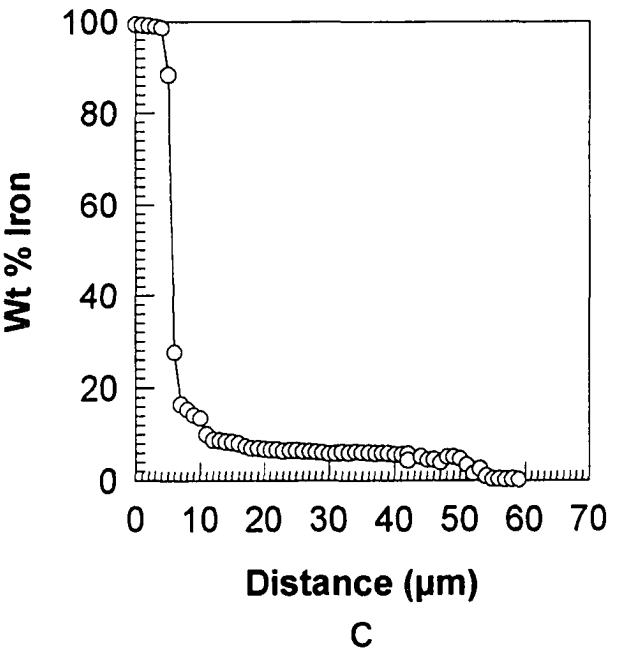

Figure 89. Iron concentration profile for the total Fe-Zn alloy layer formed on the non P-ion implanted low carbon steel surface hot-dip galvanized in a 0.00 wt% Al-Zn bath for (c) 300 seconds of immersion.

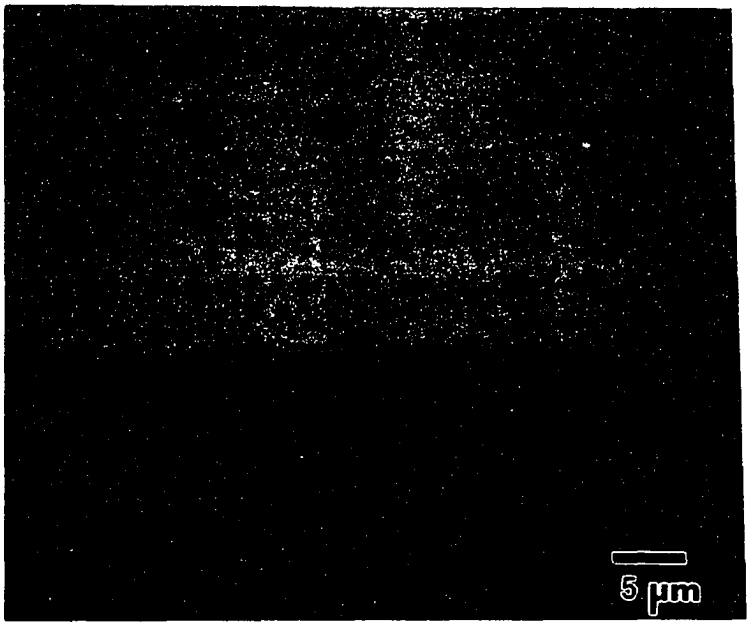

A

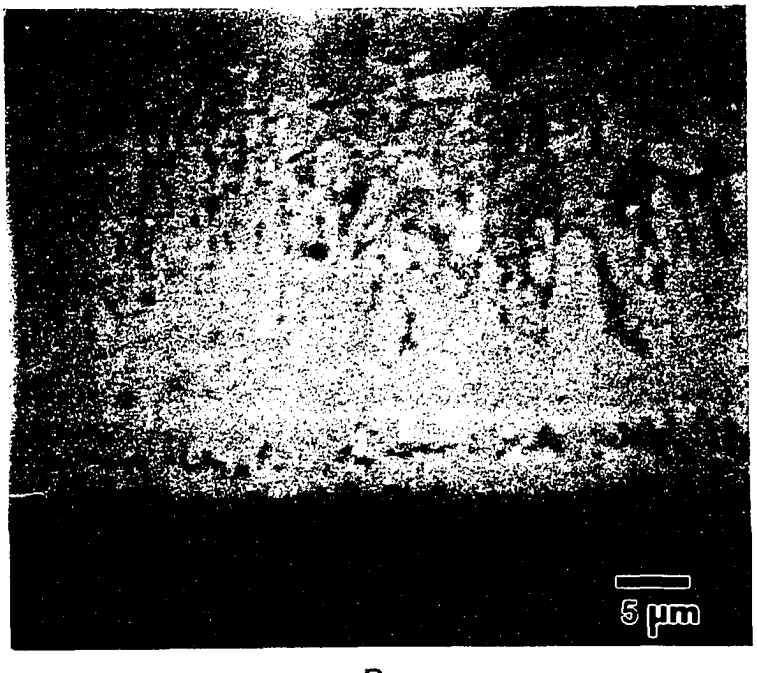

B

Figure 90. BSE images of the Fe-Zn phase layers formed on the P ion implanted low carbon steel surface hot-dip galvanized in a 0.00 wt% Al-Zn bath for (a) 5 and (b) 60 seconds of immersion. The micrographs are the areas which were analyzed for compositional analysis presented in Figure 88a and b.

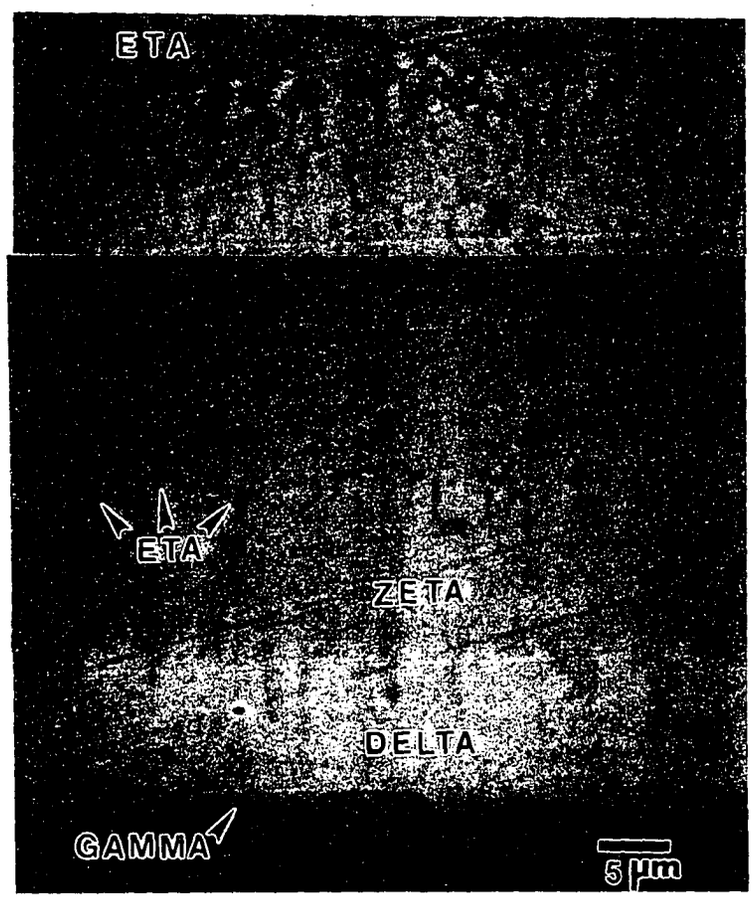

C

Figure 90. BSE images of the Fe-Zn phase layers formed on the P ion implanted low carbon steel surface hot-dip galvanized in a 0.00 wt% Al-Zn bath for (c) 300 seconds of immersion. The micrograph is the area which was analyzed for compositional analysis presented in Figure 88c.

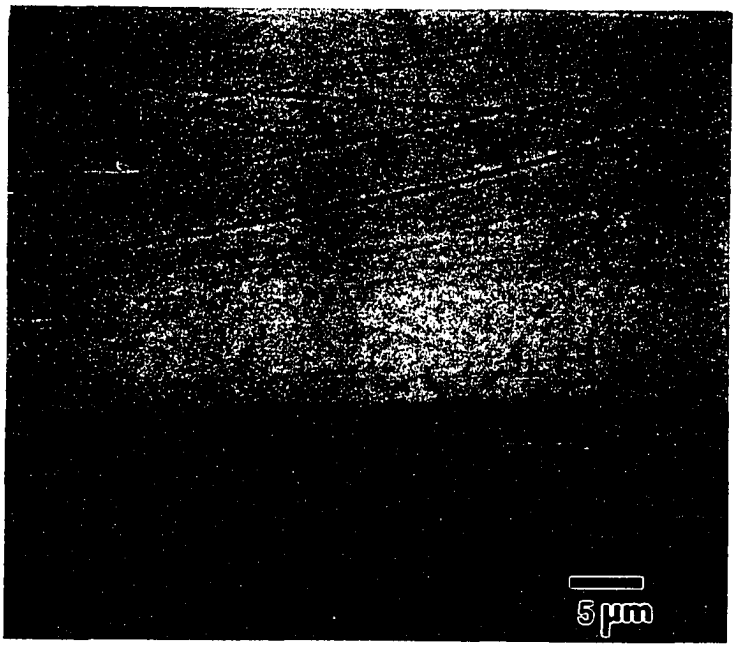

A

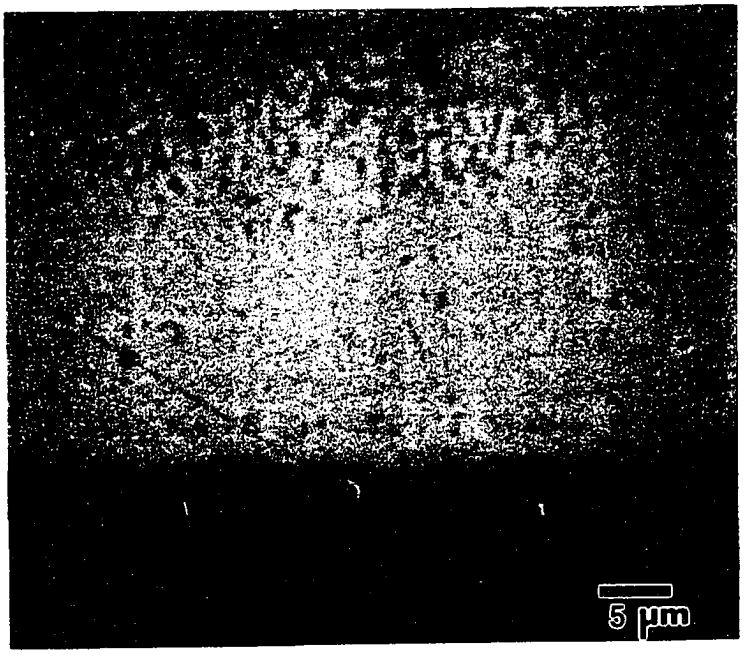

B

Figure 91. BSE images of the Fe-Zn phase layers formed on the non P ion implanted low carbon steel surface hot-dip galvanized in a 0.00 wt% Al-Zn bath for (a) 5 and (b) 60 seconds of immersion. The micrographs are the areas which were analyzed for compositional analysis presented in Figure 89a and b.

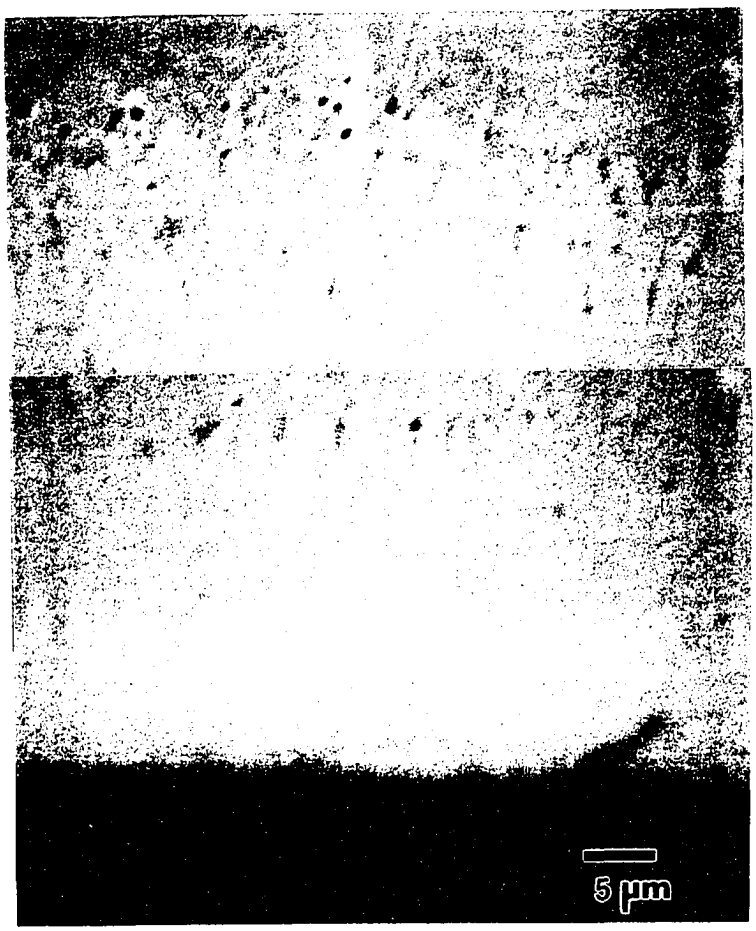

C

Figure 91. BSE images of the Fe-Zn phase layers formed on the non P ion implanted low carbon steel surface hot-dip galvanized in a 0.00 wt% Al-Zn bath for (c) 300 seconds of immersion. The micrograph is the area which was analyzed for compositional analysis presented in Figure 89c.

(ii). Delta Phase Layer Growth

Growth rate time constant values of 0.29 and 0.49 for the P and non P-ion implanted surfaces were determined. Although these values appear vastly different the error associated with each n value causes the values to fall within the error range of one another, indicating the kinetics of delta layer growth to be similar for both P and non P-ion implanted surfaces (Table XX). Delta layer growth can be assumed to follow parabolic diffusion controlled growth based upon the delta layer growth observed on other steel substrates in the 0.00 wt% Al-Zn bath, and also accounting for the large error associated with the determined n values.

(iii). Zeta Phase Layer Growth

The zeta layer was analyzed as a total layer (including the solidified eta phase present within the zeta phase layer), and growth rate time constants of 0.43 and 0.36 for the P and non P-ion implanted surfaces, respectively were determined (see Table XX). The n values are within the error of one another and indicate that the kinetics of zeta layer growth is similar for both the P and non P-ion implanted surfaces.

The kinetics of the total alloy layer and individual alloy layer growth were not influenced by the ion implantation of P when compared to the reaction kinetics observed on the ULC steels discussed in section V. B. 2. The total alloy layer growth as well as the individual

phase layer growth followed the same growth-time relationships on both the P and non P-ion implanted surfaces. Coverage of the steel/coating interface by the total Fe-Zn alloy layer was complete on both surfaces, indicating that P-ion implantation did not retard or inhibit the overall Zn attack of the steel surface.

c. Alloy Layer Growth - 0.20 wt% Al-Zn Bath

The P and non P implanted surfaces of the low carbon steel galvanized in the 0.20 wt% Al-Zn bath are shown in Figure 92. The P and non P-ion implanted surfaces were galvanized for 5-300 seconds in a 0.20 wt % Al-Zn bath which resulted in no significant Fe-Zn growth at the steel/coating interface which could be evaluated. Small crystals on the order of approximately 1.0 μm in size which formed at the steel/coating interface on both the P and non P-implanted surfaces were analyzed in the electron microprobe and the results are reported in Table XXI.

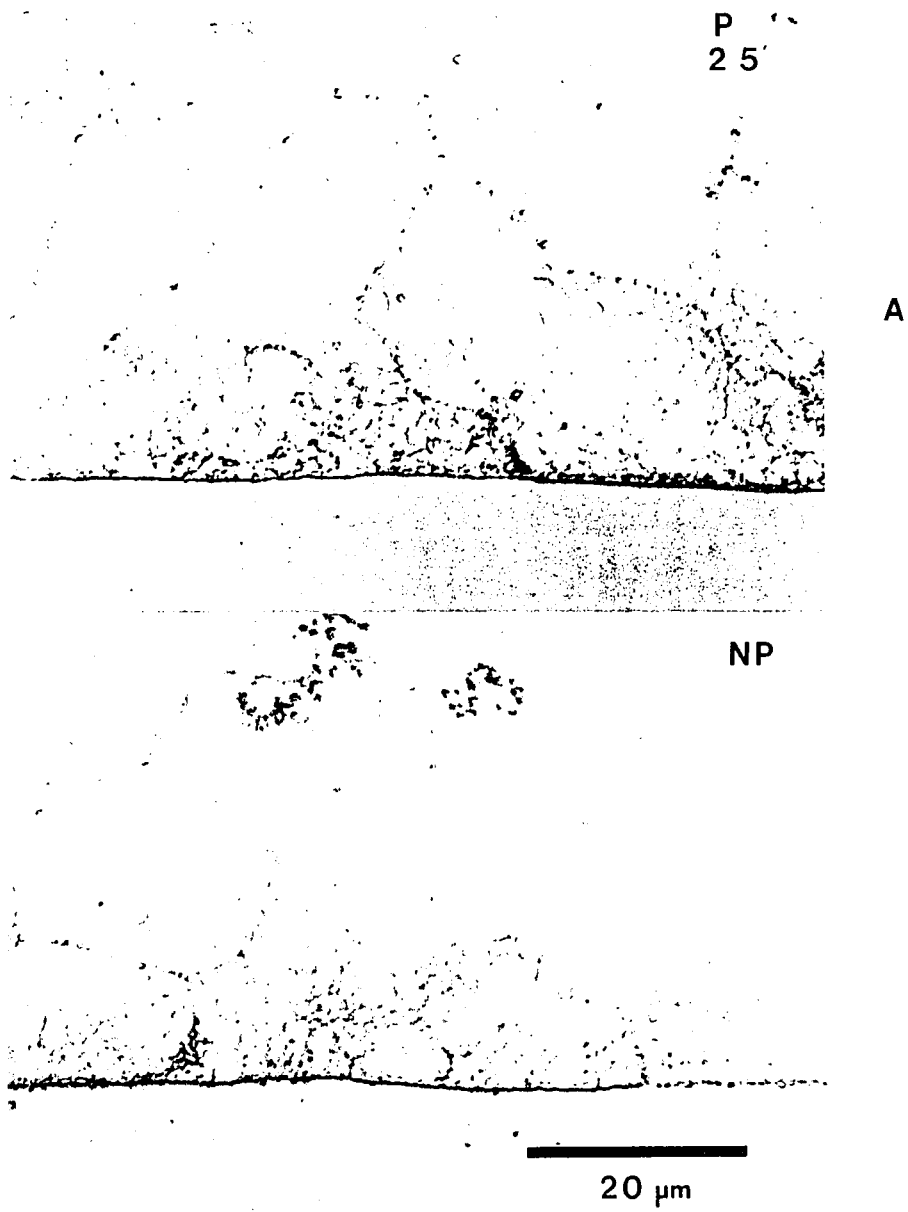

Figure 92. Phosphorous (P) and non phosphorous (NP) ion implanted low carbon steel surfaces hot-dip galvanized in a 0.20 wt% Al-Zn bath for (a) 5 seconds of immersion.

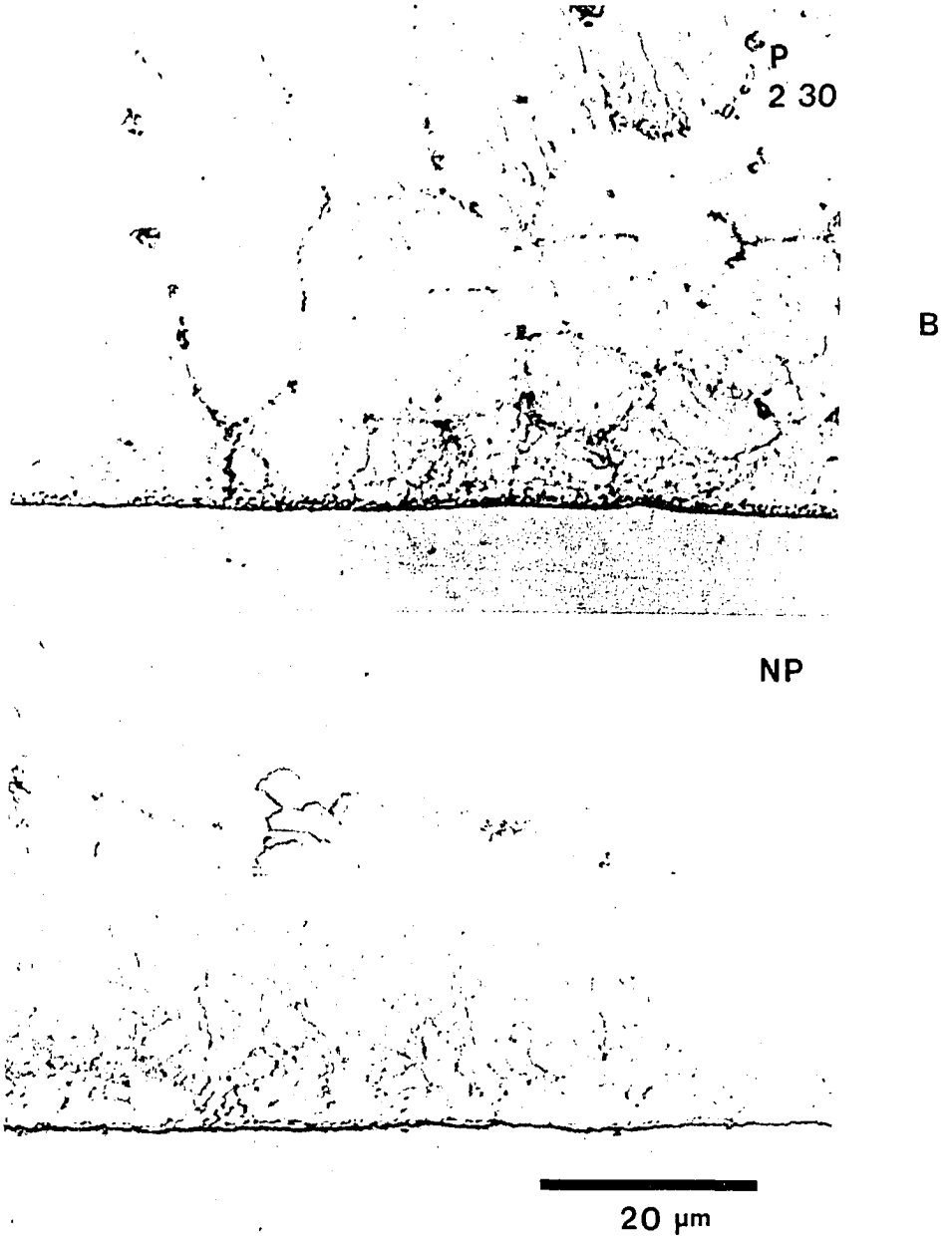

Figure 92. Phosphorous (P) and non phosphorous (NP) ion implanted low carbon steel surfaces hot-dip galvanized in a 0.20 wt% Al-Zn bath for (b) 30 seconds of immersion.

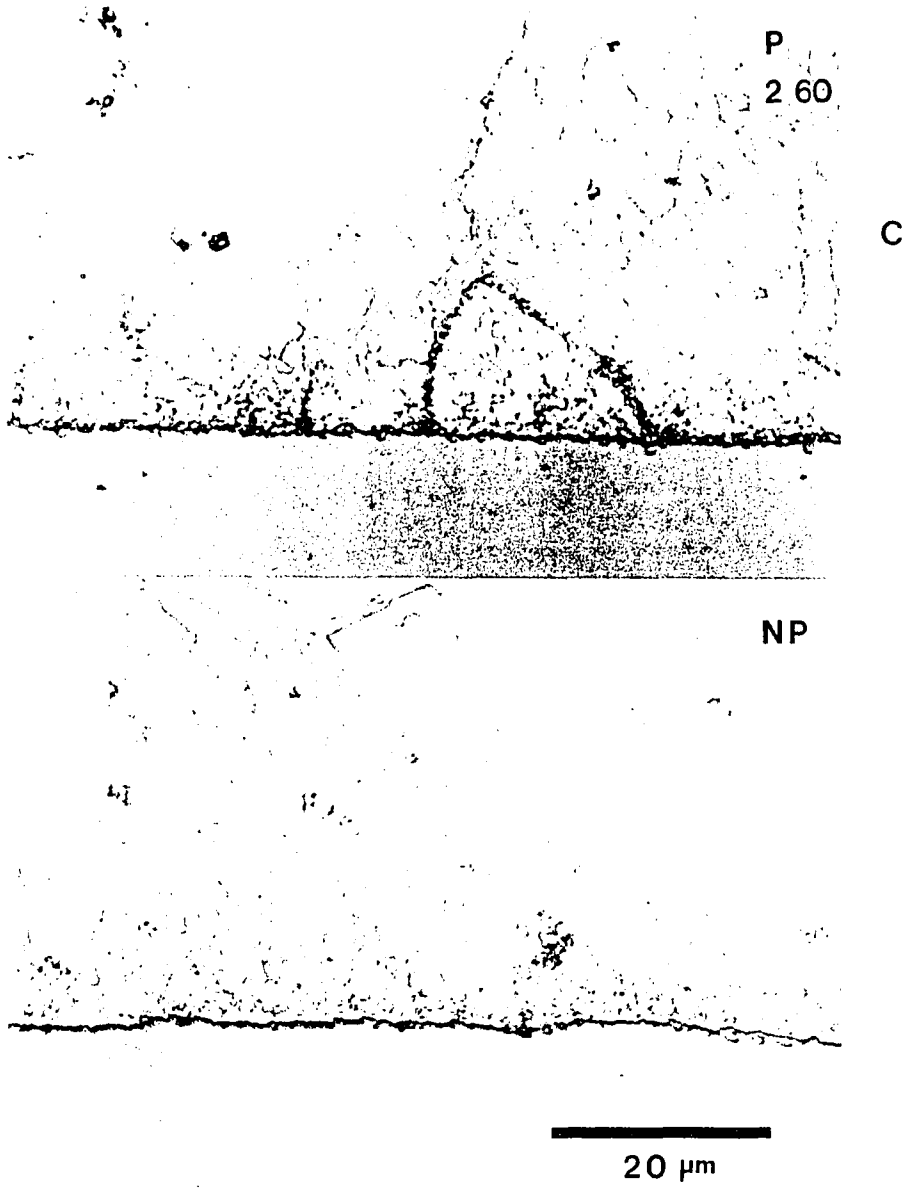

Figure 92. Phosphorous (P) and non phosphorous (NP) ion implanted low carbon steel surfaces hot-dip galvanized in a 0.20 wt% Al-Zn bath for (c) 60 seconds of immersion.

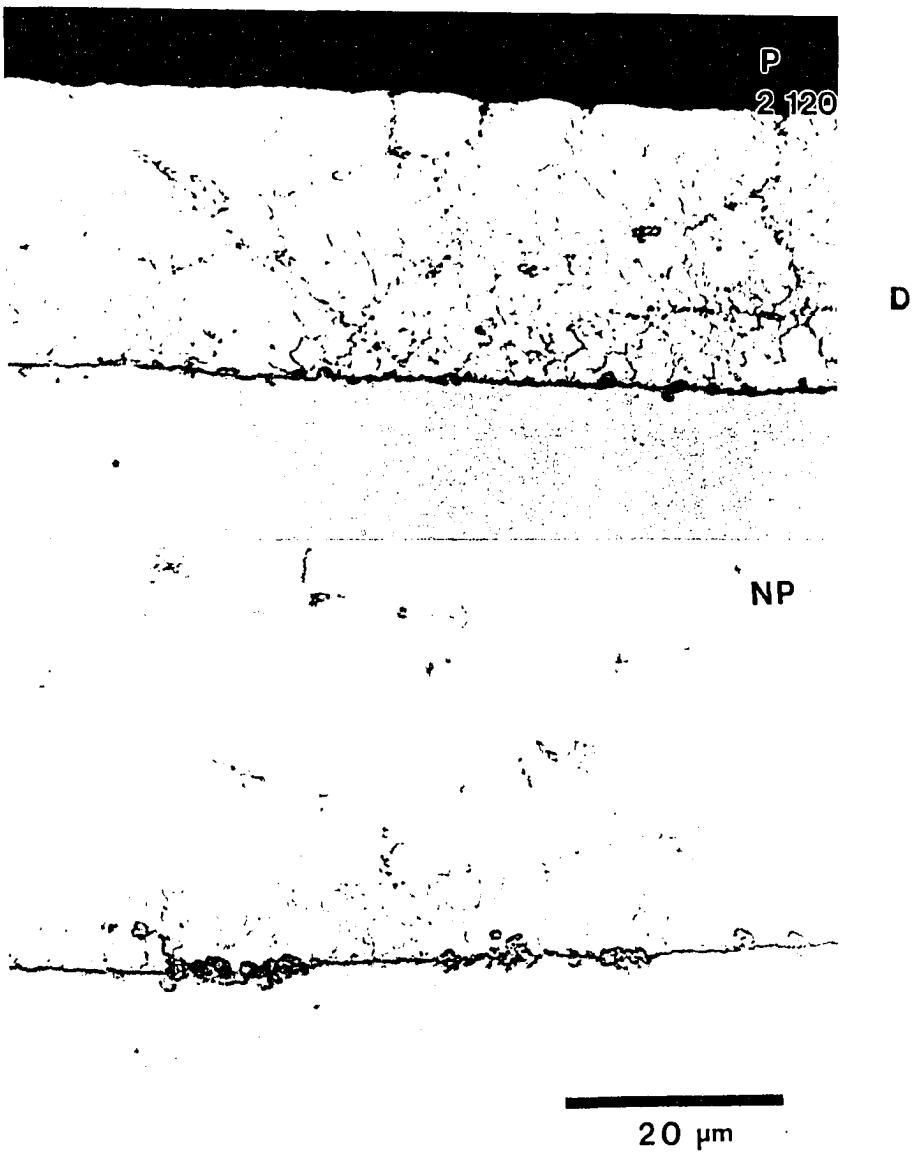

Figure 92. Phosphorous (P) and non phosphorous (NP) ion implanted low carbon steel surfaces hot-dip galvanized in a 0.20 wt% Al-Zn bath for (d) 120 seconds of immersion.

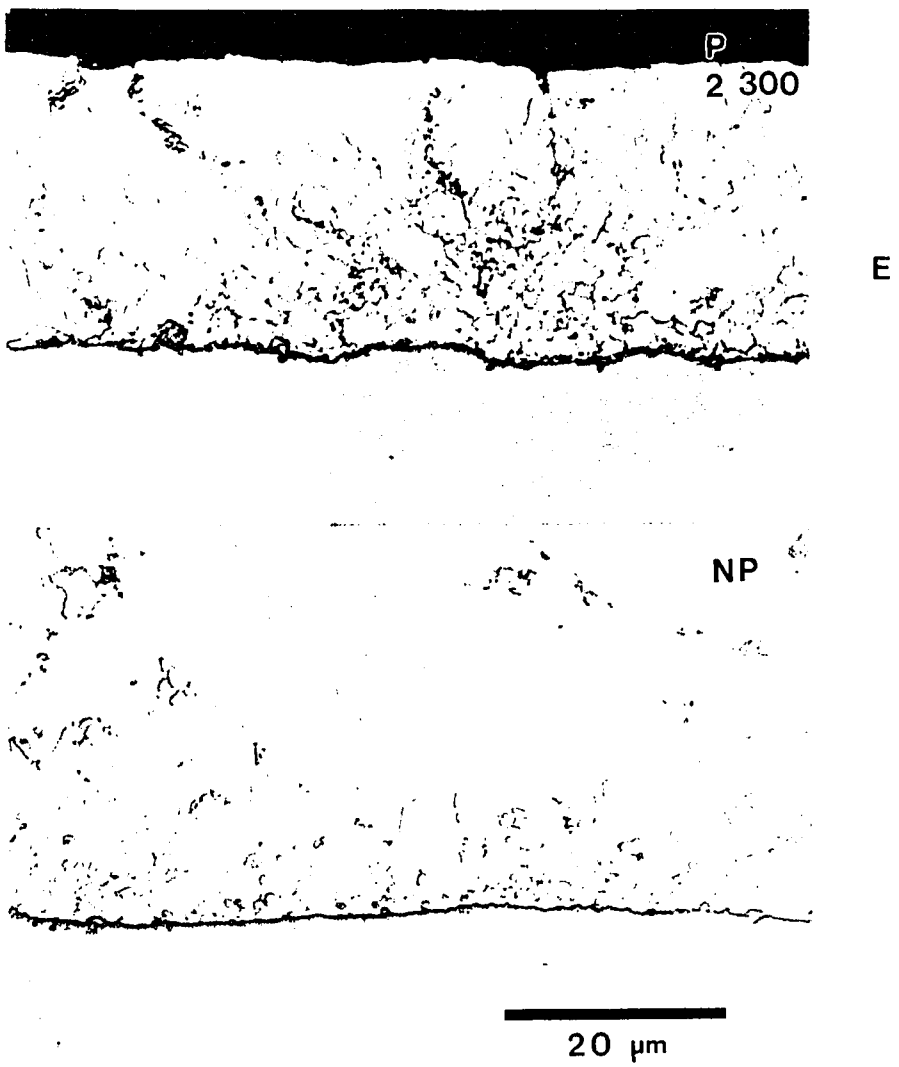

Figure 92. Phosphorous (P) and non phosphorous (NP) ion implanted low carbon steel surfaces hot-dip galvanized in a 0.20 wt% Al-Zn bath for (e) 300 seconds of immersion.

Table XXI. Microprobe Spot Analysis of Interfacial Growths formed on P and Non P-Ion Implanted Low Carbon Steel Galvanized in a 0.20 wt% Al-Zn Bath for 5, 60, and 300 seconds of immersion.

Sample / Growth description	wt% Fe (at%)	wt% Zn (at%)	wt% Al (At%)	Phase ID*
P Ion implanted sample surface				
5s / reaction layer ~ 1μm	8.00 (8.47)	85.50 (77.29)	6.50 (14.24)	$\delta + Fe_2Al_5$
5s / round phase growth	23.10 (17.93)	43.95 (29.14)	32.95 (52.94)	$\delta + Fe_2Al_5$ or $\eta + Fe_2Al_5$
60s / faceted growth	6.68 (7.49)	91.03 (87.20)	2.29 (5.31)	δ
60s / faceted growth (near steel/coating interface)	10.17 (10.35)	80.51 (70.02)	9.32 (19.63)	$\delta + Fe_2Al_5$
300s / faceted growth	5.11 (5.88)	94.28 (92.67)	0.61 (1.45)	$\zeta + \eta$
300s / faceted growth	4.93 (5.66)	94.31 (92.52)	0.76 (1.81)	$\delta + \zeta + \eta$ or $\delta + \eta$
Non P Ion implanted sample surface				
5s / faceted growth	22.90 (17.50)	42.48 (27.74)	34.62 (54.76)	$\delta + Fe_2Al_5$ or $\eta + Fe_2Al_5$
60s / growth (appears to be part of steel substrate)	95.14 (95.42)	4.51 (3.87)	0.34 (0.71)	$\alpha + \Gamma$
300s / faceted growth	4.53 (5.19)	94.37 (92.23)	1.09 (2.59)	$\delta + \eta$
300s / faceted growth	4.10 (4.69)	94.8 (92.69)	1.11 (2.62)	$\delta + \eta$

* based upon metastable Fe-Zn-Al ternary isotherm at 450°C [24].

The metastable Fe-Zn-Al ternary isotherm at 450°C [24] was used to identify the phases observed as discrete isolated growths and the phase identification is listed in Table XXI. Table XXI shows that for the P-ion implanted surface Fe_2Al_5 and Fe-Zn delta phase

growths were formed at short reaction times of 5 and 60 seconds, and at longer times of immersion (300 seconds) growths of delta and zeta phase subsequently formed at the steel/coating interface. Based upon the diffusion path through the metastable ternary isotherm previously discussed (Figure 51) zeta phase is not expected to form because it was found not to be in metastable equilibrium with the eta phase. Therefore the growths identified as zeta phase could possibly have been misidentified due to a microprobe spot size which was broad enough to sample both a delta phase growth and the surrounding Fe supersaturated eta phase. The non P-ion implanted surface showed the same behavior with Fe_2Al_5 and delta phase growths forming at the steel/coating interface first, followed at longer reaction times by delta phase growths alone. The growths measured in Table XXI were on the order of 1-5 μm in diameter, and oversampling of the growths by a broad microprobe spot size could have occurred, resulting in an error of the composition determined, and improper identification of the phases formed at the steel/coating interface.

As in the case of the 85 μm grain size ULC steel galvanized in a 0.20 wt% Al-Zn bath for 5-300 seconds of immersion, the Fe-Al inhibition layer (identified as Fe_2Al_5) in the bath was stable on the P and non P ion implanted surfaces and did not allow for localized liquid Zn attack of the steel substrate as was observed to occur for the 15 μm grain size ULC steel over the same reaction times, thus confirming the fact that increased substrate steel grain size retards Fe-Zn reactions in 0.20 wt% Al-Zn baths (see section V. B. 2). Previous investigators [27] have shown that 0.20 wt% Al-Zn baths delay the formation of Fe-Zn phases for immersion times greater than 300 seconds. Therefore long time

immersion samples of 1800, 2700 and 3600 seconds in the 0.20 wt % Al-Zn bath were chosen for further study of the P and non P-ion implanted surfaces.

Long time immersion samples were thus produced in an attempt to study the breakdown of the Fe_2Al_5 inhibition layer. Light optical micrographs of the P and non P-implanted surfaces after extended immersion time in the 0.20 wt% Al-Zn bath are shown in Figure 93. The alloy layer formed was not a series of localized Fe-Zn alloy phase growths made up of 2 individual phase layers of gamma and delta as expected, but instead a continuous Fe-Zn-Al layer formed at the steel/coating interface (Figure 93). Electron microprobe composition data of the Fe, Zn, and Al chemistry of the Fe-Zn-Al growth layer are listed in Tables XXII and XXIII. Table XXII is a listing of the microprobe spot composition analysis conducted on the P-ion implanted surface. At each immersion time the Fe-Zn-Al layer was measured at 3 locations: (1) near the steel/reaction layer interface (s/r), (2) in the middle of the reaction layer (mid) and (3) at the reaction layer/Zn melt interface (r/m), as shown in Table XXIII. According to the metastable ternary Fe-Zn-Al isotherm at 450°C (Figure 9a), the phase layer has been identified based upon composition and is also listed in Table XXII. The metastable isotherm did not show an extended solubility of Zn for Fe_2Al_5 as found by Chen [5, 25] and others [13], therefore often the phase identification based upon the metastable isotherm is representative of a composition corresponding to a Fe_2Al_5 + delta phase, or Fe_2Al_5 + eta phase two phase field. Most likely the Fe_2Al_5 phase field in Figure 9a should be extended toward the Zn corner of the isotherm to allow for the greater solubility of Zn in the Fe_2Al_5 phase. Based upon thermodynamic calculations,

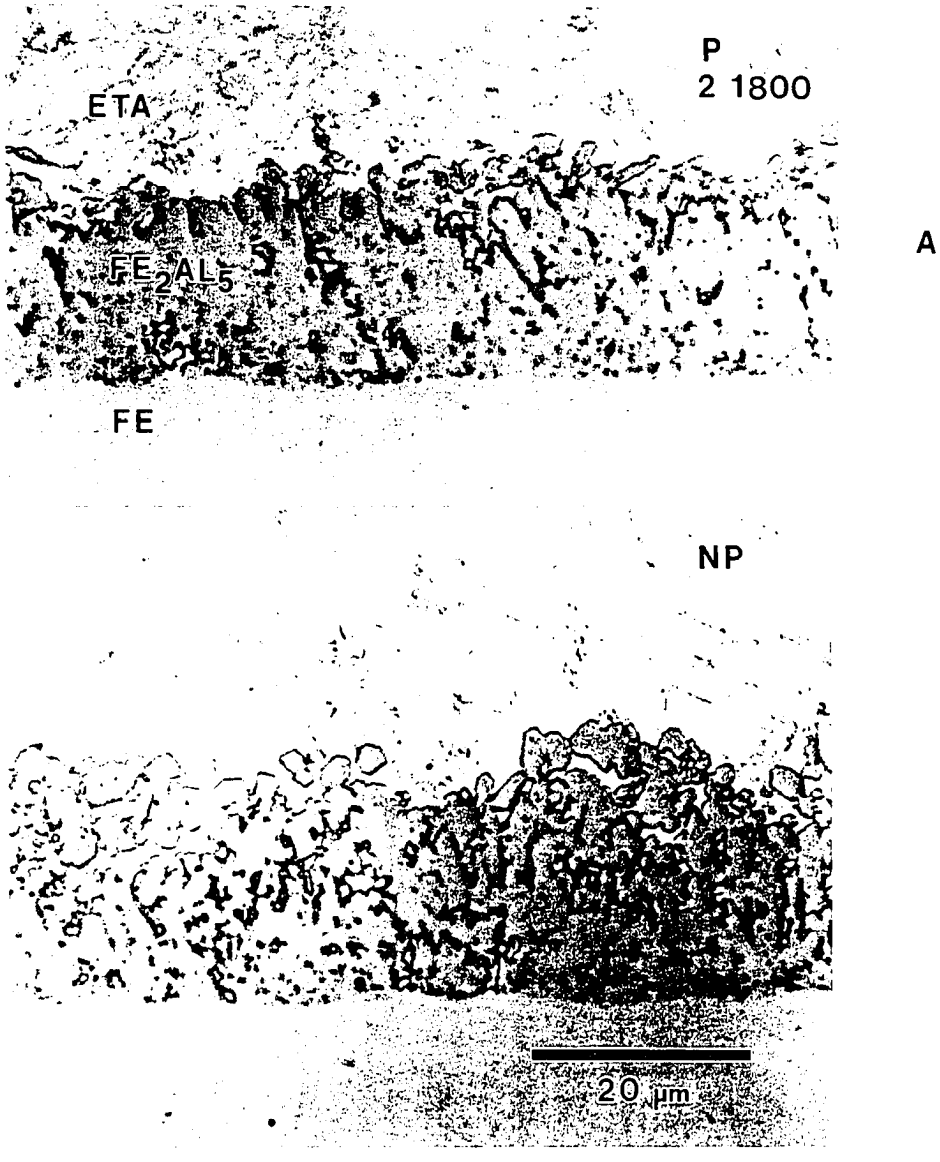

Figure 93. Phosphorous (P) and non phosphorous (NP) ion implanted low carbon steel surfaces hot-dip galvanized in a 0.20 wt% Al-Zn bath for (a) 1800 seconds of immersion.

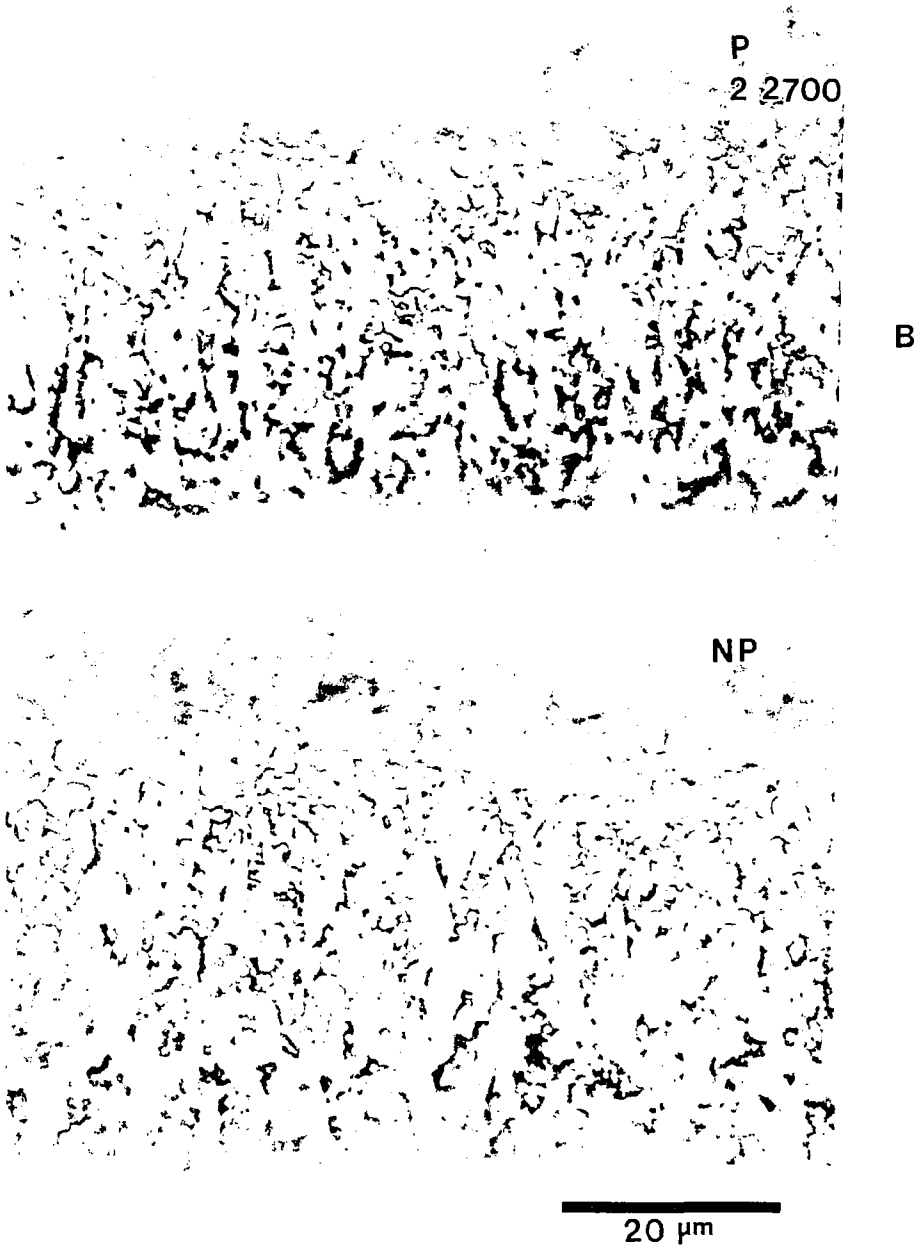

Figure 93. Phosphorous (P) and non phosphorous (NP) ion implanted low carbon steel surfaces hot-dip galvanized in a 0.20 wt% Al-Zn bath for (b) 2700 seconds of immersion.

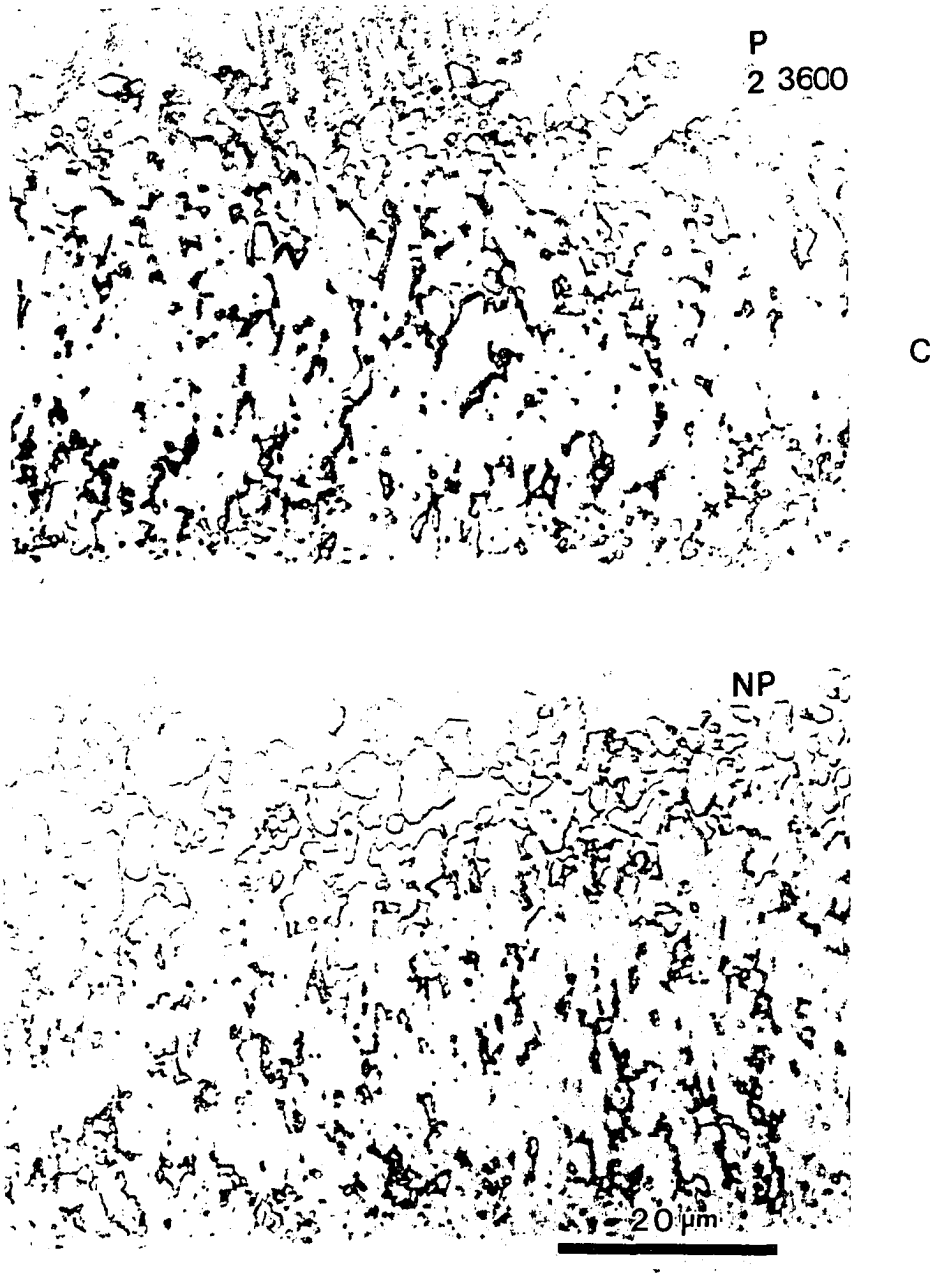

Figure 93. Phosphorous (P) and non phosphorous (NP) ion implanted low carbon steel surfaces hot-dip galvanized in a 0.20 wt% Al-Zn bath for (c) 3600 seconds of immersion.

Table XXII. Microprobe Spot Analysis of a Continuous Reaction Layer formed on P-Ion Implanted Low Carbon Steel Surface Galvanized in a 0.20 wt% Al-Zn Bath for 1800, 2700, and 3600 seconds of immersion.

Sample / Location*	wt% Fe (at%)	wt% Zn (at%)	wt% Al (at%)	Phase ID*
1800s / (s/r)	33.55 (25.15)	31.03 (19.87)	35.03 (54.98)	$\delta + Fe_2Al_5$
1800s / (s/r)	32.43 (24.40)	32.40 (20.82)	35.17 (54.77)	$\delta + Fe_2Al_5$
1800s / (mid)	30.53 (22.98)	34.14 (21.96)	35.34 (55.06)	$\delta + Fe_2Al_5$
1800s / (mid)	32.25 (24.08)	31.69 (20.21)	36.05 (55.71)	$\delta + Fe_2Al_5$
1800s / (r/m)	32.54 (23.55)	27.96 (17.28)	39.50 (59.17)	$\delta + Fe_2Al_5$ or $\eta + Fe_2Al_5$
1800s / (r/m)	34.71 (24.77)	24.46 (14.91)	40.83 (60.31)	$\delta + Fe_2Al_5$ or $\eta + Fe_2Al_5$
2700s / (s/r)	36.04 (26.86)	28.17 (17.93)	35.79 (55.21)	$\delta + Fe_2Al_5$
2700s / (s/r)	35.27 (25.99)	27.59 (17.37)	37.14 (56.64)	$\delta + Fe_2Al_5$
2700s / (mid)	37.44 (26.63)	21.67 (13.17)	40.89 (60.20)	Fe_2Al_5
2700s / (mid)	33.71 (24.30)	26.48 (16.31)	39.80 (59.39)	$\delta + Fe_2Al_5$ or $\eta + Fe_2Al_5$
2700s / (r/m)	34.58 (24.73)	24.83 (15.17)	40.59 (60.09)	"
2700s / (r/m)	32.87 (23.81)	27.75 (17.17)	39.87 (59.02)	"
3600s / (s/r)	34.51 (24.80)	25.44 (15.62)	40.05 (59.58)	"
3600s / (s/r)	34.71 (25.24)	26.61 (16.54)	38.68 (58.22)	"
3600s / (mid)	35.47 (25.41)	24.24 (14.84)	40.29 (59.75)	"
3600s / (mid)	32.60 (24.35)	31.44 (20.06)	35.95 (55.58)	$\delta + Fe_2Al_5$
3600s / (r/m)	38.10 (26.90)	20.22 (12.20)	41.67 (60.90)	Fe_2Al_5
3600s / (r/m)	28.52 (21.02)	33.58 (21.15)	37.90 (57.83)	$\delta + Fe_2Al_5$

* (s/r) = steel/reaction layer interface, (mid) = middle of reaction layer
(r/m) = reaction layer/Zn melt interface

* based upon metastable Fe-Zn-Al ternary isotherm at 450°C [24].

Table XXIII. Microprobe Spot Analysis of a Continuous Growth Layer formed on Non P-Ion Implanted Low Carbon Steel Galvanized in a 0.20 wt% Al-Zn Bath for 1800, 2700, and 3600 seconds of immersion.

Sample / Location*	wt% Fe (at%)	wt% Zn (at%)	wt% Al (at%)	Phase ID*
1800s / (s/r)	36.43 (26.45)	24.92 (15.46)	38.65 (58.09)	$\delta + Fe_2Al_5$ or $\eta + Fe_2Al_5$
1800s / (s/r)	36.99 (26.73)	23.88 (14.74)	39.13 (58.53)	"
1800s / (mid)	36.41 (26.02)	23.09 (14.09)	40.50 (59.89)	"
1800s / (mid)	34.28 (24.71)	25.96 (15.98)	39.76 (59.31)	"
1800s / (r/m)	28.71 (21.28)	34.01 (21.53)	37.28 (57.19)	"
1800s / (r/m)	36.45 (26.03)	23.01 (14.04)	40.55 (59.93)	"
2700s / (s/r)	36.16 (26.47)	26.11 (16.33)	37.74 (57.19)	$\delta + Fe_2Al_5$
2700s / (s/r)	35.85 (25.89)	24.79 (15.29)	39.36 (58.82)	"
2700s / (mid)	35.19 (25.39)	25.30 (15.60)	39.51 (59.01)	"
2700s / (mid)	36.38 (25.92)	22.80 (13.88)	40.82 (60.20)	Fe_2Al_5
2700s / (r/m)	35.29 (25.43)	25.06 (15.43)	39.65 (59.15)	$\delta + Fe_2Al_5$
2700s / (r/m)	38.73 (27.40)	19.93 (12.05)	41.34 (60.55)	Fe_2Al_5
3600s / (s/r)	35.20 (26.04)	28.11 (17.77)	36.69 (56.19)	$\delta + Fe_2Al_5$
3600s / (s/r)	32.88 (24.02)	28.75 (17.95)	38.37 (58.03)	"
3600s / (mid)	33.15 (24.08)	27.85 (17.28)	39.00 (58.64)	"
3600s / (mid)	34.64 (25.13)	26.41 (16.37)	38.95 (58.50)	"
3600s / (r/m)	37.64 (26.57)	20.61 (12.43)	41.76 (61.01)	Fe_2Al_5
3600s / (r/m)	32.40 (23.41)	27.87 (17.20)	39.73 (59.40)	$\delta + Fe_2Al_5$

* (s/r) = steel/reaction layer interface, (mid) = middle of reaction layer
(r/m) = reaction layer/melt interface
* based upon metastable Fe-Zn-Al ternary isotherm at 450°C [24].

Tang [13] has recently developed an updated Fe-Zn-Al equilibrium ternary isotherm, Figure 94, in which he defines an Fe-Zn-Al eta phase (Fe_2Al_5 - Zn_x) which has a solubility of up to approximately 20 wt% Zn. The data presented in Tables XXII and XXIII more closely match the Fe_2Al_5 - Zn_x phase composition defined by Tang [13], than that of the Fe_2Al_5 phase in the metastable Fe-Zn-Al ternary isotherm of Perrot [24]. The Fe_2Al_5(Zn) layer formed on the P and non P implanted surfaces contained more Zn than the solubility limit defined in Figure 94 for the Fe_2Al_5-Zn_x phase, and this is most likely related to the morphology of the Fe_2Al_5(Zn) layer.

The reaction layer was one phase, Fe_2Al_5 (Zn), which was porous (Figure 93). Thus the Fe_2Al_5(Zn) layer contained enclosed areas of eta phase. Microprobe spot analysis was conducted away from these regions of eta phase, yet regions of eta phase underneath the surface could have contributed to the higher than expected analysis for Zn, and thus resulted in the composition being identified as an Fe_2Al_5 + delta phase, or Fe_2Al_5 + eta phase as defined by the metastable Fe-Zn-Al ternary diagram in Figure 9. All analysis of the Fe, Zn, and Al composition data was evaluated according to the metastable ternary diagram because it was specifically developed for reaction times less than 30 minutes or 1800 seconds. The ternary isotherm presented in Figure 94 is an equilibrium diagram, and therefore is better suited for long time annealing studies. Another source of error in the composition analysis of the Fe-Al-Zn layer could be due to the correction method (phi-rho-z, $\varphi(\rho z)$) used for all coating compositional analysis. The $\varphi(\rho z)$ correction method is best suited for the analysis of small amounts of a light atomic weight element (in this case

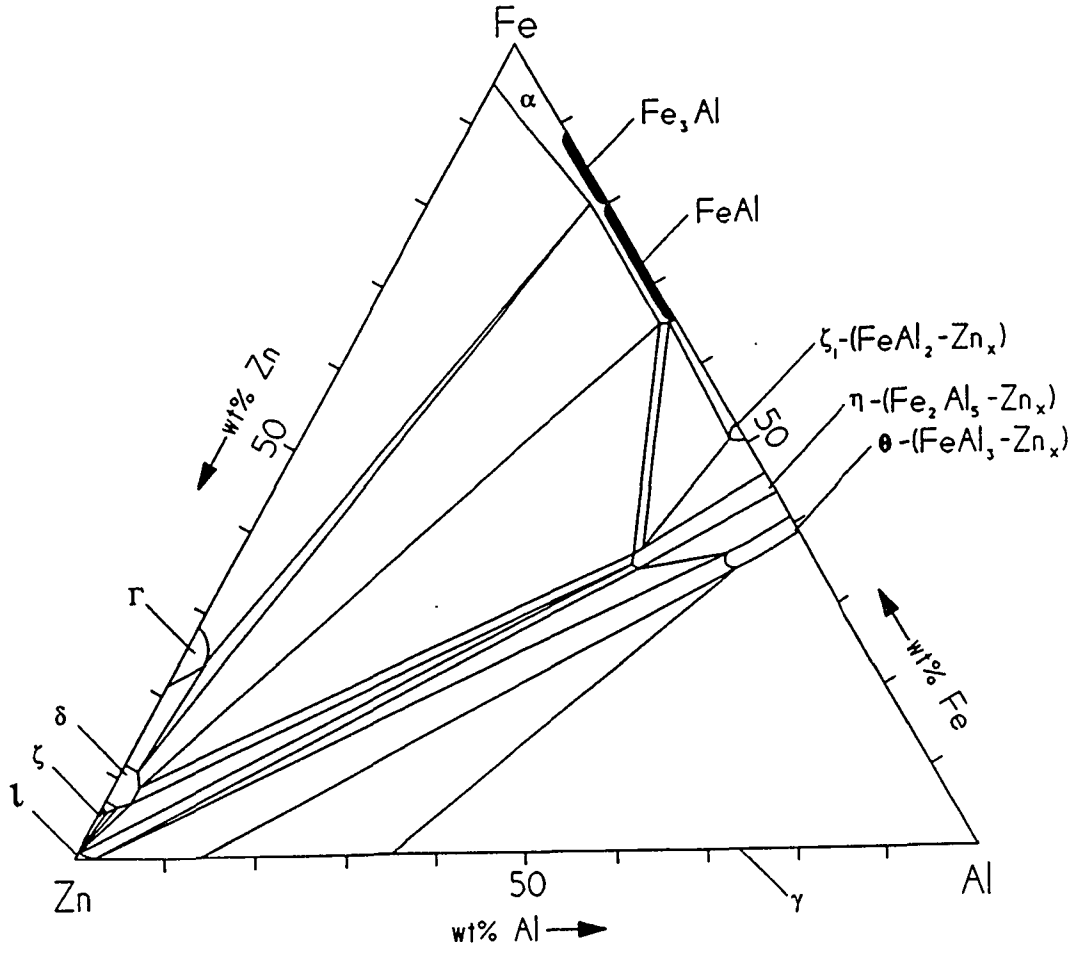

Figure 94. Revised 450°C isotherm of the Fe-Zn-Al ternary phase diagram [13].

Al) present in heavy atomic weight element or alloy matrix. While Al was present in small amounts for the coatings discussed previously, in the Fe-Zn-Al reaction layer Al is a major component and thus some error associated with the correction method may also explain some compositional irregularities. The reaction layer on the non P sample surface was also porous, containing regions of entrapped eta phase (Figure 93). The non P implanted surface also showed the Fe-Zn-Al reaction layer to be of the same composition ($Fe_2Al_5(Zn)$) as that for the P implanted surface at all of the extended reaction times studied (Table XXIII). Thus P-ion implantation did not affect the composition of the Fe-Zn-Al reaction layer.

The metastable $Fe_2Al_5(Zn)$ phase has been reported by other investigators [5, 13, 25] to have a chemistry that is in general agreement with that of the Fe-Al-Zn alloy layer analyzed in this work. The Fe-Al-Zn coverage of the steel/coating interface was complete on both the P and non P ion implanted surfaces, and the Fe_2Al_5 (Zn) layer had a porous morphology as entrapped eta phase was visible in its structure (Figure 93).

(i). Fe-Zn-Al Layer Growth

The growth of the Fe-Zn-Al compound was measured over the three extended immersion times studied, and the data for the P and non P implanted surfaces are shown in Figure 95. The total thickness of the $Fe_2Al_5(Zn)$layer was found to be greater at all reaction times for the non P ion implanted surface. Determining the growth rate time constant (n) value for

the Fe-Al-Zn layer resulted in values of 1.3 and 1.1 for the P and non P-ion implanted surfaces, respectively (Table XXIV). The n values are within error range of one another and indicate that the kinetics of the $Fe_2Al_5(Zn)$ layer is the same for both surfaces, and an n value of approximately 1.0 implies linear interface controlled kinetics. A porous reaction layer has been found by other investigators [88] to grow according to linear kinetics.

The growth data indicate there was also an incubation time associated with the formation and growth of the $Fe_2Al_5(Zn)$ layer and this incubation time occurred between 300 seconds (5 minutes) and 1800 seconds (30 minutes) as shown in Figure 95. At short reaction times of 5 seconds a metastable Fe-Al-Zn compound forms (Table XXI, 5 second data), and later, over time transforms into a more Fe and Al rich layer, Fe_2Al_5 (Zn) (Table XXII and XXIII). Thus the reaction layer progresses from that shown in Figure 92, a thin Fe_2Al_5 layer with discrete 1-5 μm growths of delta and/or zeta phase to a reaction layer like that shown in Figure 93, a porous Fe_2Al_5 (Zn) phase containing areas of entrapped eta phase. The equilibrium Fe-Zn-Al isotherm at 450° C [13] indicates that Fe_2Al_5 (Zn) should be in local equilibrium with liquid Zn. However, the 85 μm ULC steel immersed in the bath for the same time of immersion (1800 seconds), Fe-Zn growths formed in association with grain boundaries of the substrate steel, and Fe_2Al_5 formed between the Fe-Zn growths. The possible cause of this difference in P and non P-ion implanted 1800 second sample and the 85 μm ULC steel 1800 second sample may be due to kinetics,

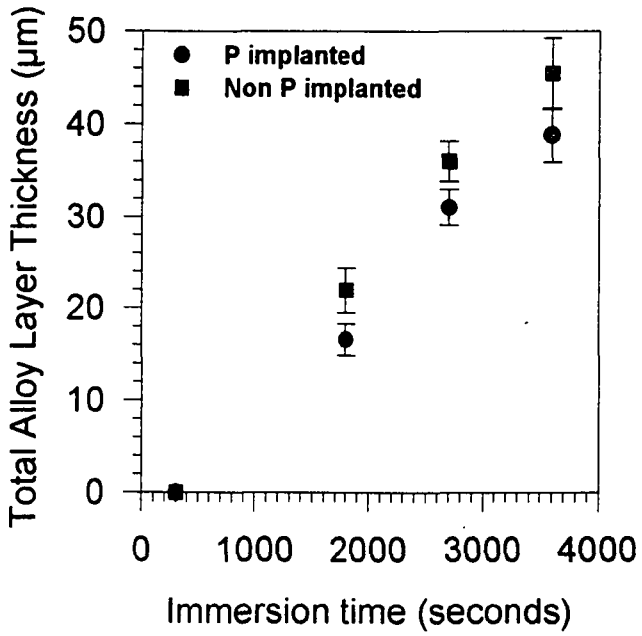

Figure 95. Total Fe-Zn alloy layer growth for the P and non P-ion implanted low carbon steel surfaces hot-dip galvanized in a 0.20 wt% Al-Zn bath.

Table XXIV. Total Fe_2Al_5-Zn Alloy Layer Growth Rate Time Constant (n) Values for the P and Non P-Ion Implanted Low Carbon Steel Galvanized in a 0.20 wt% Al-Zn Bath for 1800-3600 seconds of immersion.

Sample	Growth Rate Time Constant (n)
P implanted	1.3 ± 0.2
Non P implanted	1.1 ± 0.1

specifically grain boundary kinetics, controlling the reaction and not thermodynamic phase equilibrium criteria.

(ii). Fe-Zn Growth

Only in one or two locations on each P and non P-ion implanted sample surface did a localized Fe-Zn outburst structure form, as shown in Figure 96. Each of the few individual outburst structures appeared to be associated with a substrate grain boundary on both the P and non P-ion implanted surfaces, as shown in Figure 97. Using dark field LOM the substrate grain boundary contrast was enhanced (Figure 98), and the Fe-Zn phase growth events did appear to be associated with the substrate grain boundary, as evidenced by a trailing tail of Fe-Zn phase that progressed down a substrate grain boundary (arrows) where a localized Fe-Zn growth event occurred, shown in Figures 98b and 98d.

Due to the small number of Fe-Zn growths, the individual phase layer growth within the outbursts could not be quantified statistically. The morphology of the outbursts was similar to that found on other 0.20 wt% Al-Zn coatings and consisted of a thin gamma layer of approximately 1.0 μm at the interface, and a thick 10-100 μm delta phase layer adjacent to the gamma layer. Similar to other 0.20 wt% Al-Zn coatings, the delta layer was in contact with the liquid Zn.

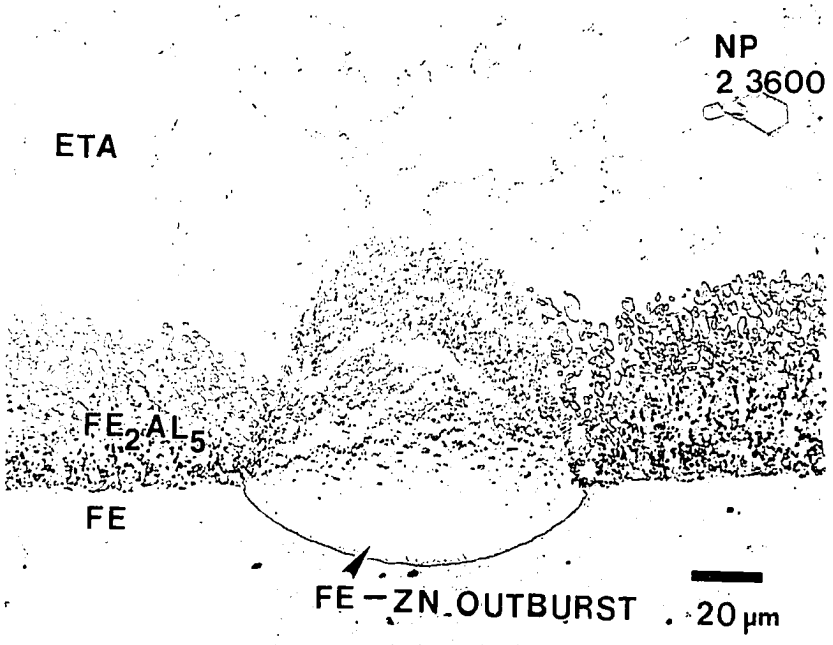

Figure 96. Non P-ion implanted low carbon steel surfaces hot-dip galvanized in a 0.20 wt% Al-Zn bath for 3600 seconds of immersion.

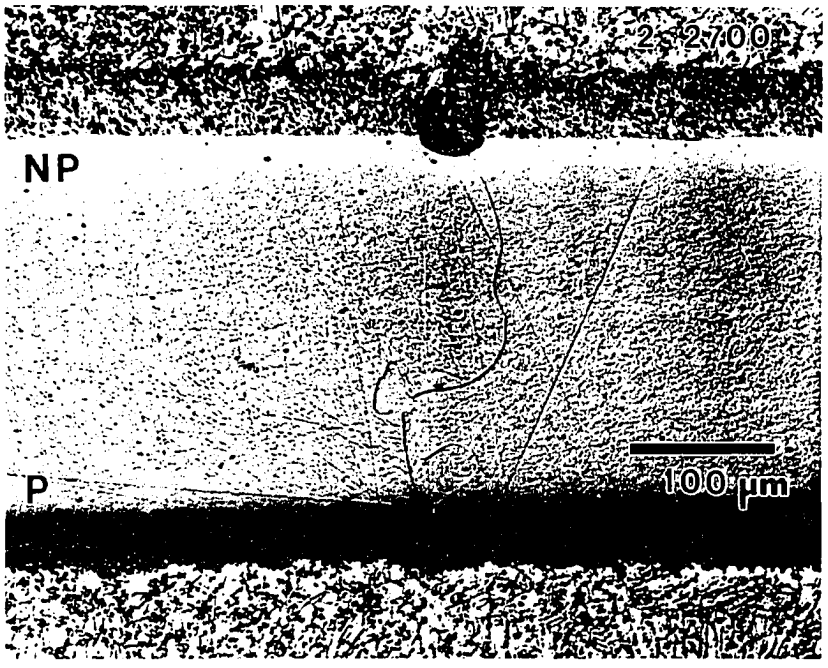

Figure 97. Localized Fe-Zn alloy phase growths formed on the phosphorous (P) and non phosphorous (NP) ion implanted low carbon steel surfaces hot-dip galvanized in a 0.20 wt% Al-Zn bath for 2700 seconds of immersion.

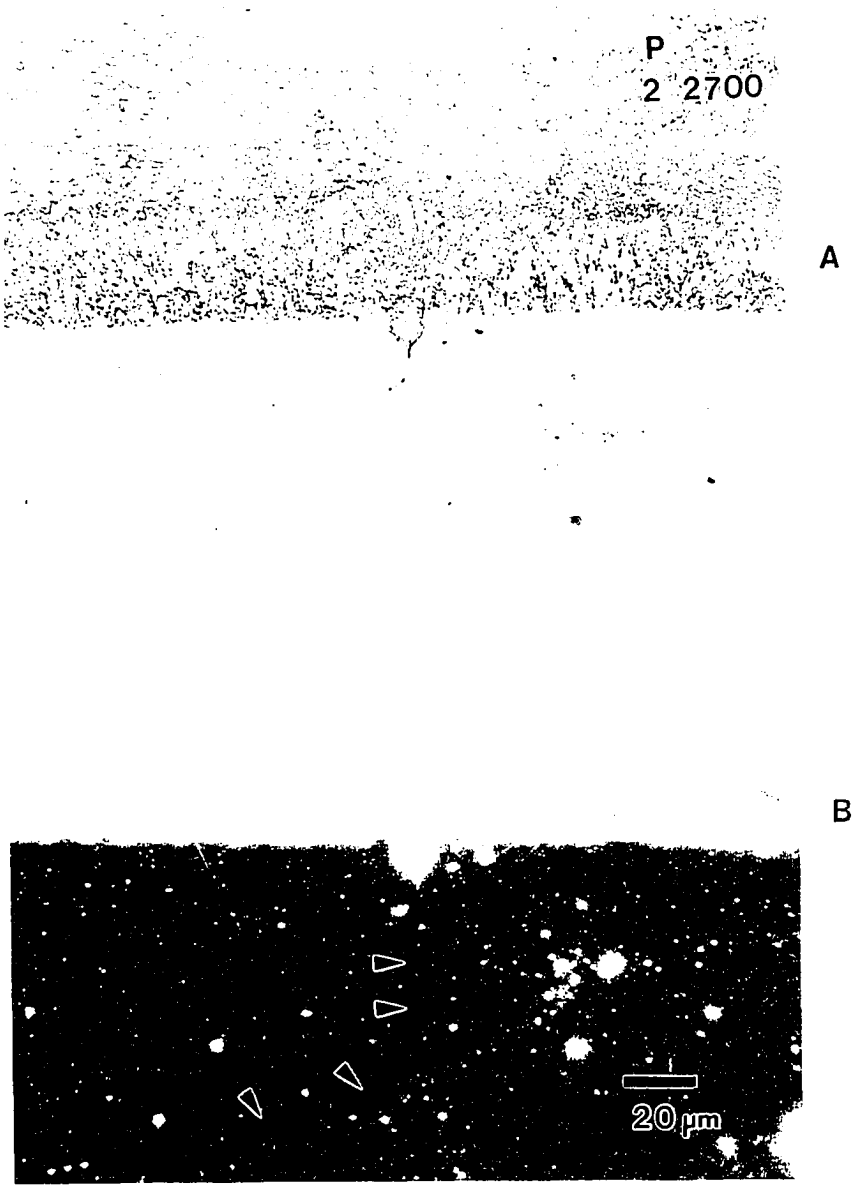

Figure 98. Localized Fe-Zn alloy phase growth formed on the P-ion implanted low carbon steel surface hot-dip galvanized in a 0.20 wt% Al-Zn bath for 2700 seconds of immersion (a) bright field LOM image and (b) dark field LOM image.

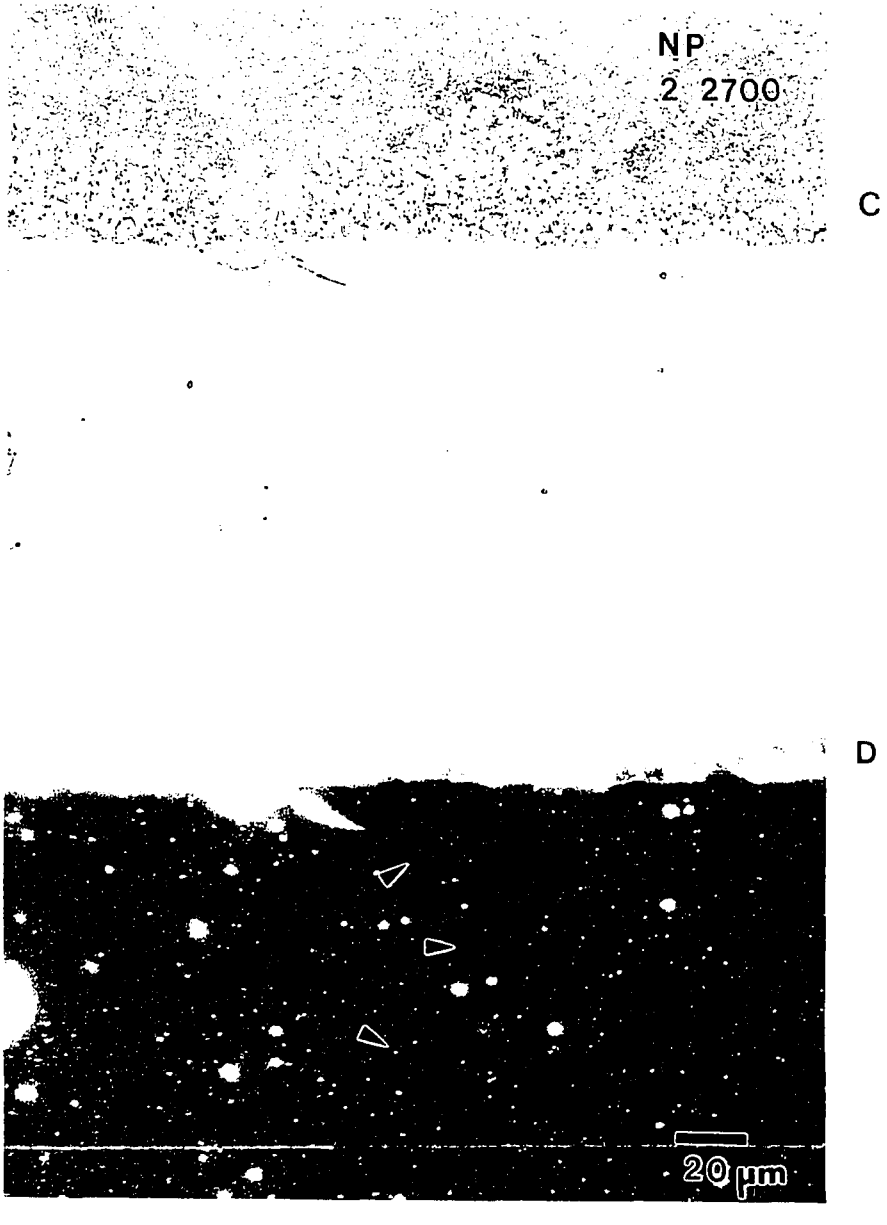

Figure 98. Localized Fe-Zn alloy phase growth formed on the non P-ion implanted low carbon steel surface hot-dip galvanized in a 0.20 wt% Al-Zn bath for 2700 seconds of immersion (c) bright field LOM image and (d) dark field LOM image.

Because a limited number of localized Fe-Zn growths were observed to form on both the P and non P-ion implanted surfaces, P surface segregation appears to have no effect on the nucleation and growth kinetics of Fe-Zn structures. It appears that the grain size of the substrate and its effect on the grain size of the Fe-Al-Zn inhibition layer is the dominant reaction mechanism as compared to surface chemistry (P surface segregation). Guttmann [44, 53] proposed a mechanism that liquid Zn diffusion is the most rapid at random high angle boundaries of the Fe_2Al_5 inhibition layer, and these high angle boundaries correspond in location to the sites of underlying substrate steel grain boundaries. This mechanism would suggest that only 1 or 2 Fe-Zn outburst structures would be expected to form on the P and non P-ion implanted surfaces, because the low carbon steel substrate had a grain size of 10-20 mm, which would result in only 1 or 2 substrate grain boundaries intersecting the substrate surface when viewed in cross section.

Furthermore Guttmann's mechanism [44, 53] can also explain the localized Fe-Zn growth at extended immersion times for the 85 μm ULC steel, while no growth occurred for the large grain size P and non P implanted surfaces at the same time of reaction. The incubation time for localized growth or outburst formation to occur as a function of substrate steel grain size is shown in Figure 99. As the grain size of the substrate steel increased from 15 to 10000 μm, the incubation time for outburst formation increased from 5 to 1800 seconds in a 0.20 wt% Al-Zn bath. The large grain size difference between the ULC and P/non P implanted low carbon substrates most likely results in many more high angle Fe_2Al_5 boundaries formed on the 15 μm ULC steel. Hence, many fast diffusion

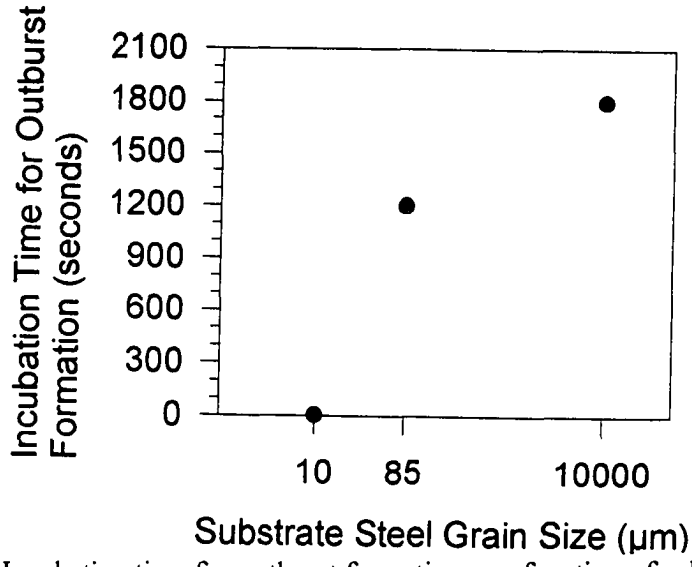

Figure 99. Incubation time for outburst formation as a function of substrate steel grain size (on a log scale) for the 15 and 85 μm ULC steel and the P/non P-ion implanted steel galvanized in a 0.20 wt% Al-Zn bath.

paths for Zn were available in the Fe_2Al_5 layer formed on the 15 μm ULC steel, resulting in much more localized Zn attack and Fe-Zn formation and growth on this substrate, compared to the 85 μm ULC steel and the 10000 μm grain size P and non P-ion implanted steel. It should be noted that the ULC and P/non P low carbon steel substrate chemistries are not the same (the P/non P substrate contained 0.015-0.032 wt% carbon, the ULC steel contained 0.003 wt% carbon) and any direct comparison of the two substrates must take this chemistry difference into account. Thus in contradiction to the suggestion by Lin and Meshii [58], P segregation to substrate steel grain surfaces is not an important mechanism in the Fe-Zn reaction, instead substrate grain size dominates the nucleation and formation of Fe-Zn phases with P only acting to retard Zn diffusion along substrate steel boundaries by segregating in these boundaries in agreement with Allegra [55].

VI. Conclusions

The main conclusions of the present research study are:

1. In a Zn galvanizing bath containing 0.20 wt% Al, the initial formation of Fe-Zn phases was significantly retarded by a large substrate steel grain size. A 15 μm grain size ULC steel showed many areas of localized Fe-Zn growth while no Fe-Zn phase growth was observed on the 85 μm grain size ULC steel over the same time of reaction in the Al containing bath. Only after extended reaction times was Fe-Zn growth found to occur on the 85 μm grain size steel, and this growth typically corresponded to the location of substrate grain boundaries. The observed effect of substrate grain size on Fe-Zn phase formation and growth supports the mechanism that the Fe-Al inhibition layer is first attacked by liquid zinc at sites corresponding to substrate steel grain boundaries.

2. In a Zn galvanizing bath containing 0.00 wt% Al, ultra low carbon substrate steel grain size had no significant effect on the kinetics of phase growth, as both the 15 and 85 μm grain size ULC steel exhibited the same growth kinetics for the gamma, delta, and zeta phase layers.

3. Phosphorus surface segregation had no apparent effect on the kinetics of Fe-Zn phase growth for the individual phase layers formed on low carbon steel in Zn

Zn phase growth occurred on both the P-ion implanted and non P-ion implanted surfaces only after extended reaction times, and Fe-Zn phase growth was found to correspond to the location of substrate grain boundary sites.

4. Substrate steel grain size (and not P surface segregation) appears to be the dominant substrate surface condition which controls the initial formation of Fe-Zn phases in a 0.20 wt% Al-Zn bath.

5. In a Zn galvanizing bath containing 0.00 wt% Al, P solute additions to ultra low carbon steel and interstitial free steel were found to retard the kinetics of Fe-Zn gamma phase layer growth, but did not affect the growth kinetics of any other Fe-Zn phase. Ti and Nb solute additions had no effect on the growth kinetics of any of the Fe-Zn phase layers present in the coating.

6. In a Zn galvanizing bath containing 0.20 wt% Al, substrate steel Ti and Nb solute additions resulted in more rapid growth kinetics of the gamma and delta phase layers. Solute additions were also found to influence the incubation time for the formation of the gamma phase. Phosphorus solute additions to ULC and Ti IF steels prolonged the incubation time for gamma phase formation, while the TiNb and TiNb-P IF steels showed the most reactive behavior and had the lowest incubation time for gamma phase formation.

7. An iron oxide present on the surface of a low carbon steel substrate acts as a physical barrier which inhibits Fe and Zn reactions in a 0.00 wt% Al-Zn bath. The inhibition effect of the oxide was found to be similar in nature to that of the Fe_2Al_5 layer which formed in the 0.20 wt% Al-Zn baths. The inhibition effect of the oxide was temporary, and defects in the oxide acted as fast diffusion paths for Zn. The oxide was eventually penetrated by liquid Zn, and localized Fe-Zn growth (outbursts) formed at the steel/coating interface. Since the wettability of the iron oxide in a 0.20 wt% Al-Zn bath was poor, no significant liquid Zn penetration of the oxide layer occurred, resulting in an absence of Fe-Zn growth.

8. In a Zn galvanizing bath containing 0.00 wt% Al, uniform attack of the substrate steel led to the development of a three phase Fe-Zn alloy layer containing gamma, delta and zeta phases. Zeta was the first Fe-Zn phase to form, followed by delta and then gamma phase. The growth kinetics of the total Fe-Zn alloy layer followed that of the zeta phase, indicating that the Fe-Zn phase layer in contact with the liquid Zn during galvanizing (zeta phase) controlled the growth kinetics of the total Fe-Zn alloy layer. The zeta phase layer followed a two stage growth process with its overall growth governed by $t^{1/3}$ kinetics. The delta phase layer also showed two stage growth, with delta phase following parabolic $t^{1/2}$ growth kinetics after an initial period of no growth. The gamma phase grew according to $t^{1/4}$ kinetics, which is indicative of grain boundary diffusion controlled growth, accompanied by grain growth.

9. In a Zn galvanizing bath containing 0.20 wt% Al, discontinuous Fe-Zn phase growth (outburst formation) was observed at the steel/coating interface, due to the inhibition effect of an Fe-Al layer that first formed upon immersion of the substrate into the bath. A two phase layer morphology developed within the localized Fe-Zn growth regions. Delta phase was the first phase to form, followed by the formation of gamma phase. The growth kinetics of the total Fe-Zn alloy layer followed that of the delta phase. Therefore, the Fe-Zn phase layer in contact with the liquid Zn during galvanizing (delta phase, in this case) was again found to control the growth kinetics of the total Fe-Zn alloy layer. The delta phase followed $t^{1/2}$ parabolic growth, while the gamma phase showed essentially no growth after its initial formation.

VII. References

1. Hisamatsu, Y.: "Science and Technology of Zinc and Zinc Alloyed Coated Steel Sheet", Proceedings of the International Conference on Zinc and Zinc Alloy Coated Steel Sheet (GALVATECH), 1989, Tokyo, Japan, ISIJ, p. 3.

2. Denner, S. G.: "An Overview of the Manufacture and Application of Zinc and Zinc Alloy Coated Steel Sheet in North America", (GALVATECH), 1989, Tokyo, Japan, ISIJ, p. 101.

3. Hada, T.: "Present and Future Trends of Coated Steel Sheet for Automotive Use", (GALVATECH), 1989, Tokyo, Japan, ISIJ, p. 111.

4. Kalson, A. M.: "Coated Steel Sheets in North America An Automotive Perspective", (GALVATECH), 1989, Tokyo, Japan, ISIJ, p.271.

5. Chen Z.W., Gregory, J.T., and Sharp, R.M.: "The Formation and Growth of Intermetallic Phases During Galfanising of Low Carbon Steel at 450°C", 18th Australasian Chemical Engineering Conference, (CHEMECA), 1990, Auckland, New Zealand, p. 296.

6. Selverian J.H. , Marder A.R., and Notis M.R. : "The Reaction between Solid Iron and Liquid Al-Zn Baths", *Metall. Trans.*, vol. 19A, 1988, p. 1193.

7. Kirkaldy, J. S., and Urednicek, M.: "Mechanism of Iron Attack Inhibition Arising from Additions of Aluminum to Liquid Zinc (Fe) During Galvanizing at 450°C", *Z. Metallkde*, Bd. 64, 1973, p. 899.

8. Osinski, K.: "The Influence of Aluminum and Silicon on the Reaction Between Iron and Zinc", Doctoral thesis, Eindhoven, Netherlands, 1983.

9. Ghuman, A. R. P., Goldstein, J. I.: "Reaction Mechanisms for the Coatings Formed During Hot Dipping of Iron in 0 to 10 Pct Al-Zn Baths at 450-700°C", *Metall. Trans.*, vol. 2A, 1971, p. 2903.

10. Borzillo, A. R., and Hahn, W. C.: "Growth of the Inhibiting Aluminum-Rich Alloy Layer on Mild Steel During Galvanizing in Zinc That Contains Aluminum", *Trans. ASM*, vol. 62, 1969, pp. 729.

11. Tang, N-Y. and Adams, G.R.: "Studies on the Inhibition of Alloy Formation in Hot-Dip Galvanized Coatings", The Physical Metallurgy of Zinc Coated Steel, Ed. A.R. Marder, TMS, Warrendale, PA ,TMS , 1994, p. 41.

12. Kirkaldy, J. S., and Urednicek, M.: "An Investigation of the Phase Constitution of Iron-Zinc-Aluminum at 450°C", *Z. Metallkde*, Bd. 64, 1973, p.419.

13. Tang, N-Y., Cominco, Canada, private communication, 1994.

14. Kubaschewski, O.: Binary Phase Diagrams, Springer-Verlag, NY, 1982.

15. Bastin, G.F, van Loo, F.J.J., and Rieck, G. D.: "On The Delta-Phase in the Fe-Zn System", *Z. Metallkde*, Bd. 68, 1977, p. 359.

16. Horstmann, D.: "Reactions Between Iron and Molten Zinc", Zinc Development Association, 1978.

17. Macowiak, J. and Short, N.R.: "Metallurgy of Galvanized Coatings", *International Metals Review*, 1979.

18. ASM Handbook, ASM International, Metals Park, OH, 1992, vol. 3, p. 206.

19. Gellings, P. J., de Bree, E. W., and Gierman, G.: "Synthesis and Characterization of Homogeneous Intermetallic Fe-Zn Compounds", *Z. Metallkde*, Bd. (70), 1979, p. 315.

20. Brown, P. J.: "The Structure of Transition Metal - Zinc Alloy Systems", *Acta Crystall.*, vol. 15, 1962, p. 608.

21. Gellings, P. J., de Bree, E. W., and Gierman, G.: "Synthesis and Characterization of Homogeneous Intermetallic Fe-Zn Compounds", *Z. Metallkde*, Bd. (70), 1979, p. 312.

22. Bastin, G. F., van Loo, F., and Rieck, G. D.: "A New Compound in the Iron Zinc System", *Z. Metallkde*, Bd. (65), 1974, p. 656.

23. Gellings, P. J., Gierman, G., Koster, D., and Kuit, J.: "Synthesis and Characterization of Homogeneous Intermetallic Fe-Zn Compounds", *Z. Metallkde*. Bd. (71), 1980, p. 70.

24. Perrot, P., Tissier, J-C., and Dauphin, J-Y.: "Stable and Metastable Equilibria in the Fe-Zn-Al System at 450°", *Z. Metallkde*, 83, 1992, p. 11.

25. Chen Z.W., Sharp, R.M, and Gregory, J.T.: "Fe-Al-Zn ternary phase diagram at 450°C", *Mat. Sci. and Technol.*, vol. 6, p. 1173.

26. Nishimoto, A., Inagaki, J., and Nakaoka, K.: "Effects of Surface Microstructure and Chemical Composition of Steels on Formation of Fe-Zn Compounds during Continuous Galvanizing", *Trans. ISIJ*, vol. 26, 1986, p. 807.

27. Yamaguchi, H., Hisamatsu Y.: "Reaction Mechanism of the Sheet Galvanizing", *Trans. ISIJ*, vol. 19, 1979, p. 649.

28. Blickwede, D.J.: "Kinetics of Galvanizing", *J. Metals*, vol. 5, 1953, p. 807.

29. Blickwede, D.J.: "Growth of Alloy Layers during Hot-Dip Galvanizing", Proceedings of the Galvanizers Committee of America, Zinc Institute, 1959, p.40.

30. Shewmon, P., Abbas, M. and Meyrick, G.: "Anomalously Fast Diffusion in the Fe-Zn System", *Metall. Trans.*, vol. 17A, (9), 1986, p. 1523.

31. Onishi, M., Wakamatsu, Y., and Miura, H.: "Formation and Growth Kinetics of Intermediate Phases in Fe-Zn Diffusion Couples", *Trans. JIM*, vol. 15, 1974 p. 331.

32. Porter, D., and Easterling, K. E., Phase Transformations in Metals and Alloys , Van Nostrand Reinhold (UK) Co. Ltd., 1981.

33. Kirkaldy, J. S.: "Diffusion in Multicomponent Metallic Systems", *Can. J. Phys.*, vol. 36, 1958, p. 917.

34. Oleford, I., Leijon, W., and Jelvestam, U.: "Selective Surface Oxidation During Annealing of Steel Sheets in H_2/N_2", *App. Surface Sci.*, vol. 6, 1980, p. 241.

35. Blickwede, D. J.: "The Importance of Surface Composition", *Metal Prog.*, 1969, p. 77.

36. Servais, J. P., Gras, H., and Leroy, V.: "Influence of Heat Treatments on the Surface of Low Carbon Steels", CRM Report, vol. 44, 1979, p. 29.

37. Hudson, R. M., Biber, H. E., Oks, E. J., and Warning, C. J.: "Kinetic Studies in Surface Segregation of Manganese During Annealing of Low Carbon Steel", *Metall. Trans.*, vol. 8A, 1977, p. 1713.

38. Janssen, E.: "Chemical Characterization of Industrial Steel and Aluminum Sheet Surfaces by Secondary Ion Mass Spectrometry, Glow Discharge Optical Spectroscopy and Other Surface-Sensitive Techniques", *Mat. Sci. and Engr.*, vol. 42, 1989, p. 309.

39. Leijon, W., Oleford, I.: "Surface State of Batch Annealed Low-Carbon Steel Sheets", *Scand. J. Metallurgy*, vol. 12, 1984, p. 239.

40. Marder, A. R.: "Zinc Coating of Interstitial-Free Steel Sheet", Interstitial Free Steel Sheet: Processing, Fabrication, and Properties Conference, Proceedings of the Metallurgical Society of the Canadian Institute of Mining and Metallurgy, 1991, Ottowa, Canada, p. 157.

41. Dubois, M., Cockerill Sambre, Belgium, private communication, 1993.

42. Graham, M. J., Beaubien, P. E., and Sproule, G. I.: "A Mossbauer study of Fe-Zn phases on galvanized steel", *J. Mat. Sci.*, vol. 15, 1980, p. 626.

43. Toki, T., et al.: "Effect of P Content in Ultra-Low Carbon Ti Stabilized Steel on the Rate of Fe-Zn Alloy Formation through ferrite grain boundary diffusion during Hot-Dip Galvanizing", The Physical Metallurgy of Zinc Coated Steel, Ed. A.R. Marder, TMS, Warrendale, PA ,TMS , 1994, p. 169.

44. Guttman, M.: "Diffusive Phase Transformations in Hot-Dip Galvanizing", Materials Science Forum, Vols. 155-156, Trans Tech Publications, Switzerland, 1994, p.527.

45. Faderl, J., Voest Alpine, Austria, private communication, 1995.

46. Smith, H., Batz, W.: "Iron-Zinc Alloy Formation During Galvannealing", *J. ISIJ*, December, 1972, p. 895.

47. Faderl, J., Pimminger, M., and Schonberger, L.: "Influence of Steel Grade and Surface Topography in the Galvannealing Reaction", Proceedings of the 2nd International Conference on Zinc and Zinc Alloy Coated Steel Sheet (GALVATECH), 1992, Amsterdam, The Netherlands, Verlag Stahl Eisen, p. 194.

48. Faderl, J., Maschek, M., and Strutzenberger, J.: "Spangle Size and Aluminum Pick Up for Hot-Dip Zinc Coatings", Proceedings of the 3rd International Conference on Zinc and Zinc Alloy Coated Steel Sheet (GALVATECH), 1995, Chicago, IL, Iron and Steel Society, p. 675.

49. Krauss, G., Wilshynsky, D. O., and Matlock, D. K.: "Processing and Properties of Interstitial Free Steels", Interstitial Free Steel Sheet: Processing, Fabrication, and Properties Conference, Proceedings of the Metallurgical Society of the Canadian Institute of Mining and Metallurgy, 1991, Ottowa, Canada, p. 1.

50. Kino, N., Yamada, M., Tokunga, Y., and Tsuchiya, H.: "Production of Ti-Nb Added Ultra Low Carbon Steel for Galvannealed Application", Metallurgy of Vacuum-Degassed Steel Products, Ed. R. Pradhan, TMS, 1990, p. 197.

51. Fukuzuka, T., Urai, M., and Wakayama, K.: "Galvannealing Characteristics of Galvanized Steel containing Titanium", *Trans. ISIJ.*

52. Mercer, J.D.: "Factors which Affect the Alloy Growth Rate in Galvannealed Coatings", Proceedings of the 2nd International Conference on Zinc and Zinc Alloy Coated Steel Sheet (GALVATECH), 1992, Amsterdam, The Netherlands, Verlag Stahl Eisen, p. 204.

53. Guttman, M. et al.: "Mechanisms of the Galvanizing Reaction: Influence of Ti and P Contents in Steel and of its Surface Microstructure After Annealing", Proceedings of the 3rd International Conference on Zinc and Zinc Alloy Coated Steel Sheet (GALVATECH), 1995, Chicago, IL, Iron and Steel Society, p. 295.

54. Abe, M., Kanbara, S., and Okuyama, T.: "Iron Zinc Alloy Behavior in Galvannealing of P and P-Si Containing Steel", *Trans. ISIJ*, vol. 25, 1985, p. B15.

55. Allegra, L., Hart, R.G., and Townsend, H.E.: "Intergranular Zinc Embrittlement and Its Inhibition by Phosphorous in 55Pct-Al-Zn Coated Sheet Steel, *Metall. Trans.*, vol. 14A, p.401.

56. Lin, C.S., Chiou, W.A., and Meshii, M.: "Effect of Phosphorus Content in Base Steel on the Formation of Alloy Layer of Hot-Dip Coated Steel Sheets", The Physical Metallurgy of Zinc Coated Steel, Ed. A.R. Marder, TMS, Warrendale, PA ,TMS , 1994, p. 31.

57. Coffin, C., and Thompson, S.W.: "The Effect of 0.07 Weight Percent Phosphorus on the Galvannealing Behavior of a Niobium/Titanium-Stabilized Interstitial-Free Sheet Steel", Proceedings of the 3rd International Conference on Zinc and Zinc Alloy Coated Steel Sheet (GALVATECH), 1995, Chicago, IL, Iron and Steel Society, p. 121.

58. Lin, C.S., and Meshii, M.: "The Effect of Steel Chemistry on the Formation of Fe-Zn Intermetallic Compounds of Galvanneal-Coated Steel Sheets", *Metall. and Mat. Trans.*, vol. 25A, p. 721.

59. Abe, M. and Kanbara, S., Tetsu-to-Hagane, vol. 69, 1983, p. S1061.

60. ASTM Standard E8-E9, American Society for Testing and Materials, Philadelphia, 1989, p. 131.

61. Antonione, C., et al., "Grain growth and secondary recrystallization in iron", *J. Mat. Sci.*, vol. 8, 1973, p.1.

62. Ashbrook and Marder, A.R., *Metall. Trans.*, 1985.

63. Vander Voort, G.F.: Metallography Principles and Practice, McGraw-Hill Series in Materials Science and Engineering, McGraw-Hill, New York, 1984.

64. A. O. Benscoter, Lehigh University, Bethlehem, PA, private communication, 1994.

65. Clayton, C.R., et al.: "Modification of the Corrosion Behavior of 304 Stainless Steel by Phosphorus Implantation", Ion Implantation Metallurgy, Ed. C.M. Preece and J.K. Hirvonen, TMS-AIME, 1980, p. 65.

66. Clayton, C.R., et al.: "RHEED, AES and XPS Studies of the Passive Films formed on Ion Implanted Stainless Steel", Ion Implantation into Metals, 3rd International Conference on Modification of Surface Properties of Metals by Ion Implantation, UMIST, UK, 1981, p. 67.

67. Zuhr, R., Oak Ridge National Laboratory, Oak Ridge, TN, private communication, 1994, 1995.

68. Jordan, C.E.: "Morphology Development in Hot-Dip Galvannealed Coatings", Masters thesis, Lehigh University, Bethlehem, PA, 1991.

69. Gerenrot, Y., FERROTECH, Pittsburgh, PA, private communication, 1993.

70. Dubois, M., Cockerill Sambre, Belgium, private communication, 1995.

71. Jordan C.E., et al., *Mater. Characterization*, 1993, vol. 31, p. 107.

72. ASTM Standard E112-84, American Society for Testing and Materials, Philadelphia, 1984, p. 117.

73. Bastin, G.F., Heijligers, H.J.M., and van Loo, F.J.J.: "The Performance of the Φ(ρz) Modified Approach as Compared to the Love and Scott, Ruste and Standard ZAF Correction Procedures in Quantitative Electron Probe Microanalysis", *Scanning*, 1984, vol. 6, p. 58.

74. Gu, M., and Marder, A.R., *Powder Diffraction*, vol. 6, no. 2, 1991.

75. van Loo, F.J.J.: "Multiphase Diffusion in Binary and Ternary Solid-State Systems", *Prog. Sold St. Chem.*, 1990, vol. 21, p. 47.

76. Esperance, L. et al.: "Analytical Transmission Electron Microscopy of Galvanneal Coatings" Proceedings of the 2nd International Conference on Zinc and Zinc Alloy Coated Steel Sheet (GALVATECH), 1992, Amsterdam, The Netherlands, Verlag Stahl Eisen, p. 442.

77. Adachi, Y., Nakamori, T., and Kamei, K.: "Nano-Characterization of Diffusional α-Fe/Zn Interface Structure", Proceedings of the 3rd International Conference on Zinc and Zinc Alloy Coated Steel Sheet (GALVATECH), 1995, Chicago, IL, Iron and Steel Society, p. 471.

78. van Loo, F.J.J. and Rieck, G.D.: "Diffusion in the Titanium-Aluminum System-I. Interdiffusion between Solid Al and Ti or Ti-Al Alloys", *Acta Met.*, 1973, vol. 21, p. 61.

79. Dybkov, V.I.: " Reaction diffusion in heterogeneous binary systems, Part 1 Growth of the chemical compound layers at the interface between two elementary substances: one compound layer", *J. Mat. Sci.*, 1986, vol. 21, p. 3078.

80. Millares, M., Pieraggi, B., and Lelievre, L.: " Multiphase Reaction-Diffusion in then Au-In System", *Scripta Met.*, 1992, vol. 27, p. 1777.

81. Coffey, K.R., et al.: "Experimental evidence for nucleation during thin-film reactions", *Appl. Phys. Lett.*, 1989, vol. 55 (9), p. 852.

82. Kim, H.K., and Tu, K. N.: "Kinetic Analysis of the soldering reaction between eutectic SnPb alloy and Cu accompanied by ripening", submitted for publication to Physical Review B, 1995.

83. Farrell, H.H., and Gilmer, G.H.: "Grain Boundary diffusion and growth of intermetallic layers: Nb_3Sn", *J. Appl. Phys.*, 1974, vol. 45 (9), p. 4025.

84. Jordan, C.E., Goggins, K.M., and Marder A.R.: " Interfacial Layer Development in Hot-Dip Galvanneal Coatings on Interstitial Free (IF) Steel", 1994, *Metall. and Mater. Trans.*, vol. 25A, 1994.

85. Darken, L.S., and Gurry, R.W., Physical Chemistry of Metals, Metallurgy and Metallurgical Engineering Series, McGraw-Hill Book Co., Inc., NY, 1953.

86. Bahnweg, P., Moreau, T.: Unpublished internal report, IRSID, 1993.

87. Philibert, J. , Atom Movements, Diffusion and Mass Transport in Solids, Les Editions de Physique, France, 1991.

88. van Loo, F.J.J., Eindhoven University, The Netherlands, private communication, 1996.

VIII. Appendicies

Appendix A. Zinc Bath Chemical Analysis (wt%).

0.00 wt% A-Zn Bath	Fe	Zn	Al
start (t=0 samples)	0.029	99.96	<0.001
t=36 samples, 5-300 seconds of immersion	0.020	99.98	<0.001
t=67 samples, 5-300 seconds of immersion	0.021	99.98	-
0.20 wt% Al-Zn Bath	Fe	Zn	Al
start (t=0 samples)	0.009	99.79	0.198
t=36 samples, 5-300 seconds of immersion	0.007	99.81	0.179
new bath (t=0 samples)	0.008	99.78	0.206
t=31 samples, 5-300 seconds of immersion	0.010	99.73	0.195
t=36 samples, 5-300, and 1200-3600 seconds of immersion	0.012	99.79	0.194

Appendix B. Total Coating Weight and Iron Content of 0.00 wt% Al-Zn Coatings Deposited onto ULC and IF Steels.

Steel Substrate	5	10	30	60	120	300
ULC						
CW*	486	453	441	530	690	802
Fe**	4686	5885	9986	13358	16940	25268
ULC-P						
CW	461	463	580	643	690	753
Fe	4519	5809	9669	12874	15467	20906
Ti IF						
CW	488	439	647	653	701	778
Fe	5192	6366	10962	12715	17420	23183
Ti-P IF						
CW	483	451	528	612	644	721
Fe	4929	6806	9196	11738	15405	20370
TiNb IF						
CW	348	493	564	721	685	777
Fe	3342	7121	9590	12829	16820	24028
TiNb-P IF						
CW	583	514	559	623	701	761
Fe	5343	6567	9407	12486	15151	20876

*CW = coating weight (gm), **Fe = total Fe content (mg/m^2)

Appendix C. Total Coating Weight and Fe Content of 0.20wt% Al Coatings Deposited onto IF Steels {*CW = coating weight (gm), **Fe = total Fe content (mg/m^2), ***Al = total Al content (mg/m^2)}

Steel Substrate	5	10	30	60	120	300
ULC						
CW*	537	540	653	649	564	588
Fe**	869	2040	2716	8009	4998	12744
Al***	265	366	810	2214	2089	3539
ULC-P						
CW	524	459	571	588	741	668
Fe	1804	2405	5306	2187	12069	10369
Al	372	579	875	1136	2550	3946
Ti IF						
CW	518	475	568	592	760	893
Fe	2704	4125	4901	4726	16442	24093
Al	345	497	1112	1528	2575	3824
Ti-P IF						
CW	483	553	583	658	574	1080
Fe	1930	1326	4913	8629	5231	28250
Al	350	353	1233	1991	2203	5135
TiNb IF						
CW	646	612	520	584	752	1033
Fe	4023	2926	2646	7654	16596	31071
Al	355	531	1090	2098	2297	5033
TiNb-P IF						
CW	475	534	568	653	596	1162
Fe	1685	1685	1789	6293	8643	27315
Al	334	427	1212	1998	2283	5954

Appendix D. Linear Parabolic Kinetics and Analysis of Growth Data

For a growth reaction initially following linear kinetics and then changing over to parabolic growth, the growth equation can be written as

$$t = x^2 / K_p + x / K_l$$

where t = reaction time, and x = layer thickness

dividing by x

$$t / x = x / K_p + 1 / K_l$$

or

$$t / x = x (1 / K_p) + 1 / K_l$$

then plotting t / x as a function of x, the slope of a fitted line is equivalent to $1/ K_p$ and the intercept of the line on the y axis is equal to $1 / K_l$. A linear regression analysis would then give the linear (K_l) and parabolic (K_p) growth rate constants of a growth layer which follows linear parabolic kinetics.

The total Fe-Zn alloy layer and individual growth layers that formed on the ULC steel hot-dip galvanized in a 0.00 wt % Al-Zn bath were evaluated for linear parabolic kinetics. The plots of immersion time / layer thickness as a function of layer thickness are shown in Figures D1-D4. Evident from the figures is that the total Fe-Zn alloy layer, and the individual gamma, delta and zeta phase layers showed nonlinearity, or that linear parabolic kinetics over the entire reaction time of 5-300 seconds was not operative. Of note was that for the total Fe-Zn alloy layer, and for the delta and zeta phase layers a transition in the plotted data occurred at 60 seconds of reaction time. Similar results were found for other steel substrates hot-dip galvanized in a 0.00 wt% Al-Zn bath. Fe-Zn growth layers that developed during hot-dip galvanizing in 0.20 wt% Al-Zn bath also showed the same behavior, with a break in the total Fe-Zn alloy layer and delta layer data occurring at 60 seconds of immersion. More data are necessary on either side of the 60 second data point in order to further study the possibility of linear parabolic kinetics for Fe-Zn reactions during hot-dip galvanizing.

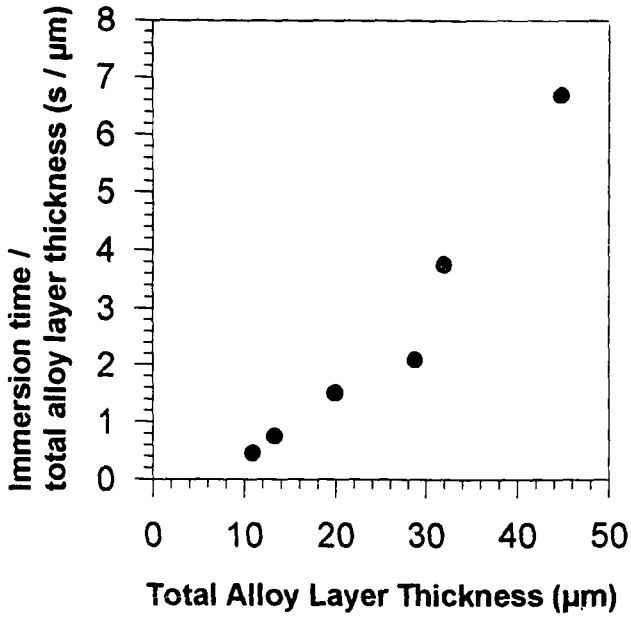

Figure D1. Immersion time divided by total Fe-Zn alloy layer thickness (t/x) plotted as a function of layer thickness (x).

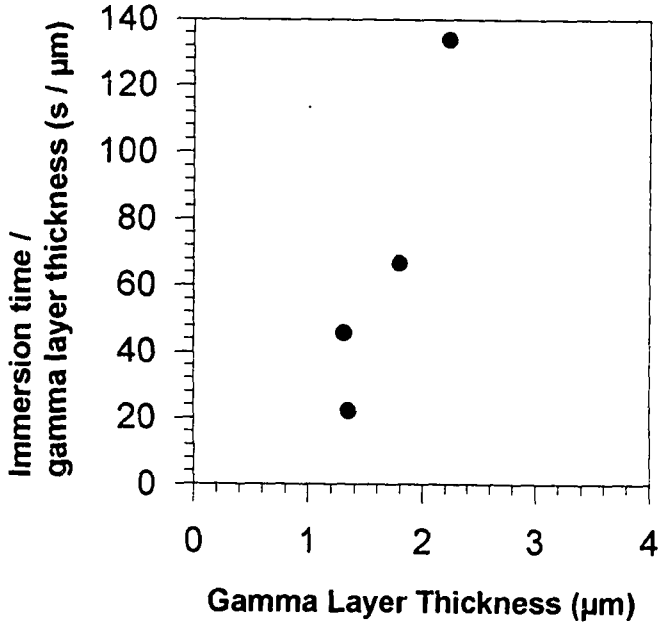

Figure D2. Immersion time divided by gamma layer thickness (t/x) plotted as a function of layer thickness (x).

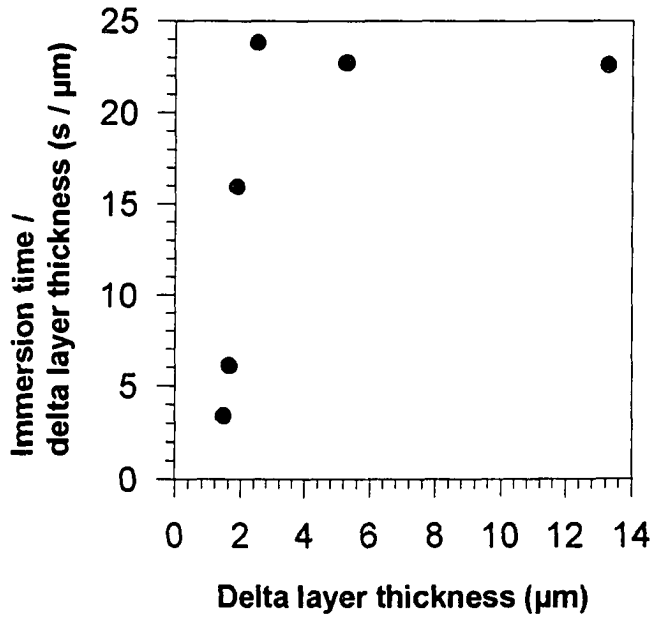

Figure D3. Immersion time divided by delta layer thickness (t/x) plotted as a function of layer thickness (x).

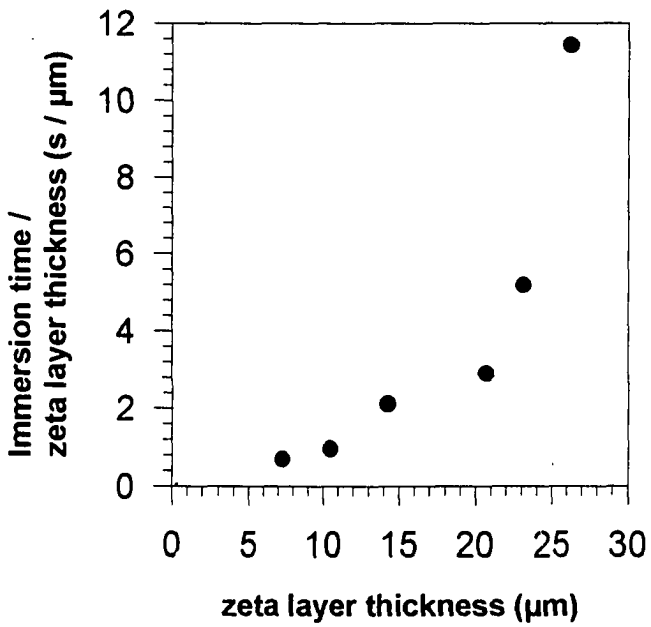

Figure D4. Immersion time divided by zeta layer thickness (t/x) plotted as a function of layer thickness (x).

IX. Vita

Catherine E. Jordan was born in 1967 in the Bronx, New York to April and Mike Jordan. She graduated valedictorian of her high school senior class at Dover High School in Dover Plains, New York. From high school she moved on to Lafayette College in Easton, Pennsylvania, where she graduated with Honors in Metallurgical Engineering in May 1989. Cathy continued her studies in the department of Materials Science and Engineering at Lehigh University, and earned a Master of Science degree in 1991. Her M.S. thesis was titled, "Morphology Development in Hot-Dip Galvannealed Coatings". At present, seven technical papers have been published, including 2 publications in Metallurgical and Materials Transactions as a result of the M.S. work and additional research on the microstructural characterization of zinc coatings. Cathy was married to Steven Attanasio in October 1995, and is currently employed at Knolls Atomic Power Laboratory in Schenectady, New York as a metallurgist in the Structural Materials Engineering Division.